The Influence of Binder Type and Cracking on Reinforcing Steel Corrosion in Concrete

Allan Nye Scott

Thesis Presented for the Degree of
DOCTOR OF PHILOSOPHY
in the Department of Civil Engineering
UNIVERSITY OF CAPE TOWN

February, 2004

DECLARATION

I declare that this dissertation is my own, unaided work. It is being submitted in fulfillment for the Degree of Doctor of Philosophy in Engineering at the University of Cape Town. It has not been submitted before for any degree or examination at any other university.

Signed by candidate

06 day of February 2004

ABSTRACT

The Influence of Binder Type and Cracking on Reinforcing Steel Corrosion in Concrete

Allan Nye Scott

February, 2004

The service life of a reinforced concrete structure is a function not only of the time taken for chlorides to reach the steel in sufficient concentration to initiate corrosion, but also of the length of time before corrosion results in an unacceptable degree of damage. Where there is cracking of the concrete the service life of a structure may be substantially reduced.

Two of the main factors affecting the durability of reinforced concrete structures therefore are the level of chlorides required to initiate corrosion and the subsequent rate of corrosion. Cement extenders have been shown to significantly affect the rate of penetration of chloride ions through concrete. The primary focus of the current work is the study of how cement extenders impact on the corrosion characteristics of embedded steel in concrete. The investigation was limited to those materials commonly used in South Africa (slag, fly ash and condensed silica fume) and performed under laboratory conditions at 30°C.

The process of the corrosion of steel in concrete is affected by both physical factors such as the resistivity of the concrete and chemical factors associated with the pore solution of the concrete. In order to more fully understand the mechanism by which steel corrodes in concrete it was necessary to first examine the chemical influences on steel corrosion through aqueous phase investigations based on the pore solution compositions determined from paste samples. Critical chloride concentrations for initiating corrosion were determined for both the aqueous phase, based on simulated pore solutions, and the case of reinforcing steel embedded in concrete. Thereafter, corrosion rates for steel in cracked concrete were determined for two crack widths of 0.2 mm and 0.7 mm at cover depths of 20 mm and 40 mm.

One of the primary contributions to knowledge of this thesis is in the study of sulphides and their influence on corrosion. The results of the aqueous phase investigation revealed a dependence of the chloride threshold concentration and corrosion rate on not only the hydroxide and chloride concentrations, as expected, but also the presence of sulphide and thiosulphate ions. Those samples which had high sulphide concentrations, representative of slag-bearing concrete, were found to have lower chloride threshold concentrations and higher corrosion rates than otherwise identical sulphide free samples. The detrimental impact of sulphides was again evident in the study on chloride threshold concentrations of steel embedded in concrete. Prior to activation of corrosion by chloride ions the slag-bearing

materials were shown to have higher corrosion rates in the passive state compared to the other concretes using OPC, fly ash and condensed silica fume. The elevated corrosion rates were attributed to the presence of sulphides and thiosulphate in the pore solution.

The negative impact of the slag material ceased however once the specimens moved from a state of passive corrosion to active corrosion. The inclusion of slag, fly ash or condensed silica fume was found to substantially increase the resistivity of the concrete thus limiting the maximum possible corrosion rate. The passive corrosion rates of steel in slag-bearing concrete were not limited by the resistivity of the concrete. The limiting effects of resistivity were evident however in the active state with the slag-bearing specimens having higher resistivities and lower corrosion rates than the OPC control.

A further contribution of this thesis is in the determination of the relationship between corrosion rate, cover and binder type. It was shown that an increase in cover depth is only effective in limiting the corrosion rates where the steel is under oxygen control, such as the case of OPC concrete. If cement extenders are used then the corrosion of steel is generally controlled by the resistivity of the concrete and variations in cover depth have little effect.

The results of the critical chloride concentrations and corrosion rates can be used in conjunction with existing damage prediction and chloride ingress models to estimate the service life of reinforced concrete structures for various concrete binder combinations. An example of their use is provided in the final chapter.

During the course of this investigation many issues were raised which require further investigation that were beyond the scope of this thesis. One of the most pressing issues is the need for further directed research into the effect of binder type on chloride threshold concentrations. The dependence of chloride threshold concentration on binder type was clearly demonstrated but more work is needed to comprehensively investigate a broader range of values with greater repeatability in the results.

ACKNOWLEDGEMENTS

I would like to express my gratitude to the following people and organizations for their assistance in my research and preparation of this dissertation:

- Professor M. G. Alexander, my supervisor for his assistance and guidance throughout my work.

- Professor Knutsen and the Department of Mechanical and Materials Engineering for their assistance and use of their equipment.

- Department of Geology for use of their laboratories and advice in analysis of samples.

- Professor Loewenthal and the water quality group in the Department of Civil Engineering for the use of their facilities and suggestions.

- Dr. G. Glass and Samuel Ginsberg for development and production of the corrosion monitoring system.

- Civil Engineering workshop and materials group for their assistance.

- H. Bueshausen for his assistance in various laboratory activities.

- And my parents for their continued support and assistance.

LIST of ABBREVIATIONS and TERMS

cement extenders	mineral admixtures or supplementary cementitious materials
corrosion rate	refers to rate at which corrosion is occurring and is generally expressed as a corrosion current density in $\mu A/cm^2$
FA	fly ash, also mix design with 30% replacement by FA
PC	Portland cement
SL	mix design with low replacement by slag (25%)
SM	mix design with medium replacement by slag (50%)
SH	mix design with high replacement by slag (75%)
SF	silica fume, also mix design with 7% replacement by SF
slag	ground granulated blast furnace slag
SPS	standard pore solution
TR	ternary blend of 50% PC, 43% slag and 7% SF

TABLE OF CONTENTS

LIST OF FIGURES

LIST OF TABLES

CHAPTER 1: INTRODUCTION

The premature degradation of reinforced concrete represents a serious problem from both a theoretical and practical perspective. According to Mehta (1991) 'tremendous strides have been made in the understanding of durability in corrosive environments, yet it still remains the foremost problem facing structural concrete used today'. Mehta's comments about concrete degradation made in 1991 remain true today more than 10 years later. Considerable research has been directed towards increasing the fundamental understanding of both the transport of aggressive ions through concrete and the subsequent corrosion of reinforcing steel (Mackechnie, 1996, Tuutti, 1982, Schiessl, 1988, and Glass and Buenfeld, 1997). The degradation of reinforced concrete generally involves two processes. Aggressive ions, usually chlorides, initially move through the concrete cover layer towards the steel before any damage occurs. Corrosion of the steel, and thus damage to the concrete, is only initiated once these ions have reached the steel in sufficient concentration. Tuutti (1982) has defined an overall damage model as shown in Figure 1.1.

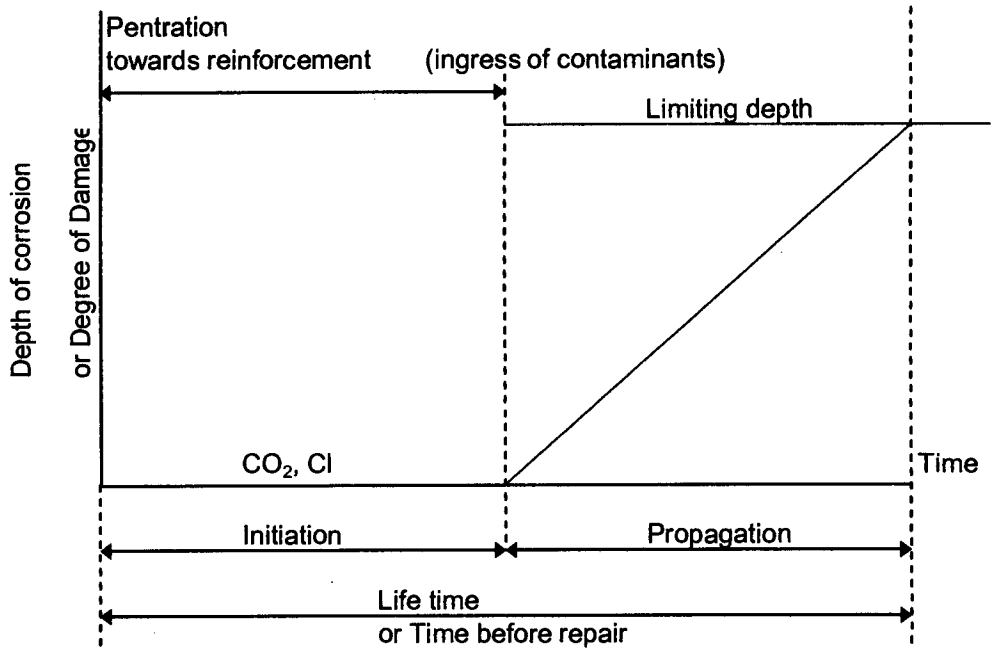

Fig 1.1: Effects of corrosion on life cycle (based on Tuutti 1982)

The damage model of Tuutti (1982) shows two periods: the initiation period of corrosion during which chloride and other harmful substances penetrate through the cover of the concrete but no damage to concrete occurs, and the propagation period during which the steel

reinforcing corrodes and leads to damage. Cement extenders (supplementary cementitious materials such as slag, fly ash and condensed silica fume) have been shown to significantly increase the time to initiation of corrosion (Mangat, Khatib and Molloy, 1994, Mackechnie and Alexander, 1996). There is however less understanding and agreement on the influence of cement extenders on the corrosion rate of steel in concrete. The issue of cracking is another area which tends to complicate the phenomenon of corrosion and little work has been done on the influence of cement extenders on the corrosion of steel in cracked concrete.

Concern has been raised about slag concretes in regard to the presence of sulphides in the pore water. Tromans (1980) has suggested that sulphides may be incorporated into the oxide layer thus reducing its ability to protect the steel. Valentini et al. (1990) conducted an investigation into the corrosion rates of steel in blastfurnace slag mortars at slag replacement levels of 20, 45 and 75%. The initial corrosion rates for the slag-containing samples were approximately 10 times higher than PC but this difference decreased with time. Arya and Xu (1995) examined the performance of a number of cement extenders using steel anodes with cast-in chlorides at 1 and 3%. For 3% chlorides it was shown that corrosion rates occurred in decreasing order of Fly Ash > OPC > Slag > Silica Fume, for cement replacement levels of 35, 0, 65 and 10% respectively. Sirivivatnanon et al. (1994) investigated the influence of similar binder types in mortar samples and found somewhat different results with macrocell corrosion rates at 6 months in the order of OPC > FA > Slag > SF. There was a significant difference in corrosion rate between the 5% and 10% SF replacement levels which would alter the corrosion ranking order.

The influence of service cracking on corrosion rate is also the subject of active debate with Beeby (1983) and Arya and Wood (1995) suggesting that there is no direct relationship between crack width and corrosion rate. The more important factors are considered to be: 1) crack properties, for instance whether the crack is active or dormant, 2) concrete-steel properties, whereby low permeability of the concrete will limit ionic transport, high moisture contents will limit oxygen ingress and increased strength leads to better bond and less slip at the steel-concrete interface, and 3) service environment (Arya and Wood, 1995) . Controlling the environment around the steel-concrete interface is therefore more important than the presence of the crack itself. Pettersson and Jorgensen (1996) however showed an indirect relationship between crack width and corrosion rate by means of the influence of cover for a given crack width.

Disagreement therefore still exists as to the exact influence of cement extenders on the corrosion rate of steel in concrete. The issue of cracking is also subject to much debate and

the interaction of the two variables, cracking and binder type, even more so. The problem of reasonable and representative values for corrosion rates of steel in concrete under cracked conditions and with various binder types was determined to be one of the primary factors limiting predictions for the service life of a structure and in need of investigation. Another significant problem in determining service life is the determination of what level of chlorides are necessary to induce corrosion. As with the issues of corrosion rates and cracking, there are no generally accepted values for chloride threshold level which accounts for deviations caused by the inclusion of cement extenders.

1.1 Problem Definition

The primary problem in the design of adequate serviceability in reinforced concrete structures stems from an inability to accurately quantify and compare the various construction options. In particular there is insufficient information as to the relationship between binder type and the corrosion rate of steel in concrete under various service conditions. The case of the corrosion of steel in cracked concrete is one such area still in need of considerable attention. The objectives of the current work are presented in section 1.2.

1.2 Objectives

The objectives of this thesis are as follows:

1) To study the influence of various binder systems incorporating cement extenders, namely: portland cement (PC), fly ash (FA), silica fume (SF), slag and a ternary blend of PC, slag and SF, on the corrosion rates of steel in concrete. A proper understanding of the influence of cement extenders on the corrosion of steel requires an assessment of the chemical, physical and physico-chemical parameters.

2) To compare results from aqueous phase testing with results from corrosion monitoring of steel in concrete to help separate physical and chemical effects and more accurately assess the mechanisms at work in promoting and controlling corrosion. Particular attention to be paid to the effect of sulphides in both passive and active corrosion states.

3) To investigate the influence of crack width and cover depth on the corrosion rates of steel in concrete containing cement extenders.

4) To attempt to quantify binder specific chloride threshold values.

5) To attempt to correlate corrosion rate data with durability index values as predictive tools for assessing performance of the material.

6) To develop a model framework or use an appropriate existing damage model for predicting the remaining service life of a structure associated with the propagation period based on the information derived from the first four objectives.

1.3 Scope and Limitations

The scope of work involved in this thesis was limited to the study of the corrosion of reinforcing steel and mild steel bar in two different environments. An aqueous phase investigation of mild steel in simulated pore solutions was conducted to determine the chemical impact of the pore solution on some of the characteristics of both passive and active corrosion. The second environment was that of steel in concrete where chloride threshold concentrations, as well as passive and active corrosion rates were determined. Chloride threshold concentrations for the various binder types were also determined for steel in mortar specimens but only limited data are available due to the length of time before active corrosion initiated. A number of specific limitations are provided in the following discussion.

The investigation of the relationship between binder type and corrosion rate is limited to seven binder combinations as provided in Table 1.1.

Table 1.1 Percentage of binder type used in the investigation

Binder Type	*Portland Cement*	*Slag*	*Fly Ash*	*Silica Fume*
PC	100	0	0	0
SL	75	25	0	0
SM	50	50	0	0
SH	25	75	0	0
FA	70	0	30	0
SF	93	0	0	7
TR	50	43	0	7

The seven mix compositions representing a wide cross section of binder types likely to be employed were chosen for study. SL and SH, with slag replacement levels of 25% and 75% replacement levels respectively, were included in the investigation to provide a basis for examining the impact of different levels of slag replacement on the corrosion characteristics, even though those specific replacement levels are outside the normal range of values encountered in practice.

The investigation of the pore solution was conducted by means of pore expression of paste samples at 7, 28 and 90 days. General trends with respect to pore solution chemistry can

be determined, but the concentration of sulphides was variable over this period, preventing accurate long term predictions. One of the major factors affecting the reliability of pore solution results is the necessity of minimizing the contact of the pore solution with the external environment. While all reasonable effort was taken to minimize exposure of the pore solution to the atmosphere, some limited contact undoubtedly took place.

The study of corrosion rates and binder type is limited to two cover depths of 20 mm and 40 mm. Two crack widths of 0.2 mm and 0.7 mm were chosen as being representative of service cracking. The corrosion rates were determined for specimens stored at a constant temperature of 30°C. Any use of the corrosion rates presented in this thesis should therefore be limited to the range over which the materials were investigated.

A damage prediction model was chosen from work already published by other investigators and was used to investigate the potential service life of structures. The primary objective of the current work was the determination of the relationship between corrosion rate and binder type. It was deemed acceptable therefore to select a reasonable damage model, using the corrosion rate data obtained in the current investigation, for the purpose of illustrating the impact of binder type on the potential service life of a structure, although further verification of the model for the specific materials used in this investigation would be required.

1.4 General Outline of Thesis

A review of the basic principles involved in electrochemical corrosion is presented in chapter 2. The derivation of the Nernst equation, which permits the calculation of cell and half-cell potentials at a range of temperatures, and ionic concentrations for the reactants and products, is presented in this section. The stability of the various iron oxides and factors associated with the passivity of metal are also discussed. The use of Tafel equations and knowledge of the polarization resistance allows for the estimation of corrosion rates. The role of chlorides and sulphides in promoting corrosion is also presented.

Understanding the corrosion of steel in concrete first requires a knowledge of certain material and chemical characteristics. The chemistry of the pore solution was determined by means of pore expression of cement paste representing the mix designs under consideration, the values and methodologies of which are provided in chapter 3. The interaction between sulphides, from the slag bearing materials, and dissolved oxygen concentrations are highlighted in this section.

Given knowledge of the individual chemistry associated with the inclusion of cement extenders, it is possible to isolate the chemical effects in the concrete by subjecting steel to simulated pore solutions as demonstrated in chapter 4. The relationship between corrosion rate and pore solution composition is presented in this section. The effects of binder specific pore solution chemistry on the chloride threshold concentration is also discussed. The residual impact of sulphides on the passivity of steel in solution, even after their oxidation, was investigated under both passive and active corrosion conditions.

The effects of cement extenders on the corrosion of steel cannot be measured by pure chemical analysis alone but also require incorporation of physical and physicochemical effects. Chapter 5 provides corrosion rate measurements for steel embedded in concrete made with the different binder types under cracked conditions. Two crack widths of 0.2 mm and 0.7 mm and two cover depths of 20 mm and 40 mm are investigated. In addition to corrosion rate data the material properties were assessed by use of durability index testing. Binder specific chloride threshold values were determined based on mortar and concrete samples.

The corrosion rates and durability index values presented in chapter 5 are used in chapter 6 to provide a corrosion prediction model based on 90 day chloride conductivity values. The effects of binder specific chloride threshold values are coupled with existing chloride ingress models to show the effect of specific threshold values on the time to corrosion initiations. Various damage models are also investigated and the prediction of service life is based on a combined initiation and propagation approach using the corrosion rate data derived from this work. The deterioration estimates would only be applicable for the situation currently investigated and should ultimately be correlated with site data for the model to be validated.

1.5 References

Arya, C. and Wood, L. 1995, **The relevance of cracking in concrete to corrosion of reinforcement,** (Concrete Society Technical Report No. 44).

Arya, C. and Xu, Y. 1995, *Effects of cement type on chloride binding and corrosion of steel in concrete*, **Cement and Concrete Research**, Vol. 25, No. 4, 1995, pp. 893-902.

Beeby, A. 1983, *Cracking, cover and corrosion of reinforcement*, **Concrete International**, February, pp. 35-40.

Glass, G. and Buenfeld, N. 1997, *The presentation of the chloride threshold level for corrosion of steel in concrete*, **Corrosion Science**, Vol 39, No. 5, pp. 1001-1013.

Mackechnie, J. 1996, **Predictions of Reinforced Concrete Durability in the Marine Environment,** PhD Thesis, University of Cape Town.

Mackechnie, J. and Alexander, M. G. 1996, *Marine exposure of concrete under selected South African conditions*, **Proceedings third ACI/CANMET Int. conference on the performance of concrete in marine environment**, St. Andrews by-the-Sea, Canada, pp. 205-216.

Mangat, P., Khatib, J. and Molloy, B. 1994, *Microstructure, chloride diffusion and reinforcement corrosion in blended cement paste and concrete*, **Cement and Concrete Composites**, Vol. 16, pp. 73-81.

Mehta, P. 1991, *Durability of Concrete-Fifty Years of Progress?*, **Durability of Concrete, Second International Conference, ACI SP-126,** Montreal, pp. 1-31.

Pettersson, K. and Jorgensen, O. 1996, *The effect of cracks on reinforcement corrosion in high-performance concrete in a marine environment*, **Proceedings third ACI/CANMET Int. conference on the performance of concrete in marine environment**, St. Andrews by-the- Sea, Canada, pp. 185-200.

Schiessl, P. ed. 1988, **Corrosion of steel in concrete: Report of the Technical Committee 60-CSC** RILEM, Chapman & Hall.

Sirivivatnanon, V., Bucea, L., Meck, E., Yozghatlian, S. and Cao, H. 1994, *Influence of fly ash, ground granulated blast furnace slag and silica fume on chloride induced corrosion of steel in reinforcement,* **2nd International Symposium on Blended Cements,** Malaysia, pp. 114-120.

Tromans, D. 1980, *Anodic polarization behavior of mild steel in hot alkaline sulfide solutions*, **Journal of Electrochemical Society**, June, 1980, pp. 1253-1256.

Tuutti, K. 1982, **Corrosion of steel in concrete**, Swedish Cement and Concrete Research Institute.

Valentini, C., Berardo, L., and Alanis, I. 1990, *Influence of blast furnace slags on the corrosion rate of steel in concrete*, **Corrosion Rates of Steel in Concrete: ASTM STP 1065**, Philadelphia, pp. 17-28.

CHAPTER 2: PRINCIPLES OF STEEL CORROSION

The principles of corrosion of steel in concrete and corrosion in general have been well documented by a number of authors (Schiessl, 1988, Bockris et al., 1981). It is not the objective of this thesis to present a detailed description of the fundamentals of electrochemistry, but for the purposes of review and explanation of the research some principles governing corrosion are discussed. Steel rebar in concrete essentially behaves as normal aqueous corrosion with the pore water acting as the interface for the solution and means of ion transport. The study of aqueous phase corrosion therefore is essential to understanding the nature of steel corrosion in concrete. The specific influence of concrete and pore water chemistry will be discussed in the subsequent chapters 3 and 4.

Corrosion of steel in concrete is an electro-chemical process in which iron enters solution at the anode and an oxidizing agent is reduced at the cathode. The corrosion half cell reactions for iron are given as follows (Stansbury, 2000):

Anodic reaction:

$$Fe \rightarrow Fe^{2+} + 2e^{-} \qquad \ldots 2.1$$

Cathodic reaction:

$$O_2 + 2H_2O + 4e^{-} \rightarrow 4OH^{-} \qquad \ldots 2.2$$

To verify that the reaction will proceed in the direction indicated, it is necessary to look at the change in energy under normal conditions for the steel. The thermodynamics of a system can provide information on the direction of the reaction and the likely corrosion products under a given set of conditions but it cannot provide information on the likely rate, or kinetics, of the reaction. It is necessary therefore to explore both the thermodynamics and kinetics of aqueous corrosion.

2.1 Chemical Thermodynamics

Thermodynamics can be defined as the study of heat in a changing physical and chemical process (West, 1980). By examining the change in heat it is possible to gain an understanding of the nature of the process and possibilities for changes to the system. The first law of thermodynamics states that "in a system of constant mass, energy can neither be created nor destroyed, although it may be converted from one form to another". From the first law of

thermodynamics it can be shown that the change in internal energy must be balanced by the heat absorbed and the work done giving rise to (Stansbury and Buchanan, 2000 rewritten as):

$$dU = dq - w \qquad \ldots 2.3$$

Where:

dU - change in internal energy

dq - change in heat absorbed

w - work done

The work done can be divided into two forms with one component PdV, where P is pressure and V volume, being received from the atmosphere and the other w' attributed to electrical energy.

The entropy (S) of a system derives from the second law of thermodynamics which states that for a process to proceed spontaneously there must be an increase in the disorder of he universe. The change in entropy or disorder (dS) of a system therefore is equal to the amount of heat added (dq) at a controlled temperature (T), equation 2.4 (West, 1980).

$$dS = \frac{dq}{T} \qquad \ldots 2.4$$

Combining equations 2.3 and 2.4 yields:

$$dU = TdS - PdV - w' \qquad \ldots 2.5$$

Assuming T and P are constants equation 2.5 can be rewritten as :

$$-w' = d(U - TS + PV) \qquad \ldots 2.6$$

2.1.1 Gibbs Free Energy

The total heat energy known as enthalpy (H) of a system, as taken from the first law of thermodynamics, is described as $H = U + PV$. The maximum available energy of a system, known as Gibbs free energy (GFE) or free enthalpy, is given as (Shreir, 1979):

$$G = H - TS \qquad \ldots 2.7$$

where G is Gibbs free energy.

Therefore (Stansbury and Buchanan, 2000):

$$dG = -w' \qquad \ldots 2.8$$

with $$dG = d(U - TS + PV) \qquad \ldots 2.9$$

For a reaction to proceed spontaneously the change in available free energy (ΔG) must be negative.

The GFE of a reaction is a sum of the energy of the products minus the reactants. Absolute values for G however do not exist and are therefore determined under constant conditions of one atmosphere and T = 298 K, which give rise to the standard G denoted as G^o. As a reference, the G^o of an element is taken as zero and tables of standard free energies for various compounds are provided in numerous books including West (1980). For standard conditions the change in GFE for a reaction can be written as (rewritten from Stansbury and Buchanan, 2000):

$$\Delta G^o_{react} = \sum \Delta G^o(products) - \sum \Delta G^o(reactants) \quad \ldots 2.10$$

As Stansbury and Buchanan (2000) rightly note, the conditions for a spontaneous reaction to occur are not that changes in the standard G of a reaction ($\Delta G^o_{reactants}$) are negative but rather the changes under actual conditions ($\Delta G_{reactants}$) are negative. It is therefore necessary to relate the standard G to the actual conditions under which the reaction is occurring. The relationship between the standard GFE and the actual GFE for a pure substance is given as (West 1980):

$$G = G^\circ + RT \ln a \quad \ldots 2.11$$

where a is the activity, R is the gas constant 8.314 (J/mol K), and T is temperature (K).

2.1.2 Gibbs free energy and chemical potential

The energy of a system can be changed through addition or subtraction of moles of various substances in the system. The chemical potential refers to the change in free energy of the i^{th} component of a system when 1 mol of component i is added to the system with everything else (T, P n_j) being held equal. The chemical molar potential μ_i therefore is given as (Shreir, 1979):

$$\mu_i = \left(\frac{\partial G}{\partial n_i}\right)_{p,T,n_j} \quad \ldots 2.12$$

where $n_{i,j,\ldots}$ are the number of moles.

As with G, the standard chemical potential of a pure element is considered to be zero, and the relationship between the μ^o_i and μ_i given by Shreir (1979):

$$\mu_i = \mu_i^\circ + RT \ln a_i \quad \ldots 2.13$$

The direction or likelihood of a reaction can therefore be determined based on the chemical molar potentials of a system according to (West, 1980):

$$\Delta G = \left(\sum n_i \mu_i\right)_{prod} - \left(\sum n_i \mu_i\right)_{react} \quad \ldots 2.14$$

By incorporating equation 2.13 it can be shown that

$$\Delta G = \sum n_i \mu_i^\circ + RT \sum n_i \ln a_i \quad \ldots 2.15$$

where the term Σ includes both reactants and products. If ΔG is less than zero then the reaction will proceed spontaneously in the direction written. Under conditions of thermodynamic equilibrium $\Delta G = \sum n_i \mu_i = 0$ (rewritten from Bockris et al., 1981).

Considering a general reaction $aA + bB = cC + dD$ the second term of equation 2.15 yields:

$$\sum n_i \ln a_i = \sum n_i \ln\left[\frac{\left(a_C^c a_D^d\right)}{a_A^a a_B^b}\right]$$

$$= \ln K \quad \ldots 2.16$$

where K is the equilibrium constant for the system (West 1980). Since $\Delta G^o = \sum n_i \mu_i^o$ for equilibrium conditions equation 2.15 may be rewritten as:

$$\sum n_i \mu_i^\circ = -RT \sum n_i \ln a_i$$

or

$$\Delta G^\circ = -RT \ln K \quad \ldots 2.17$$

The preceding derivations and explanations provide a brief background to the development of chemical thermodynamics which underpins the basis of electrochemical thermodynamics which can then provide vital information on the possible corrosion conditions of a particular system. In summary it shows that:

- the change in free energy provides a means determining the direction or likelihood of a reaction occurring
- the chemical potential of each component in a mixture is a function of the molar free energy in its standard state adjusted for departures from ideality (West 198).

The following sections will further develop the basic principles involved in the electrochemical study of corrosion.

2.2 Electrochemical Thermodynamics and the Nernst Equation

Bockris et al. (1981) state that an electrochemical reaction may be defined as a reaction in which chemical bodies and free electrical charge in the form of electrons take part. The chemical potential μ must therefore be augmented by an additional electrical energy given as

zFφ where φ is the electrical potential and F is Faraday's constant (Bockris et al., 1981, West, 1980). The electrochemical potential (μ_i') therefore can be expressed as:

$$\mu_i' = \mu_i + z_i F \varphi_i \qquad \ldots 2.18$$

The corrosion of metal in a solution can generally be viewed as two individual half cells combined to produce an overall reaction as shown in equations 2.1 and 2.2. The individual electrode contributes a potential difference of $\varphi^M - \varphi^S$ where M represents the metal immersed in a solution S (West, 1980). Where two individual half-cells are combined there is a tendency for electrons to flow from the anode where oxidation is occurring to the cathode which supports reduction. By convention, the cell is shown as having an anode on the left and cathode on the right. The potential difference $\varphi_R - \varphi_L$ measured on the open circuit is known as the electromotive force (emf) of the cell and is designated ε and is a measure of the free energy change that would result if the reaction were allowed to occur (West, 1980). The relationship between the electrical potential difference and the chemical free energy difference available to drive the cell is given as (West, 1980):

$$\Delta G = -nF\varepsilon \qquad \ldots 2.19$$

At equilibrium, the GFE driving the transfer of an ion from the metal to the solution is balanced by the electrical potential difference attracting the ion back to the metal (Stansbury and Buchanan, 2000).

Since it is not possible to measure a single electrode directly, relative values are determined against a suitable standard reference electrode. The right hand electrode given as $2H^+ + 2e = H_2$ occurring on a platinum wire with hydrogen ion activity of 1, hydrogen gas pressure of 1 atmosphere and 25°C is known as the standard hydrogen electrode (SHE) for which the half cell potential $E^o_{H_2,H^+}$ is zero (Stansbury and Buchanan, 2000). For a half-cell measured against the SHE, the emf of the cell is represented by the term E_M where M is the metal under consideration (West, 1980).

Consider the general reaction:

$$xM + mX^{x+} \leftrightarrow xM^{m+} + mX \qquad \ldots 2.20$$

consisting of two half cell reactions:

$$xM \leftrightarrow xM^{m+} + (x.m)e$$

$$mX^{x+} + (x.m)e \leftrightarrow mX$$

where M is the oxidant, X^{x+} is the reductant, m is the charge of the oxidized species, and x is the number of oxidants. The direction of current and electron flow for the combined cell can be seen in Figure 2.1.

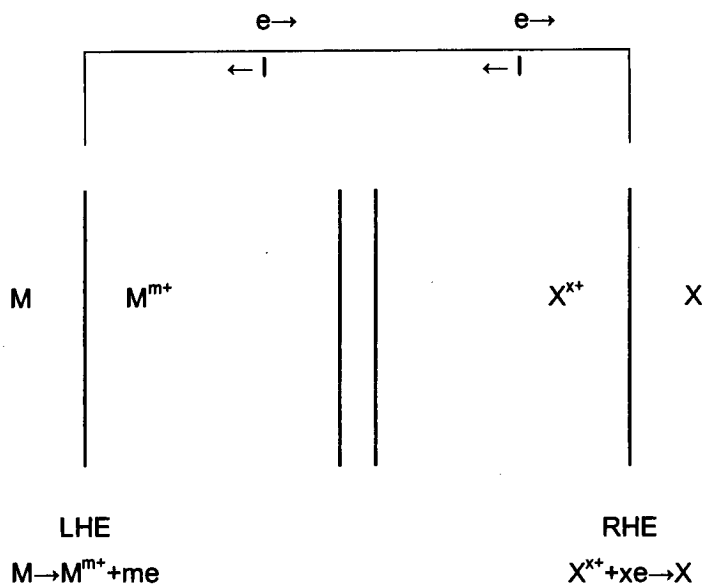

Fig 2.1: Current and electron flow for coupled half- cells
(Stansbury and Buchanan, 2000)

According to electrical current convention, current flows from the high potential X to the low potential M, thus providing electrical energy capable of doing work (Stansbury and Buchanan, 2000). For equation 2.20 to proceed spontaneously from left to right $\Delta G_{react} < 0$. Since $E_{cell}=E_{RHE}- E_{LHE,}$ for consistency with equation 2.19, therefore $E_{cell} > 0$ for the reaction to proceed spontaneously. From equation 2.20 the GFE can be written as (Stansbury and Buchanan, 2000):

$$\Delta G = \Delta G^{\circ} + RT \ln \frac{a_X^m \cdot a_{M^{m+}}^x}{a_M^x \cdot a_{X^{x+}}^m} \qquad \ldots 2.21$$

Given $\Delta G = -nFE$ and $\Delta G^{\circ} = -nFE^{\circ}$ where $n = x \cdot m$ it follows,

$$E = E^{\circ} - \frac{RT}{nF} \ln \frac{a_{M^{m+}}^x}{a_{X^{x+}}^m} \qquad \ldots 2.22$$

Since $E_{cell}=E_{RHE}- E_{LHE} = E_{X,X^{x+}} - E_{M,M^{m+}}$ and $E^{\circ} = E^{\circ}_{X,X^{x+}} - E^{\circ}_{M,M^{m+}}$ substituting into

equation 2.21 yields the Nernst half-cell equations:

$$E_{X,X^{x+}} = E^{\circ}_{X,X^{x+}} + \frac{RT}{xF} \ln a_{X^{x+}} \quad \ldots 2.23$$

$$E_{M,M^{m+}} = E^{\circ}_{M,M^{m+}} + \frac{RT}{mF} \ln a_{M^{m+}} \quad \ldots 2.24$$

The general form for redox equilibrium reaction therefore is given as:

$$E = E^{\circ} + \frac{RT}{nF} \ln \frac{a_{Ox}}{a_{\mathrm{Red}}} \quad \ldots 2.25$$

where a_{Ox} and a_{Red} are the products of the oxidized and reduced sides of the equation.

The Nernst equations are essential for the use and presentation of thermodynamic data. The equations allow for the calculation of the cell and half-cell potentials at any range of temperatures, and ionic concentrations for reactants and products under consideration. From this information it is possible to determine the likelihood of a reaction occurring in the manner indicated and thus determine the range of situations in which corrosion may occur. The Nernst equations led to the development of Pourbaix diagrams, discussed in the following section, which provide a useful graphical means of showing the susceptibility of metals to corrosion and the range of corrosion products. The potentials for various individual half-cell reactions have been determined and are presented in numerous books (West, 1980, Stansbury and Buchanan, 2000, Shreir, 1979).

2.3 Pourbaix Diagrams

The measurement of half-cell potentials, when compared to equilibrium potentials, allows for the determination of the state of a particular metal (and its oxide) in solution. If the measured electrode potential (E) is greater than the calculated equilibrium potential (E') then oxidation is possible. Where $E < E'$ then reduction is possible and if $E = E'$ then neither oxidation nor reduction is possible and the system is in equilibrium (Bockris et al., 1981). The stability of a metal and its oxides in solution is conveniently displayed through the use of Pourbaix diagrams. The Pourbaix diagram shows the relationship between electrode potential and pH at equilibrium for a metal in an aqueous environment.

A simplified form of the Pourbaix diagram for the iron-water system is shown in figure 2.2. There are broadly three domains in which iron can exist (West, 1980):

a) immune – no corrosion takes place and iron exists in its metallic states (Fe)

b) corrosion – where iron exists in its stable ionic states (Fe^{II}, Fe^{III}) and $HFeO^{-}_{2}$ (Stansbury and Buchanan, 2000)

c) passive – stable passivating compounds of Fe_2O_3 and Fe_3O_4 are formed

The nature of the passive state and further discussion of the various iron oxides and their influence on corrosion will be presented subsequently in more detail. The construction of the Pourbaix diagram shown in Figure 2.2 is based on the Nernst equations as previously established. When constructing a Pourbaix diagram for a particular metal one of the first areas steps is the determination of the region of stability of water given by lines *a* and *b* corresponding to equations 2.26 and 2.27 respectively.

$$H_2O + e = \frac{1}{2}H_2 + OH^- \qquad \ldots 2.26$$

$$2H_2O = O_2 + 4H^+ + 4e \qquad \ldots 2.27$$

Below line *a* H_2 is produced and above line *b* O_2 is produced. Thus the effective stable range for water lies between *a* and *b*.

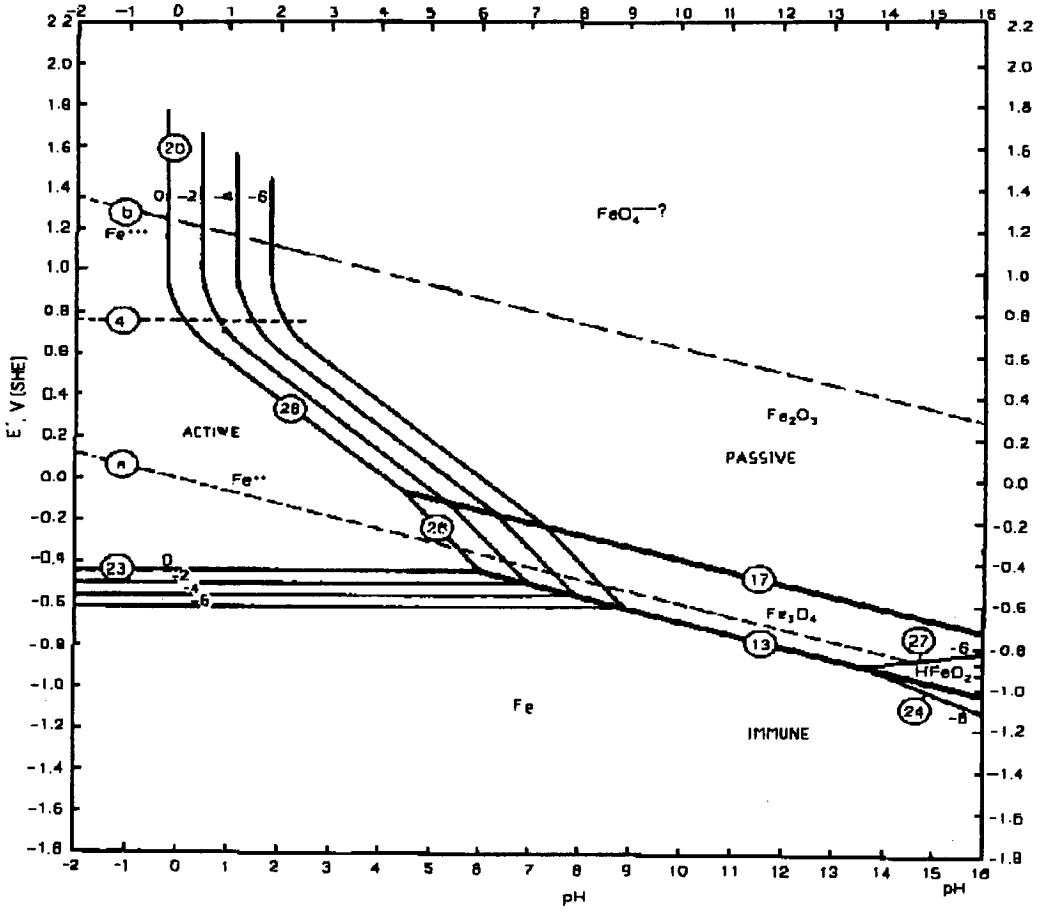

Figure 2.2: Pourbaix Diagram for iron in water (base on Stansbury and Buchanan, 2000)

There are a number of aspects of the various oxide states of the metal which are evident in the Pourbaix diagrams. The equilibria between Fe(s) | Fe^{II}(aq) and Fe^{II}(aq) | Fe^{III}(aq) are

given by horizontal lines indicating the reaction is independent of hydrogen ions and thus pH, equation 2.28.

$$Fe^{III} + e = Fe^{II}$$

$$E = E^o + \frac{RT}{nF}\log\left(\frac{a_{Fe^{III}}}{a_{Fe^{II}}}\right) \qquad \ldots 2.28$$

$$= +0.77 \quad V, SHE$$

Conversely the conversion of $Fe^{III}(aq)$ to $Fe_2O_3(s)$ as shown by the vertical line (20) indicates no exchange of electrons. The equilibria between $Fe^{II}(aq) \mid Fe_3O_4(s)$ however is somewhat more complicated involving both hydrogen and electrons as shown in equation 2.29 and accounts for the slope in the line, (West 1980).

$$Fe_3O_4 + 8H^+ + 2e = 3Fe^{II} + 4H_2O$$

$$E = E^o + \frac{RT}{2F}\log\left(\frac{a_{H^+}^{\ 8}}{a_{Fe^{II}}^{\ 3}}\right) \qquad \ldots 2.29$$

$$= +1.08 - 0.177pH \quad V, SHE$$

The effect of activity on the E-pH diagram is clearly demonstrated by line 23, of figure 2.2, which is representative of the equilibrium half-cell reaction for Fe, Fe^{II}, at 25°C, equation 2.30.

$$E_{Fe:Fe^{II}} = -0.44 + 0.0295\log(a_{Fe^{II}}) \qquad \ldots 2.30$$

The activities of Fe^{II} (10^0 and 10^{-6}) in solution are shown as parallel lines corresponding to electrode potentials of –440 and –610 mV respectively. Potentials more positive than the equilibrium value lead to dissolution of metallic iron into Fe^{II}. A further increase in potential will results in the conversion of Fe^{II} to Fe^{III}. There is an inverse relationship therefore between the degree of ionic activity in solution and the corrosion domain. Increases in temperature will also result in an enlarged corrosion domain.

Figure 2.2 applies to iron in pure water at 25°C, thus the effects of other complexing agents such as sulphides or chlorides are not considered. Figure 2.3 has been determined for iron in salt water. The Pourbaix diagram of iron in sea water shows a stark contrast to pure water and highlights the effects of chlorides on the corrosion of iron. The domains of iron in seawater, represented by chloride concentrations between 10^{-1} M and 1.0 M, are clearly shown in Figure 2.3 where there is a substantial increase in the area of corrosion and the formerly passive domain is also marked by an area which is susceptible to pitting corrosion.

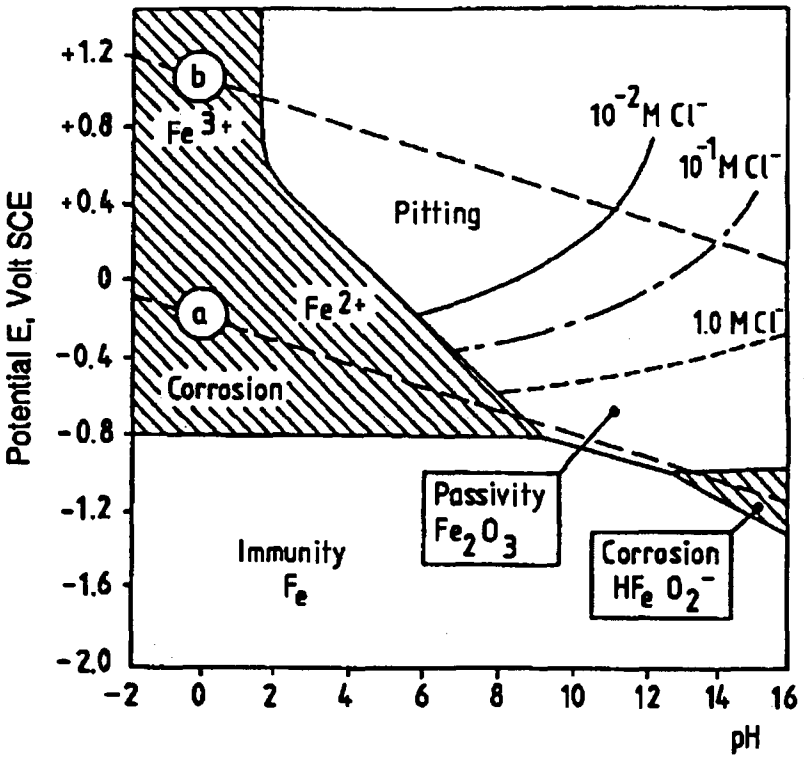

Figure 2.3: Pourbaix diagram for iron exposed to chloride solutions (Pettersson and Sandberg, 1997)

While Pourbaix diagrams are useful for determining the regions in which corrosion of iron is possible and likely form of the corrosion product, they do not provide any information on the rate at which the reaction will proceed. Before examining reaction rates and process it is useful to further investigate the types of corrosion products which can form and their influence on the corrosion process.

2.4 Iron Oxide Stability and Passivity

There are numerous oxides, hydroxides and oxide hydroxides of iron which may exist under various conditions of temperature, pressure, potential and pH. Cornell and Schwertmann (1996) have identified 16 which are listed in Table 2.1. Not all of the oxides listed will be present in the corrosion of steel in concrete and only those which are significant will be briefly discussed.

Table 2.1: Iron oxides

Oxide hydroxides and hydroxides	*Oxides*
Goethite α-FeOOH	Haematite α-Fe_2O_3
Lepidocrocite γ-FeOOH	Magnetite Fe_3O_4
Akaganeite β-FeOOH	Maghemite γ-Fe_2O_3
Schwertmannite	β-Fe_2O_3
$Fe_{16}O_{16}(OH)_y(SO_4)_z \cdot nH_2O$	
δ-FeOOH	ε-Fe_2O_3
Feroxyhyte δ'-FeOOH	Wustite FeO
High pressure FeOOH	
Ferrihydrite $Fe_5HO_8 \cdot 4H_2O$	
Bernalite $Fe(OH)_3$	
$Fe(OH)_2$	

The primary reaction for the corrosion of iron was given in equation 2.1 which is the conversion of Fe(s) to Fe^{II} in the aqueous solution. The iron (II or III) will precipitate as an oxide or hydroxide, as listed in table 2.1, once the solubility product is exceeded (West, 1980). Consider equations 2.31 and 2.32 in which $Fe(OH)_2$ and $Fe(OH)_3$ are formed respectively:

$$Fe^{II} + 2OH^- = Fe(OH)_2(s) \quad \ldots 2.31$$

$$Fe^{III} + 3OH^- = Fe(OH)_3(s) \quad \ldots 2.32$$

where the ionic product, given as the product of the individual ionic Henrian activities (h), is $h_{Fe^{III}} \bullet h^3_{OH^-} = 10^{-39}$. The critical ferric ion activity ($h_{Fe^{III}}$) therefore is a function of the hydroxyl ion concentration. At a pH of three ($h_{OH^-}=10^{-11}$), hence $h_{Fe^{III}} = 10^{-39}/10^{-33}=10^{-6}$. At a pH of 8 however the $h_{Fe^{III}}$ is reduced to only 10^{-21} (West 1980). In the case of $Fe(OH)_2$ with a solubility product of 10^{-15}, a pH of 9.5 requires an $h_{Fe^{II}}$ of 10^{-6}. Thus the improved stability and lower solubility of the ferric hydroxide is readily seen. The ferric hydroxide is readily transformed to its oxide counter part (Fe_2O_3) through the removal of water molecules.

The ferrous compounds adjacent to the steel may include $FeOH^+$, $HFeO^-_2$ and FeO^-_2 which are distinguished by their green colouring. These cations and anions are converted to ferrous hydroxide $Fe(OH)_2$, which is a white slightly soluble jelly-like substance (Beeby, 1978), and magnetite (black) for pH above 6 to 7 (Bockris et al., 1981). Ferrous hydroxide is however thermodynamically unstable compared to magnetite and will in time convert to this substance. The ferrous compounds may be further oxidized into various ferric oxides and hydroxides. Cornell and Schwertmann (1996) state that goethite is often the end product of many oxide transformations due its high thermodynamic stability. Other relatively stable and

common ferric corrosion products include: Lepidocrocite, Maghemite and Akaganetite, the latter of which is only formed in a chloride-rich environment.

The various corrosion products may be deposited in layers of varying thickness, with the Fe^{II} generally found closest to the metal and the Fe^{III} further away. Marcotte and Hansson (1998) observed goethite and akaganeite around steel embedded in two types of cracked concrete exposed to simulated sea water. Maghemite however was observed on only one set of bars which suggests an oxygen deficiency at the steel concrete interface in those samples.

Suda et al. (1993) similarly examined the corrosion product of steel embedded in concrete with the samples exposed to sea water over a 5 year period. The corrosion products of magnetite, goethite and lepidocrocite were found to occupy 30% of the total corrosion product with the remainder being composed of amorphous material which was assumed to be similar to δ-FeOOH. The overall volume expansion of corrosion product in concrete was found to be between 3.0 and 3.2.

The variations in volume change associated with individual iron oxides are clearly illustrated in Figure 2.4.

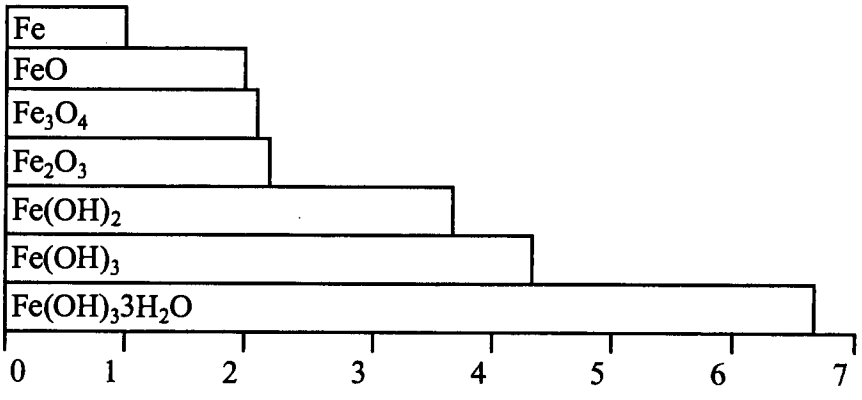

Fig 2.4: Relative volume of iron corrosion products (Liu, 1996)

There is considerable variation in the volume of the corrosion products as illustrated in Figure 2.4. There is however another corrosion situation in which a passive film is formed over the iron which limits further corrosion. Theses films are often very thin, being only a few molecules thick, and firmly adhere to the metal base (Cornell and Schwertmann, 1996). The exact nature of the passive layer is still subject to some debate but is generally characterized by two layers with an inner layer of magnetite and outer of γ-Fe_2O_3 (or γ-FeOOH), (Bockris et al 1981). It has been suggested that only the overlaying film of γ-Fe_2O_3 provides protection and that a previously nonprotective layer of Fe_3O_4 can be made passive by covering it with the γ-Fe_2O_3.

Although the passive film is considered to provide an effective barrier between the metal and the electrolyte, it is sufficiently thin to permit the transfer of electrons and thus sustain a cathodic reaction. West (1980) further states that passive films do not display the same bulk semiconducting properties of the other oxides but rather tend to more closely approximate metallic behaviour. The result is a lower electron concentration in the double layer which may account for lower exchange current densities and secondly an increase in the Tafel slope. The general attributes of a passive layer have been defined by Schreir (1979) to include:

1. very low ion conductivity
2. appreciable electron conductivity
3. very low chemical solubility and dissolution rate
4. a large range of potential thermodynamic stability
5. high compressive strength and good adhesion to the metal

The exchange current density and Tafel slope are issues related to corrosion rates and kinetics and will be discussed in the following section. In short they may account for the much lower rates of corrosion observed in the passive domain for iron.

The particular type of corrosion product and mechanism by which it is formed therefore are critical elements in the overall evaluation of the corrosion of steel in concrete. The formation of passivating films results in such a slow dissolution of the underlying iron that the steel can survive in that environment almost indefinitely. Where active corrosion has begun, variations in the environment around the steel due to differences in mix design including addition of cement extenders will result in the formation of different corrosion products. The various corrosion products will occupy a certain volume thus leading to expansive pressures on the concrete and eventually to cracking and spalling of the concrete cover layer. Thus the rate of deterioration can be related to the type of corrosion product and hence the environment in which it exists. Some specific aspects of how quickly corrosion occurs will now be examined in the following sections.

2.5 Kinetics of Corrosion Reactions

The previous sections on thermodynamics and passivation provided some insight into the various domains of iron in aqueous solution and regions where corrosion is likely to occur. This area of study is very useful for determining if steel in concrete is actively corroding but tells nothing of the rate at which the reaction may be occurring. The study of kinetics therefore provides information as to the speed at which a particular reaction is occurring.

The development of Pourbaix diagrams and thermodynamic considerations is based on conditions of electrochemical equilibrium. Where there is corrosion there can be no equilibrium of the electrochemical cells. Any local region of the metal-solution interface is either consuming electrons (cathodic reaction) or releasing electrons from the metal (anodic reaction). Where the cathodic reaction is greater than the supply of electrons from the anode, electrons may be provided from regions external to the immediate area. The source of current could include nearby or distant half-cell reactions, stray current from power lines or electrical equipment. Deviations in potentials from half-cell equilibrium are a function of the current density regardless of the source of the current flow (Stansbury and Buchanan, 2000).

Any deviation in potential of the electrode from its reversible value is termed overpotential and the electrode is said to be polarized. The overpotential η is given by (Shreir, 1979):

$$\eta = E_p - E_r \qquad \ldots 2.33$$

where E_r is the reversible or equilibrium potential and E_p is the polarized potential, which according to Stansbury and Buchanan (2000), is a function of the current density. The cathodic overpotential η_c, $(\eta_c = E_{pc} - E_{rc} < 0)$ is always negative while the anodic overpotential η_a, $(\eta_a = E_{pa} - E_{ra} > 0)$ is always positive. Figure 2.5 provides an overview of these interactions with anodic and cathodic curves showing the relationship between potential and current. Zn and H were used in this example but the principles are the same regardless of the oxidizing agents and that which is being oxidized (for instance Fe and O_2).

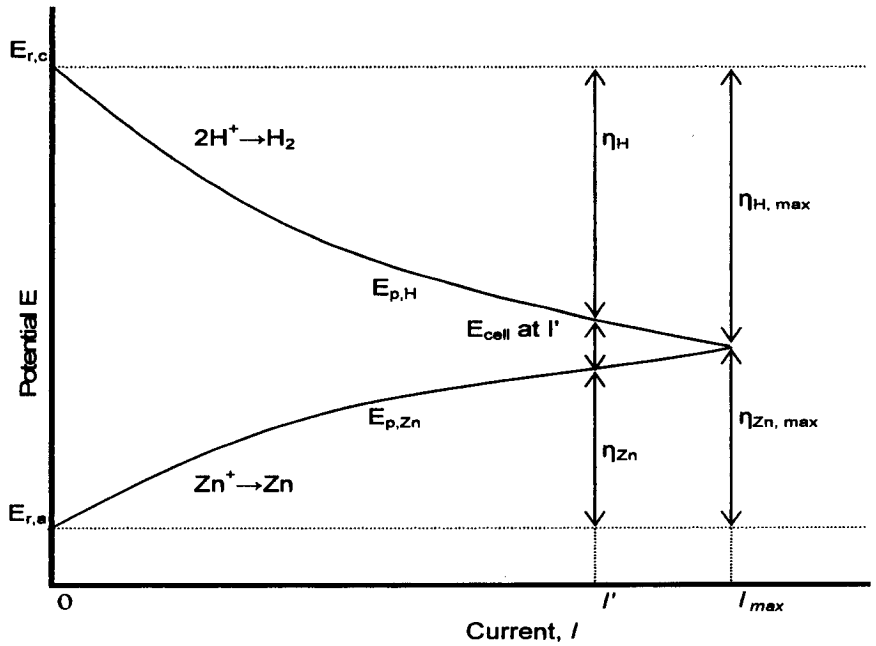

Fig 2.5: Relationship between E and I for half-cell reactions of Zn and H (Shreir, 1979)

There are essentially three types of overpotentials or polarization which will be discussed: activation, concentration and resistance. All three of these contribute to the overall polarization of the cell and are necessary to accurately determine the corrosion rate of a particular material. The total overpotential shown in Figure 2,5, excluding concentration polarization, is a combination of η_H, η_{Zn}, and the differences between Zn and H curves, resistance overpotential. The effects of polarization resistance are evident with the reduction in current from I_{max} to I'.

2.5.1 Activation Polarization

West (1980) states that according to rate process theory there are three components to a chemical process: a) molecular collision, b) formation of intermediate complexes of high energy and short life, and c) immediate decomposition of intermediate complexes to form products. For a reaction to occur only those molecules which have a sufficiently large free energy will be able to react to form the final product. The required energy for the formation of the activated complexes is termed the free energy of activation ΔG^*. As there is a difference in the free energy between the initial and final state, the free energies of activation for the forward and reverse reactions will be quite different.

The rate of a reaction is related to the free energy of activation through the rate constant k_a, where 'a' denotes the anodic reaction and 'f' represents the vibration frequency of the activated complex as seen in equation 2.34 (West, 1980):

$$k_a = f \exp\left(\frac{-\Delta G^*}{RT}\right) \qquad \ldots 2.34$$

Faraday's law can be used to show the relationship between corrosion current I and general rate of charge transfer K according to (Shreir, 1979):

$$K = \frac{I}{zF} \text{ (mol s}^{-1}\text{)} \qquad \ldots 2.35$$

where the current I is measured in amperes, and 1 ampere = 1 coulomb of charge (6.2×10^{18} electrons) per second. Faradays constant F ≈ 96,500 coulombs, z is the number of electrons required to complete one electron transfer process (for $Fe \rightarrow Fe^{2+} + 2e^-$, Z = 2). The corrosion current can be rewritten in the form of a current density i such that $i = I/A$ where A is the area of the corroding metal. For a current density of i (A/m^2) the anodic rate of charge transfer would be given in mol/m^{2}s.

West (1980) states that at the equilibrium single potential the charge flux across the double layer is the same in both directions which gives rise to the exchange current density i_o.

The double layer refers to the electric field around the negatively charged electrode surface and Helmholtz plane which represents the closest approach of postively charged cations (Jones, 1996). Furthermore the species taking part in the formation of the activated complexes are the 'kink site' metal atoms on the surface and hydroxyl ions of the double layer. The rate therefore in mol/m^2 for the anodic reaction is given as (West, 1980):

$$k_a a_{kink} h^n{}_{OH^-} = \frac{i_o}{zF} \qquad \ldots 2.36$$

where a_{kink} is the activity of the kink site metal atoms.

Substituting the rate constant from equation 2.34 into 2.36 the exchange current density becomes:

$$i_o = zFfa_{kink} h^n{}_{OH^-} \exp\left(\frac{-\Delta G^*}{RT}\right) \qquad \ldots 2.37$$

The activation complex is assumed to exist at fraction α of the double layer thickness from the metal surface. If the free energy of a metal ion on the surface is raised by a given amount ($zF\eta$) then the energy of activation must also be raised by an amount $(1-\alpha)zF\eta$ such that the new energy of activation becomes $\Delta G^* - \alpha zF\eta$ as illustrated in figure 2.6. Note that the symbol $\Delta\tilde{G}^{\pm}$ in Figure 2.6 is written as ΔG^* in this text.

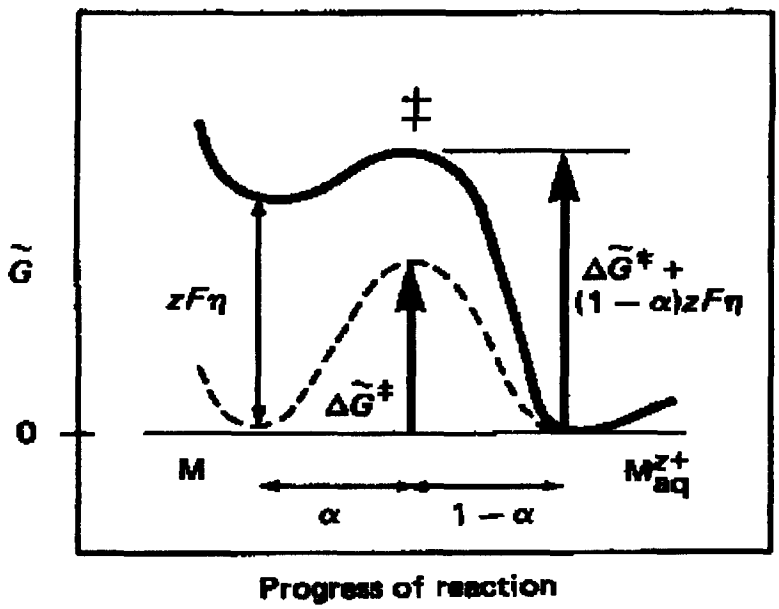

Fig 2.6: Polarization of activation energy (West, 1980)

The rate of charge transfer for the anodic current density is therefore (West, 1980):

$$i_a = zFfa_{kink}h^n{}_{OH^-}\exp\left(\frac{-(\Delta G^* - \alpha zFn)}{RT}\right)$$

$$= i_o \exp\left(\frac{\alpha zFn}{RT}\right) \quad \ldots 2.38$$

By rearranging equation 2.38 the activation overpotential becomes:

$$n_{act,a} = \frac{2.303RT}{\alpha zF}\log\left(\frac{i_a}{i_o}\right) \quad \ldots 2.39$$

for the anodic activation overpotential and by similar argument

$$n_{act,c} = -\frac{2.303RT}{(1-\alpha)zF}\log\left(\frac{i_c}{i_o}\right) \quad \ldots 2.40$$

for the cathodic activation overpotential. Equations 2.39 and 2.40 are known as the Tafel equations where $\frac{2.303RT}{\alpha zF}$ and $-\frac{2.303RT}{(1-\alpha)zF}$ can be replaced by the Tafel constants b_a and b_c respectively. Note the Tafel constants represent the slope of the line for the anodic and cathodic polarization curves. The Tafel region for which b_a and b_c are valid is the linear portion of the polarization curve as shown in Figure 2.7.

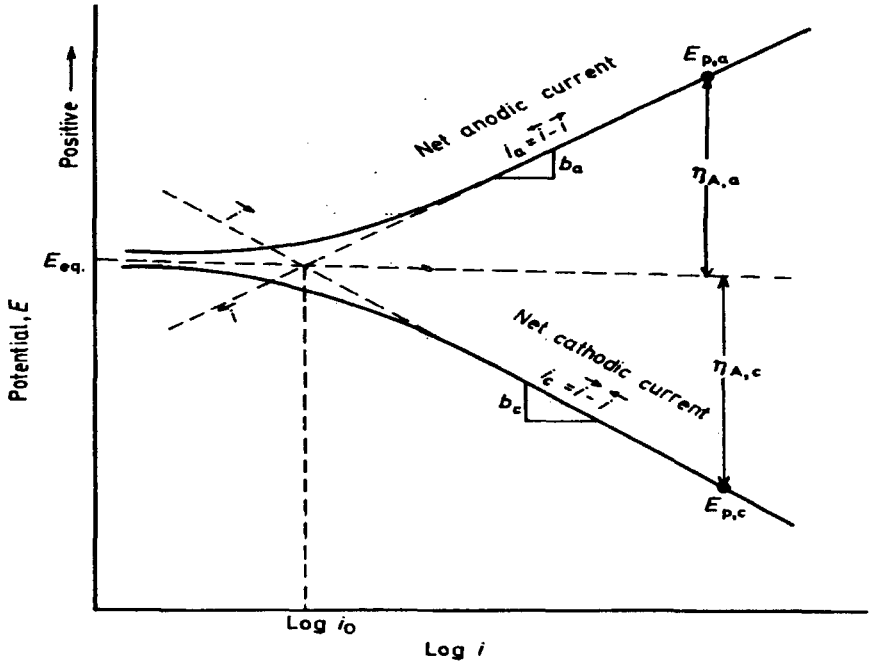

Fig 2.7: Tafel slopes and exchange current density (Shreir, 1979)

The equilibrium exchange current density i_o is shown graphically as the intersection of the anodic and cathodic polarization curves and represents the most significant parameter in

controlling the corrosion process (Shreir, 1979). A single half cell exchange current density essentially sets a minimum rate at which the process can occur. Consider two metals with otherwise identical characteristics, such as Tafel slopes, the one with the highest exchange corrosion current density must be corroding at a faster rate.

While the exchange current densities and Tafel slopes are the primary determinants of corrosion rates both concentration polarization and solution resistance polarization can affect the observed corrosion current.

2.5.2 Concentration polarization

When the rates of a reaction are sufficiently large, the availability of reactants at the cathode will be limited by the transport of ions to that site. The overall rate of the reaction therefore will be controlled by this transport of ions to the cathode. While concentration and ionic transport limitations are possible at anodic sites at very high corrosion rates, they can generally be ignored as there is almost an unlimited supply of metal atoms at the interface (Jones, 1996). Where the transport of ions to the cathode is based on diffusion, a Fick's Law model assuming a linear activity gradient across the diffusion layer of defined thickness (δ)

will yield (West, 1980):

$$\frac{i_c}{zF} = \frac{-D(a_{Mz+}^{\ surface} - a_{Mz+}^{\ bulk})}{\delta} \qquad \ldots 2.41$$

where D is the diffusivity of the metal ions, and i_c is the cathodic current density, and a_{Mz+} is the activity of the metal ions. If the surface concentration of ions tends to zero the chemical potential difference $RT\ln\left(\frac{a_{Mz+}^{\ bulk}}{a_{Mz+}^{\ surface}}\right)$ will approach infinity yielding a limiting diffusion flux of (West, 1980):

$$i_L = \frac{zFDa_{Mz+}}{\delta} \qquad \ldots 2.42$$

Due to the limiting diffusion flux and hence activity of the surface ions the Nernst equation for the equilibrium single potential becomes:

$$E = E^{\circ} + \frac{RT}{zF}\ln\left[1 - \left(\frac{i_c}{i_L}\right)\right]a_{Mz+}^{\ bulk} \qquad \ldots 2.43$$

and the concentration overpotential is given as:

$$n_{conc} = \frac{RT}{zF}\ln\left[1-\left(\frac{i_c}{i_L}\right)\right] = \frac{2.303RT}{zF}\log\left[1-\left(\frac{i_c}{i_L}\right)\right] \quad \ldots 2.44$$

The limiting current density and hence concentration overpotential is affected by a number of factors including temperature which impacts the diffusion coefficient, ion concentration, and solution agitation which decreases δ. The effects of increasing solution velocity, temperature and concentration on the limiting current density are shown in Figure 2.8 where the dark curve represents the cathodic current.

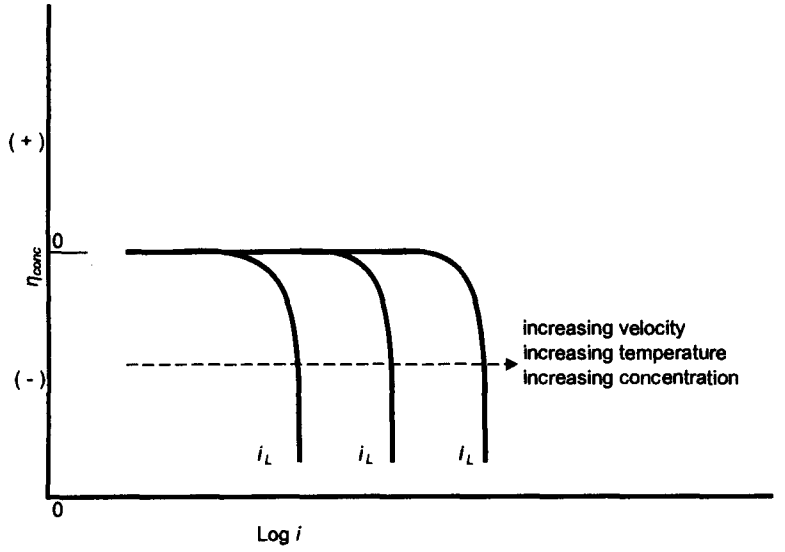

Fig 2.8: Cathodic concentration polarization (Jones, 1996)

As the temperature, mixing of the solution as a given by solution velocity, or concentration of oxidant increases the curves moves to the right resulting in a higher limiting current density. The current exchange density i_o defined the relationship between current and potential and provided a minimum corrosion rate. Limiting current density thus sets a maximum corrosion rate under a given set of environmental conditions through cathodic control of the reaction.

2.5.3 Resistance polarization

There is a third form of polarization which can affect the kinetics of a reaction, particularly where there is a considerable distance between the anode and cathode. For coupled half-cell reactions there must be both a flow of electrons through the metal and a movement of ions through the solution to complete the circuit. The resistance along a metallic pathway is negligible, thus the resistance overpotential is a function of the solution or the metal solution interface and is defined as (Shreir, 1979):

$$n_R = I(R_{Soln} + R_f) \quad \ldots 2.45$$

where R_{soln} is the electrical resistance of the solution and R_f is the resistance due to films or coatings on the metal surface. The effects of solution resistivity on overpotential will be discussed in greater detail in the following section.

The total polarization effects (excluding resistivity) can therefore be seen as simply the addition of the individual polarization effects. The total cathodic overpotential therefore will be:

$$n_{T,c} = -\frac{2.303RT}{(1-\alpha)zF}\log\left(\frac{i_c}{i_o}\right) + \frac{2.303RT}{zF}\log\left[1-\left(\frac{i_c}{i_o}\right)\right] \quad \ldots 2.46$$

while the total anodic overpotential remains:

$$n_{T,a} = \frac{2.303RT}{\alpha zF}\log\left(\frac{i_a}{i_o}\right) \quad \ldots 2.47$$

The combination of the total anodic and cathodic overpotentials can therefore be used to determine the corrosion rates of a particular metal in a certain environment, thus the relevance to the corrosion of steel in concrete.

2.6 Combined kinetic half-cell reactions and the Evans diagram

The corrosion of steel in concrete is generally a situation in which both anodic dissolution of the metal and cathodic reduction occur on the same surface. The previous discussion generally focused on the individual half-cell reactios of oxidation and reduction. These individual reactions may now be combined to show the interaction between these mechanisms. Where there is a separation between the anode and cathode, there will be a marked change in potential along various points of the bar dependant on solution, or in the case of concrete, matrix resistivity.

Consider an example by Stansbury and Buchanan (2000) with two uncoupled equilibrium half-cell reactions with E_M=-1000 mV and E_X=0 mV, the cell driving force $E_{cell}=E_x-E_m$= +1000 mV, where E_M represents the metal half cell potential and E_x the oxidant half cell potential. Where the solution resistivity is sufficiently high, the solution potential of the anode would approach + 1000 mV while that of the cathode would approach 0 mV. In Figure 2.9 current paths or channels linking the anode and cathode are shown to perpendicularly intersect iso-potential lines since the current flux travels in approximately semi-circular channels. The mean current flowing through each channel is given as $I_n=\Delta\psi_s/R$, where $\Delta\psi_s$ is the potential difference of the solution between the anode and cathode.

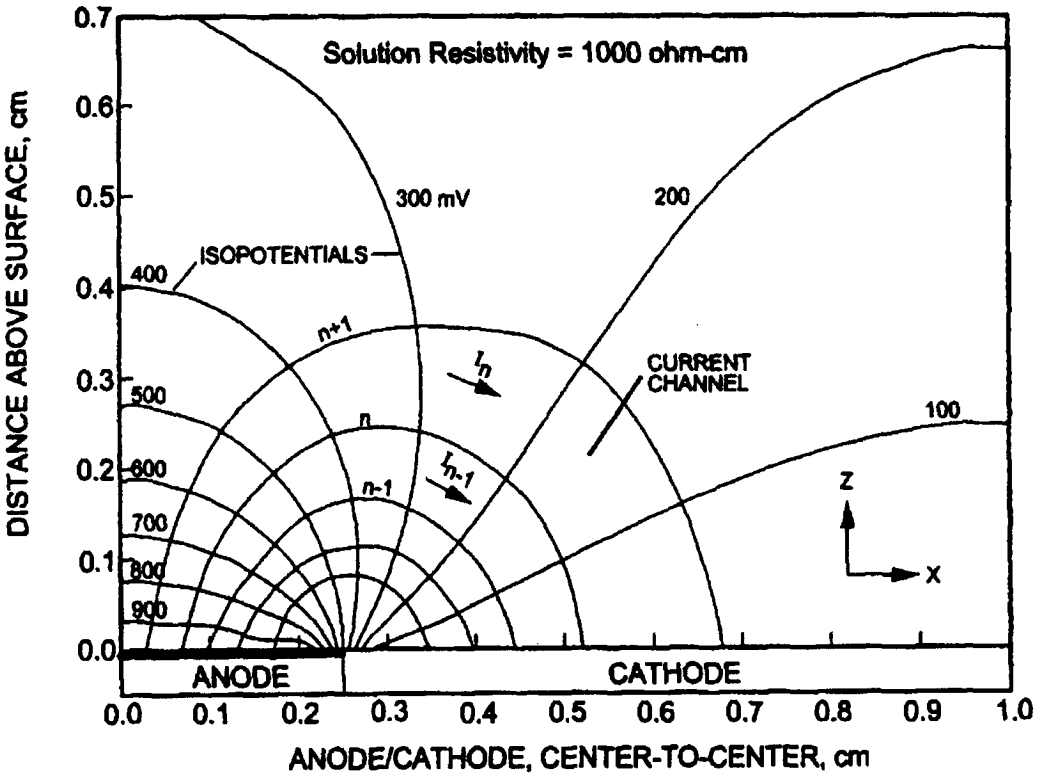

Fig 2.9: Anodic, cathodic potential and current flux (Stansbury and Buchanan, 2000)

Where the solution resistivity is reduced, the magnitude and gradient of the potential difference across the anode and cathode is diminished and the size of a channel for a given current I_n is also reduced. In the extreme case for a very low resistivity the potential gradient is almost flat and approaches the equilibrium corrosion potential for coupled half-cells (250 mV in this example). The effects of resistivity on the potential gradient are clearly illustrated in Figure 2.10.

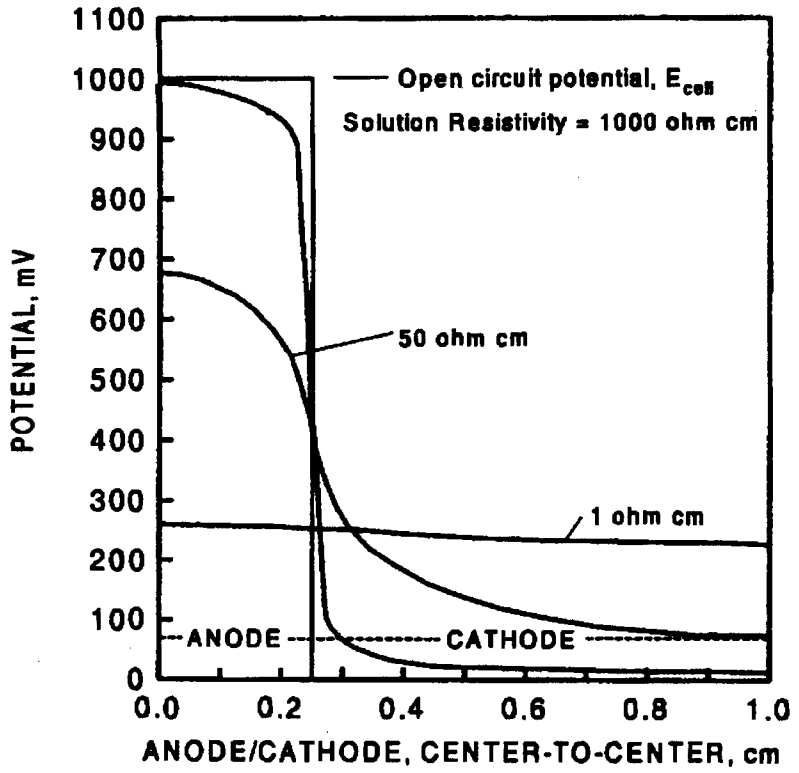

Fig 2.10: Effect of resistivity on potential gradient (Stansbury and Buchanan, 2000)

For the case of a freely corroding system the overall corrosion current I_{corr} must be equal to both the anodic current I_a and the cathodic current I_c. Since Ohm's law must be satisfied for each channel (Stansbury and Buchanan, 2000),

$$(I_{corr})_n = \frac{(E_X - E_M)_n}{(R_s)_n} \quad \ldots 2.48$$

From the Tafel equations 2.39 and 2.40 for activation polarization where A_c and A_a are the surface areas for the anode and cathode respectively the corrosion current for a given channel n (Stansbury and Buchanan 2000):

$$(I_{corr})_n = \frac{\left[E_x - b_c \log \frac{I_{corr}/A_c}{i_o}\right] - \left[E_M + b_a \log \frac{I_{corr}/A_a}{i_o}\right]}{(R_s)_n} \quad \ldots 2.49$$

the overall reaction can therefore be written as:

$$E_{cell} = E_x - E_m = \eta_a + \eta_c + IR_s \quad \ldots 2.50$$

Where the resistivity of the solution or the distance between the anode and cathode is sufficiently small equation 2.50 becomes:

$$E_{cell} = \eta_a + \eta_c \quad \ldots 2.51$$

It is evident therefore that the total electromotive force (emf) E_{cell}, driving the reaction is the sum of the magnitudes of η_a, η_c and IR. As the IR increases so does its contribution to the total emf thus reducing the effective driving force and lowering the overall corrosion rate (West 1980). Where the resistance is negligible as given in equation 2.51 the intersection of the cathodic and anodic coupled half-cell polarization curves results in a potential of E_{corr} at a maximum corrosion current of I_{corr}. Equation 2.51 is of fundamental importance in that it shows the corrosion rate is dependant upon both the thermodynamic parameter E_{cell} and kinetic parameters of η_a, η_c.

The relationship between two coupled half-cell reactions is best shown graphically by means of an Evans diagram where the individual half-cell reactions have their origins at the exchange current densities and equilibrium potentials. The resultant slope of the lines for the oxidation and reduction of each half-cell is therefore the respective Tafel constants b_a and b_c. Figure 2.11 shows the Evans diagram for the dissolution of an assumed metal with hydrogen reduction.

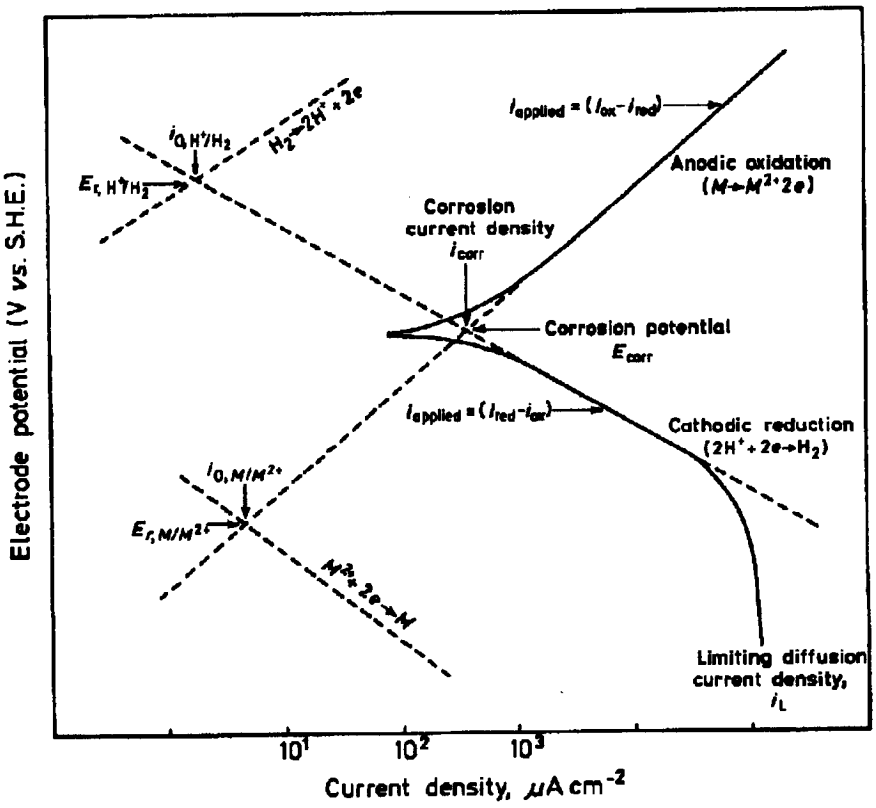

Fig 2.11: Evans diagram for couple half-cell reactions (Shreir, 1979)

The intersection of the anodic and cathodic polarization curves is thus E_{corr} and corrosion current density i_{corr} for the couple half-cell reactions.

The intersection of the linear portion of the Tafel lines for the anodic and cathodic provides a unique value for the corrosion rate and potential of the system. The polarization of the system through application of an external current thus allows for the study of the system and determination of the corrosion rate of a material in its environment. The change in potential associated with the application of a current is termed polarization resistance R_p and the relationship between the corrosion current and R_p is presented in the work of Stern and Geary (1957). It is not necessary to fully derive this relationship as it has been effectively presented in numerous sources including Mansfeld (1970) and the basic electrochemical principles already addressed in the current work. The equation is therefore given as (Mansfeld, 1970):

$$I_{corr} = \frac{b_a b_c}{2.303(b_a + b_c)}\left(\frac{\partial I}{\partial E}\right)_{E_{corr}} = \frac{B}{R_p} \qquad \ldots 2.52$$

where:

$$R_p = \left(\frac{\partial E}{\partial I}\right)_{E_{corr}} \qquad \ldots 2.53$$

and

$$B = \frac{b_a b_c}{2.303(b_a + b_c)} \qquad \ldots 2.54$$

The study of corrosion rates of materials, regardless of the specific system employed, are often based on the principle of polarization resistance and hence equation 2.52. It should be noted that this relationship applies for values sufficiently close to E_{corr}, generally less than +/- 10mV (Stansbury and Buchanan, 2000). The constants used in the Stern-Geary equation (2.52) are clearly derived from the Tafel slopes b_a and b_c. The range of possible B values, for any system, varies by a factor of 8 from 6.5 to 52.1 mV as shown in Table 2.2.

Table 2.2: Theoretical values for B (Mansfeld, 1970)

	b_c			
b_a	*30 mV*	*40 mV*	*120 mV*	∞
30 mV	6.51	7.44	10.42	13.03
40 mV	7.44	8.68	13.03	17.37
120 mV	10.42	13.03	26.05	52.11
∞	13.03	17.37	52.11	-

According to Stansbury and Buchanan (2000) the 'normal' range of extreme values for B range between 13 and 52 thus an assumed value of 26 would provide for a maximum possible error of 2. Given the nature of corrosion rate measurements and other uncertainties this error

is normally considered quite acceptable. An explanation of the chosen method for corrosion rate determination in the current work will be provided chapter 4.

2.7 Passivity and kinetic considerations

The entire anodic polarization curve for a metal however is not linear and the thermodynamic effects of stability of various oxide formation become evident in the relationship between potential and corrosion current. In the passive state most pure metals exhibit an anodic current independent of potential under steady state conditions, though some metals such as nickel show an anodic dissolution current which increases with potential (Sato, 1978). As previously discussed in sections 2.3 and 2.4 iron in an aqueous solution forms passive oxides generally attributed to a dense thin layer of γ-Fe_2O_3 or γ-FeOOH. The effects of the passive film result in a substantial deviation of the anodic current from the linear Tafel slope. West (1980) states that the limited vacancy activity results in a diffusion control of the anodic current which is similar to equation 2.42 for cathodic concentration control. Stansbury and Buchanan (2000) however state that it has not been clearly established whether the low passive current density is due to low conductivity of migrating cations and anions through the film, slow transfer of ions across the interface, or low conduction of electrons. Regardless of the exact cause of the reduced current density, the general shape of the anodic polarization curve including passive conditions has been reasonably well defined for various metals and alloys in numerous environments.

The shape of the anodic polarization curve with respect to passivation can be characterized by three quantities: i_p anodic passive current density, i_{crit} and E_{pp} the current density and potential at which the transition from active to passive corrosion occurs. The influence of passivity on the anodic current density is shown in Figure 2.12.

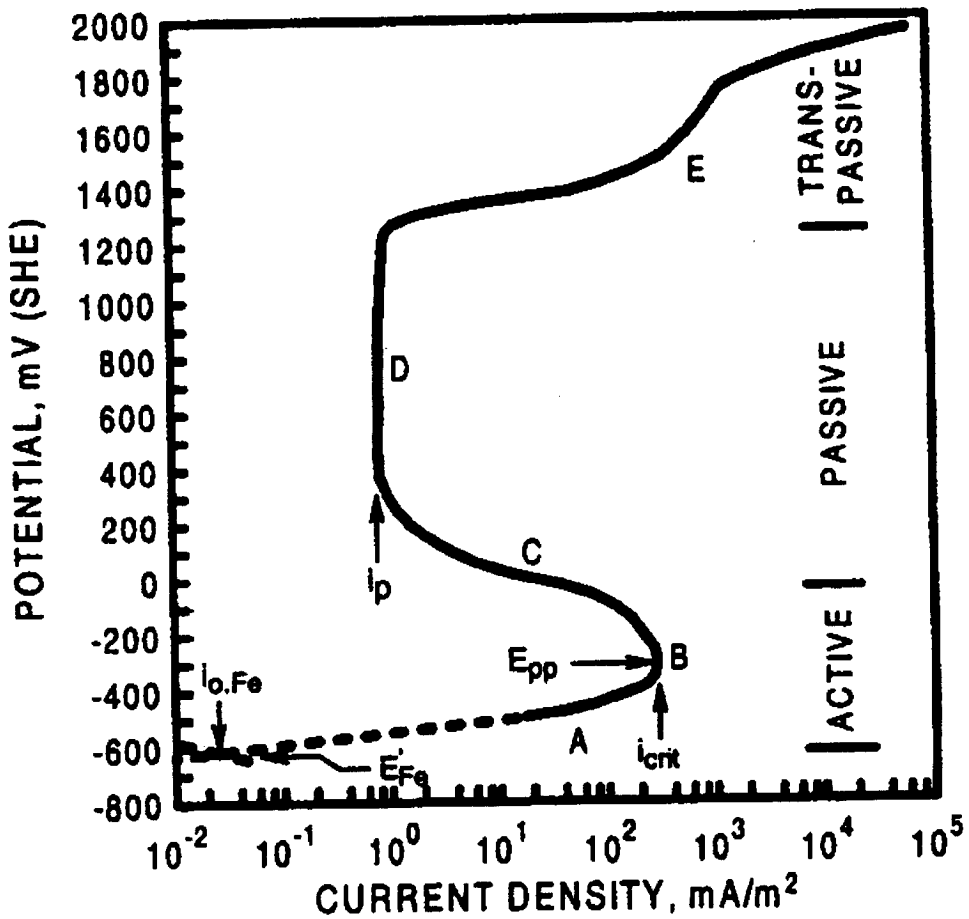

Fig 2.12: Typical anodic polarization curve for iron (Stansbury and Buchanan, 2000)

As the potential continues to increase above E_{pp} two further reactions involving the ferric oxide may occur (Stansbury and Buchanan, 2000):

$$(2-x)Fe_2O_3 + 3xH_2O \rightarrow 2Fe_x^{VI}Fe^{III}_{(2-2x)}\Diamond_x O_3 + 6xH + +6xe \quad \ldots 2.55$$

and

$$Fe_2O_3 + 5H_2O \rightarrow 2FeO_4^{2-} + 10H^+ + 6e \quad \ldots 2.56$$

where $\Diamond$ represents a vacant iron lattice site and x the fraction of iron lattice occupied by Fe^{VI}. The region of passivity is still maintained for a considerable range in potential above E_{pp} despite the presence of the defective iron oxides. Eventually however in the trans-passive region iron is converted to Fe^{III} or FeO_4^{2-} and current increases substantially. At these high potentials water will also decompose to oxygen thus reducing the potential at which trans-passive corrosion may begin. Transpassivity is characterized by a sudden increase in the

dissolution current and uniform corrosion on the metal surface. As the potential continues to rise the anodic current generally approaches a limiting value (Sato 1978).

The passive current i_p will depend upon the material in its specific environment. The influence of pH, for instance, on the passivation of iron in 0.15M Na_3PO_4 solution is clearly shown in Figure 2.13. It is interesting to note that at a pH of 11.50 there is no active corrosion peak in the anodic polarization curve.

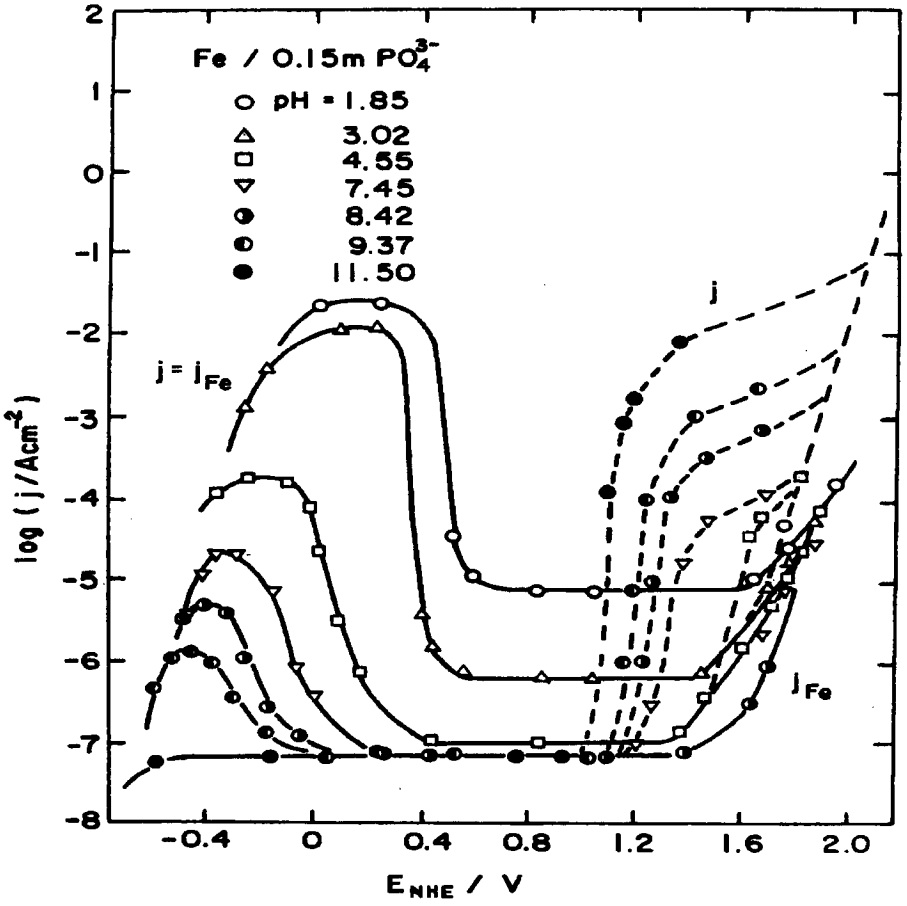

Fig 2.13: Anodic polarization curve for iron in 0.15M Na_3PO_4 (Sato, 1978)
(Note that the corrosion current density in this example is given as *j*)

The dashed section of the curve show the combined current density associated with both iron dissolution and oxygen evolution.

As previously stated E_{corr} and I_{corr} are determined by the intersection of the anodic and cathodic polarization curves. Due to the passive nature of many materials the cathodic polarization curve may intersect the anodic curve at more than one location, particularly where there is a weak oxidizer or concentration polarization is significant. Figure 2.14 clearly

shows the possible corrosion values for two cathodic conditions. Curve A indicates that both active and passive corrosion are possible. The oxidizer is not sufficiently strong to passivate a non-passive metal thus point 1 will yield the most likely E_{corr} and I_{corr}. If however the material is already passive, the cathodic reaction is sufficient to maintain passivity at point 2, under these conditions. Jones (1996) states that any surface damage will destroy the passive film resulting in active corrosion, thus point 1 should be conservatively considered as the representative E_{corr} and I_{corr} given cathodic curve A. An increase in concentration of oxidizing species will result in curve B which is sufficiently strong to both maintain and initiate passivity on the metals surface. Under such cathodic polarization passivity would be obtained corresponding to point 3.

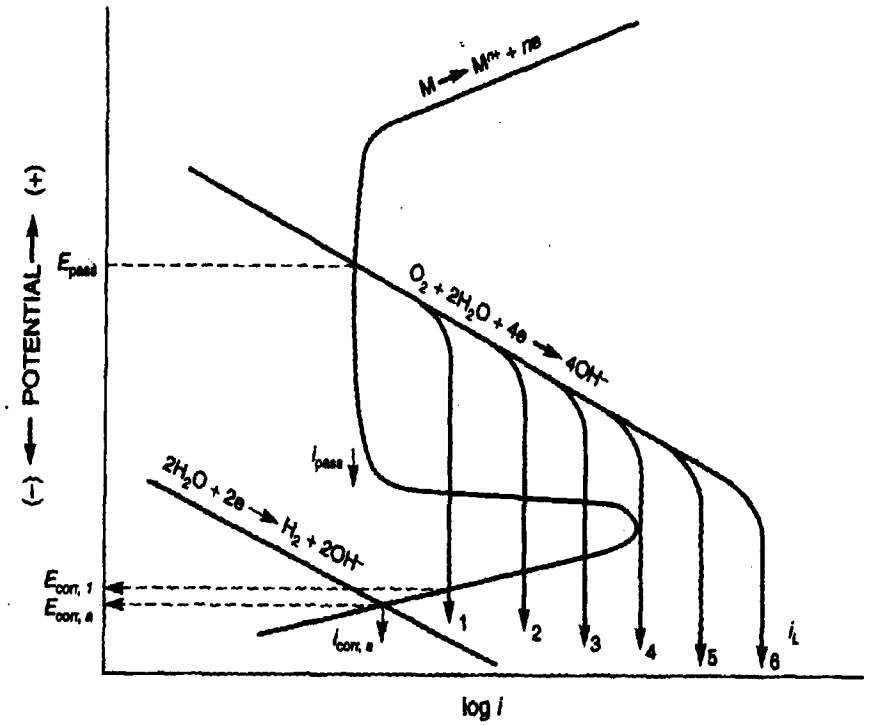

Fig 2.14: Impact of cathodic reaction on E_{corr} and I_{corr} (Jones, 1996)

A fairly simple model for passivation kinetics is provided by Sato (1978) in which there is a competition between active dissolution of the metal and passive film formation. The total anodic current therefore is a function of the rate of anodic dissolution, film formation and amount of the surface covered by the passivating film. The idea of competition between anodic dissolution and film formation is of significance when studying the breakdown of passivity and effect of various anions such as chlorides and sulphides on the passive film. These anions may enhance either the anodic dissolution or film formation thus affecting the

corrosion rate of the material. The primary ions, which are observed in practice and may influence the corrosion of steel in concrete, are either chlorides or various sulphur species anions which will be discussed in the following sections.

2.8 Effect of chlorides

The exact role which chlorides play in the breakdown of the passive layer has been the subject of much debate and uncertainty. There are a number of views as to how the chloride ions actually depassivate iron under otherwise stable conditions, including:

1) The traditional view on the role of chloride ions states that the small size of the chloride ion gives it high penetrating power through the oxide layer (Shreir, 1979).
2) Chloride ions result in local acidification thus destabilizing the anodic film at low pitting potentials. At higher pitting potentials local acidification is a necessity but not sufficient to induce pitting. Further anion adsorption is also required (Alvarez and Galvele, 1984).
3) Breakdown in film passivity is a result of the destabilization of the film substrate bond with little or no chemical dissolution of the film (Leek and Poole, 1990).
4) Chloride ions are preferentially adsorbed in competition with oxygen and may displace passivating species, thus allowing for increased corrosion of the metal (Foley, 1970).
5) Complex formation of iron halides (Cl^-) on the surface. The overall process occurs with a chemico-adsorption reaction between a surface atom of the metal and the chloride. The complex can then pass into solution once a certain potential is reached. Once in solution the halide complex will dissociate and other more stable complexes (hydroxides) will be formed (Foley, 1970).

The exact mechanism of chloride-induced corrosion, while theoretically and scientifically interesting, is not essential for the general understanding of the influence of chlorides on corrosion of steel in concrete.

Passivity should not be viewed as a complete protection of the underlying metal but rather an extreme or limiting value of corrosion. The passive layer is in a continual state of breakdown and repair under normal conditions. The presence of chloride ions will contribute towards the breakdown of the passive layer while other anions such as OH^- are responsible for its stability and have inhibiting properties. There is a point therefore at which the concentration of aggressive ions overcomes the inhibiting ions and 'corrosion' can initiate. This point is known as the pitting potential, below which passivity is maintained (Bockris et

al., 1981). The struggle to maintain passivity in the presence of aggressive ions is shown in Figure 2.15 where chlorides are added to passive steel in a borate solution. The current densities for Fe^{III} and Fe^{II} are initially flat. Once chloride ions are added the fluctuations in the Fe^{III} passive film dissolution current can be seen almost immediately where there is an initial competition between passivating and activating species. After a short period the passivity is overcome and the Fe^{II} pitting current increases substantially.

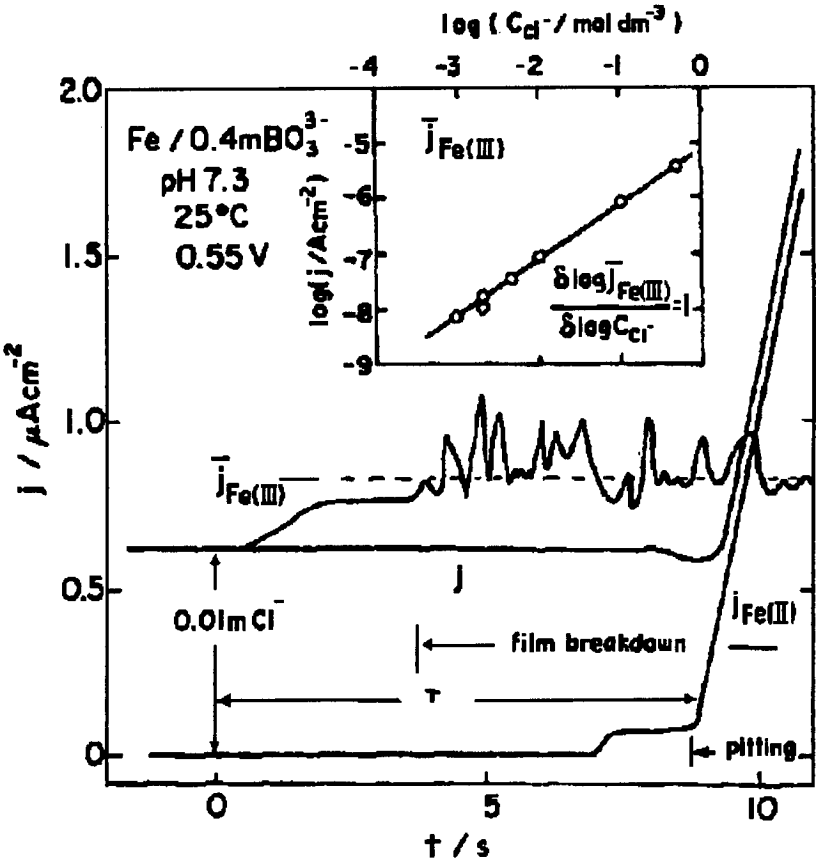

Fig 2.15: Change in anodic current with addition of chlorides (Bockris et al., 1981)

Regardless of the mechanism by which chloride ions attack the passive layer, the corrosion is characterized by the formation of pits at the point where there is a breakdown in the passive layer. The intiation of pitting on steel generally occurs at weak points in the film which according to Shreir (1979) and Jones (1996) have been associated with the inclusion of sulphides (MnS) present in the steel. A pit generally consists of three regions of interest: a pit interior where the metal enters solution; pit mouth of iron oxide which acts to isolate the interior from the external environment and controls the ingress and egress of Fe^{II}, chlorides

and oxygen; and external environment where oxygen reduction occurs. The general characteristics and development of a pit can be seen in Figure 2.16.

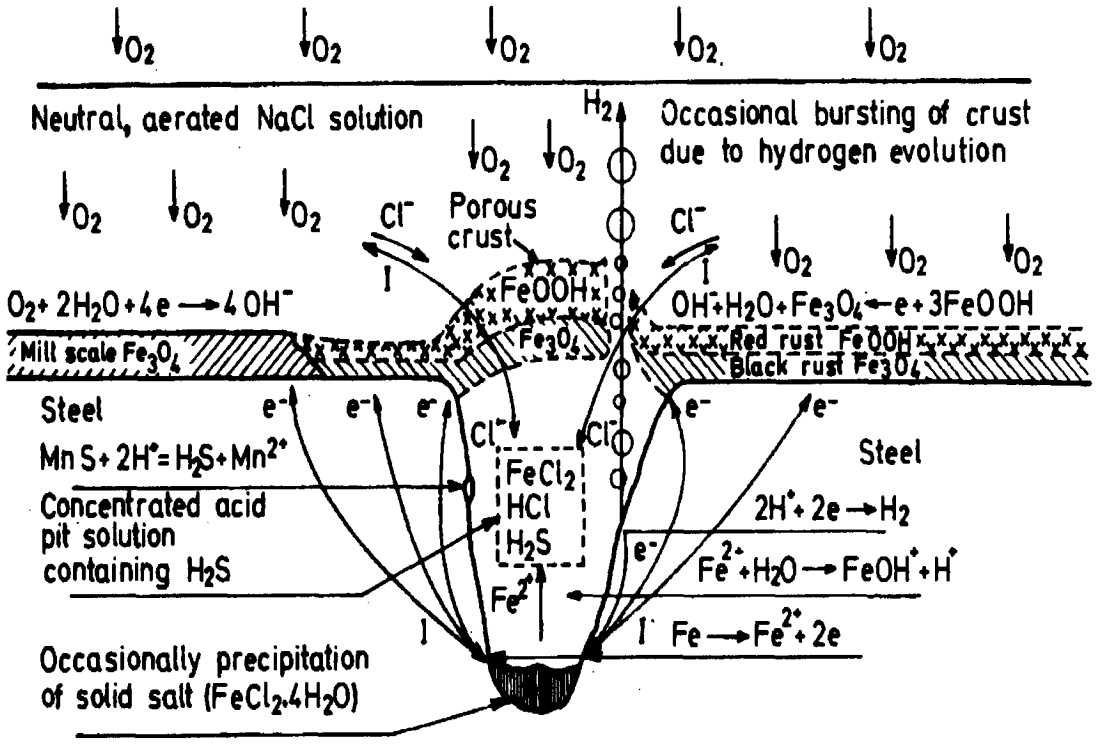

Fig 2.16: Pitting of carbon steel at MnS inclusion site (Shreir, 1979)

The pit interior is the site of active dissolution of iron. Due to the generation of H^+ the pH in a pit can be substantially lower than the bulk solution. The interior of the pit essentially contains an acid chloride solution and possibly S^{2-} and HS^-. The sulphides are associated with the dissolution of MnS contained in the steel. Shreir (1979) states, that sulphides stimulate the attack by decreasing the activation potential for the dissolution of iron. The continued migration of chlorides into the pit will also enhance the dissolution of the iron.

The pit interior is separated from the bulk solution by the pit mount which is typically a membrane of magnetite Fe_3O_4 and lepidocrocite or akaganeite (FeOOH), rust. The membrane is formed as the Fe^{II} and $FeOH^+$ migrates away from the pit interior and are oxidized to magnetite and rust thus quasi-sealing the interior of the pit.

The area outside the pit is substantially different and the passivity of the surrounding steel is somewhat enhanced by the production of hydroxide due to the reduction of oxygen. The exterior of the pit provides the cathodic process thus driving the reaction. The rust which was previously formed is subsequently converted to magnetite or other iron oxide as discussed in section 2.4.

2.8.1 Influence of chloride concentration on corrosion process

It has already been noted that increased chlorides levels will stimulate the dissolution of iron. The possible effects of chloride ions on the corrosion rates of steel are evident from anodic polarization curves which show progressive lowering of the transpassive portion of the curve with increasing chloride content as seen in Figure 2.17. Figure 2.17 shows the anodic curve for stainless steel in neutral solution but the same principle would apply for carbon steel in a variety of solutions with different chloride concentrations.

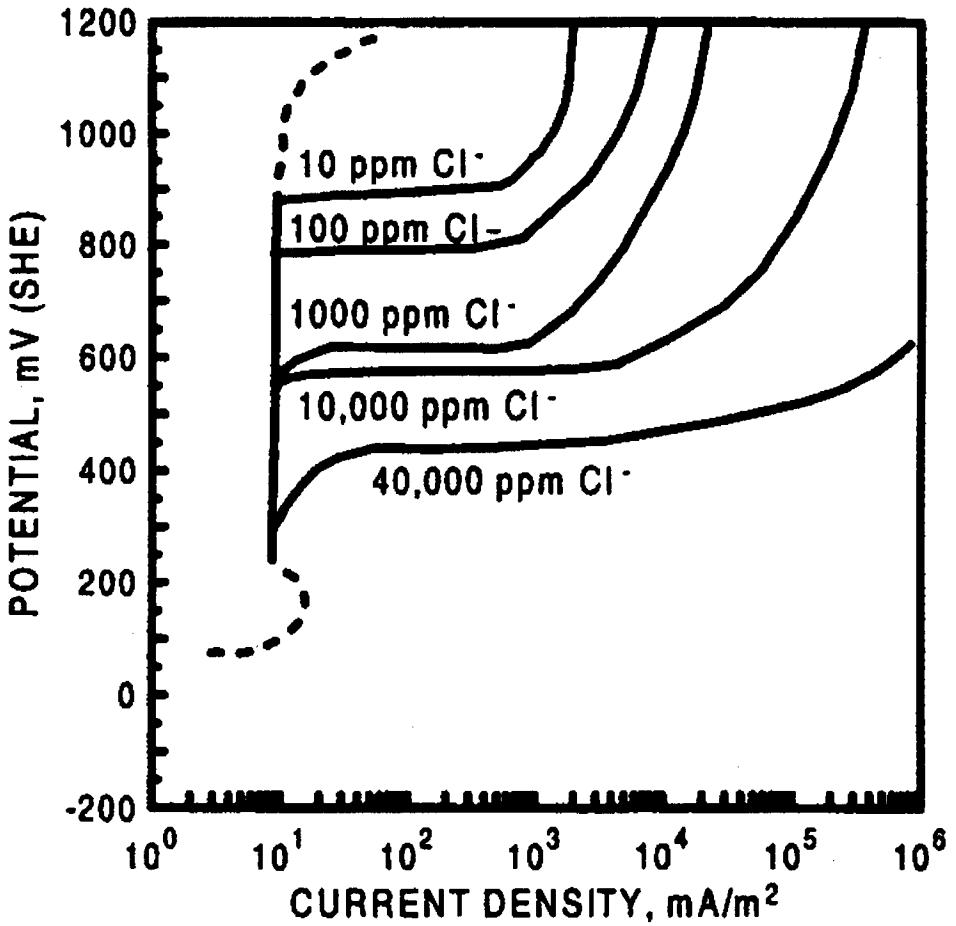

Fig 2.17: Effects of chloride ion concentration on the anodic polarization curve of stainless steel in a neutral solution (Stansbury and Buchanan, 2000)

The effects of chloride ions on the pitting potential of pure iron-alkali solutions has been studied by Alvarez and Galvele (1984) and shown to follow the relationship:

$$E_p = -0.364 - 0.064 \log C_{Cl^-} \qquad \ldots 2.57$$

for NaCl concentrations between 0.01 and 1.0 M for a pH of 10 and potential measured against normal hydrogen electrode (NHE). The influence of pH at a constant chloride concentration was also measured and the pitting potential found to increase with pH according to:

$$E_p = -0.560 + 0.020 pH \qquad \ldots 2.58$$

for 1.0M NaCl and pH $\geq$ 10. Thus the effect of chloride ions is to successively lower the pitting potential, and thus transpassive portion of the anodic polarization curve, while increasing pH results in raising of the pitting potential. This competitive process between chloride ions and hydroxyl ions (increasing pH) is already evident and will be shown to be one of the central ideas in determining the influence of various cement extenders on the corrosion of steel in concrete. The chloride to hydroxide (Cl/OH) ratio is widely attributed as being the main parameter in controlling the onset of corrosion and hence chloride threshold values.

For a given cathodic polarization curve the progressive lowering of the transpassive portion of the curve would result in an increasing corrosion current density with chloride concentration. While this is true to some extent the effects of chloride concentration on the solubility of oxygen and thus cathodic processes must also be considered. Figure 2.18 shows the weight loss versus solution normality for various chlorides. According to Foley (1970) there is an optimal chloride concentration where the decrease in the cathodic reaction due to oxygen depletion is countered by the increase in anodic dissolution. The solubility of oxygen in various concentrations of salts is shown in Table 2.3. It is evident that the greatest corrosion rate from Figure 2.18 occurs at a sodium chloride content of approximately 0.5N.

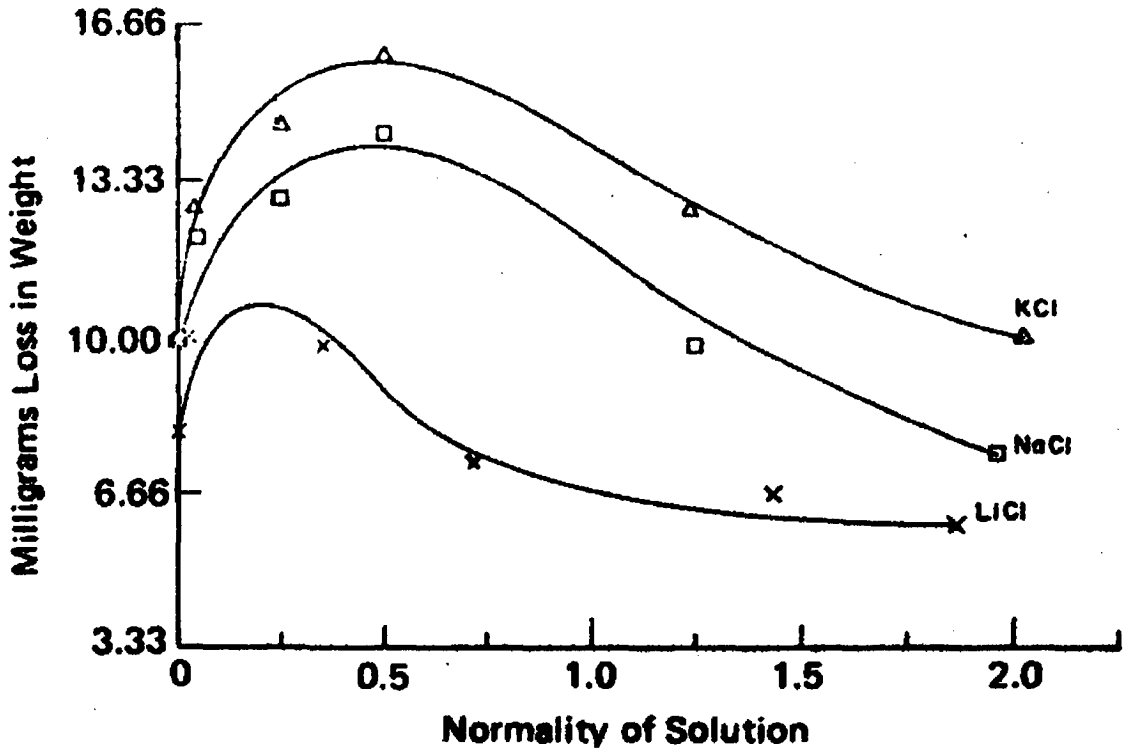

Fig 2.18: Corrosion rate versus chloride content (Foley, 1970)

Table 2.3: Oxygen solubility with respect to salt concentration (Foley, 1970)

Salt Concentration (N)	*Solubility of O_2 in cc/litre*		
	KCl	*NaCl*	*Na_2SO_4*
0.0	6.13	6.13	6.13
0.5	5.23	5.20	4.87
1.0	4.51	4.46	3.98
2.0	3.41	3.19	2.67
3.0	2.55	2.31	

Considerable work has been done to determine the critical level of chlorides necessary to initiate corrosion of steel in concrete, with most of the early work focusing on aqueous phase testing of steel in simulated pore solutions. The composition of these solutions and implications for chloride threshold levels and corrosion rates will be discussed in a subsequent chapter.

2.9 Effect of sulphides

The impact of sulphide ions is of particular concern as they may be present in significant concentration in ground granulated blastfurnace slag and hence slag-bearing concretes. As

with chlorides, sulphide ions have also been shown to contribute to the depassivation and corrosion of iron and steel in solution. West (1980) states that S^{2-} and HS^- considerably accelerate corrosion through two processes: enhancement of the cathodic reaction, and reduction in the anodic Tafel slope. As previously noted by Shreir (1979) sulphides can decrease the activation potential for the dissolution of iron.

Where sulphides are initially present in a solution, they will affect the steel in two ways: firstly the sulphides will be oxidized to sulphate by the available oxygen thus depleting the oxygen concentration at the steel and creating a potentially reducing environment; secondly the sulphides will form a precipitate of FeS on the steel surface thus affecting the formation of the passive layer. The depletion of oxygen is of particular concern where there may be limitations on the initial total quantity of oxygen available and subsequent diffusion processes. As previously shown the development of the passive layer is reliant upon sufficient oxygen to supply the cathodic reaction. MacPhee and Cao (1993) have suggested that the more reducing environment therefore favours the formation of a porous Fe^{II} layer rather than the Fe^{III} which has been shown to be fairly broad but more diffuse.

Salvarezza et al. (1982) have suggested that there is initially a competitive process for the adsorption of OH^- and SH^- by the iron according to equations 2.59 and 2.60. The iron hydroxides through further reactions tend towards passivating species while the sulphide-bearing compounds lead to the formation of mackinawite (FeS).

$$(H_2O)Fe + OH^- \rightarrow Fe(OH^-) + H_2O \quad \ldots 2.59$$

$$(H_2O)Fe + SH^- \rightarrow Fe(SH^-) + H_2O \quad \ldots 2.60$$

Salvarezza et al. (1982) have suggested that the SH^-/OH^- ratio is the determining factor for which reaction will be favoured; where the SH^-/OH^- ratio is low, oxygen-containing film is favoured, where the SH^-/OH^- ratio is high the porous sulphide-containing layer becomes dominant. The actual mechanism for sulphide attack is attributed to the solubility of FeS in the presence of high concentrations of SH^- and not the direct attack of the Fe_2O_3 layer by sulphide species. At high SH^-/OH^- ratios the FeS dissolves yielding soluble Fe^{II}, thus leading to corrosion of the metal.

The anodic polarization curve for a solution containing sulphide ions has been characterized by Salvarezza et al. (1982) showing two large peaks. The first peak, which corresponds to the same potential in sulphide-free solution, is attributed to the formation of the ferric, ferrous passive layer, though somewhat defective. The exact cause of the second

current peak however is not as clear. Figure 2.19 shows the anodic polarization curves for mild steel in solutions of 10^{-2}M NaOH, pH 11.54 and 10^{-2}M Na_2S, pH 11.54.

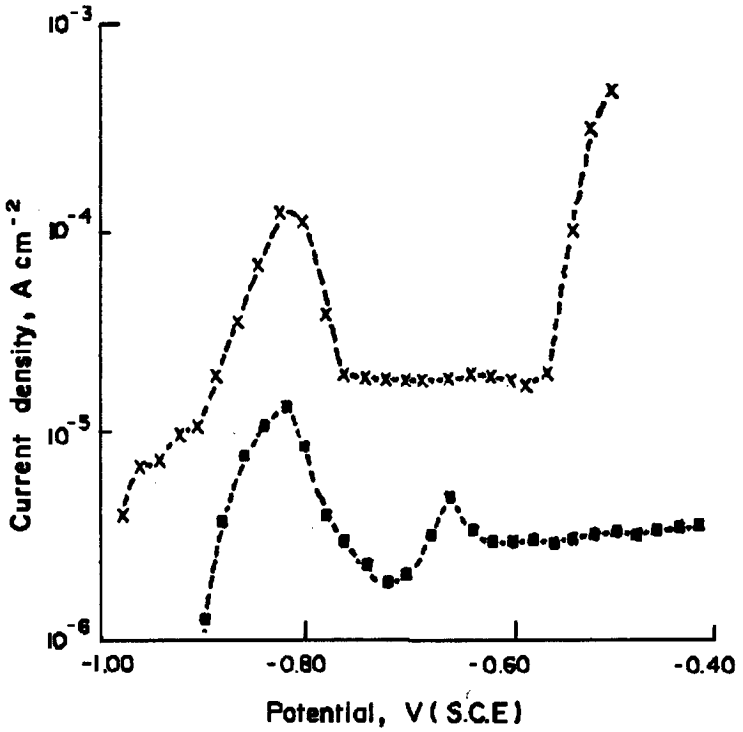

Fig 2.19: Anodic polarization curves (Salvarezza et al., 1982)

The anodic current for sulphide-containing solution was an order of magnitude higher than the NaOH solution over the potential range. The passive oxide layer present in the sulphide solution contained sulphide ions incorporated into the lattice of the Fe_3O_4 layer. The sharp increase in anodic current at –0.60 V_{SCE} may be a result of the oxidation of sulphide ions present on the metal surface to free sulphur or a soluble polysulphide. The current peak may also be attributed to the deposition of sulphur on top of the passive layer of Fe_3O_4 and Fe_2O_3. Further possibilities include the oxidation of aqueous sulphide to $S_2O_3^{2-}$ (thiosulphate) and finally the dissolution of iron at the metal surface through a beakdown in the passive layer.

The work of Tromans (1980) seems to support the argument of the oxidation of sulphide to thiosulphate as seen in the polarization curve for mild steel in a solution of NaOH and NaS_2, pH 12.01 at 92°C in Figure 2.20. The equilibrium potential for sulphide- thiosulphate ($E_{S_2O_3^{2-}/S^{2-}}$) reaction under the given conditions was -0.68 V_{SHE} as seen in the anodic

polarization curve which would explain that portion of the curve. The $E_{S_2O_3^{2-}/S^{2-}}$ for a variety of solution compositions at 100°C can be calculated according to (Tromans 1980):

$$E_{S_2O_3^{2-}/S^{2-}} = 0.034 - 0.056pH + 0.0093\log\left(\frac{[S_2O_3^{2-}]}{[S^{2-}]^2}\right) \quad \ldots 2.61$$

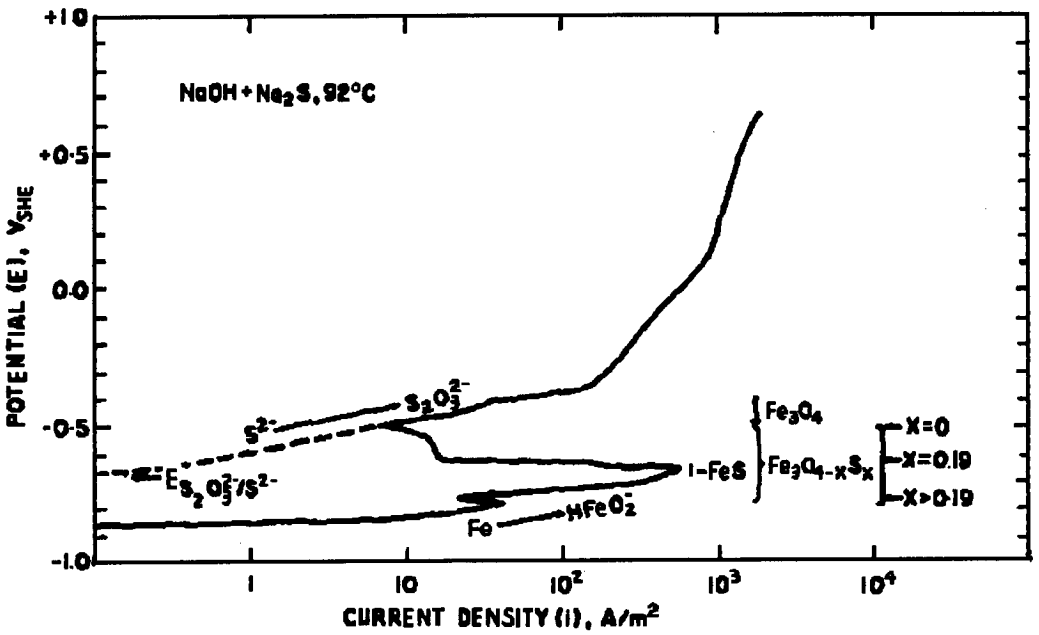

Fig 2.20: Anodic polarization curve for mild steel in NaOH + NaS_2 solution at 92°C (Tromans, 1980)

The effects of sulphide ions on the passivity and corrosion of steel in hot alkaline solutions can therefore be summarized as (Tromans, 1980):

1) Passivitiy in the NaOH solution started with the formation of Fe_3O_4 and reached a maximum during the formation of γFe_2O_3.
2) Passivity in the NaOH + NaS_2 solution was retarded due to the inclusion of S_2- into the lattice Fe_3O_4 forming a non-protective film. FeS was also deposited as a non-protective film on the surface.
3) Passivity in the NaOH + NaS_2 solution commenced when the S^{2-} concentration in the Fe_3O_4 lattice reduced to a sufficient level. The reduction in S^{2-} can be attributed to the oxidation of S^{2-} to $S_2O_3^{2-}$ in solution. Passivity therefore is attributed to Fe_3O_4 and not γFe_2O_3 as is normally the case.

The acceptance of negative impact of sulphides on the corrosion process however is not universal Cao et al. (1990) suggest that sulphide ions may inhibit the pitting of steel in the presence of chlorides. Anodic polarization curves for steel in simulated pore solution for OPC and FA and Slag concretes, were determined for various chloride concentrations. The increase in chloride concentrations for the Slag concretes was in part attributed to the higher sulphide contents. Greater understanding and research into the effects of sulphides on the corrosion processes, particularly with respect to the corrosion of steel in concrete medium is therefore needed. The role the sulphide ion and other data directly pertaining to steel corrosion in simulated pore solutions and concrete itself is discussed in chapter 4 and 5.

2.10 Chapter Summary

A general overview of some of the principles involved in the corrosion of steel has been presented in this chapter. Chemical thermodynamics has shown the actual Gibbs Fee Energy (GFE) of a substance can be determined from the standard GFE modified by the temperature, gas constant and activity of the substance. The change in GFE is related to the electro motive force, also known as potential difference, of the cell by means of electrochemical thermodynamics and permits derivation of the Nernst equations 2.23, 2.24 and 2.25.

The Nernst equations allow for the calculation of the cell and half-cell potentials at any range of temperatures, and ionic concentrations for reactants and products under consideration. This information can be used to determine the likelihood of a reaction occurring in the manner indicated and thus determine the range of situations in which corrosion may occur.

The Pourbaix diagrams are essentially graphical representations of the Nernst equations and show the relationship between electrode potential and pH at equilibrium for a metal in an aqueous environment. The three domains of iron, immunity, passivitiy and active corrosion are clearly represented in the Pourbaix diagrams. The passivity of ion in solution has been attributed to the formation of double layer film of Fe_3O_4 and γFe_2O_3. Only the outer film of γFe_2O_3 is considered to afford passive protection to the underlying steel.

While thermodynamics is useful for determining the likelihood of a reaction occurring, it does not say anything about the rate at which the reaction will occur. Knowledge of reaction rates is obtained from the study of the kinetics of the reactions. Any change in potential of an electrode from its equilibrium half-cell potential is termed overpotential and the electrode is said to be polarized. The Tafel equations, 2.39 and 2.40, provide a relationship between the change in half-cell potential and current. The three forms of polarization which will determine

the over corrosion rate are activation, concentration and resisitance. The intersection of anodic and cathodic curves from two different half-cells can be used to estimate the corrosion current of a combined half-cells, for instance the anodic dissolution of Fe and the cathodic reduction of oxygen.

Chloride ions have been shown to disrupt the passive layer which normally protects steel in alkaline environments. The effect of chlorides is to progressively lower the transpassive portion of the anodic polarization curve with increasing concentrations of Cl^-. Since the solubility of oxygen in solution decreases with increasing Cl^- concentration, a maximum corrosion rate is reached at slat Cl^- concentrations of approximately 0.5M. Sulphides generally have a similar effect result in the development of a more porous passive layer around the steel thus limiting its effectiveness against Cl^- for instance.

An understanding of the fundamental corrosion process provides the basis of any attempt to study the corrosion of steel in concrete. The corrosion of steel in concrete is complicated by the physical environment of the concrete but the pore solution essentially provides an aqueous medium in which corrosion can occur. The following chapter will outline the specifics of the pore solution of concrete and the principles factors which will affect the corrosion of steel.

2.11 Reference

Alvarez, A. and Galvele, J. 1984, *Mechanism of Pitting of High Purity Iron in NaCl Solutions*, **Corrosion Science**, Vol. 24, No. 1, pp. 27-48.

Bockris, J., Conway, B., Yeager, E and White, R. ed. 1981, **Comprehensive Treatise of Electrochemistry, Volume 4**: Electrochemical Materials Science, Plenum Press: New York.

Cao, H., Baweja, D. and Roper, H. 1990, *Corrosion Characteristics of Steel in Solutions Derived from Cement and Blended Cements*, **Cement and Concrete Research**, Vol. 20, pp. 325-334.

Cornell, R. and Schwertmann, U. 1996, **The Iron Oxides: Structure, Properties, Reactions, Occurrence and Uses,** VCH, Weinheim.

Foley, R. 1970, *Role of the Chloride Ions in Iron Corrosion*, **Corrosion**, Vol. 26, No. 2, pp. 58-70.

Jones, D. 1996, **Principles and Prevention of Corrosion, Second Edition**, Prentice Hall: New Jersey.

Leek, D. and Poole, A. 1990, *The Breakdown of the Passive Film on High Yield Mild Steel by Chloride Ions*, **Corrosion of Reinforcement in Concrete**, Society of Chemical Industry, London, pp. 65-73.

Liu, Y. 1996, **Modeling the Time-to-Corrosion Cracking of the Cover Concrete in Chloride Contaminated Reinforced Concrete Structures, Dissertation for Doctor of Philosophy**, Virginia Polytechnic Institute and State University.

Macphee, D. and Cao, H. 1993, *Theoretical Description of Impact of Blast Furnace Slag (BFS) on Steel Passivation in Concrete*, **Magazine of Concrete Research**, Vol. 45, No. 162, pp. 63-69.

Mansfeld, F. 1970, *The Polarization Resistance Technique for Measuring Corrosion Currents*, **Advances in Corrosion Science and Technology**, pp. 163-261.

Marcotte, T. and Hansson, C. 1998, *A Comparison of the Chloride-Induced Corrosion Products from Steel-Reinforced Industrial Standard versus High Performance Concrete Exposed to Simulated Sea Water*, **International Symposium on High-Performance and Reactive Powder Concretes: Sherbrooke**, Vol. 4, pp. 145-162.

Pettersson, K. and Sandberg, P. 1997, *Chloride Threshold Levels, Corrosion Rates and Service Life for Cracked High-Performance Concrete*, **Durability of Concrete: Proceedings Fourth CANMET/ACI International Conference, Sydney, Australia, SP 170, ed. Malhotra**, pp. 451-472.

Sato, N. 1978, *The Passivity of Metals and Passivating Films*, **Passivity of Metals: Proceedings of the Fourth International Symposium on Passivity**, Electrochemical Society, pp. 29-58.

Salvarezza, R., Videla, H. and Arvia, A. 1982, *The Electrodissolution and Passivation of Mild Steel in Alkaline Sulphide Solutions*, **Corrosion Science**, Vol. 22, No. 9, pp. 815-829.

Stern, M. and Geary, A. 1957, *Electrochemical Polarization, A Theoretical Analysis of the Shape of Polarization Curves*, Journal of the Electrochemical Society, Vol. 104, pp. 56-63.

Shreir, L. ed. 1979, **Corrosion Volume1, Metal/Environment Reactions**, Newnes-Butterworths: London.

Schiessl, P. ed. 1998, **Corrosion of Steel in Concrete**, Chapman and Hall Ltd: London.

Stansbury, E. and Buchanan, R. 2000, **Fundamentals of Electrochemical Corrosion**, ASM International, Ohio.

Suda, K., Misra, S. and Motohashi, K. 1993, *Corrosion Products of Reinforcing Bars Embedded in Concrete*, **Corrosion Science**, Vol. 35, No. 5-8, pp. 1543-1549.

Tromans, D. 1980, *Anodic Polarization Behaviour of Mild Steel in Hot Alkaline Sulfide Solutions*, **Journal of Electrochemical Society**, June, pp. 1253-1256

West, J. 1980, **Basic Corrosion and Oxidation**, Ellis Horwood Limited: London.

CHAPTER 3: PORE WATER CHEMISTRY

The general thermodynamic and kinetic principles governing the corrosion of steel in aqueous media have been presented in chapter 2. It is now possible to more specifically investigate the corrosion of steel under conditions which simulate the pore solution chemistry of concrete. Concrete is a heterogeneous material with voids filled by a solution known as pore water or pore solution. The study of corrosion in aqueous media therefore is an attempt to examine one component or phase of the overall corrosion of steel in concrete. These aqueous solutions should ideally be representative of the actual pore solution found in the concrete.

The overall objective of the current work is to investigate the influence of cement extenders on the corrosion rates of steel in concrete. It is well know that simulated solutions do not accurately reflect the true mechanisms of steel corrosion in concrete as there is no bonding of hydrates to the steel or specific variability in pore solution chemistry which may exist within localized regions of the concrete. Aqueous phase corrosion investigations can however provide very meaningful information as to the influences of specific chemical effects on the corrosion, as the chemistry of the pore solution can be accurately controlled and determined. An understanding of the chemical processes at work where specific cement extenders are employed is therefore necessary.

As considerable variations in pore solution chemistry may exist in concretes with nominally the same extenders and with time, it is essential to accurately quantify the pore solutions of the concretes under investigation. Once the chemistry of the pore solution is known, it is then possible to develop simulated pore solutions which can be used to perform rapid aqueous phase testing of the materials. The separation of chemical, physical and physico-chemical effects is essential if progress is to be made in optimizing the use of extenders so as to prolong the life of reinforced concrete structures.

3.1 Pore Solution Chemistry

The study of pore solution chemistry has been the subject of much work for a considerable period of time. The first methods of assessing the pore solution chemistry generally involved suspensions of cement in water, followed by filtering of the particles and subsequent analysis of the liquid. It is obvious therefore that pore solution chemistry could only be determined prior to hydration. The development of the pore press, for expressing solution from hardened mortar and cement paste, allowed for the long term study of the pore

water chemistry during after hydration. A further method of pore solution extraction was recently developed by Cromie et al., (2002) which employed a heavy liquid coupled with centrifuge to displace the pore solution in a fractured sample. The heavy liquid extraction method appears quite promising but, as it was only recently developed and not employed in the current investigation, no further mention of it will be made.

Barneyback and Diamond (1981) provide a fairly detailed description of the pore expression device (PED) with its application and use. The operating pressure of their device was approximately 550 MPa which is considerably greater than the 350 MPa employed by Longuet et al (Barneyback and Diamond, 1981). Duchesne and Berube (1994[a]) investigated; the influence of pressure on the alkalinity of pore solution, and the comparison of pore fluid extracted from mortars and cement paste of the same w/c ratio. Pore solution was extracted in pressure ranges from 0-560, 0-200, and 200-560 MPa and they concluded that the alkalinity of the pore solution was independent of the pressure at which it was extracted. Similarly there was little variation in the alkali concentration of pore solution extracted from mortars or cement pastes, though over extended periods of time there may be some effects if reactive aggregates are used due to AAR.

Constantiner and Diamond (1997) provide similar results in their study of pressure effects, though they note some dependence of sulphate concentration on pressure; 0.047 N for 414 to 490 MPa, and 0.027 N for 0 to 220 MPa. The collection of pore solution through the normal operating range of 350 to 550 MPa of most PEDs should result in only small variation in concentration of most ions, though sulphate ions appeared to vary slightly. It is therefore possible to make meaningful comparisons between results of pore solution extraction from either mortars or pastes and taken at different operating pressures. Glasser (2003) suggests that the efficiency of most collection devices to be no more than 50% of the total pore solution and confirms that pressure effects are unlikely to significantly influence the pore solution composition. Glasser (2003) does state however that two more important considerations are to ensure the sample is adequately protected from the environment and the geometry of the collection. Uniaxial devices for instance result in uneven compression and only part of the sample may be subject to sufficient pressure to express the pore solution. As a triaxial device for expressing pore solution was unavailable, this effect has not been considered in the current investigation.

3.1.1 Major Anion and Cation Composition of Pore Solution

The pore solution composition of OPC and various cement extenders has been investigated by numerous researchers. The majority of work however has been focused on the evaluation of hydroxyl ion concentration or Na^+ and K^+ levels. According to Duchesne and Berube (1994[b]) at high pH, $[Na^+]+[K^+] \approx [OH^-]$ since other ionic species are relatively insignificant. In their work paste samples containing Cement, FA, Slag and SF with a *w/c* ratio of 0.5, where *c* refers to all cementitious material, were cast in sealed plastic bottles and analyzed for alkali content over a period of approximately 1.5 years. Their 84 day alkali results, taken as hydroxyl ion concentration, are summarized in Table 3.1 together with data from other researchers.

The inclusion of cement extenders significantly affects the alkali content of the pore solution with all extenders shown in Table 3.1, entrapping more alkali than they release. Duchesne and Berube (1994[a]) state that the effects of extenders are more than simply inert fillers as a 10% replacement by SF results in 60% or more decrease in alkali. While FA results in only a 25 to 35% decrease in alkali at 7 days it continues to remove alkali at later stages. Slag is also said to act primarily as an inert diluent at early ages. Duchesne and Berube (1994[b]) do however note that a 5% SF-B type results in greater alkali content than the control at 84 days and shows an increasing trend over time.

The results of pore water chemistry have generally been derived from cement pastes or mortars made with *w/c* ratios of 0.5 or 0.6, for example work by Byfors, et al (1986), Andrade and Page (1986), Constantiner and Diamond (1997), Page and Vennesland (1983) and Longuet (1976) shown in Table 3.1. From these results it is apparent that the normal range of hydroxyl ion concentration for OPC exists between a low of 0.53 mol/l and a high of 0.71 mol/l with a mean of approximately 0.62 mol/l. The inclusion of cement extenders generally results in lower hydroxyl ion concentrations (mol/l) with typical values of:

Slag:	30%	0.600	SF:	5%	0.480
	35%	0.416		10%	0.239
	76%	0.142		30%	0.010
FA:	25%	0.410			
	40%	0.256			

Table 3.1: Summary of chemical analysis of pore water

	Concentration in mol/l				
	OH^-	Na^+	K^+	Ca^{2+}	SO_4^{2-}
Byfors, et al (1986)					
3 months. 1% Cl added. *w/c* 0.6					
PC, Swedish	0.610				
FA (25%)	0.410				
SF (10%)	0.110				
Slag (30%) Australian	0.600				
Duchensne and Berube (1994[b])					
84 day, *w/c* 0.5					
PC	0.640				
Slag (35%)	0.416				
Slag (50%)	0.290				
FA-B (20%)	0.380				
FA-B (40%)	0.256				
SF-A (5%)	0.480				
SF-A (10%)	0.290				
Andrade and Page (1986)					
28 day, 1% Cl added, *w/c* 0.5					
PC –british	0.620				
Spanish Portland Blastfurnce Cem.	0.754				
Cao et al (1990)					
7 day, *w/c* 2					
Cem I high C_3A	0.046				
Cem I low C_3A	0.039				
Slag (35%)	0.035				
FA (25%)	0.035				
Constantiner and Diamond (1997)					
2 year, *w/c* 0.5					
PC, low alkali	0.452	0.070	0.398	NA	0.0150
PC, mod-high alkali	0.530	0.187	0.387	NA	NA
Page and Vennesland (1983)					
84 day, *w/c* 0.5					
PC	0.713	0.323	0.639	0.0020	0.0270
PC/Silica 10%	0.239	0.114	0.202	0.0010	0.0160
PC/Silica 20%	0.078	0.051	0.069	0.0020	0.0250
PC/Silica 30%	0.010	0.030	0.030	0.0070	0.0320
Longuet (1976)					
3 months, *w/c* 0.5					
A 95.5% Clk, 4.5% gy	0.625	0.133	0.532	0.0030	0.0000
B 19.1% Clk, 4.5% gy, 76.4% slag A	0.142	0.050	0.086	0.0025	0.0008
C 19.1% Clk, 4.5% gy, 76.4% slag C	0.225	0.078	0.160	0.0000	0.0009

Note: For Longuet Clk – clinker, gy – gypsum, Sample C taken at 2 months

However, as Duchesne and Berube (1994[b]) have shown, there can be significant variations in hydroxyl ion concentration between different types of the same extenders and at the similar replacement levels. These concentrations also vary as a function of the age of the specimens, and therefore direct comparisons between the results presented from various sources is not entirely possible, though they do provide for a reasonable expected range of values. It should also be noted that chloride was added to the samples in a number of cases, thus further influencing the pore solution.

Tritthart (1990) investigated the influence of *w/c* ratio on the hydroxyl ion concentration of pore water taken from hardened cement paste samples containing 1% chloride as NaCl. The results from pore expression tests taken at 3 months can be seen in Figure 3.1.

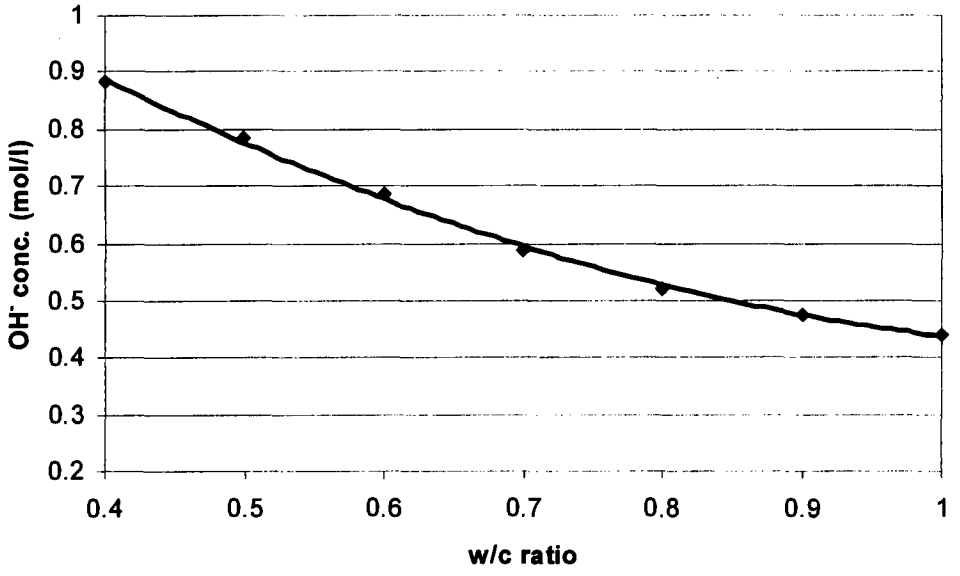

Fig 3.1: *w/c* ratio versus hydroxyl ion concentration (from Tritthart 1990)

Tritthart's results of 0.78 mol/l of hydroxyl ion for a *w/c* ratio of 0.5 are somewhat higher than the mean value determined from other researchers. The main contribution of the work is the qualification of the relative change in hydroxyl ion concentration with respect to *w/c* ratio, which may allow for partial standardization of various *w/c* ratios to a common value thus eliminating one further variable. That is, a proportional shift in hydroxyl ion content for a particular measurement or set of measurements can be made to adjust to a common *w/c* ratio for the purposes of comparison across various mix designs.

The results of Cao et al. (1990), see Table 3.1, confirm the reduction of hydroxyl ion concentration associated with use of cement extenders. Their *w/c* ratio of 2 is much higher than would normally be expected, thus results for pore water chemistry comparisons to other

work is not possible. The results of their tests on the anodic polarization of steel in pore water solutions however will be subsequently discussed.

The concentrations of the major cations and hydroxide have been reasonably well established and summarized in the preceding discussion. For the maintenance of passivity of the steel the importance of hydroxide concentration upon the corrosion of steel in concrete is quite evident, as is the need for controlling the levels of chlorides required to cause initiation of active corrosion. Thus knowledge of hydroxide levels in pore solutions as a major indicator of the steel protection is probably reasonable in most concretes including FA and SF bearing concretes. It would appear therefore that FA and SF should perform less favourably than PC with respect to the corrosion of steel in concrete. In practice we see quite the opposite, thus a significant non-pore solution chemistry component must be present as will be discussed later in this chapter, and in chapter 4. The use of slag however results in significant variations to the pore solution chemistry through a reduction in alkalinity, as described by Duchesne and Berube (1994[a]), and also through the inclusion of soluble sulphur species such as HS^-, S^{2-} and $S_2O_3^{2-}$. Consequently, the next section will deal with the role of sulphides and other minor anions on the pore solution.

3.1.2 Role of sulphides and other minor anions in pore solution chemistry

The effects of slag on pore water composition were investigated in the early work of Longuet (1976). A number of mixes containing various proportions of gypsum, clinker and slag were investigated over a period of approximately two years. Numerous elements and compounds were analyzed including: Si, Al, Fe, S^{2-}, SO_4^{2-}, Ca^{2+}, Na^+, and K^+, in addition to electrochemical measurements of pH, redox potential and conductivity. For the purposes of the current investigation only the results for S^{2-}, SO_4^{2-}, OH^-, and redox potential of three mixes are presented in Table 3.2. The results of Longuet (1976) indicate a distinct difference in pore solution chemistry between the slag and non-slag bearing materials. The slag bearing samples all contained sulphides to some degree while no sulphides were detected in the non-slag bearing samples.

Table 3.2: Sulphide, sulphate, redox and OH^- measurements over time (mg/kg unless otherwise stated), (base on Longuet, 1976)

Sample		*5h*	*2d*	*7d*	*28d* *30d	*3m* #2m	*6m* *5m	*13m* *11m	*2y*
A	S^{2-}								
	SO_4^{2-}	4417	58	443			185	703	1225
mol/l	OH^-	0.176	0.435	0.623	0.717	0.625	0.670	0.635	0.671
mV	redox		+96	+80	+88	+79	+112	+91	
B*	S^{2-}		17	36	10	30	14	25	
	SO_4^{2-}	1483	13			53	38	58	
mol/l	OH^-	0.078	0.135	0.162	0.149	0.142	0.146	0.144	
mV	redox		-106	+4	-16	+142	-25	-350	
C#	S^{2-}			74	28	46	29	85	201
	SO_4^{2-}	1442		65	109	61	98	150	391
mol/l	OH^-	0.081		0.183	0.219	0.225	0.230	0.235	0.228
mV	redox			-236	-230		-300	-370	+78

Sample A: (Clinker 95.5%, Gypsum 4.5%)

B: (Clinker 19.1%, Gypsum 4.5%, Slag-A 76.4%)

C: (Clinker 19.1%, Gypsum 4.5%, Slag-C 76.4%)

The results of Longuet are generally somewhat lower than those of Tuutti (1982) who investigated both mortars and pastes with slag replacement levels of 70%. Tuutti found sulphide concentrations of approximately 160 ppm at 0.8 and 15 months for pastes made with a w/c ratio of 0.5. Variations in sulphide concentration for the 0.4 w/c ratio mix over time were somewhat greater; 15 months 250 - 300 ppm, 21 months 160 - 300 ppm, but still reasonably consistent. The sulphide levels taken from mortars compared to pastes however were significant different. The maximum sulphide concentration for any of the mortar samples was determined to be 20 ppm. Tuutti states the mortar specimens were exposed to large amounts of oxygen compared to the paste samples which were sealed. This could also be observed visually as the initial dark colouring of the material had disappeared by the time of the measurements.

Early age data from the study by Vernet (1982) of the sulphur chemistry of slag cements (73% slag) showed that a maximum concentration of 80.2 mg/l of S^{2-} was reached 35 hours after mixing. After reaching a peak concentration the S^{2-} level reduced over the remaining period placing the concentrations roughly between those of Longuet and Tuutti. Vernet stated that the sulphide concentration should have been 805 mg/l and that the measured value 10 times lower is a result of S^{2-} forming precipitates and not as a result of oxidation. The author further states that variation in sulphide concentration is a result of change in flux between

dissolution of anhydrites and the precipitation of hydrates. The influence of different materials, particularly with respect to the slag component, must again be emphasized. The need for individual pore solution analysis of the slags to be employed in any investigation is therefore essential. The method of measurement and extraction are also important factors as sulphides are readily oxidized thus distorting measured values.

The kinetics of the oxidation of sulphide is relatively complex but can be described by the equation (Chen and Morris, 1972):

$$-\left[\frac{d\left(\sum S^{2-}\right)}{dt}\right]_{t=0} = k\left(\sum S^{2-}\right)^{1.34}(O_2)^{0.56} \qquad \ldots 3.1$$

where (O_2) is the concentration of oxygen, (ΣS^{2-}) is the total concentration of sulphides, t is time in hours and k is the rate constant. The rate constant k and thus oxidation rate of sulphide is dependant upon the initial O_2 and ΣS^{2-} concentration and pH of the solution. The rate constant k is approximately 15 $M^{-0.9}hr^{-1}$ for a pH in the order of 12 to 13. The rate constant decreases as the alkalinity of the solution increases above a pH of 11. Thus the overall oxidation of sulphides is relatively rapid and great care must be taken when determining their concentration in pore solutions.

The effects of sulphides and slag replacement levels are also manifest in the redox potential of the solution. The non-slag bearing material (sample A) of Longuet displayed redox potentials of at least + 79 mV over the entire study period. The slag bearing samples showed quite a range of values from -350 to + 142 mV for slag A and -370 to +78 mV for slag C. It is particularly interesting to note that there does not appear to be any significant trends associated with redox potential or sulphide concentration.

While there may not be a definite trend in Redox potential with time, Angus and Glasser (1985) have shown a fairly significant relationship between redox potential, sulphide concentration and slag replacement levels with highly negative potentials associated with sulphide concentrations in excess of 100 ppm as shown in Table 3.3. Redox potentials were measured against a platinum electrode while the sulphides were determined by ion chromatography. The data from Table 3.3 was obtained after 25 days of hydration during which time approximately 25% of the slag reacted, thus much of the total S would still remain locked in the unhydrated portion (Angus and Glasser, 1985).

Table 3.3: Redox potential and S^{2-} concentration (Angus and Glasser, 1985)

OPC	*BFS*	*E_h (mV)*	*S^{2-} (ppm)*
100	0	+82	0
75	25	+79	NR
50	50	+68	12
25	75	+35	6
15	85	-240	120
10	90	-269	110
5	95*	-330	1000
2.5	97.5*	-259	1100

* 0.5% Ca(OH)2 added to ensure setting

Slag replacement levels of up to 75% appear to have little effect on the redox potential or sulphide concentration. Angus and Glasser suggest that break level of 75% may be a result of the relatively short aging and further data is required to verify the existence of this point.

Glasser et al (1988) investigated additional sulphur species present in the pore solution of slag bearing materials. It was found that thiosulphate ($S_2O_3^{2-}$) was also present in appreciable quantities of pore water derived from an 85% slag, 15% cement mix. The test cylinders were cured for 25 days at 20°C in individual polythene plastic bags which according to Glasser et al. would have inhibited though not totally prevented the ingress of oxygen. Thus some oxidation may have occurred resulting in slightly lower S^{2-} and $S_2O_3^{2-}$ values than expected. S^{2-} was determined using a S^{2-} selective AgS electrode while $S_2O_3^{2-}$ and SO_4^{2-} were determined by ion chromatography. The results of the pore solution analyzed are shown in Table 3.4.

Table 3.4: Sulphur species concentration from 85% slag pore solution (Glasser et al., 1988)

Parameters	*25 d at 20°C*
pH	12.6
E_h (mV)	-227
S^{2-} (mg/l)	120
$S_2O_3^{2-}$	310
SO_4^{2-}	297

The variation in redox potential (E_h) and, by association, sulphide concentration with time have been attributed to competition between the reduced species ***R*** of the slag and the oxidized species ***Ox*** of the cement (Macphee and Cao, 1993). Where the E_h is positive the effectiveness of ***R*** is insufficient to overcome the oxidized content and dissolved oxygen of

the pore solution. Similarly where E_h is negative the ***R*** species are dominant. The poising capacity essentially refers to electrochemical buffering capacity of the system in a manner analogous to pH buffering. The redox poising capacity is a function of the concentration of the redox couple, the number of electrons required for its oxidation or reduction and the difference between the potential of the solution and the formal potential of the couple (Glasser et al., 1988). According to Macphee and Cao (1993) in the short term the ***R*** of the slag is insufficient to overcome the poising capacity of the rapidly hydrating cement, thus the redox potential remains positive until such time as the ***Ox*** are consumed and a reducing environment dominates. The effects of slag concentration on the redox potential with time are illustrated in Figure 3.2. A reducing environment is established after approximately 28 days for an 85% slag content with a 75% slag content taking approximately 3 months to reach a similar state. The 50% slag cement is also expected to develop a reducing environment though at a later date.

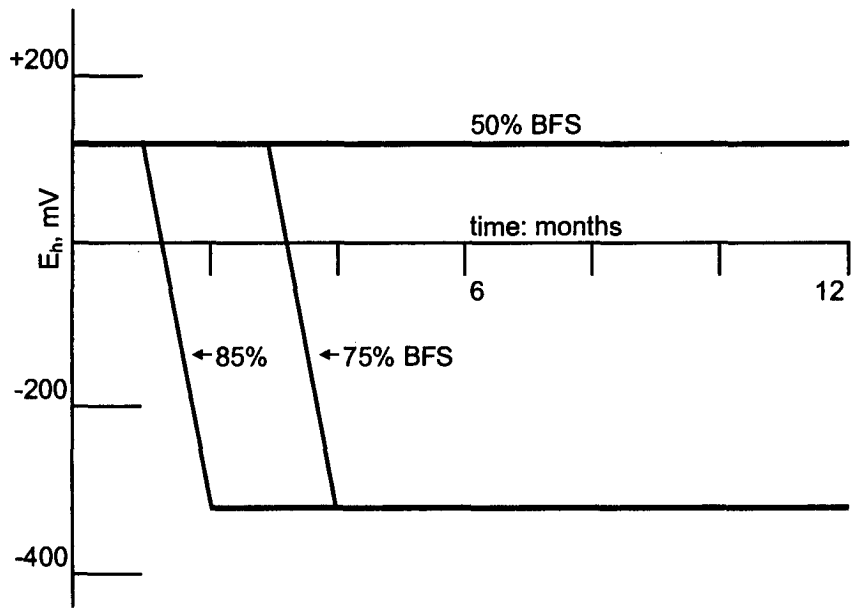

Fig 3.2: Effect of slag replacement levels and time on the redox potential of the pore solution (Macphee and Cao, 1993).

The general range of sulphide concentrations for slag replacement levels greater than 75% and less than 90% appear to be in the range of 110 to 300 mg/l in addition to thiosulphate. As previously noted Longuet's (1976) results displayed somewhat lower values in the order of 20 to 80 mg/l, for a 76% slag paste, though one value of 201 mg/l was recorded. The values for redox potential were correspondingly negative in the range of -227 to -270 mV for samples containing appreciable levels of sulphides, though Longuet (1976)

recorded a value of -370 mV with an associated sulphide concentration of approximately 85 mg/l and + 78 mV with S^{2-} of 201 mg/l. The E_h of commercially available cements was found to lie between +75 and +100 mv (Glasser et al., 1988). There is however a general indication that reasonably negative redox values are associated with the high slag replacement levels which result due to the presence of substantial quantities of reduced sulphur species in the pore solution. The variation in sulphide concentration with time has been attributed to changes in the hydration reactions and competition among dissolution and precipitation of various hydrates and anhydrates.

The range of concentrations for sulphides, thiosulphate and redox potentials present in the literature shows the dependence of the pore solution chemistry on the specific cement and slag. Therefore any attempt to understand the influence of cement extenders, particularly slag, on the corrosion rates of steel in concrete must first examine the individual constituents of the mix and associated chemical properties. The methodology and results of the pore solution chemistry for the specific materials employed in the current investigation will now be discussed in the following section.

3.2 Experimental Procedures

The method for examining the pore water chemistry of concrete is based on the principle of pore expression as described by Barneyback and Diamond (1981). Seven sets of cement pastes, corresponding to the seven mix designs chosen for the corrosion rate studies, were cast in sealable plastic bottles of 48 mm diameter and 80 mm height. The mix proportions are as follows:

PC: 100% OPC
SL: 75% OPC:25% Slag
SM: 50% OPC:50% Slag
SH: 25% OPC:75% Slag
FA: 70% OPC:30% FA
SF: 93% OPC:7% SF
TR: 50% OPC:43% Slag:7% SF

The oxide content and mineralogy of the materials employed in the current investigation are provided in Appendix 3A. A *w/c* ratio of 0.58 was used which resulted in a fluid composition and thus continuous mixing was required during preparation. Once an individual container was filled it was sealed and placed in a rotating device for approximately 24 hours. A sufficient number of samples were cast to allow for analysis at 7, 28 and 90 days. The samples

were stored at a constant temperature of 20°C. Minimal oxygen penetrated the containers as upon removal at the desired age, the characteristic dark blue colour of the slag bearing samples was observed either at the surface or just beyond the first few millimeters of the sample.

The pore expression device generally resembled those in the literature with a central plunger surrounded by a confining cylinder in which the sample is placed, as seen in Figure 3.3. The base plate contains a grooved ring where the pore solution is collected and which then flows through an opening to the side of the base plate. A syringe was used to extract the pore solution to minimize contact with the air and thus limit oxidation of the sulphides or ingress of carbon dioxide causing reduction of the pH. The pore press was slowly loaded to a maximum pressure of approximately 450 MPa at which point the pressure was maintained for several minutes.

Fig 3.3: Pore expression device used in the experimental work

Once the solution was obtained from the pore press the following analytical procedures were followed:

1) The collected solutions were filtered through a 45 μm membrane to remove any suspended solids or particulate.

2) Sulphide and thiosulphate were analyzed be means of colorimetric spectroscopy as described in appendices B and C respectively. The colorimetric method allows for accurate determination of the concentrations at fairly low levels

3) Sulphate was determined by means of a Merck Spectroquant Nova 60 system used with a sulphate cell test kit 1.14548.0001. The pH was adjusted to less than 10 and 5 ml of the adjusted sample was added to the vial. The reagent was then added and after shaking allowed to stand for one minute at which point the reading was taken.

4) Dissolved oxygen was measured, immediately after filtering, by YSI 55 dissolved oxygen meter which uses the potential across a membrane to determine oxygen concentration.

5) Redox potential measurements were taken against a platinum reference electrode and recorded once a stable value was reached.

6) Hydroxyl ion concentration was determined by means of a Gran titration against HCl (Loewenthal et al., 1989).

7) The solution conductivity measurements were taken with a Hanna Instruments HI 9033, multi-range conductivity meter.

8) The cations of Na, K, Ca, Mg, Fe were analyzed by both ion chromotography and atomic absorption. There was fairly close agreement between the two methods and an average value of the two taken as the concentration.

Proper laboratory procedures were used to limit contamination of the samples, for instance use of a syringe to minimize contact with the atmosphere. The equipment was calibrated prior to each set of readings to ensure accuracy and confidence in the results.

3.3 Results and Discussion

3.3.1 Hydroxyl and Conductivity Measurements

The results of the pore water analyses showed general trends similar to previous work conducted by other researchers. A complete summary of the results may be found in Appendix D. The results for hydroxyl ion concentration are shown in Figure 3.4 and indicate a maximum concentration of 0.32 mol/l after 90 days for the PC sample. There is some variation in the literature, as previously seen in Table 3.1, from a low of 0.452 mol/l to a high of 0.713 mol/l for a PC at w/c of 0.5.

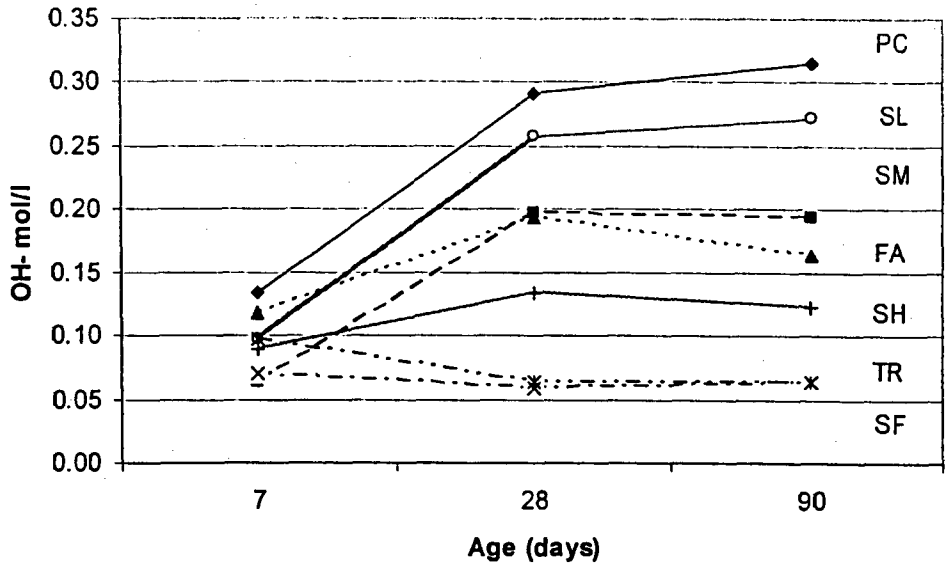

Fig 3.4: Influence of cement extenders on hydroxyl ion concentration

The current hydroxyl ion concentrations while somewhat lower, due to factors such as w/c ratio and C_3A content, do not significantly fall outside the normal range of values. The use of the Gran titration approach ensured an accurate assessment of the hydroxyl content of the solution. There was generally an increasing trend in the hydroxyl ion concentration with age as hydration continued. Some slight reductions from 28 to 90 days were observed for the FA and SH mixes. Only the SF and TR blends showed an overall decrease from the initial 7 day measurements to 28 and 90 days. The results from the slag samples, SF and TR shows that slag dominates the early hydration chemistry while SF has a greater influence on the ternary blend chemistry at later ages. The effects of SF may be delayed by the presences of the slag. The lowest hydroxyl ion concentration of 0.059 mol/l for SF at 28 days is still sufficient to provide full passivation for the steel. Steel in any of the cement extenders should therefore remain fully passive until the ingress of chloride or other harmful anions have penetrated to the required depth in sufficient concentrations.

The relative concentration of hydroxyl ions, as shown in figure 3.5, associated with the inclusion of cement extenders bears greater resemblance to other work than the absolute values for the hydroxyl ions. Duchesne and Berube (1994[b]) have shown a relative concentration ($[OH^-]_{extender}/[OH^-]_{PC}$) of hydroxyl ions of 0.45 for a 50% slag, and 0.59 and 0.4 respectively for 20% and 40% FA which is comparable to the 0.61 obtained for 50% slag and 0.52 for a 30% FA replacement at 90 days. Byfors et al. (1986) have shown a minor decrease

in hydroxyl concentration compared with OPC to 0.98 for a 30% slag replacement which is of a similar order to the 0.86 observed for 25% slag replacement.

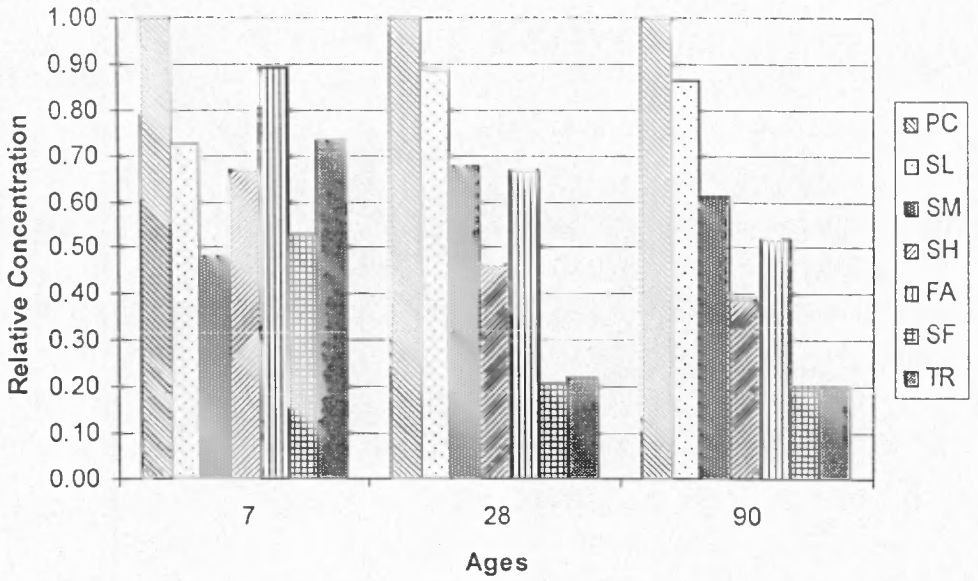

Fig 3.5: Relative concentrations of hydroxyl ion for cement extenders
(PC taken as 1 for each age)

The observed 0.20 relative concentration for 10% SF is also consistent with the 0.19 obtained by Byfors et al. (1986). Finally the work of Longuet 1976 indicated a relative hydroxyl concentration of approximately 0.22 and 0.36 for A and C type slags at a 76% replacement which is similar to the 0.39 which was determined for 75% slag. It is evident that the inclusion of cement extenders has a significant effect on the hydroxyl ion concentration of the pore solution. The greatest reductions were obtained using 7% replacement by SF. The ternary blend of OPC, slag and SF showed essentially the same level of hydroxyl ions which would indicate the dominance of SF in the determination of this component of the pore water chemistry. The hydroxyl ion concentration can therefore be summarized in decreasing order according to: PC > SL > SM > FA > SH > TR and SF at 28 or 90 days.

The conductivity measurements are closely related to the hydroxyl ion concentration as expected. The relationship between conductivity and hydroxyl concentration is shown in Figure 3.6 with a correlation of 0.996. The conductivity values for the extender replacements follow the same pattern as the hydroxyl ions. Conductivity therefore is almost entirely dependant upon the hydroxyl concentration of the pore solution. The high conductivity value of the solutions should assist in the required ionic flow in an electro-chemical corrosion reaction.

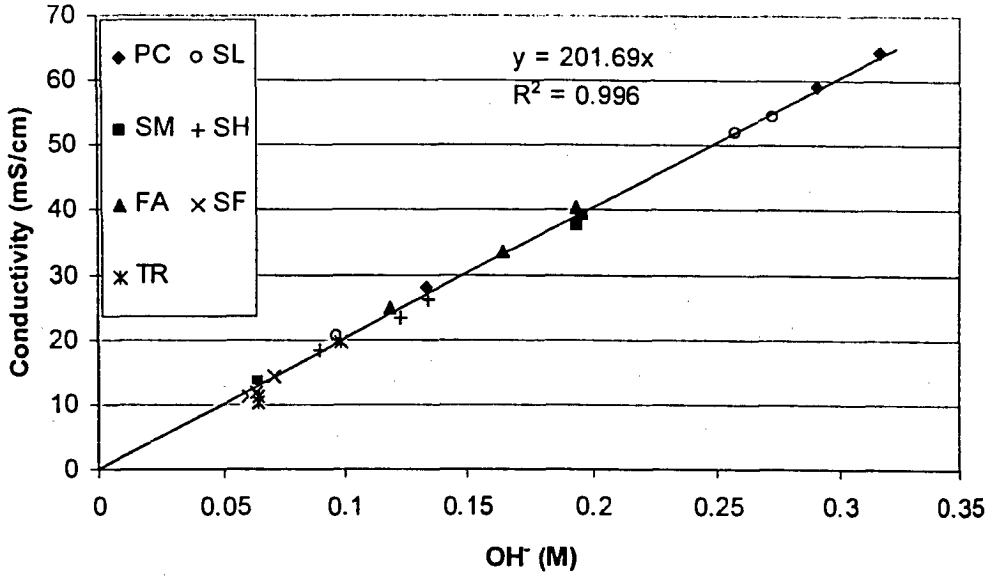

Fig 3.6: Conductivity versus hydroxyl ion concentration

The resisitivity of any of the solutions would be fairly low and thus not significantly impede or slow the corrosion process.

3.3.2 Cation Measurements

The major cations under investigation were Na^+, K^+, and Ca^{2+}. The results for Na^+ and K^+ are generally lower than those reported elsewhere but this would be expected due to the lower hydroxyl concentration. The 90 day results of the Na^+, Ka^+, Ca^{2+} and the K^+/Na^+ ratio are presented in Table 3.5.

Table 3.5: K^+, Na^+, Ca^{2+} and K/Na ratio for 90 day pore expression results (mg/l)

Sample	K^+	Na^+	Ca^{2+}	K^+/Na^+
PC	8449	2057	40	4.1
SL	7038	1846	23	3.8
SM	4538	1245	29	3.6
SH	2742	882	10	3.1
FA	4195	1073	24	3.9
SF	788	202	506	3.9
TR	772	301	347	2.6

The K^+/Na^+ ratios for PC of 4.1, slag 3.1 to 3.8 and SF of 3.9 are fairly close to those reported by Duchesne and Berube (1994[b]) of 4.5, 3 and 4 to 4.5 respectively for similar cement replacement proportions. A fairly significant divergence occurs with respect to the FA sample

for which a measured value of 3.9 was recorded compared to Duchesne and Berube (1994[b]) who reported their lowest value of approximately 1. The lowest K/Na ratio in the current investigation was that of the ternary blend 2.6. The K^+/Na^+ ratio showed little variation with time and did not display the more consistent trends associated with the hydroxyl ions. The relative proportion of Na^+ and K^+ for all the samples are shown in Figure 3.7.

The measured values for Ca^{2+} appear reasonable for the PC, slag and FA samples with concentrations less than 40 mg/l. The SF and TR samples however displayed high levels in the range of 347 to 506 mg/l. The lower pH of the solution would allow for some increase in Ca^{2+} concentration due to the nature of its solubility product.

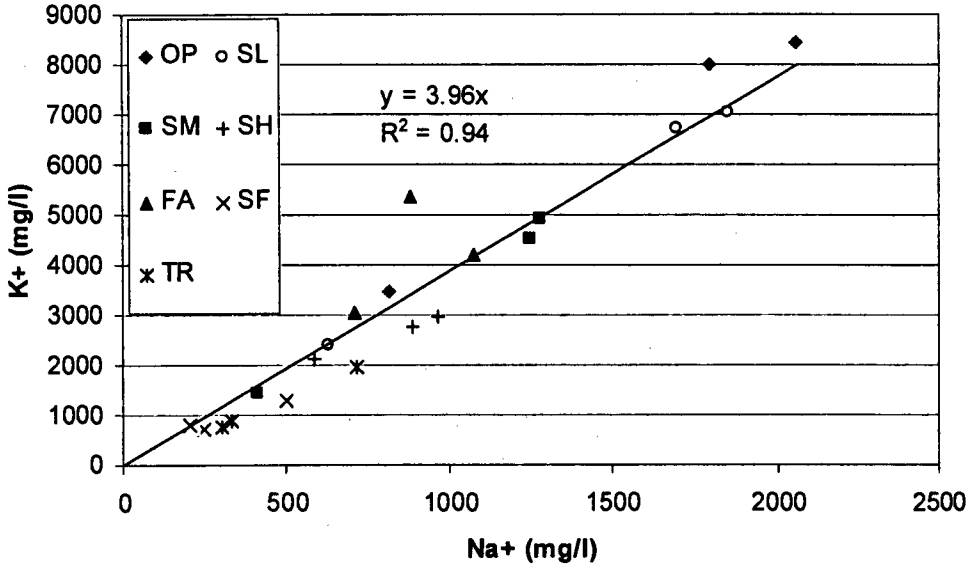

Fig 3.7: Relationship between K^+ and Na^+ for all samples

Page and Vennesland (1983) show similar Ca^{2+} levels of approximately 320 mg/l for a 20% SF cement mix with a corresponding hydroxyl concentration of 0.055 mol/l. The Ca^{2+} concentration, as shown in Table 3.5, of the non SF bearing samples decreased with time as the hydroxyl ion concentration increased. Similarly the Ca^{2+} concentration of SF bearing samples increased over the same period from 7 to 90 days as the hydroxyl ion concentration of the solution decreased. Though the value of 506 mg/l for Ca^{2+} is somewhat higher than reported elsewhere, it is consistent with the chemical behaviour of the pore solution. The calcium hydroxide contribution while almost irrelevant to non SF bearing samples represents a considerable contribution to the cation and thus hydroxide composition of both SF and TR pore solutions. Clearly in such cases the representation given by Duchensene and Berube

(1994[b]), $[Na^+]+[K^+]=[OH^-]$ should be rewritten as $[Na^+]+2[Ca^{2+}]+[K^+]\approx[OH^-]$ thus more correctly representing the true nature of the pore solution chemistry.

Two minor cations of Mg and Fe were also investigated. The results for Mg showed essentially background levels of less than 0.003 mg/l for all samples. The Fe concentrations for the 7, 28 and 90 days results are shown in Table 3.6. Generally, concentrations increased over the evaluation period for the non SF bearing samples while the SF bearing samples show a modest decrease in concentrations. The total Fe contribution for any of the samples was however low at < 5.1 mg/l or $9x10^{-5}$ M.

Table 3.6: Fe concentrations mg/l

Sample	*7 day*	*28 day*	*90 day*
PC	3.4	5.1	4.5
SL	1.7	2.8	4.0
SM	0.5	1.9	1.6
SH	0.2	1.1	1.2
FA	0.2	0.3	0.4
SF	2.9	1.8	1.7
TR	1.5	0.9	0.8

The various cations are not expected to significantly affect the overall corrosion processes of steel in concrete. The correlation between hydroxyl concentration and Na^+, K^+, and Ca^{2+} is important however if assumptions of the hydroxyl concentration are to be made purely on cation measurements. Fe concentrations have been shown in Figure 2.2 of chapter 2 to influence the shape of the Pourbaix diagram, particularly the potential and pH at which passivation or corrosion begins. For the normal case of steel in concrete (pH 12 - 14) there should be no effect from the variations in the Fe concentration measured here. Furthermore the Fe concentration of the solution around the rebar is likely to be quickly dominated by the dissolution of metal from the steel as opposed to the initial bulk solution properties. Thus the presence of the various cations should have a negligible impact upon the corrosion of steel in concrete, though they are indirectly relevant as they are necessary to maintain a charge balance with the anions, particularly OH^-.

3.3.3 Anion Measurements

The determination of the anions and their interaction between Redox potential and dissolved oxygen concentration represents some of the more interesting findings of the pore

solution investigation. The sulphate results are provided in Table 3.7 and generally show an increase from 7 to 90 days.

Table 3.7: SO_4^{2-} concentrations mg/l

Sample	*7 day*	*28 day*	*90 day*
PC	104	242	218
SL	56	110	210
SM	22	27	87
SH	17	15	45
FA	9	30	64
SF	NR	NR	NR
TR	NR	NR	4

The results for the concentration of sulphate ions are generally lower than those reported elsewhere such as Page and Vennesland (1983) who obtained 2,592 mg/l SO_4^{2-} for an OPC solution. Longuet (1976), while obtaining similar concentrations to the current investigation, has shown a decrease in sulphate levels from 5 hrs to 3 months with subsequent gains after 6 months.

The results of the sulphate ions are of particular interest when compared to the other sulphur species of sulphide and thiosulphate. The concentration of sulphate ions decreased substantially with addition of cement extenders and particularly where SF was employed. The SF and TR samples showed no detectable level of sulphates at any of the ages measured, except for 90 day TR.

When other reduced sulphur species are measured however, a somewhat different picture emerges. PC has generally been shown to contain little or no S^{2-} with Angus and Glasser (1985) showing no S^{2-} in 100% PC, no result at 25% slag replacement and only 12 ppm at 50% slag. The current investigation has revealed low S^{2-} and $S_2O_3^{2-}$ levels in PC with a substantial increase in both ions associated with 25, 50% and 75% slag replacement as shown in Table 3.8. The S^{2-} and $S_2O_3^{2-}$ levels found in PC pore solution are likely a result of the raw materials, particularly sulphur components found in the clay, which were used in the production process at that time.

Table 3.8: Concentrations of reducing sulphur species (mg/l)

	7 day			28 day			90 day		
Mix	S^{2-}	$S_2O_3^{2-}$	*Total S*	S^{2-}	$S_2O_3^{2-}$	*Total S*	S^{2-}	$S_2O_3^{2-}$	*Total S*
PC	3	14	11	7	15	16	2	22	15
SL	36	7	40	59	75	102	22	181	126
SM	41	16	50	49	99	106	25	63	61
SH	44	18	54	12	29	29	19	119	87
FA	2	0	2	7	12	14	1	8	6
SF	0	0	0	0	5	3	0	4	2
TR	17	12	24	8	10	14	4	16	13

The total reduced sulphur (*TRS*) concentrations, taken as S^{2-} plus the sulphur component of $S_2O_3^{2-}$, in the slag bearing samples was considerably higher despite the unhydrated slag having a slightly lower sulphur concentration of 1.1% compared to 1.3% for PC. The 25% slag showed an increasing *TRS* concentration over the entire period from 7 to 90 days, while the 50% slag peaked at 28 days before decreasing considerably at 90 days. The 75% slag had the highest early *TRS* concentration at 7 days but decreased somewhat at 28 days before increasing again at 90 days.

The variability in *TRS* concentrations over time seems to be consistent with the work of Longuet (1976). The lower sulphur concentrations of the SH samples however appears counter intuitive, but may be due to the lower pH and slower hydration mechanisms of the system thus limiting the release of new S^{2-} and $S_2O_3^{2-}$. The higher initial concentrations may have been partially oxidized and subsequent release of the sulphur species taken longer to develop.

The inclusion of FA and SF significantly limited the *TRS* concentration. though the difference between PC and FA at 28 days was small. While the pore solution chemistry of the ternary blends seems to be dominated by the SF component in most respects at later stages there was an appreciable component of reduced sulphur present in the 7 day samples, with lower levels comparable to PC at 28 and 90 days. The suppressed S^{2-} and $S_2O_3^{2-}$ concentrations in the ternary blend seems to support the role of hydroxyl ions in activating the slag component and thus the development of the pore solution sulphur chemistry. Further S^{2-} is only stabilized at pH greater than 12.9, below which HS^- is favoured and the eventual oxidation of the sulphur species to SO_4^{2-} (Faure, 1992). The kinetics of the oxidation of the reduced sulphur species to sulphate are also very interesting as there is a maximum

conversion rate around pH 8 before reducing to a minimum at pH 9 and then increasing again to a second maximum at pH 11. The oxidation rate then continues to decrease with increasing alkalinity of the solution (Chen and Morris, 1972). Thus the higher pH of SL solution is likely to retard the oxidation of sulphides and the lower pH of TR accelerate this process.

The high early age concentration of *TRS* in the TR samples is likely to result in the formation of a passive layer more characteristic of slag bearing materials than SF, despite having virtually identical hydroxide concentrations. The *TRS* concentration of TR is very similar to PC or FA at later stages but since the development of passivity occurs rapidly, lasting effects of high early age *TRS* concentrations are likely despite lower subsequent levels. The combination of low hydroxide concentration with a defective passive layer should seriously limit the effectiveness of steel in TR pore solutions to resist attack from chloride ions. These effects will be shown in chapter 4 on the corrosion of steel in simulated pore solutions.

3.3.4 Redox Potential and Dissolved Oxygen

The redox potential and dissolved oxygen concentrations appear closely related to the sulphides and thiosulphates in the pore solution. As seen in Table 3.9 the highly negative redox values are found in those samples containing the highest reduced sulphur levels. as expected. The redox potential is also shown to vary with dissolved oxygen (DO) content and presence of reduced sulphur species.

It can be seen that the redox potential decreased markedly with a reduction in oxygen content and increased sulphide concentration of the PC samples from 7 to 28 days. It should be noted that there is not an appreciable difference in dissolved oxygen concentration between 0.06 and 0.1 mg/l, in the case of SL, SM or TR 7 day and 28 day results, and given the accuracy of measurement devices no real distinctions should be drawn. The SL, SM and SH samples all showed low DO levels of approximately 0.10 mg/l at 90 days with the TR increasing slightly to 0.40 mg/l. The increase in DO from 7 to 28 days in the SH accords well with the *TRS* concentrations and redox potential. The 28 day results had the highest oxygen content coupled with the lowest *TRS* readings for period of study. The slag bearing samples, at any replacement, show more negative potentials and lower DO concentrations than those samples without slag.

Table 3.9: Redox (mV) and DO levels (mg/l)

Sample	*7 day*	*28 day*	*90 day*
PC Redox	-289	-419	-346
D.O.	2.20	0.14	2.10
SL Redox	-545	-610	-594
D.O.	0.09	0.10	0.11
SM Redox	-554	-527	-585
D.O.	0.06	0.10	0.10
SH Redox	-460	-448	-465
D.O.	0.10	0.44	0.10
FA Redox	-297	-427	-374
D.O.	2.24	1.40	3.17
SF Redox	-171	-185	-200
D.O.	2.75	3.40	3.70
TR Redox	-430	-422	-395
D.O.	0.09	0.10	0.40

The relationship between *TRS* concentration and dissolved oxygen at 90 days can be seen graphically in Figure 3.8.

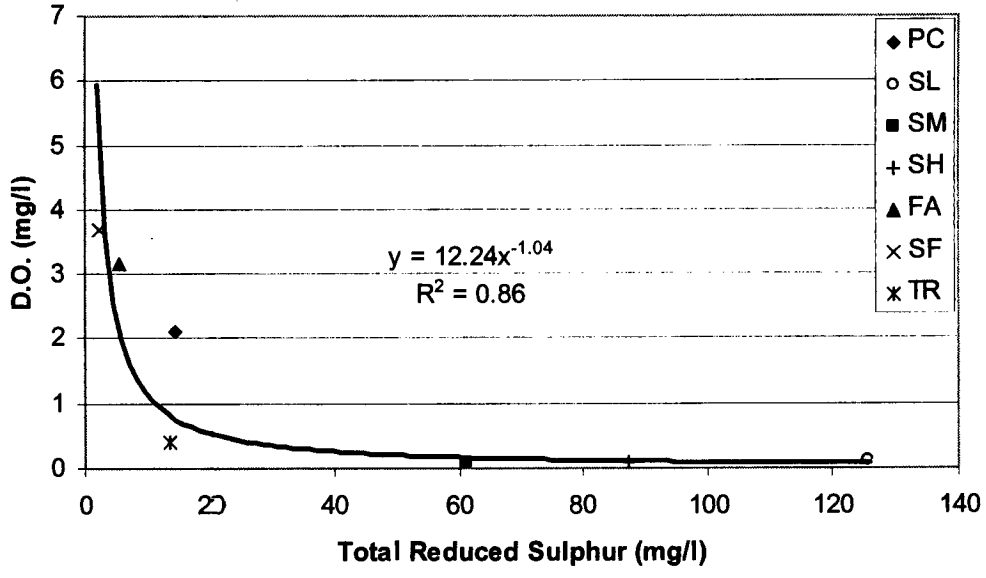

Fig 3.8: Relationship between D.O. and total reduced sulphur for 90 day results

It is not the objective of the current investigation to provide a definitive relationship between DO and *TRS* concentration in the pore solution, but rather to investigate corrosion rates of steel in concrete associated with the inclusion of various cement extenders. The relationship

between DO and *TRS* found in this work is:

$$DO = 12.24 TRS^{-1.04} \quad \ldots 3.2$$

where: *TRS* is the total reduced sulphur species (mg/l) and *DO* is the dissolved oxygen concentration (mg/l).

The relationship provides reasonable correlation with a correlation coefficient of 0.85.

From the results it is perhaps better said that for a *TRS* concentration above approximately 60 mg/l the DO of the solution is minimal. Further research would be required to more accurately define this relationship but it is sufficient for the current investigation to state that the presence of high levels of *TRS* is associated with a depletion of the oxygen in the pore solution. Again the likely cause of this depletion of oxygen is the conversion of the sulphides and thiosulphate to sulphate. The lower redox potential and particularly DO concentrations associated with slag bearing materials may have a significant effect on the development of the passive layer of steel in concrete. The low DO levels, associated with the slag bearing pore solution, may inhibit the formation of an effective passive layer resulting in a somewhat higher corrosion rate even under passive conditions. The maximum possible corrosion rate would however be limited by the level of DO. While the measured corrosion rate of steel in a DO limited solutions might be higher than steel in a solution with a high DO level, the maximum possible corrosion rate would likely be reduced as the availability of oxygen would effectively result in a cathodically controlled limiting current density.

A lower level of chlorides may also be required to initiate corrosion due to a comprised passive layer thus leading to premature active or pitting corrosion compared to non-sulphide bearing materials. Furthermore the presences of sulphides in their own will result in some changes to the passive layer with their possible inclusion as FeS in the passive layer. Site of sulphides in the passive layer may limit its effectiveness in protecting the steel against chlorides. There is clearly a need therefore to investigate the effects of variations in the pore solution chemistry on the stability of the passive layer of steel and ultimately the corrosion rates of steel in both the aqueous phase and more representative cast concrete samples.

3.4 Chapter Summary

The study of the composition of the pore solution of the different binder types under investigation is the first step in investigating the influence of cement extenders on the corrosion of steel in concrete. The specific materials used in this investigation must be characterized and their effects on the physical and in this chapter chemical component of the

overall concrete determined. There has been considerable work done in the analysis of pore solution of various binder types. The literature generally shows that the inclusion of cement extenders results in a progressive reduction of the hydroxyl ion concentration with increasing replacement levels. SF was shown to be the most effective in reducing the hydroxyl ion concentration.

The results from current work show that hydroxyl ion concentration in the order from highest to lowest at 28 and 90 days: PC > SL > SM > FA > SH > TR ≈ SF. The seven day results for all the samples were generally fairly similar, 0.064 to 0.133 mol/l, but changed quite markedly with time. SM in particular went from having the lowest hydroxyl concentration at 7 days to the third highest at 28 ad 90 days, resulting in over a 3 fold increase.

The sulphur chemistry of the pore solution and the influence of various binder types is more uncertain. In an investigation of pore solution composition over time, Longuet (1976) showed considerable variability in the concentration of sulphide ions with no discernable trend for 76% replacement by slag. There also appeared to be fairly little correlation between redox potential and sulphide concentration though at no point did the PC samples show negative potentials whereas the slag bearing materials generally showed negative redox potentials. The results from the seven mixes investigated in this chapter seem to verify the lack of consistent trend with respect to sulphide concentrations over time. The sulphide levels for SL increased from 7 to 28 days before declining at 90 days. The thiosulphate concentrations generally showed an increase in concentration with time which would be expected if sulphides were being oxidized to thiosulphate.

The 75% break-point for the replacement level of slag affecting sulphur chemistry, as suggested by Angus and Glasser (1985) was not observed with the materials used in this investigation. Redox potentials more than 200 mv negative to PC were observed for 25% replacement by slag. At 7 days SH showed the highest sulphide level but at 28 days the SL was found to have the greatest concentration of sulphides. PC was also found to have low levels of both sulphides and thiosulphate with only SF having zero mg/l of sulphides over the study period. The inclusion of slag at replacement levels between 25 and 75% therefore results in elevated levels of sulphides and thiosulphate causing a reducing environment in the pore solution. Very low dissolved oxygen levels were also found in any of the slag bearing materials.

A comparison of TR and SF shows that the slags dominated the early age process around 7 days while SF appeared to expert more control over the later stages. The 28 and 90 day

hydroxyl concentrations were virtually identical for SF and TR. TR showed a reasonable concentration of sulphides 7 days but these decreased quite markedly at 28 and 90 days. The suppressed hydroxyl concentrations likely resulted in the rapid oxidation of sulphides to thiosulphate and sulphate. Both the redox potential and dissolved oxygen level slowely shifted levels from those indicative of slag bearing materials to those more representative of SF.

The reduced hydroxyl concentration of the cement extenders is likely to limit their ability to protect the steel in the presence of chloride ions. The effects of limited DO coupled with high levels of sulphides found with slag bearing materials is likely to further weaken the passive layer around the steel and may result in lower chloride threshold levels and elevated corrosion rates. The effects of the pore solution chemistry on the corrosion of steel will be shown in the following chapter where steel was placed in simulated pore solutions as determined from the work discussed in this chapter.

3.5 Appendices

3A Oxide content and mineralogy of binder type

Oxide	*PC*	*Slag*	*FA*	*SF*	*Mineralogy (OPC)*	*%*
SiO_2	21.5	35.7	53.1	91.9	C_3S	74.7
CaO	65.9	34.3	4.2	0.0	C_2S	5.3
Al_2O_3	3.7	13.6	33.7	0.7	C_3A	3.8
Fe_2O_3	3.6	0.7	3.6	0.8	C_4AF	10.9
Mn_2O_3	0.06	1.10	0.05	0.09		
TiO_2	0.18	0.60	1.77	0.11		
MgO	0.88	10.20	1.02	0.26		
SO_3	3.28	2.86	0.30	0.46		
K_2O	0.54	0.80	0.75	1.33		
Na_2O	0.19	0.20	0.40	0.42		

3B Determination of Sulphide Concentrations using Cline Solution

The sulphide concentrations of the expressed pore water where determined through a variation on colorimetric methylene blue method as described in standard methods (Eaton et al 1995). The general approach involves measuring the absorbance of light, at a given wave length, through a sample which is then correlated to a set of known standards. There is a range of wave lengths from 644 nm (Truper and Schlegel, 1964), 663nm (Plas et al., 1992), 664 nm (Eaton et al., 1995), to 670 nm (Cline 1969) which have been used to measure the absorbance of methylene blue.

The reactions are given by Truper and Schlegel (1964) as:

$$2(\text{dimethyl} - \text{p} - \text{phenylenediamine}) + S^{2-} \rightarrow 1(\text{leuco} - \text{methylene blue})$$
$$(\text{leuco} - \text{methylene blue}) + Fe^{3+} \rightarrow (\text{methylene blue}) + Fe^{2+} \quad \ldots 3B.1$$

The sulphides are incorporated into the methylene blue stiochiometrically thus the correlation between colour development and sulphide concentration.

There are however a number of interferences which may limit colour development. Thiosulphate concentrations above 10 mg/l are known to either retard colour formation or prevenet the reaction completely. Similarly sulphide itself may limit the reaction if the concentrations are high enough. Interferences from thiosulphate, sulphite and many other soluble substances can be accomplished through precipitating the sulphide as ZnS in a solution of Zn acetate, removing the supernatant and replacing it with distilled water (Eaton et al., 1995). The precipitation of the sulphides by Zn acetate also stabilized the samples until they could be analyzed.

3B.1 Reagents

0.01M Zn acetate

20 g of Zn acetate•$2H_20$ and 0.2 ml acetic acid made up to 1000 ml with distilled water, (Plas et al. 1992).

Cline Solution

Dissolve 2 g of *N,N*-dimethylene-*p*-phenylenediamine sulphate and 3 g of $FeCl_3$•$6H_2O$ in 500 ml of 50 %, by volume, hydrochloric acid (Cline 1969).

Sulphide standards

Sulphide standards were generally prepared according to Eaton et al (1995), but using 541 mg of Na_2S•$9H_2O$ in 1 l of de-aerated water which produced as a stock solution containing 72

mg/l of S^{2-}. The solutions were further diluted to produce 7.2 mg/l and 0.72 mg/l of S^{2-} standards.

3B.2 Method

Vessels with a capacity of approximately 55 ml were filled with 10 ml of Zn acetate. After the pore water from the paste samples was extracted and filtered 5 ml of sample were added to the vessels. The samples were then filtered through a 45 μm membrane. The substrate was retained and returned to the vessels and made up to 50 ml through addition of distilled water. 4 ml of the diamine reagent was added to the vessel and mixed gently to limit volatilization of the hydrogen sulphide (Cline 1969). The absorbance was measured with a Biochrom Novaspec II spectrophotometer at a wave length of 665 nm. The absorbance measurements were then recorded once they had stabilized which generally occurred after the first few minutes.

3B.3 Calibration curve for S^{2-}

As previously noted sulphide standard were prepared for correlating known sulphide concentrations with measured absorbances. The sulphide concentrations for the 50 ml samples and corresponding absorbances are given in Table 3B.1 and Figure 3B.1.

Table 3B.1 Absorbance vs. S^{2-} Concentration

S^{2-} Concentration mg/l	*Absorbance λ = 665 nm*
7.20	2.876
3.60	2.025
1.44	0.924
0.72	0.518
0.14	0.118
0.072	0.064

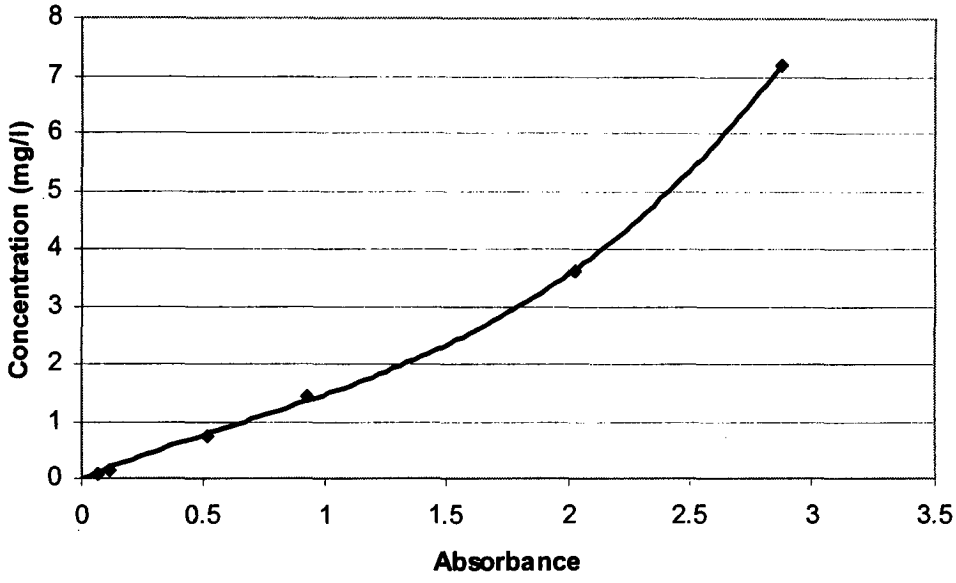

Fig 3B.1: Sulphide calibration curve for methylene blue absorbance ($\lambda = 665$ nm)

The calibration curve indicates a generally linear relationship between concentration and absorbance up to a concentration of approximately 3.6 mg/l where upon substantial deviation occurs. The equation of the line is taken as (with a correlation coefficient of 0.999):

$$c = 0.276a^3 - 0.52a^2 + 1.712a \qquad \ldots 3B.2$$

where c - sulphide concentration in mg/l, and a - absorbance measured at $\lambda = 665$ nm.

Values above 3.6 mg/l may note therefore be entirely accurate but should still provide a reasonable approximation of the likely occurrence of sulphide.

3C Determination of Thiosulphate Concentrations

The thiosulphate concentration of the pore water was obtained through determination of the 'total' sulphur component, excluding sulphate, less the sulphide contribution. It was assumed that the primary sulphur components which may be present included: sulphate, thiosulphate and sulphide. Other various sulphur ions may also exist but are not expected in appreciable quantities. A variation on the colourometric method, as developed by Nor and Tabatabai (1976), was used for the determination of total sulphur. The original method was developed for the determination of thiosulphate, but it appears to be affected by the presence of sulphides which further increases the absorbance of the sample.

The reactions for thiosulphate are described as follows (Nor and Tabatabai, 1976):

$$S_2O_3^{2-} + CN^- \xrightarrow{Cu^{2+}} SO_3^{2-} + SCN^-$$
$$SCN^- + Fe^{3+} \rightarrow Fe \bullet SCN \text{ complex} \qquad \ldots 3C.1$$

The inclusion of sulphide S^{2-} also results in increased absorbance measurements which would indicate a further reaction to form Fe•SCN complex.

3C.1 Reagents

0.1M Lithium Chloride

4.2 g of LiCl dissolved in distilled water made up to 1 liter.

0.1M Potassium Cyanide

6.51 g of KCN in distilled water made to 1 liter.

0.033M Cupric Chloride

5.63 g of $CuCl_2 \cdot 2H_2O$ in distilled water made to 1 liter.

0.25M Ferric nitrate-nitric acid

Dissolve 50 g $Fe(NO_3)_3 \cdot 9H_2O$ in 100 ml of concentrated HNO_3 made to 500 ml with distilled water.

3C.2 Method

A volumetric flask of 25 ml was filled with 5 ml filtered of sample. 1 ml of 0.1M KCN solution was then added and swirled to ensure adequate mixing. After 15 minutes 2 ml of 0.033M $CuCl_2$ and 1ml of $Fe(HNO_3)_3$-HNO_3 was then added. The sample was inverted several times and left to stand for 1 minute. The absorbance of the ferric thiocyanate complex was then measured at a wave length of 460 nm using the Biochrom Novaspec II spectrophotometer (Nor and Tabatabai 1976). The measured absorbance is then compared to

the calibration curves for the standard solutions and the quantity of thiosulphate determined. As previously noted colour development was affected by the presence of sulphide ions thus the measured values include both thiosulphate and sulphide which must be subtracted to determine the actual thiosulphate component. The inclusion of sulphate ions was shown to have no effect on the colour development.

Colour instability has been noted by Nor and Tabatabai (1976) who state the colour remains stable under dark condition for up to 2 hours but fades slowly in laboratory light. In the current investigation fairly rapid initial colour loss was observed under more alkaline conditions as would be expected in the concrete pore water. The absorbance decreased quickly over the first few minutes but generally stabilized prior to 5 minutes at a pH of approximately 13. Measurements were therefore recorded once the colour development had stabilized but no later than 5 minutes.

Initial attempts were made to measure the thiosulphate concentrations after the sulphide was precipitated as ZnS and removed. The measured absorbances however were not consistent and the remaining Zn acetate probably interfered with the formation of the ferric thiocyanate complex. Thus this approach had to be abandoned.

3C.3 Calibration curve for $S_2O_3^{2-}$

Fairly good calibration where obtained for thiosulphate standards made with LiCl solutions as described by Nor and Tabatabai (1976). The pore solution of concrete however generally has a pH in the range of 12.5 to 13.5. The colour development was significantly retarded by the increase in pH. New standards therefore were required which accounted for increased in pH. At a pH range between 12.5 and 13.5 little difference in the measured absorbance was observed, thus one set of standards would be sufficient for the various samples under investigation. As previously noted there was also an initial rapid loss of colour, measurements were taken once a more stable reading was observed or prior to 5 minutes after mixing.

Separate calibration curves at pH 13 were developed for $S_2O_3^{2-}$, S^{2-} and combined $S_2O_3^{2-}$:S^{2-}. Good correlation coefficients ($R^2 \approx 0.99$) were observed with the standard curves for the isolated sulphur ions in addition to the combined standards. The combined or 'total' S, expressed as the quantity of S^{2-} (μg) plus the sulphur component of $S_2O_3^{2-}$ (μg), calibration curve was bounded by $S_2O_3^{2-}$and S^{2-} curves as shown in Figure 3C.1.

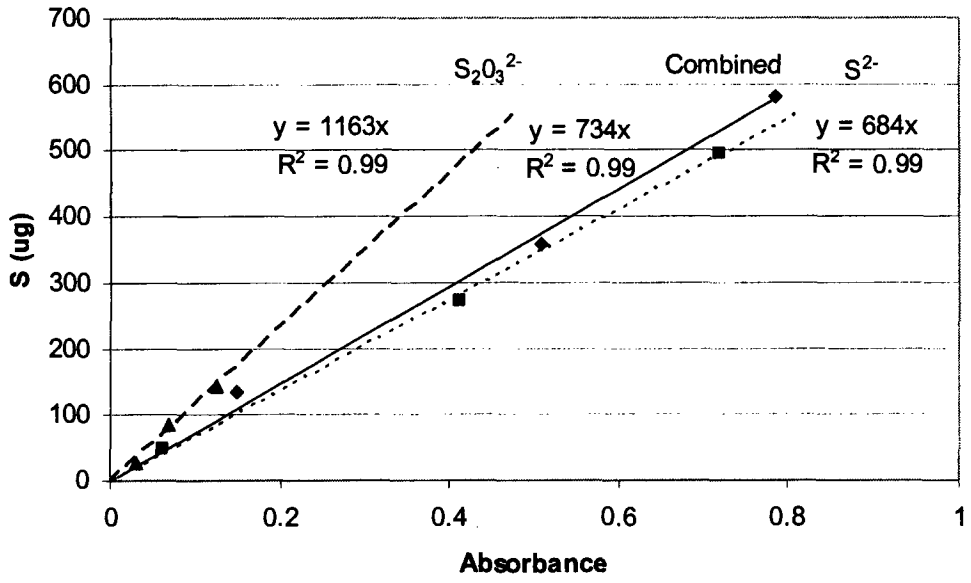

Fig 3C.1: Total reduced sulphur calibration curve for ferric thiocyanate complex (λ = 460 nm)

The accuracy of the method for determining total S and hence $S_2O_3^{2-}$ may be somewhat reduced at high $S_2O_3^{2-}/S^2$ ratios. The method does however provide for a reasonable estimate of $S_2O_3^{2-}$ and ability to distinguish between high and low concentrations of the substance among various samples. The relationship between absorbance and total S content is given as:

$$s = 734a \qquad \ldots 3C.2$$

where s is the total measured sulphur species components in μg and a is the measured absorbance at λ = 460 nm. The results from the colorimetric method generally agree moderately well with those from Ionic Chromotography so use of the method to provide approximate $S_2O_3^{2-}$ concentrations appears valid.

Sample	pH	OH^- mol	Conduc (mS/cm)	Redox (mv)	D.O. (mg/l)	Na mg/l	Ca mg/l	K mg/l	Mg mg/l	Fe mg/l	SO_4^{2-} mg/l	S^{2-} mg/l	$S_2O_3^{2-}$ mg/l	Total S mg/l
PC 7D	13.2	0.1331	28.1	-289	2.20	812	56	3486	<0.003	3.4	104	3	14	11
PC 28D	13.6	0.2905	59.1	-419	0.14	1796	61	8006	<0.003	5.1	242	7	15	16
PC 90D	13.6	0.3155	64.3	-346	2.10	2057	40	8449	<0.003	4.5	218	2	22	15
SL 7D	13.1	0.0964	20.5	-545	0.09	626	53	2382	<0.003	1.7	56	36	7	40
SL 28D	13.5	0.2575	51.9	-610	0.10	1693	57	6738	<0.003	2.8	110	59	75	102
SL 90D	13.5	0.2723	54.6	-594	0.11	1846	23	7038	<0.003	4.0	210	22	181	126
SM 7D	12.9	0.0640	13.5	-554	0.06	412	153	1443	<0.003	0.5	22	41	16	50
SM 28D	13.4	0.1967	39.3	-527	0.10	1279	47	4924	<0.003	1.9	27	49	99	106
SM 90D	13.3	0.1935	37.6	-585	0.10	1245	29	4538	<0.003	1.6	87	25	63	61
SH 7D	13.0	0.0892	18.5	-460	0.10	586	117	2110	<0.003	0.2	17	44	18	54
SH 28D	13.2	0.1343	26.0	-448	0.44	965	22	2976	<0.003	1.1	15	12	29	29
SH 90D	13.1	0.1226	23.3	-465	0.10	882	10	2742	<0.003	1.2	45	19	119	87
FA 7D	13.0	0.1183	25.0	-297	2.24	704	152	3028	<0.003	0.2	9	2	0	2
FA 28D	13.3	0.1942	40.6	-427	1.40	881	87	5364	<0.003	0.3	30	7	12	14
FA 90D	13.2	0.1642	33.6	-374	3.17	1073	24	4195	<0.003	0.4	64	1	8	6
SF 7D	12.9	0.0701	14.2	-171	2.75	499	223	1267	<0.003	2.9	NR	0	0	0
SF 28D	12.8	0.0594	11.2	-185	3.40	246	460	706	<0.003	1.8	NR	0	5	3
SF 90D	12.8	0.0633	11.8	-200	3.70	202	506	788	<0.003	1.7	NR	0	4	2
TR 7D	13.0	0.0978	19.7	-430	0.09	714	192	1970	<0.003	1.5	NR	17	12	24
TR 28D	12.8	0.0635	11.3	-422	0.10	331	345	886	<0.003	0.9	NR	8	10	14
TR 90D	12.8	0.0637	10.3	-395	0.40	301	347	772	<0.003	0.8	4	4	16	13

Note: 1) NR represents SO_4 values below detection limits 2) pH has been adjusted to 20 deg C

3) Total S refers to combined measurement of S^{2-} and the sulphur component of $S_2O_3^{2-}$

3.6 References

Andrade, C. and Page, C. 1986, *Pore Solution Chemistry and Corrosion in Hyrdated Cement Systems Containing Chloride Salts: A Study of Cation Specific Effects*, **British Corrosion Journal**, Vol. 21, No. 1, pp 49-53.

Angus, M. and Glasser, F. 1985, *The Chemical Environment in Cement Matrices*, **Materials Research Society Symposium Proceedings**, Vol. 50, pp. 547-556.

Barneyback, R. and Diamond, S. 1981, *Expression and Analysis of Pore Fluid from Hardened Cement Pastes and Mortars*, **Cement and Concrete Research**, Vol. 11, pp. 279-285.

Benjamin, S. and Sykes, J. 19889, *Chloride-Induced Pitting of Swedish Iron in Ordinary Portland Cement Mortars and Alkaline Solutions: The Effect of Temperature*, **Corrosion of Reinforcement in Concrete: Page, C. Treadaway, K. and Bamforth, P. ed.**, Elsevier Applied Sciences: London, pp. 59-64.

Breit, W. 1998, *Corrosion of Steel in Concrete: The Question of Corrosion Initiated by the Critical Chloride Content*, **Betonwerk + Fertigteil-Technik**, Vol. 11, pp. 37-45.

Burstein, G. and Ilevbare, G. 1996, *The Effect of Specimen Size on the Measured Pitting Potential of Stainless Steel*, **Corrosion Science**, Vol. 38, No. 12, pp. 2257-2265.

Byfors, K., Hansson, C. and Tritthart, J. 1986, *Pore Solution Expression as a Method to Determine the Influence of Mineral Additives on Chloride Binding*, **Cement and Concrete Research**, Vol. 16, pp. 760-770.

Cao, H., Baweja, D. and Roper, H. 1990, *Corrosion Characteristics of Steel in Solutions Derived from Cements and Blended Cements*, **Cement and Concrete Research**, Vol. 20, pp. 325-334.

Chen, K. and Morris, J. 1972, *Kinetics of Oxidation of Aqueous Sulfide by O_2*, **Environmental Science and Technology**, Vol. 6, No. 6, pp. 529-537.

Cline, J. 1969, *Spectrophotometric Determination of Hydrogen Sulphide in Natural Waters*, **Limnology and Oceanography**, Vol. 14, pp. 454-458.

Constantiner, D. and Diamond, S. 1997, *3: Pore Solution Analysis: Are there Pressure Effects?*, **Mechanisms of Chemical Degradation of Cement-based Systems Ed. Scrivener, K. and Young, J.**, E & FN Spon, London, pp. 22-29.

Cromie, J., Abu-Tair, A., Lyness, F. and McFarland, B. 2002, *The Extraction of Pore Fluid from Concrete using a Heavy Liquid Extraction Method*, **Magazine of Concrete Research**, Vol. 54, No. 1, pp. 1-5.

Duchesne, J. and Berube, M. 1994[a], *Evaluation of the Validity of the Pore Solution Expression Method from Hardened Cement Pastes and Mortars*, **Cement and Concrete Research**, Vol. 24, No. 3, pp. 456-462.

Duchesne, J. and Berube, M. 1994[b], *The Effectiveness of Supplementary Cementing Materials in Suppressing Expansion due to ASR: Another Look at the Reaction Mechanisms Part 2: Pore Solution Chemistry*, **Cement and Concrete Research**, Vol. 24, No. 2, pp. 221-230.

Eaton, A., Clesceri, L. and Greenberg, A. ed. 1995, **Standard Methods for the Examination of Water and Wastewater 19th Edition**, United Book Press Inc: Maryland, pp. 4-122 to 4-125.

Faure, G. 1992, **Principles and Applications of Inorganic Geochemistry**, Macmillan Publishing Company: New York, pp. 332-338.

Glasser, F. 2003, *The Pore Fluid in Portland Cement: Its Composition and Role*, **Proceedings of the 11th International Congress on the Chemistry of Cement (ICCC), South Africa**, The Cement and Concrete Institute of South Africa, pp. 19-30.

Glasser, F., Luke, K. and Angus, M. 1988, *Modification of Cement Pore Fluid Compositions by Pozzolanic Additives*, **Cement and Concrete Research**, Vol. 18, pp. 165-178.

Gouda, V. 1970, *Corrosion and Corrosion Inhibition of Reinforcing Steel I: Immersed in Alkaline Solutions*, **British Corrosion Journal**, Vol. 5, pp. 198-203.

Hausmann, D. 1967, *Steel Corrosion in Concrete, How Does it Work?* **Materials Protection**, November, pp. 19-23.

Hinczak, H., Cao, H. and Cook, D. 1989, *Anodic Behavior of Steel in Solutions of Slag Blended Cements, Durability of Concrete, Aspects of Admixtures and Industrial by-Products*, **2nd Internation Seminar**, Swedish Council for Building Research, pp. 63-76.

Loewenthal, D., Ekama, G. and Marais, G. 1989, *Mixed Weak Acid/Base Systems, Part 1: Mixture Characteristics*, **Water SA**, Vol. 15, No. 1, pp. 3-24.

Longuet, P. 1976, *La Protection des Armatures dans le Beton Arme Elabore avec des Ciments de Laitier*, **Silicates Industriels**, Vol. 7, pp. 321-328.

Macphee, D. and Cao, H. 1993, *Theoretical Description of Impact of Blast Furnace Slag (BFS) on Steel Passivation in Concrete*, **Magazine of Concrete Research**, Vol. 45, No. 162, pp. 63-69.

Mammoliti, L., Brown. L., Hansson, C. and Hope, B. 1996, *The Influence of Surface Finish of Reinforcing Steel and pH of the Test Solution on the Chloride Threshold Concentration for Corrosion Initiation in Synthetic Pore Solution*, **Cement and Concrete Research**, Vol. 26, No. 4, pp. 545-550.

Morgan, T. 1990, *Some Comments on Reinforcement Corrosion in Stagnating Saline Environments*, **Corrosion of Reinforcement in Concrete: Page, C. Treadaway, K. and Bamforth, P. ed.**, Elsevier Applied Sciences: London, pp. 29-38.

Nor, Y. and Tabatabai, A. 1976, *Extraction and Colourometric Determination of Thiosulphate and Tetrathionate in Soils*, **Soil Science**, Vol. 122, No. 3, pp. 171-178.

Page, C. and Vennesland, O. 1983, *Pore Solution Composition and Chloride Binding Capacity of Silica-Fume Cement Pastes*, **Materials and Construction**, Vol. 16, No. 91, pp. 19-25.

Plas, C., Harant, H., Danner, H., Jelinek, E., Wimmer, K., Holubar, P., and Braun, R. 1992, *Ratio of Biological and Chemical Oxidation during the Aerobic Elimination of Sulphide by Colourless Sulphur Bacteria*, **Applied Microbiology and Biochemistry**, Spring, pp. 817-822

Tritthart, J. 1990, *Pore Solution Composition and other Factors Influencing the Corrosion Risk of Reinforcement in Concrete*, **Corrosion of Reinforcement in Concrete: Page, C. Treadaway, K. and Bamforth, P. ed.**, Elsevier Applied Sciences: London, pp. 96-106.

Truper, H. and Schlegel, H. 1964, *Sulphur Metabolism in Thiorhodacea, Quantitative Measurements on Growing Cells of Chromatium Okenii*, **Antonie van Leeuwenhoek**, Vol. 30, pp. 225-238.

Tuutti, K., **Corrosion of Steel in Concrete**, Swedish Cement and Concreter Research Institute: Stockholm, 1982, pp. 288.

Vernet, C. 1982, *Comportement de l'ion S^{2-} au Cours de l'hydration des Ciments Riches en Laitier (CLK)*, **Silicates Industriels**, No. 3, pp. 85-89.

Wheat, H., Kasthurirangan, J., and Kitowski, C. 1997, *17: Behaviour of Steel in Simulated Concrete Solutions*, **Mechanisms of Chemical Degradation of Cement-based Systems: Scrivener, K. and Young, J. ed.**, E & FN Spon: London. pp. 143-150.

Yonezawa, T., Ashworth, V. and Procter, R. 1988, *Pore Solution Composition and Chloride Effects on the Corrosion of Steel in Concrete*, **Corrosion Engineering**, Vol. 44, No. 7, pp. 489-499.

CHAPTER 4: AQUEOUS PHASE CORROSION OF STEEL IN SIMULATED PORE SOLUTIONS

In the preceding section, it was shown that there is considerable variability in the chemical composition of the pore solutions of pastes made using various cement extenders at different replacement levels and with time. Variation in the major cations such as Na^+, K^+ and Ca^{2+} are unlikely to have any significant impact upon the development of the passive layer around the steel or subsequently influence the corrosion rate of steel once initiation has occurred. The effects of the anions such S^{2-} and $S_2O_3^{2-}$ are the subject of some debate, as noted in section 2.9. As seen in the study of pore solution composition, these anions may be present in both PC pastes and pastes made with cement extenders, particularly slags. The considerable differences in hydroxyl concentration will also have a marked effect on the stability of the passive layer and influence corrosion threshold levels with respect to chlorides, as well as corrosion rates. The study of corrosion of steel in the aqueous phase is valuable in investigating the chemical influences of the materials since the environment can be more precisely controlled compared to steel in mortars or concretes. The effects of specific variables can therefore be assessed with greater confidence. Furthermore the aqueous phase testing has enhanced our understanding of the nature of South African materials and allowed for the development of a data base for future investigation and comparisons.

Gouda (1970) investigated the influence of hydroxide concentration on the corrosion of steel for NaOH solutions with pH of 10.2, 11.5, 12.1, and 12.6 and $Ca(OH)_2$ solutions of pH 12.1. The results indicated that steel remained passive at a pH of 12.1 or greater for both the NaOH and $Ca(OH)_2$ solutions. Steel in the pH 10.2 solution displayed rusting within the first day and that exposed to pH 11.5 remained passive for the first two days, after which time corrosion initiated. Further anodic polarization results indicated the breakdown of passivity in the samples with pH of 10.2 and 11.5, but no similar breakdown at a pH of 11.75 or above. Thus hydroxyl concentrations with a pH of 11.75 or greater would ensure passivity of steel. There was little difference arising from the sources of the hydroxides.

The role of chlorides and sulphides in promoting corrosion of steel in aqueous environments was discussed in sections 2.8 and 2.9 respectively. It is now possible to examine in more detail and with particular attention to the nature of the aqueous phase of concrete, the role of these ions in promoting or controlling the corrosion of steel.

4.1 Chloride Threshold Values for Initiation – A Literature Survey

Much of the early work on corrosion rates and chloride threshold levels for reinforced concrete focused on steel in the aqueous environment and was a natural extension of other corrosion studies. Hausmann (1967) investigated the corrosion of bare steel bars in simulated pore solutions ranging in pH from 11.6 to 13.2. The bars were cleaned and burnished to bright steel. A cement paste cylinder was cast around the steel at the air/water interface to prevent corrosion at that point. The bars were embedded in gravel with oxygen diffused through so as to ensure the presence of free oxygen against the steel surface. Samples were also investigated where no free oxygen was available. Chlorides were mixed into pore solution at the time of preparation, thus the development of the passive layer would be impeded almost immediately. In practice the passive layer generally has a chance to form and develop before chlorides reach the steel.

The initiation of corrosion was determined by potential measurements only. Passive potentials were considered to be in the range of -100 to -200 mV relative to a saturated calomel electrode (SCE). Actively corroding samples generally showed potentials more negative than -400 mV. Some of the results of chloride content for the initiation of corrosion are provided in Table 4.1.

Table 4.1: Chloride threshold values (Hausmann, 1967)

Source of Alkalinity	*pH*	*NaCl (mol/l)*	*Cl/OH ratio*
NaOH	11.60	0.002	0.50
	11.60	0.003	0.75
	11.60	0.005	-
$Ca(OH)_2$	12.40	0.020	0.61
saturated	12.38	0.025	0.79
	12.37	0.030	0.98
	12.33	0.040	1.08
NaOH	13.20	0.250	0.83

The results indicate a Cl/OH ratio in the range of 0.50 to 1.08 for the onset of corrosion. There was little difference in Cl/OH ratio requirement between the sources of alkalinity, though there appeared to be some scatter for the saturated calcium hydroxide solutions. The availability of free oxygen was shown to have no effect on the potential of un-corroded bare steel, *ceteris paribus*. In the case of saturated calcium hydroxide with free oxygen, a chloride threshold of 700 ppm (approximately mol/l) was observed, while in the absence of free

oxygen the required chloride concentration was significantly higher. Thus the availability of free oxygen trapped against the steel resulted in a substantial decrease in the chloride threshold level. Since the presence of a void on the surface of the steel (in this case caused by the oxygen bubble) would impede the formation of the passive layer, it is reasonable that a lower chloride threshold would be required. If the void were formed by other means, the same result may be observed. Thus the lowering of the chloride threshold, as observed by Hausmann may not be a result of the presence of oxygen so much as the presence of voids on the steel surface.

Gouda (1970), having determined that steel is passivated in solutions of pH 11.75 or greater, proceeded to investigated the influence of chloride content on depassivation of steel at a range of pH starting from 11.75. Steel rods of diameter ¼ inch were polished, degreased and pickled in 50% wt. HCl prior to testing. Anodic polarization results were measured over time against a SCE at a constant current density. Sodium, calcium and potassium hydroxides were investigated and no relationship was observed between the type of cation and breakdown in passivity due to chloride ions. No corrosion was observed for sodium chloride concentrations of 0.01, 0.04 and 0.08% for pH of 11.75, 12.1 and 12.6 respectively. A log linear relationship was determined between the required chloride content to initiate corrosion and hydroxyl content, which is valid over a pH range from 11.75 to approximately 13.5, according to (Gouda 1970):

$$pH = n \log C_{Cl^-} + k \qquad \ldots 4.1$$

where n and k are constants and C_{Cl^-} is the concentration of chloride ions. According to Yonezawa et al. (1988), equation 4.1 can be rewritten as:

$$\log[Cl^-] = 0.81 \log[OH^-] - 0.65 \qquad \ldots 4.2$$

From equation 4.2 the critical Cl/OH ratios range from 0.6 for pH 11.75 to 0.3 for pH 13.3. The results from Gouda (1970) therefore are not substantially different from those of Hausmann (1967).

Anodic polarization curves, similar to those shown in section 2.8, have been developed for steel rebar in saturated $Ca(OH)_2$, pH 12.5 with various additions of Cl^- (Morgan 1990). The anodic polarization curves for both oxygenated and deaerated solutions are shown in Figure 4.1. The result of the addition of chloride ions, as previously shown in section 2.8, is to lower the pitting potential and hence transpassive portion of the polarization curve. The results correspond well with other research, with chloride concentrations in the order of

0.0375M required to initiate corrosion at a potential of approximately -200 mV (SCE) in oxygenated solutions. The Cl/OH ratio therefore is approximately 0.75.

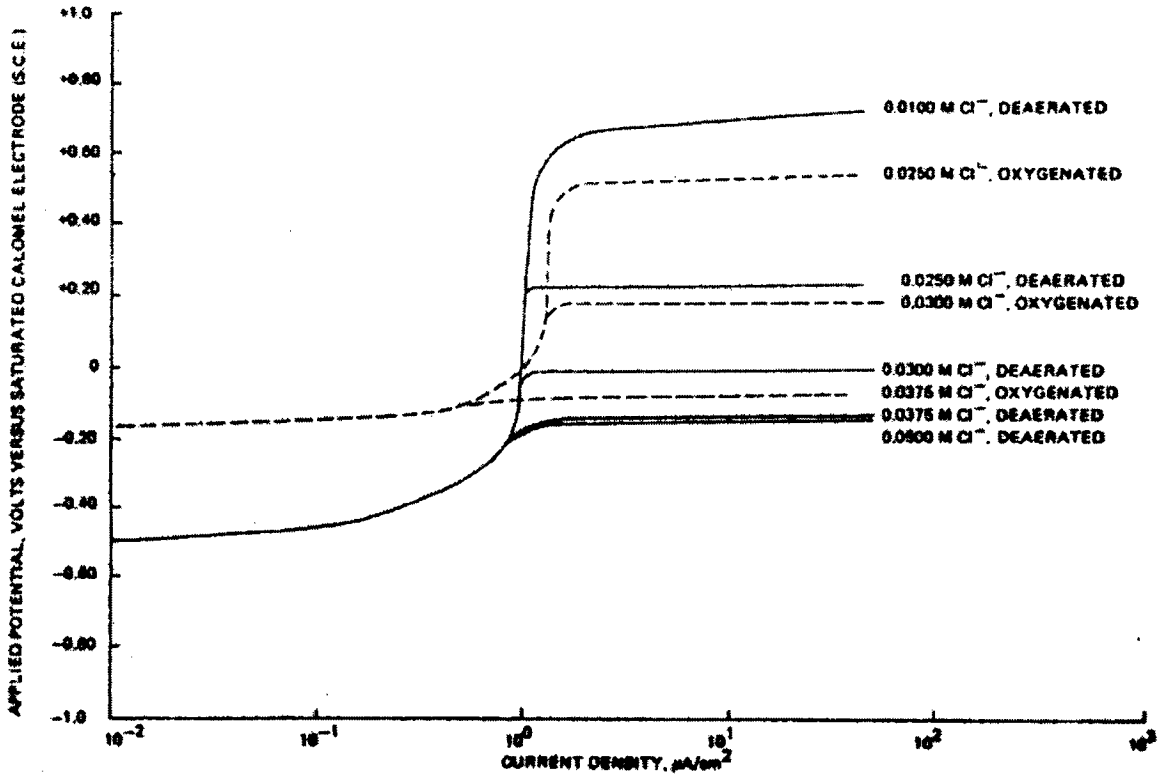

Fig 4.1: Anodic polarization of steel rebar in saturated $Ca(OH)_2$ solution with varying Cl- concentration (Morgan, 1990)

Goni and Andrade (1990) employed polarization resistance techniques to determine the corrosion rate of steel in simulated pore water solutions, pH 11.64 to 13.22, with different chloride concentrations and hence Cl/OH ratios. Their chloride threshold values ranged from 0.25 to 0.8 for OH^- as determined by pH measurements. They note however that when OH^- values were determined by titration, the Cl/OH ratios reduce to 0.15 to 0.3 which may explain some of the apparent differences from ratios reported by other authors. Determination of hydroxyl ion concentration by titration therefore provides a more accurate measurement of the pore solution and Cl/OH ratios based purely on pH measurements must be treated with some caution.

Benjamin and Sykes (1990) investigated the influence of temperature on the chloride threshold. Chloride threshold levels were found to decrease with increasing temperature with a Cl/OH ratio of approximately 0.27 for 0 °C, 0.20 at 20 °C and 0.12 at 40 °C for iron in a 0.2

M NaOH solution. While temperature will clearly have some impact upon the chloride threshold value, for the normal laboratory conditions between 15 and 25 °C there would only be a 0.04 difference in the Cl/OH ratio, which is relatively minor considering the large range of ratios that have been reported in the literature.

4.1.1 Post passivation chloride addition

All the previous determinations of chloride threshold values involved incorporating chlorides into the simulated pore solution at the time of mixing and thus the chlorides would be present before the passive layer surrounding the steel had a chance to fully develop. A weakened or less developed passive layer is less likely to resist the presence of chlorides and thus the values for chloride initiation would probably be lower than would normally be the case. Wheat et al. (1997) investigated the chloride threshold for grade 60 reinforcing steel in a simulated pore solution (SPS) of 0.6M KOH, 0.2 M NaOH, and 0.001 M $Ca(OH)_2$. The two situations of chlorides present at the time of mixing, and gradual penetration of chlorides, were investigated using a diffusion cell which permitted the slow movement of chlorides into the previously uncontaminated SPS. The reinforcing steel was either ground flat and polished with a 600 grit SiC paper or wire brushed before being ultrasonically cleaned in methanol prior to testing. Their results indicated that polished specimens became thermodynamically active at NaCl concentrations of 0.35% while the as-received bars remained passive until 3.5% NaCl. Corrosion initiation therefore occurred at a Cl/OH ratio of approximately 0.075 for the polished samples and approximately 0.75 for the as-received samples. It should be noted that there were no additional chloride concentration ranges between 0.35 and 3.5% NaCl, so the apparent large difference in Cl/OH ratios would likely be reduced if more refined chloride additions were employed. The greater corrosion resistance of the as-received samples may be a result of the protection afforded by the mil scale.

The reported decrease in chloride levels for corrosion initiation with polishing seems to contradict the work of Mammoliti et al. (1996) who clearly showed an increase in required chloride concentration with surface smoothness. A smooth or polished sample should have fewer crevices and a more uniform surface, thus inhibiting pit initiation. Variations in chloride threshold levels and corrosion rates between various researchers may also be attributed to the surface conditions of the steel. According to Mammoliti et al. it is inappropriate to use polished surfaces for reinforcing studies. The primary contribution of the work of Wheat et al. (1997) however, is their demonstration of the effect of subsequent addition of chlorides compared with initial mixing. None of the polished bars, which had chloride thresholds of

0.35% NaCl for initial mixing, showed any signs of corrosion even after 150 days at chloride levels in excess of 4000 ppm (approximately 0.66% NaCl) when chlorides were allowed to diffuse into the solution. Thus any attempt to measure chloride threshold levels should ensure that the passive layer surrounding the steel has had an opportunity to develop prior to the introduction of chlorides. The results from much of the earlier work, which did not apply this principle, must therefore be treated with some circumspection.

Breit (1998) similarly conducted investigations of chloride threshold values for steel immersed in solutions between pH 12 and 14. Chlorides were added after the passive layer had a chance to develop, thus more accurately representing the case in practice. The relationship between chloride concentration for corrosion initiation and hydroxyl ions in this case is given by:

$$\log(Cl^-)_{crit} = 1.5\log(OH^-) - 0.245 \qquad \ldots 4.3$$

where: $(Cl^-)_{crit}$ is the concentration of chloride ion initiating corrosion (mol/l)

(OH^-) is the hydroxyl ion concentration (mol/l)

which indicates a decreasing Cl/OH ratio with decreasing pH.

The study of steel in pore solutions does not sufficiently represent the unique environment of reinforcing steel in concrete. However, where a systematic attempt to quantify the various physical and chemical effects of cement extenders on the corrosion of steel is concerned, the aqueous phase experiments must simulate reality as much as possible. The normal case for reinforcing corrosion is a result of the movement of chlorides through the concrete generally allowing sufficient time for the passive layer to develop. Thus attempts to determine chloride threshold levels should represent this situation. The current investigation therefore tries to follow this principle, and chlorides are progressively added to solution once the passive layer has already formed. Furthermore, care must be taken in the preparation of the steel samples. As shown by Mammoliti et al. (1996) the surface finish of the steel can significantly affect the chloride threshold level, thus samples should as much as possible be representative of the normal state of steel in concrete.

4.1.2 Effects of cement extenders

The study of chloride thresholds has generally focused on pH effects with little consideration of other anions, such as sulphide and thiosulphate, which would be present in slag bearing cements. Cao et al. (1990), and Hinczak et al. (1989) investigated the influences of the pore solution from various blended cements on the corrosion characteristics of steel.

Cement solution liquors were derived from mixes with *w/c* ratio of 2 shaken regularly over the first 8 hours and stored for 3 and 7 days. The solutions were then extracted, filtered and frozen until testing. The response of steel to the addition of chlorides for a high C_3A and low C_3A cement, slag (35%) and FA (25%) were investigated using anodic polarization techniques. The results are summarized in Table 4.2 and show the slag bearing cement to afford the greatest protection to the steel. The critical Cl/OH ratio, with OH^- taken from approximate pH values, were in the range of 0.95 for low C_3A to 1.29 for slag. Cao et al. (1990) have suggested the increased resistance of the slag bearing material may be a result of sulphides inhibiting the pitting of the steel surface in the presence of Cl^-.

Table 4.2: Chloride threshold values for various cement extenders at 7 days (Cao et al., 1990)

Solution	*Chloride level (mol/l)*	*pH approx.*	*Cl/OH*
Cem 1 (high C_3A)	0.045	12.66	0.98
Cem 2 (low C_3A)	0.035	12.57	0.95
Slag (35%)	0.045	12.54	1.29
Fly Ash (25%)	0.035	12.54	1.00

However, the theory of sulphides impeding the corrosion process runs contrary to the generally accepted ideas on sulphides as discussed in chapter 2.9.

The chosen *w/c* ratio of 2 is very high and the cement solution liquor may not adequately represent the true pore solution where more normal *w/c* ratios are used. The variations in required chloride and pH measurements between the samples are also small and may not be substantially different from one another. Without more information on the composition of the pore solution, it is difficult to draw definitive conclusions from this work, though it is a novel attempt at evaluating the chloride threshold levels.

The work of Tuutti (1982) also seems to support the suggestions of Cao et al. (1990), and Hinczak et al. (1989) that sulphides impede the pitting of steel. Solutions of varying hydroxyl concentration with 500 ppm S^{2-} were produced and a steel bar placed in each solution. The presence of corrosion was determined based on visual examination of the test specimens. According to Tuutti (1982), small concentrations of S^{2-} had no negative effects and in fact helped to prevent the occurrence of pitting in highly alkaline solutions. The critical Cl/OH ratio therefore would likely be greater for slag cement, although whether the improvements due to sulphides offset the reduced OH^- is not clear.

One further point should be considered with respect to studies of corrosion not only in pore solutions, but also in concrete. The corrosion process, in addition to being affected by the surface conditions of the metal, is also influenced by the size of the specimen. Burstein and Ilevbare (1996) have shown an increase in the pitting potential with decrease in specimen surface area. Their investigation was based on stainless steel in acidic chloride solutions but the general principles for corrosion should still apply. That is, as the specimen size decreases there is an increasing probability that the most susceptible pit nucleation sites (those that are largest and least open) are not present on the surface and higher potentials are required to activate the next most susceptible site. The rise in mean potential with decreasing specimen size is therefore merely a function of change in probability (Burstein and Ilevbare 1996). This would seem to suggest that larger specimens are more likely to initiate corrosion somewhere along the length of the bar than smaller samples, and thus the chloride threshold on larger samples may be somewhat lower.

The evaluation of the corrosion processes of steel in concrete, by analogy to aqueous phase corrosion, represents the simplest and earliest attempts to treat this problem. Despite its apparent simplicity and ability to control the environment, there are still many unanswered questions and much debate about a number of key issues. The issue of the role of sulphides, in particular, is of some concern with at least three authors suggesting improvements in the protection of steel against pitting in the presences of sulphides despite the general view of suphides being detrimental. Further research in this area is therefore essential. Attempts to study chloride threshold levels and corrosion rates should allow sufficient time for the development of the passive layer prior to the addition of chlorides and the steel surface should be adequately representative of the normal case of steel corrosion in concrete.

4.2 Corrosion Rates for Steel in Pore Solutions

There is relatively little published work on corrosion rates for steel in solutions representative of those found in concrete. The majority of work on corrosion rate measurements has involved casting steel rods into paste, mortar or concrete samples and subsequent evaluation under those conditions. Measurements of this nature are clearly more representative of the true environment surrounding the steel, but it becomes increasingly difficult to study particular aspects of the pore solution chemistry and their effects on corrosion. The study of corrosion rates in pore solution is therefore of value when trying to determine the effects or influences of particular components, as the environment can be fairly

into solution. The corrosion rate results are dependant upon the time at which the measurements were taken as seen in Figure 4.2.

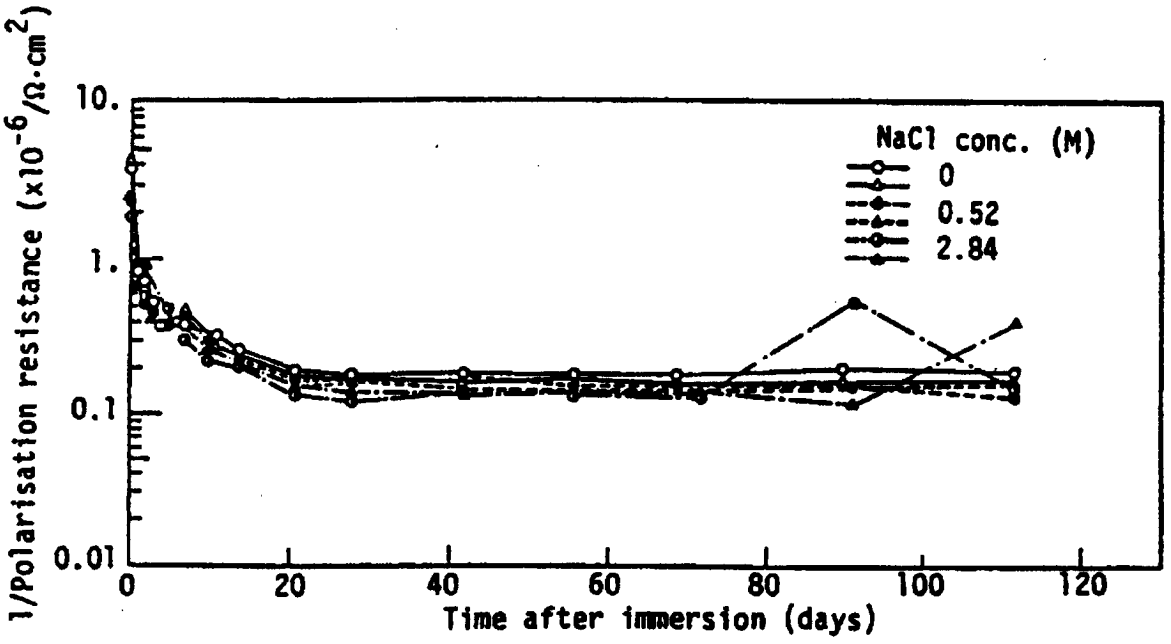

Fig 4.2: Polarization resistance measurements of steel immersed in a solution of 0.4M KaOH + 0.2M NaOH (Yonezawa et al., 1988)

The corrosion rates were approximately 10 to 40 times greater shortly after immersion of the specimens but declined quickly as the passive layer had a chance to develop.

Goni and Andrade (1990) performed similar investigations into corrosion rates of steel in pore solution from calculated pH 12.04 to 13.30 at 21°C. Only one of the samples however remained chloride free and hence passive, providing a corrosion rate of 0.060 μA/cm^2 at a pH of 13.30. The stable passive corrosion rates of Yonezawa et al. are approximately an order of magnitude less than those of Goni and Andrade under similar situations. More information on surface characteristics for instance would be required to accurately compare the two measurements, but it does highlight the variations in data which exist and the need for further investigation. The pore solution corrosion rates from Goni and Andrade do however generally resemble those seen in steel in embedded in concrete as will be shown in chapter 6.

The passive state of steel in an alkaline solution or embedded in concrete is represented by the almost vertical line of the anodic polarization curve as seen in Figure 4.1or 2.13. The work of many other researchers (Cao et al. 1990, Sato 1978, and Salvarezza et al. 1982), as previously shown, also verifies the general shape of this curve. The almost vertical nature of

accurately controlled. The results from aqueous phase corrosion studies must also be viewed in context of the real in-situ environment and the values not taken as absolutes.

4.2.1 Corrosion Rates under Conditions of Passivity

The corrosion rate for steel in pore solutions is effectively shown through anodic polarization curves as seen in figure 2.12, 2.13 or 5.1, with the passive corrosion current being represented by the portion of the curve that shows constant current with increasing potential. Morgan (1990) has determined a passive corrosion current density (i_p) of approximately 1 $\mu A/cm^2$ for steel rebar in a saturated solution of $Ca(OH)_2$ with a pH of 12.5. The corrosion rates were slightly higher for oxygenated conditions compared to de-aerated samples, though the difference appeared fairly minor. Salvarezza et al. (1982) have shown i_p for mild steel in NaOH solution of pH 11.54 to be approximately 4 $\mu A/cm^2$. The results from Sato (1978), as seen in figure 2.13, showed significantly lower passive corrosion rates (in the order of less than 0.1 $\mu A/cm^2$) for iron in a solution with a pH of 11.50. There is therefore considerable variability in the reported passive corrosion rates for iron or mild steel in alkaline solutions.

Cao et al. (1990) examined the corrosion rates for steel in a number of solutions as previously described in section 5.1 (effects of cement extenders) with pH between 12.54 and 12.66. While specific passive corrosion current densities were not given, the anodic polarization curves generally showed similar characteristics prior to the addition of chlorides, despite the pore solution being derived from different cement extenders.

Tromans (1980) determined corrosion rates for mild steel to be approximately 40 $\mu A/cm^2$ for a pH of 12.01 and at 90°C. A passive corrosion current density of 40 $\mu A/cm^2$ is substantially higher than the previous passive rates, provided by other authors which ranged from less than 0.1 to 4 $\mu A/cm^2$ for normal laboratory temperatures. The significant increase in corrosion rate may be explained by the Arrhenius equation as discussed later in section 4.2.3, which, assuming a factor of 2 increase in rate for every 10 degrees, would place it at approximately 0.42 $\mu A/cm^2$ for 25°C. Accounting for the temperature effects in this manner places the results from Tromans in good agreement with others reported in the literature.

Corrosion rate measurements over time were taken by Yonezawa et al. (1988) for steel electrodes immersed in saturated solutions of $Ca(OH)_2$ and 0.4M KaOH + 0.2M NaOH. The results of the steel immersed in the $Ca(OH)_2$ solution showed inverse polarization resistance (1/Rp) measurements of approximately 0.1×10^{-6} /$\Omega.cm^2$ which translates into a passive corrosion rate of approximately 0.003 $\mu A/cm^2$,assuming a *B* value of 26. The 0.4M KaOH + 0.2M NaOH solution was only marginally higher at approximately 40 days after immersion

the curve, such that the slope approaches infinity, implies that the corrosion rate in the absence of chlorides or other aggressive anions is almost independent of the cathodic reduction curve. Thus over the range of passivating potentials which is approximately -600 mV to + 400 mV (SHE), any change in the slope or location of the cathodic polarization curve would have little or no effect on the corrosion current and would only influence the equilibrium potential as shown in Figure 4.3.

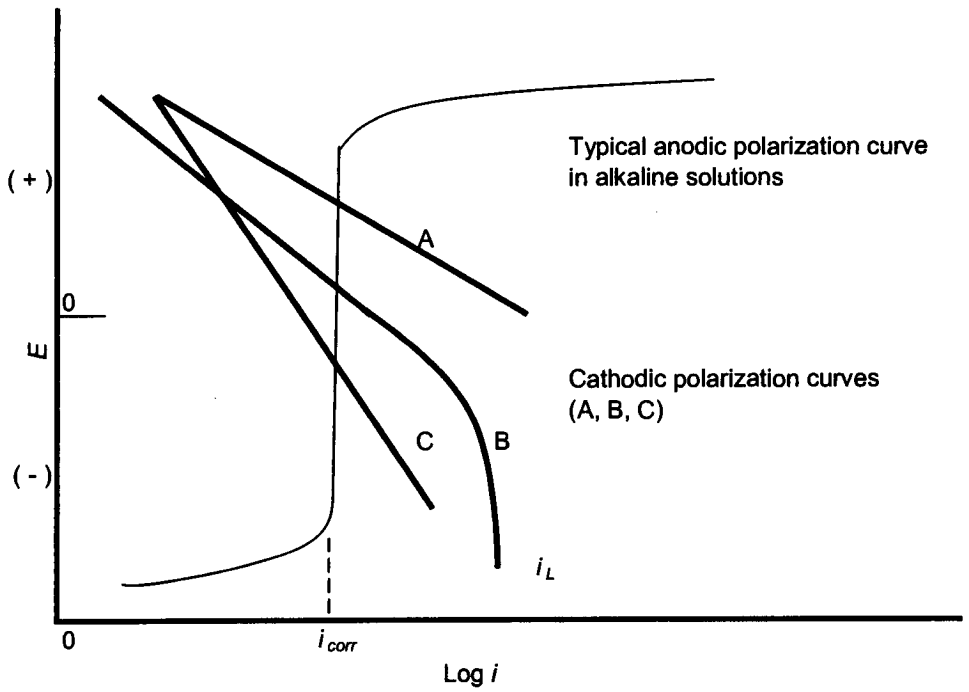

Fig 4.3: Theoretical influence of variation in cathodic polarization curve on passive corrosion current density.

Whether cathodic curve A, B, or C is used, the effect on corrosion rate is negligible. The primary influence on passive state of the metal must be a result of the nature of the passivating film surrounding the steel, and thus in turn the factors governing the rate kinetics and stability of the film, such as temperature, surface condition for metal dissolution and oxide precipitation and presence of sulphides or other anions. That is not to say the presence of oxygen is irrelevant, as it is necessary for the formation and stability of the passivating oxide layer, but rather the corrosion rate is controlled anodically rather than cathodically. A study of the passive corrosion rates of steel in alkaline solutions or concrete therefore provides valuable information on the fundamental condition of the metal and its propensity to actively corrode or remain stable.

4.2.2 Corrosion Rates for Active Conditions

The passive state is generally considered to exist for corrosion rates of steel in concrete less than approximately 0.1 $\mu A/cm^2$, at which the corrosion of the rebar is considered to be negligible (Andrade and Alonso, 1996). Such low corrosion rates would have virtually no effect on the service life of a structure. Active corrosion may be 1, 2 or even 4 orders of magnitude higher than typical passive rates, thus resulting in significant loss of rebar cross section and load-carrying capacity of the structure. It is the study of active corrosion that is of most interest to engineers as it is directly relevant to the design and serviceability of structures.

Cao et al. (1990) determined corrosion rates for steel in pore solutions with 0.05 M NaCl specific to a number of cement extenders shown in Table 4.3. All the corrosion rates appear quite high for such a low chloride concentration. It is interesting to note that corrosion rates for the slag pore solutions are almost half of those for the CEM 2 and that there was fairly little variation between the CEM 1 and Fly Ash samples.

Table 4.3: Corrosion rates ($\mu A/cm^2$) for various cement extenders at 7 days with 0.05 mol/l NaCl (Cao et al., 1990)

Solution	*Corrosion Rate ($\mu A/cm^2$)*
CEM 1 (high C_3A)	20
CEM 2 (low C_3A)	28
Slag (35%)	15
Fly Ash (25%)	19

The corrosion rate data, as expected, correlates reasonably well with the chloride threshold data provided in Table 4.2, which shows slag having the best performance followed by FA, CEM 1 and finally CEM 2 based on Cl/OH ratios. It was suggested that the presence of sulphides may inhibit pit formation thus protecting the steel. Without further information on the pore solution composition it is difficult to comment on this, but based on the majority of work pertaining to sulphides and their role in the corrosion process, this seems very unlikely. Further research is therefore needed to address this issue properly and to determine the role of sulphides in a controlled aqueous environment.

Mammoliti et al. (1996) while showing the impact of surface finish on the chloride threshold levels, also demonstrated its influence on corrosion rate. Approximate corrosion rate values for polished specimens, degreased deformed rebar, and smooth round bar in $Ca(OH)_2$ solution are given in Table 4.4.

Table 4.4: Approximate corrosion rate ($\mu A/cm^2$) of steel in solutions with various concentrations of chloride (Mammoliti et al., 1996)

Surface Condition	*0.28 M Cl*	*0.56 M Cl*	*0.84 M Cl*
Polished	very low	10	10
Deformed	10	45	115
Smooth	50	80	220

The polished specimens displayed significantly lower corrosion rates than either deformed or smooth bars. The importance of surface finish is again emphasized by these results. Not only does surface finish affect the level of chlorides required to initiate corrosion but also the rate once corrosion has begun.

The polarization measurements from Yonezawa et al. (1988) yield corrosion rates of approximately 13 and 5 $\mu A/cm^2$ for mild steel immersed in saturated solutions of $Ca(OH)_2$ with 0.52 M and 2.84 M NaCl respectively. The decrease in corrosion rate with increasing chloride concentration above 0.5 M is consistent with the work of Foley (1970) who has shown a maximum corrosion rate at approximately 0.5 M NaCl. The results do however differ from those of Mammoliti et al. who demonstrated an increasing corrosion rate with increased chloride concentration. One of the differences may be explained by the form of the measurements, with linear polarization techniques employed by Yonezawa et al. and full anodic/cathodic polarization curves used by Mammoliti et al. No reference however is made to possible oxygenation of the solution or reduction in pH due to CO_2 ingress in either case.

Goni and Andrade (1990) in their examination of corrosion rates primarily studied the impact of pH and chloride concentrations over time to determine representative average values. The use of an insulating oil layer would have minimized the ingress of CO_2 and limited the subsequent reduction in pH of the solution. Chlorides in the form of NaCl and $CaCl_2$ were added at the time of preparing the solution. The results of corrosion rate with respect to chloride concentration and pH are shown in Table 4.5.

Table 4.5: Corrosion rates ($\mu A/cm^2$) for various pH and chloride (NaCl) concentrations (Goni and Andrade, 1990)

pH	*Chlorides*			
	0.1M	*0.5M*	*0.75M*	*1.0M*
12.78		1.6	1.6	
13.30	0.2	0.9	1.0	1.15
13.60		0.46	0.54	

It is evident that the increasing pH results in lower corrosion rates for a given chloride concentration. For a given pH, the corrosion rate increases with chloride concentration according to the equation:

$$\log I_{corr} = 0.11 + 0.8 \log[Cl^-] \quad \ldots 4.4$$

with the relationship between corrosion rate and Cl/OH ratio given as:

$$\log I_{corr} = 0.43 + 0.62 \log \frac{[Cl^-]}{[OH^-]} \quad \ldots 4.5$$

The results from Goni and Andrade also fail to show a maximum corrosion rate near the 0.5 M Cl level. If chloride levels were to be increased further, this effect may become evident but is certainly not demonstrated with the existing data. Some care should therefore be taken about extrapolating these equations beyond the bounds of the region over which they were calibrated. Furthermore the inclusion of chlorides at the time of mixing would have inhibited the formation of the passive layer thus likely affecting both the reported chloride threshold levels and corrosion rates compared to the more usual case of chlorides migrating to the bar after passivation has occurred.

The slope of the anodic polarization curve under passive conditions was noted to be almost vertical or approaching infinity. In the case of active corrosion under the influence of chloride ions the transpassive portion of the curve moves to lower potentials. The slope of the chloride-affected portion of the curve, as shown by Morgan (1990) in Figure 4.1, approaches zero. Unlike the passive conditions in which the cathodic polarization curve plays only a very small part in determining corrosion rate, under active corrosion it is evident from Figure 4.4 that the slope and position of the cathodic curve must be the significant factor, for a given chloride level, in the determination of the corrosion rate.

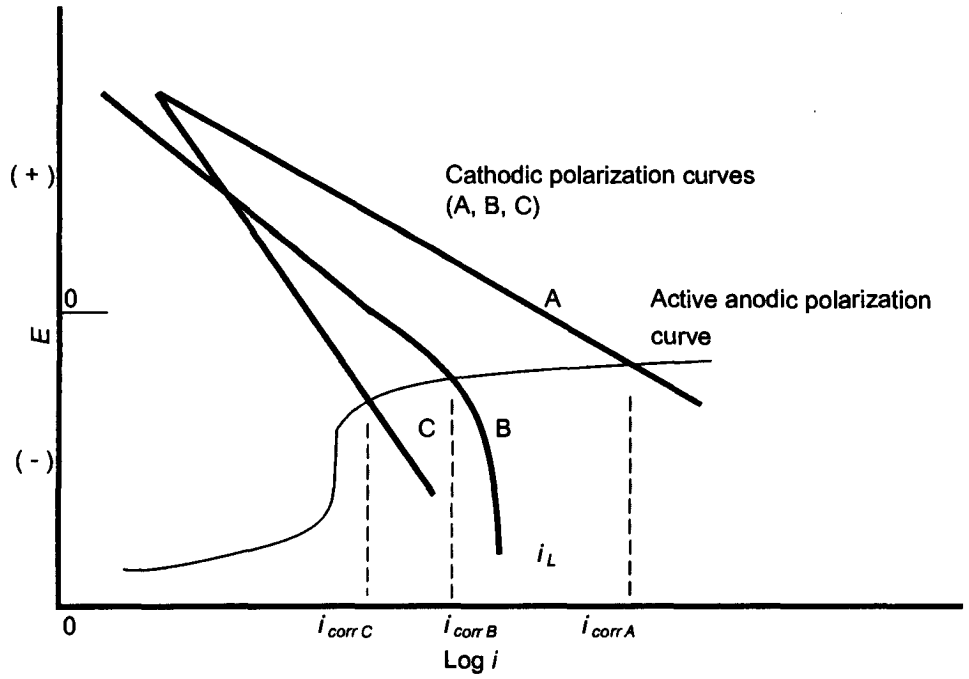

Fig 4.4: Effect of cathodic polarization curve under active corrosion conditions

The study of corrosion rates, particularly under active corrosion conditions, must account for the availability of oxygen. The need for further investigation into corrosion in the aqueous environment is thus clear. Particular attention needs to be paid to the nature of the steel surface, subsequent addition of chlorides after passivation has occurred, impact of the other anions (sulphides and thiosulphate) and the possible role of oxygen.

4.2.3 Effects of Temperature on Corrosion Characteristics

Temperature is another significant factor in controlling the corrosion rate. The temperature dependence of many thermally activated processes can generally be described by the Arrhenius equation (West, 1980):

$$k = A\exp\left(\frac{-Q}{RT}\right) \qquad \ldots 4.6$$

where:

k is the rate constant, A is the frequency factor, Q is the activation energy, R is the gas constant 8.31 (J/mol K) and T is temperature in Kelvin.

Every 10 K rise in temperature translates into approximately a 2 to 4 factor increase in reaction rate (Gillespie et al. 1989). The direct application of the Arrhenius equation to the corrosion of steel in solutions may not be entirely simple as increasing temperature, while

accelerating the corrosion process, also reduces the dissolved oxygen (DO) concentration of the solution, thus limiting the possible corrosion rate.

The effects of temperature on the anodic polarization curve for stainless steel in a 3.5% NaCl solution at pH 3 are shown in Figure 4.5.

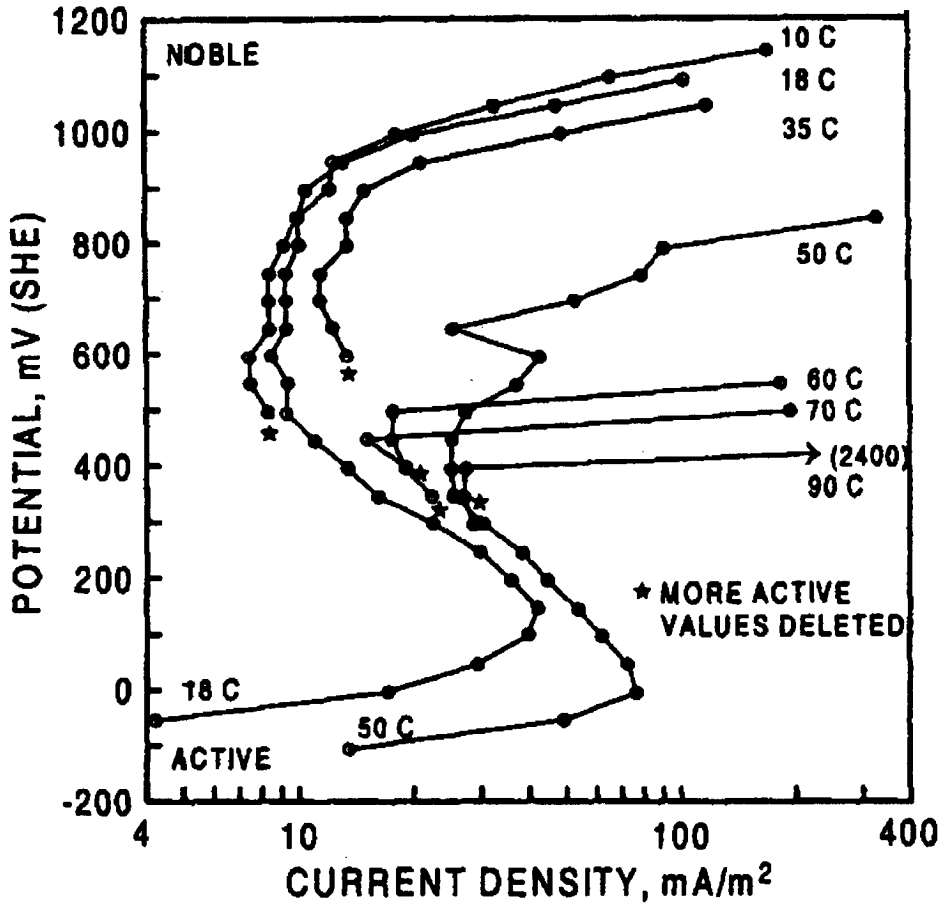

Fig 4.5: Effects of temperature on the anodic polarization of stainless steel (Stansbury and Buchanan, 2000)

It is clear that the increase in temperature significantly reduces the potential at which transpassive corrosion begins and leads to a general increase in the corrosion rates at virtually all potentials. Thus both passive and active corrosion rates will be affected by changes in temperature. The change to the polarization curves is dramatic between 35 and 60°C. Changes in temperature therefore are likely to have an effect on the chloride threshold values with increased temperatures leading to lower transpassive region which would then require less chloride to induce corrosion.

The influence of temperature on the corrosion of steel in concrete is further complicated as the increasing temperature, while increasing the rate constants, will lead to more rapid drying of the concrete and reduce the availability of pore solution, increasing the resistance to the ionic current flux and lowering the solubility of DO as previously noted. The impact of temperature on the corrosion of steel in concrete and some possible methods of standardizing for temperature will be discussed in chapter 5. Temperature was held at a constant 30°C in the current investigation of both aqueous and concrete samples thus there is no need for compensation when comparing the threshold levels or corrosion rates of the various samples.

A description of the experimental apparatus and methodology are provided in the following section. The remainder of the chapter contains a discussion of the results and a summary of the findings.

4.3 Experimental Procedure

The principle behind the development of the aqueous phase research component of the current investigation was to identify a number of major contributors to the overall corrosion process and to study their influence under controlled conditions. Corrosion rates or threshold levels derived from aqueous phase work will not be directly applicable to the real situation of steel in concrete but it does help to quantify specific aspects of the corrosion process and provide a better overall understanding of the mechanisms and factors at work.

The chemical difference between the pore solutions for various extenders was the primary motivation for this phase of the work. The results for pore solution investigations have been provided and discussed in chapter 3. The choice of an appropriate simulated pore solution (SPS) or set of solutions must therefore be based on the results from that investigation. The 7 mix designs were found to fall roughly into 4 main groups based on hydroxyl ion concentration: 1) PC, SL; 2) SM, FA; 3) SF, TR; 4) SH. The hydroxyl concentrations for the PC and SL for instance were not significantly different from one another though there was some variation. The primary difference in chemistry between the two pore solutions (PC and SL) was the presence of sulphides and thiosulphate. It was thus decided that rather than developing an absolutely specific pore solution for PC and SL, the influence of reduced sulphur species on the corrosion process would be investigated by keeping all other factors the same. Thus the PC and SL SPS, while having approximately the same hydroxyl and cation compositions, have different anion compositions. The 75% slag mix (SH) was deemed sufficiently different from any of the other pore solutions and therefore investigated separately. The chosen SPS compositions are shown in Table 4.6.

Table 4.6: Chemical composition of aqueous phase simulated pore solution

Chemical compounds	*Concentration of Compounds (g/l)*						
	PC	SL	FA	SM	SH	SF	TR
NaOH	3.12	3.12	2.20	2.20	1.88	0.64	0.64
KOH	10.86	10.86	7.62	7.62	4.59	1.34	1.34
$Ca(OH)_2$	0.11	0.11	0.13	0.13	0.04	0.74	0.74
K_2SO_4	0.23	0.23	0.07	0.07	0.03	0.00	0.00
Na_2S9H_20		0.226		0.074	0.142		0.098
$Na_2S_2O_35H_2O$		0.057		0.102	0.032		0.029
Total OH^- conc. (M)	0.275	0.275	0.195	0.195	0.130	0.06	0.06

Sulphides and thiosulphate are readily oxidized, even at high pH. The solutions were prepared using de-aerated distilled water in 5L volumetric flasks where the head space was filled with nitrogen prior to mixing. Attempts were generally made to minimize agitation or contact with the air so as to prevent carbonation and thus pH reduction of the SPS, or oxidation of the sulphur species.

The normal case for a slag-bearing concrete would have the steel situated in a sulphide-dominated environment, or at least one where sulphides are present, until oxygen from the atmosphere has oxidized the reduced sulphur species resulting in a change from a reducing environment to an oxidizing one. The process may take up to a few years, depending on depth and other details pertaining to the mix design, construction and service conditions. Chlorides would then be expected to reach the steel at some later date and initiate active corrosion. It is clearly not practical to wait for such an extended and unknown period of time in laboratory studies. Instead, the approach in this study was to place the steel rods with the SPS into the corrosion cells with a surface layer of oil to limit contact with the air and minimize contamination. After 2 weeks oxygen was bubbled through the solution daily for one week, after which time chlorides were added incrementally. The initial two week period was to allow the development of the passive layer in an environment representative of the different characteristic pore solutions. Sulphides would remain present in the SPS and thereby affect the development of the passive layer. The subsequent introduction of the oxygen had two effects:

1) The oxidation of sulphides and thiosulphate which would happen under normal circumstances though over a longer period of time. The oxidation of the sulphur species would then create a more uniform basis (similar oxygen and sulphide levels) for subsequent corrosion rate and threshold measurements between the sulphide-bearing and sulphide-free SPS.

2) Further enhance the development of and stabilization of the passive layer prior to the introduction of chlorides.

After the first week of daily oxygenation, oxygen was then pumped through the cells approximately thrice weekly to ensure a reasonably uniform oxygen concentration between cells. High corrosion rates would consume the available oxygen and, if not replaced, would stifle the subsequent corrosion rate. Oxygen was therefore added because it was not intended to be a limiting factor for corrosion rates in this investigation.

The corrosion cells were made from 5L boro-silicate glass beakers as shown in Figure 4.5. The test specimens were lengths of 12 mm diameter round mild steel taken from the same extrusion. The samples were wire brushed, degreased with acetone and the ends covered with heat shrink tubing and epoxy to provide an exposed area of 40 cm^2. Three mild steel working electrodes and one stainless steel counter electrode were placed in each corrosion cell.

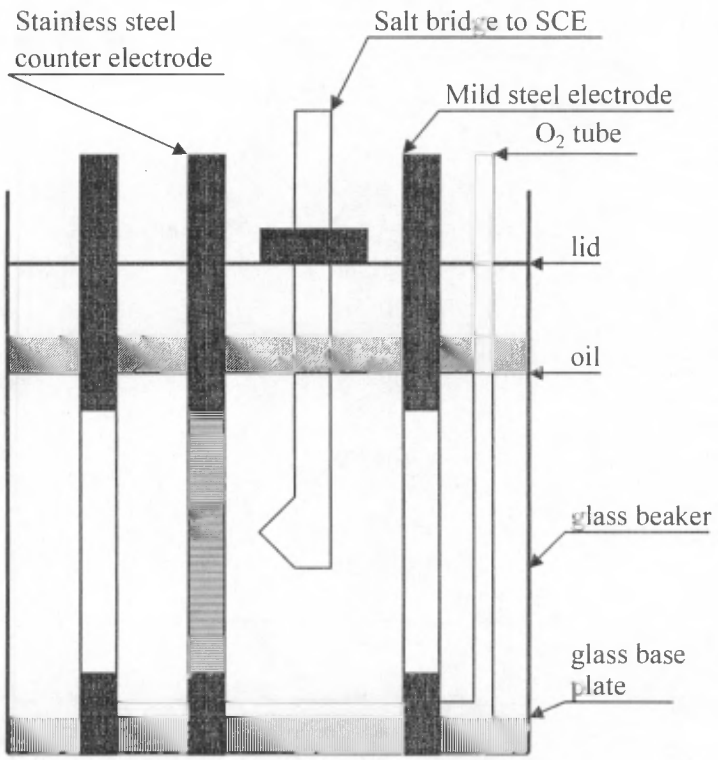

Fig 4.5: Corrosion cell schematic

Note: The corrosion cell is cylindrical with the 4 electrodes spaced at equal distances around a central opening in the lid. The opening in the lid allows for access of the movable salt bridge to the steel and a syringe to draw samples from the solution.

Tubing was provided along the bottom of the cell to allow for oxygenation of the solution. Oxygen (99.9% pure) was provided by gas cylinder attached to a peristaltic pump to ensure reasonably uniform distribution of oxygen to each cell. Aliquots for measurement of solution properties, and chloride additions, were obtained from the samples by using a syringe and long needle which penetrated the oil layer into the SPS.

Chlorides were added to the SPS such that the chloride concentration of the SPS was increased by increments of 0.05M up to 0.2M. The chloride concentration was then increased incrementally to 0.4M and finally 0.6M. The schedule for chloride additions is provided in Table 4.7. In the case of PC and SL, some samples did not show signs of corrosion initiation even after 0.2M of NaCl were added. 0.05 M NaCl increments were then added until all the corrosion threshold values were determined which resulted in a delay in the PC and SL samples reaching the 0.4M chloride level compared to the other samples.

Table 4.7: Chloride addition schedule

Day	*Samples*	*Total chloride level (M)*
22	All	0.05
28	All	0.10
35	All	0.15
42	All	0.20
70	PC, SL	0.25
	Others	0.4
73	PC	0.3
	Others	0.4
76	PC	0.35
	Others	0.4
84	All	0.4
98	PC	0.45
	Others	0.6
112	All	0.6

Samples were generally monitored at the start of the week, prior to the addition of any chlorides to the solution, and again 3 or 4 days later. Thus the measurements taken on day 28 for instance would have been before 0.05M of chlorides were added to the solution. The readings taken at the start of the week included: potential measurements, corrosion rate measurements, dissolved oxygen (DO), redox potential and pH near the start and end of the study period. Mid-week measurements were generally only taken of potential and corrosion rate. Sulphide and thiosulphate measurements were also taken for the first few weeks until oxidation of the material was complete. The samples were monitored for a total of 126 days.

The DO, redox and potential measurements were taken using the same equipment employed in the study of pore solution chemistry. DO and redox readings were allowed to stabilize for approximately 10 minutes. Potential measurements were made against a Saturated Calomel Electrode (SCE) connected to a 'salt bridge' in the solution. The salt bridge was made from 1.5 g agar-agar boiled in 50 ml of 0.1M NaOH solution. Corrosion rates were determined by a coulostatic method, as described in appendix 4A, and are presented as $\mu A/cm^2$.

4.4 Results and Discussion of Pore Solution Properties during Passivation Process

The initial three weeks of the experiment were designed to facilitate the development of the passive layer in a manner consistent with the normal exposure conditions which may be encountered in structures and consistent with the methodology employed in the examination of steel in cracked concrete described in chapter 5. That is, the steel remains in a solution relatively free from exposure to oxygen for the first two weeks, followed by oxygenation of the solution for one week prior to addition of chlorides.

It can be seen from the dissolved oxygen concentrations taken over two weeks (Figure 4.6) that the pore solution was not completely sealed from the atmosphere as the oxygen concentration of the non-sulphide bearing SPS (PC, FA, SF) increased from an initial reading of 0.9 mg/l to approximately 2 to 3 mg/l over that period. The sulphide bearing SPS continued to show lower DO readings, generally less than 1 mg/l, over the first week but then started to increase slowly after this period and before the addition of oxygen to the system. In all cases the DO readings taken after 14 days, at which point oxygen was introduced, showed significantly elevated levels compared to the levels before that period. It should be noted that a new and more accurate DO probe was used from day 21 onwards and for all the TR readings as this set of experiments was performed after the PC, SL, SM, SH, FA and SF experiments but under identical conditions.

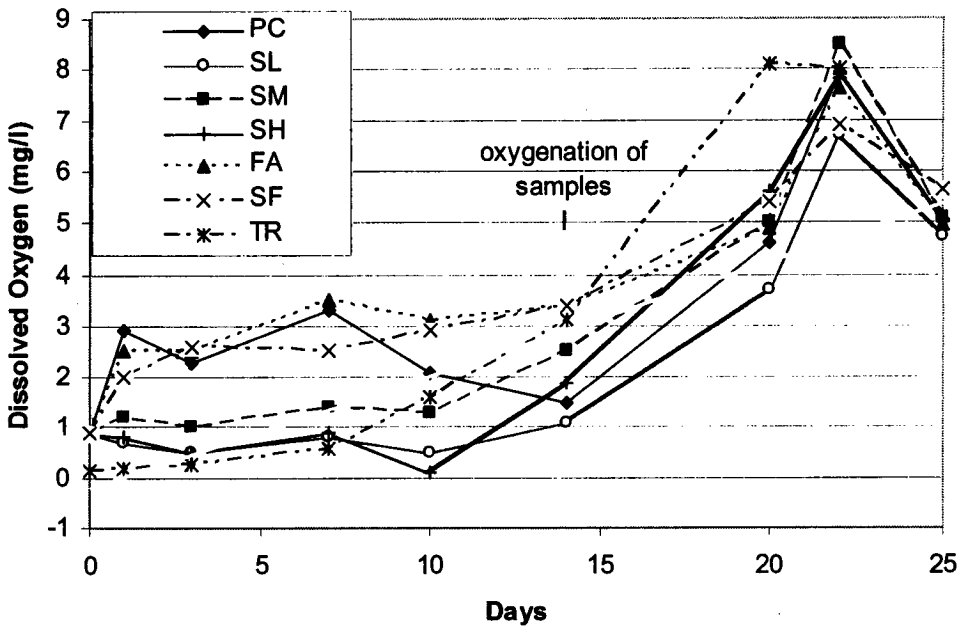

Fig 4.6: Dissolved oxygen readings over first 25 days of aqueous phase experiments

The DO values, after the introduction of oxygen, were at least 3.7 mg/l after 20 days and well over 4.5 mg/l by day 25. This level of oxygen should be more than sufficient to sustain a very active corrosion reaction for a number of days. Future active corrosion rates can therefore be compared under similar conditions of oxygenation. The dip in measured DO at day 25 was likely a result of the reading being taken two days after the samples were oxygenated and after the addition of chloride ions which would reduce the DO capacity of the solution.

The redox potentials shown in Figure 4.7 follow a similar trend to the DO readings. The non-sulphide bearing SPS displayed moderately high redox potentials, generally in the order of -150 to -100 mV, over the first week followed by a slight increase to greater than -100 mV over the remaining period with little or no change noticed after the introduction of oxygen. The sulphide bearing SPS showed characteristically low redox potentials of between -480 and -385 mV over the first week. As with the DO readings, the potentials started to creep towards more positive values prior to the introduction of oxygen. After oxygen was added, a substantial positive shift occurred to produced values comparable with the non-sulphide bearing SPS. The redox potential of the SPS is significantly affected by the presence of sulphide and thiosulphate ions.

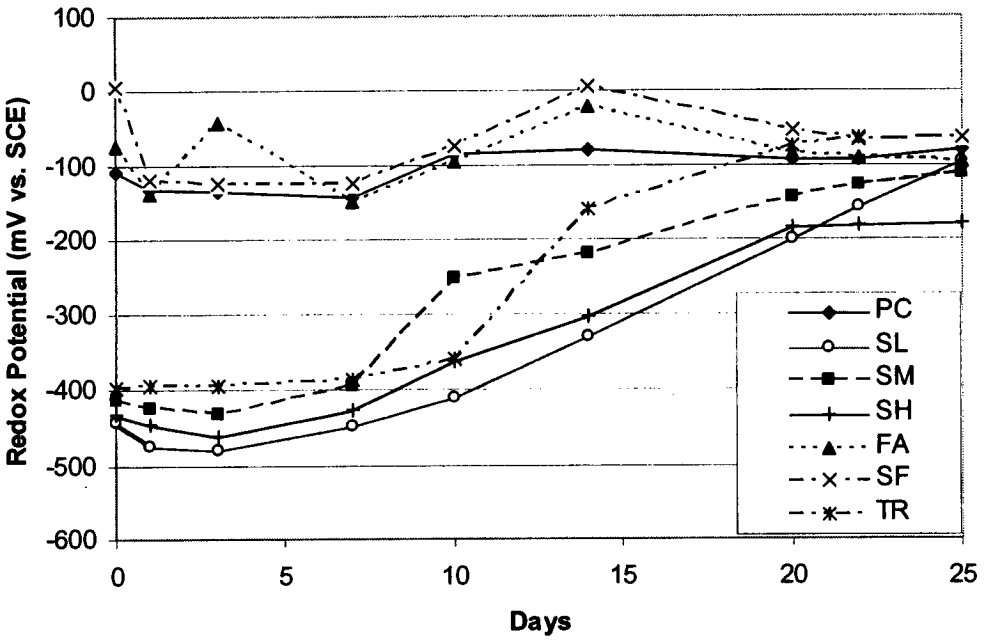

Fig 4.7: Redox potentials (SCE) over first 25 days of aqueous phase experiments

The measurements of DO and redox potential can be used as an indication of, and are a result of, the presence of reduced sulphur species, and are validated by the sulphide and thiosulphate measurements taken over the same period as shown in Table 4.8. The redox potentials are inversely proportionate to the concentration of sulphide ions. At day 14, for instance, the order of the concentration of sulphides present in the solutions was SL > SH > SM > TR with the redox potentials from most negative to positive: SL < SH < SM < TR. There is some discrepancy between redox potential and sulphide concentration for TR and SM but the differences in sulphide concentration between the two are quite small. The difference between 2.3 and 2.8 mg/l is essentially negligible, particularly if the results are viewed in the context of concrete where there may be localized variability in local pore solution. In general however there is reasonable agreement that greater concentration of sulphide ions result in more negative redox potential for the solution. The thiosulphate ions did not seem to significantly affect the redox potential as their concentration increased over the same period.

It can be seen from Table 4.8, that sulphide concentration decreased from those calculated for the initial mixing of the SPS prior to the introduction of oxygen. The sulphides were still at appreciable levels however over the initial two week period and the passive layer is considered to have developed under environments representative of slag bearing concrete.

Table 4.8: Concentration of sulphide and thiosulphate (mg/l)

	Initial	*Day*					
Sulphides	*Mix*	*1*	*4*	*11*	*14*	*21*	*25*
PC	0			0.3			
SL	30.1			22.8	18.4	0.4	0.3
SM	9.9			2.8	1.5	0.3	0.3
SH	18.9			11.3	6.8	0.8	0.5
FA	0			0.2			
SF	0			0.2			
TR	13.1	9.7	8.1	2.3	2.1	0.2	
Thiosulphate							
PC	0				< 3		
SL	25.7				31.3		47
SM	46.1				62.1		60.6
SH	14.5				30.1		39.9
FA	0				< 3		
SF	0				< 3		
TR	13.1	23.5	21.2	13.1	10.3	10.3	

The low sulphide concentrations readings for the PC, FA and SF SPS are essentially at background levels and should not be taken to mean that sulphides were present in the solution. A dramatic decrease in sulphide concentrations is observed after the introduction of oxygen, as expected since sulphides are oxidized by free O_2. No further measurements were taken after 25 days as the results from 21 and 25 days indicated essentially background levels and there was no additional source of sulphides.

The measured thiosulphate readings are interesting, particularly those of the TR SPS, which were taken a few days after mixing. The increased thiosulphate levels suggests that some portion of the sulphides were converted into thiosulphate. These concentrations then continued to decrease with time, but at a much slower rate compared to the sulphides. Even after the introduction of oxygen, the thiosulphate levels remained high and in fact greater than the initial concentrations for SL, SM and SH. After all the sulphides are converted to thiosulphate or sulphate, it is expected that the thiosulphate levels should decrease as they are progressively oxidized to sulphate. The rate of the reaction however was slower than initially anticipated. The thiosulphate measurements for SL, SM, and SH samples were obtained from ion chromatography while the TR values were derived from colourometric methods as described in chapter 3.

It has been shown that SPS were not impervious to the surrounding environment as some degree of oxygenation took place prior to bubbling of O_2 at day 14. The DO, Redox potential and sulphide and thiosulphate measurements are all in reasonable agreement in this regard. There is however a noticeable difference in oxygen, redox and sulphide / thiosulphate levels between those samples which represented slag-bearing materials (SL, SM, SH and TR) and those which did not (PC, FA, SF). The contrast was most stark over the first week, after which time the values for the representative slag-bearing samples started approaching typical non-slag bearing values. These effects are shown in the true case of steel in concrete as oxygen slowly penetrates to the steel and results in changes to the pore solution. These changes are observed through potential measurements of the steel over time as will be shown in chapter 5. There was however sufficient variability between different mixes in the aqueous investigation to suggest that the passive layer would be subject to sulphide and thiosulphate influences and that any future variation in chloride threshold value or corrosion rate could be attributed to this development stage. The one area of concern however is the continued presence of thiosulphate after one week of oxygen bubbling. The redox and oxygen levels, even in the samples containing thiosulphate, closely approximated those of the non-slag bearing samples. The influence of the thiosulphate ions on the change in redox characteristics of the SPS appears to be very limited and only sulphide ions had any real effect on the redox potential. The conversion of sulphide to thiosulphate and its continued presence would be representative of the true situation of steel in concrete. While only sulphide ions appear to determine the redox potential the continued presence of thiosulphate may effect the chloride initiation or corrosion rate measurements and their influence therefore cannot be excluded in the current investigation. The continued presence of thiosulphate may significantly affect the corrosion process and further study will be needed in this regard.

4.5 Chloride Threshold Levels for Initiating Corrosion

The determination of chloride threshold level was based on both a significant thermodynamic potential shift to more negative values and an increase in the kinetic corrosion rate of the steel. A value of 0.1 $\mu A/cm^2$ is generally seen as the level beyond which active corrosion has begun. Chlorides were added in 0.05 M increments, thus if corrosion initiated after 0.05M of Cl^- was added, that would be considered the chloride threshold level even though the true threshold may lie somewhere between 0 and 0.05M.

The potential values for the PC samples, which were generally used as an indication of activation, and chloride concentrations can be seen in Figure 4.8. The results for the SL

samples are shown in Figure 4.9. The remaining plots of potential values over the period of the study are provided in appendix 4B.

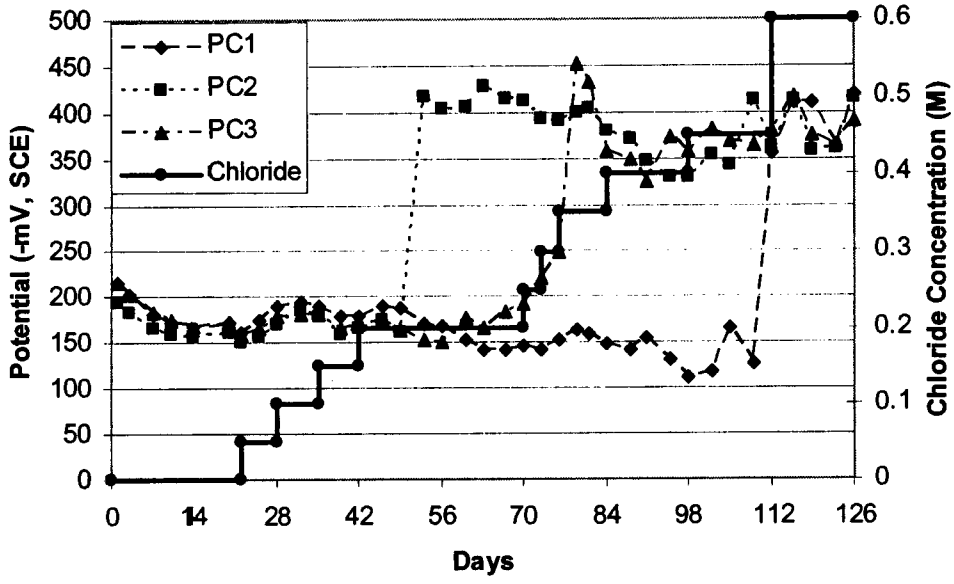

Fig 4.8: Potential values and chloride concentrations with time for PC corrosion cells

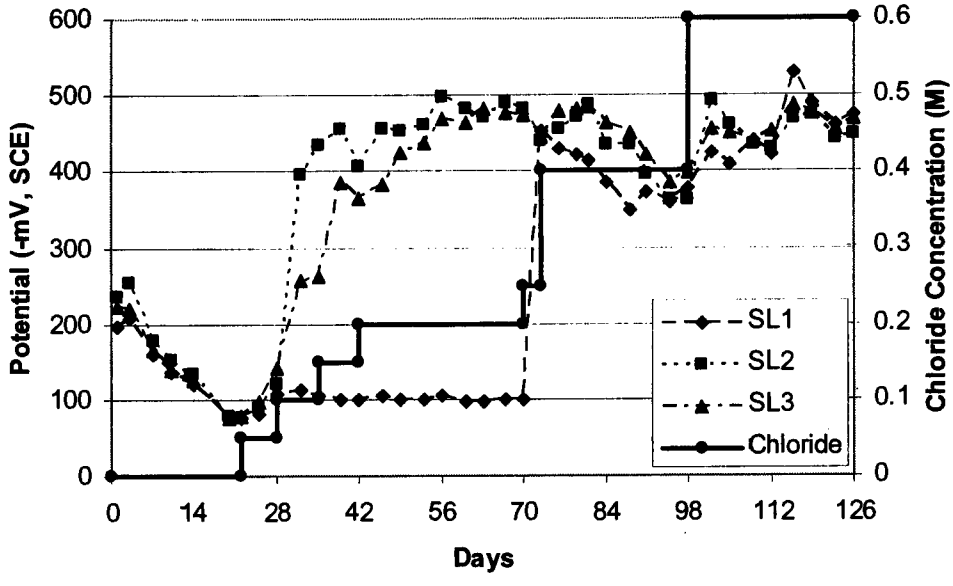

Fig 4.9: Potential values and chloride concentrations with time for SL corrosion cells

Values for the individual test specimens rather than average values were presented to highlight the variability in results associated with the testing of chloride thresholds. The potentials for both PC and SL corrosion cells showed passivating trends prior to the introduction of chlorides at day 21. The potential values of the steel in SL SPS, while initially

starting at more negative potentials than PC, increased over the initial conditioning phase to substantially more positive values (-77 mV for SL compared to -168 mV for PC) prior to the introduction of chlorides. The same trend is true for all steel in sulphide bearing solutions which had more negative initial potentials, yet increased (positively) and overtook the non-sulphide bearing solutions prior to the addition of chlorides.

It may be argued that the difference in DO levels between the sulphide-bearing and sulphide-free SPS was responsible for the lower corrosion potentials. If one examines the potential measurements of the PC and SL systems and allows a three week lag, at 22 days there was virtually no difference in DO levels between any of the samples. The average non-initiated PC potential at day 42 was -172 mV, compared to SL2 which displayed -99 mV at 42 days and -76 mV at 22 days. The effects of sulphide and thiosulphate ions on the thermodynamic and passive layer properties of steel persist, despite virtually identical DO and redox potential values of the SPS after the introduction of oxygen and chloride ions. The true impact will be seen in the subsequent section on corrosion rates (section 4.6).

The point of corrosion initiation can be clearly seen by the sudden jump to more negative potentials of the steel. Two of the three SL samples started actively corroding prior to any of the PC samples despite having the same hydroxyl concentration. The last bar to begin corroding was also in the PC solution and had a substantially higher chloride threshold than any of the bars in SL solution. The time to initiation and associated chloride threshold levels for all the samples are provided in Table 4.9 and the Cl/OH ratio in Table 4.10.

Table 4.9: Chloride threshold concentrations (M)

Sulphide free samples			*Sulphide bearing samples*		
Sample	*Day*	*Cl*	*Sample*	*Day*	*Cl*
PC1	112	0.45	SL1	73	0.25
PC2	53	0.20	SL2	32	0.10
PC3	79	0.35	SL3	32	0.10
Avg		***0.33***	***Avg***		***0.15***
FA1	39	0.15	SM1	28	0.05
FA2	32	0.10	SM2	49	0.20
FA3	32	0.10	SM3	25	0.05
Avg		***0.12***	***Avg***		***0.10***
SF1	28	0.05	TR1	25	0.05
SF2	32	0.10	TR2	32	0.10
SF3	32	0.10	TR3	25	0.05
Avg		***0.08***	***Avg***		***0.07***
			SH1	42	0.15
			SH2	39	0.15
			SH3	32	0.10
			Avg		***0.13***

The potentials for FA1 showed fairly early signs of corrosion initiation but the corrosion rate and potentials subsequently reduced somewhat, which suggests a degree of repassivation. The chloride threshold value was therefore taken at a slightly later date and at higher chloride level. While this is not a conservative assumption, it probably provides a more realistic threshold value and was thus chosen. The total chlorides required to initiate corrosion can therefore be ranked in the following order: PC > SL > SH > FA > SM > SF > TR. This trend is generally similar to the order of the concentration of hydroxyl ions, with a notable exception that SH was lower than either FA or SM.

An examination of the Cl/OH ratio in Table 4.10 should provide greater insight into the chloride initiation.

Table 4.10 Cl/OH ratios

Sulphide free samples				*Sulphide bearing samples*			
Sample	*OH⁻*	*Cl⁻*	*Cl/OH*	*Sample*	*OH⁻*	*Cl⁻*	*Cl/OH*
PC1	0.275	0.45	1.64	SL1	0.275	0.25	0.91
PC2	0.275	0.2	0.73	SL2	0.275	0.1	0.36
PC3	0.275	0.35	1.27	SL3	0.275	0.1	0.36
Avg			***1.21***	***Avg***			***0.55***
FA1	0.195	0.15	0.77	SM1	0.195	0.05	0.26
FA2	0.195	0.1	0.51	SM2	0.195	0.2	1.03
FA3	0.195	0.1	0.51	SM3	0.195	0.05	0.26
Avg			***0.60***	***Avg***			***0.51***
SF1	0.06	0.05	0.83	TR1	0.06	0.05	0.83
SF2	0.06	0.1	1.67	TR2	0.06	0.1	1.67
SF3	0.06	0.1	1.67	TR3	0.06	0.05	0.83
Avg			***1.39***	***Avg***			***1.11***
				SH1	0.13	0.15	1.15
				SH2	0.13	0.15	1.15
				SH3	0.13	0.1	0.77
				Avg			***1.03***

The Cl/OH ratios of Table 4.10 show that for the paired samples of PC-SL, FA-SM and SF-TR the inclusion of sulphides results in a lower value than in the samples which contained no sulphides. The PC-SL pair, in particular, highlights the probable effects of the addition of sulphide to the chloride resistance of the passive layer, with SL having a Cl/OH ratio approximately half that of PC despite the same hydroxyl concentration. The Cl/OH ratio for the FA samples however, appears somewhat lower than the other two corrosion cells which

were free from sulphides. The ratio of 0.60 is roughly half that of either the PC or SF. There is no immediate explanation for this reduced chloride initiation value. In general there is a fair amount of variability in the ratio and perhaps with more measurements a more accurate picture may develop. Furthermore the choice of a 0.05 M chloride increment is somewhat coarse and greater refinement might aid in the threshold determination. The corrosion rate measurements, which will be discussed in the following section, will show that while corrosion initiated fairly quickly on the FA samples the actual rate was fairly low and more consistent with a solution of its hydroxyl concentration.

The results from the SH samples pose somewhat of a problem as they had a lower hydroxyl ion concentration than either FA or SM and yet required a greater absolute chloride concentration and significantly greater Cl/OH ratio than the other two. SL and SM both had Cl/OH ratios of approximately 0.5 while the SH was 1.03. In terms of sulphide concentrations SH had the second highest initial S^{2-} concentrations and a higher S^{2-}/OH ratio compared to SL and SM, both of which had much lower Cl/OH ratios. The suggestion of the negative impact of S^{2-} on the chloride threshold values is therefore difficult to state with absolute certainty based on the assumptions of results for chloride initiation in this experiment. When chloride threshold values are viewed in conjunction with subsequent corrosion rates, a more clear and consistent picture of the influence of sulphides is observed as will be shown in section 4.6.2. One possible explanation for apparent inconsistency with respect to sulphide levels is that both SH and TR, which also showed a similar Cl/OH ratio, had the lowest thiosulphate concentrations after the three week passive layer development phase. There is therefore a possibility that the presence of thiosulphate in the SPS contributed to the earlier dissolution of the passive layer thus reducing the Cl/OH ratio of the SL and SM samples and accounting for the somewhat lower reading of TR compared to SF.

4.5.1 Prediction of Chloride Threshold Concentrations under Aqueous Conditions

Figure 4.9 shows the relationship between chloride and hydroxide concentrations for the initiation of corrosion of steel in SPS. The paired samples showed a consistently lower Cl/OH ratio where sulphides were present but the somewhat anomalous case of SH presents some problem in making an absolute statement. The relationship between chloride content and hydroxyl concentration for the samples of PC, FA and SF provide a moderate correlation coefficient of 0.73, but for only three points which are presented as average values. The chloride threshold values determined in the present work are generally higher than those determined elsewhere and may be attributed to development of the passive layer prior to the

introduction of chlorides, though Breit (1998) also waited until the passive layer was developed prior to the addition of chlorides.

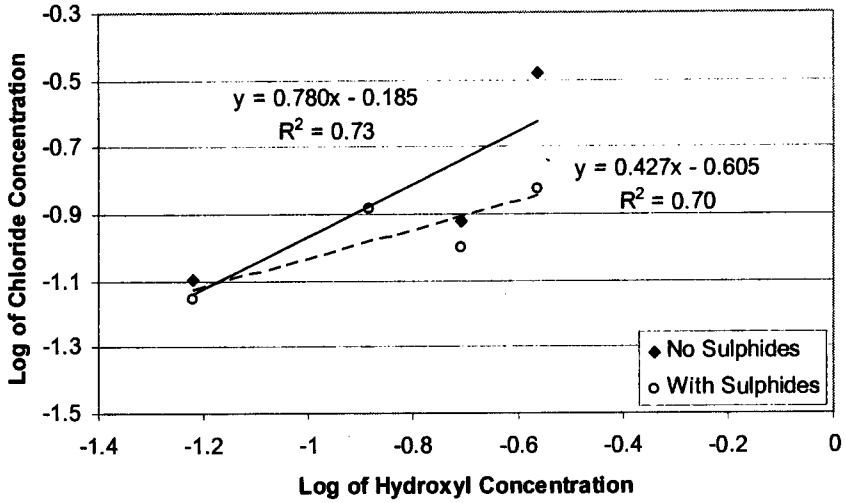

Fig 4.9: Chloride initiation levels versus OH^- concentration

Figure 4.10 provides a comparison of the chloride threshold values for sulphide free and sulphide-bearing solutions, shown in bold, and results from other researchers.

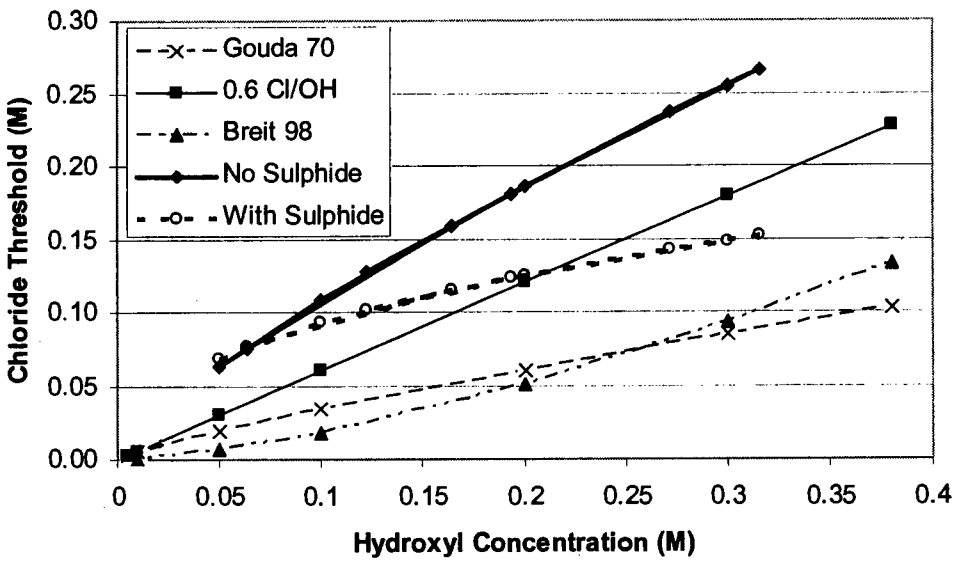

Fig 4.10: Predicted chloride threshold values from various sources

The effects of the sulphides are evident with a lower chloride threshold required to initiate corrosion. Based on the present work, the relationship between critical chloride concentration

for initiating corrosion and hydroxyl ions is given by:

a) Sulphide free samples (PC, FA, SF)

$$\log(Cl) = 0.78\log(OH) - 0.19 \quad \ldots 4.7$$

b) Sulphide bearing samples (SL, SM, SH, TR)

$$\log(Cl) = 0.43\log(OH) - 0.61 \quad \ldots 4.8$$

The precise influence of sulphides on corrosion thresholds or rates cannot be directly determined from this investigation since both the variables of sulphide and hydroxyl concentration changed between samples. The purpose of the investigation was to simulate the pore solutions of the various cement extenders and in that regard the inclusion of slags between 25 and 75% replacement levels is expected to have an effect on the chloride threshold level as shown in Figure 4.9, 4.10 and with equation 4.8 compared to 4.7.

The presence of sulphides (and thiosulphates) clearly has an impact upon the development of the passive layer, as indicated by the corrosion potentials already discussed and the generally lower chloride levels required to initiate corrosion. The uncertainty in the chloride threshold measurements may be a reflection of fundamental variability in the corrosion initiation process. While sulphides and hydroxyl ions will have a significant influence on the chloride threshold, the inherent variability in the underlying process may be equally important. If it there are difficulties in obtaining consistent chloride threshold information in the controlled aqueous environment, there are likely to be even greater difficulties where steel is embedded in concrete due to the significantly greater number of variables and inconsistencies. The following section will definitively show the negative implications of the role of sulphides in enhancing corrosion in all cases, including SH, for aqueous phase corrosion.

4.6 Corrosion Rates of Steel in Simulated Pore Solution

Corrosion rate measurements, reported in $\mu A/cm^2$, were determined using the coulostatic technique (discussed in appendix 4A). Measurements were generally taken at the start of the week and then three or four days later. The corrosion rates measured prior to the introduction of chlorides generally follow a similar trend to those of the redox potentials, with the sulphide-containing SPS showing higher initial corrosion rates for the immersed steel than those which were sulphide free, but moving to more consistent values over time, as seen in Figure 4.11.

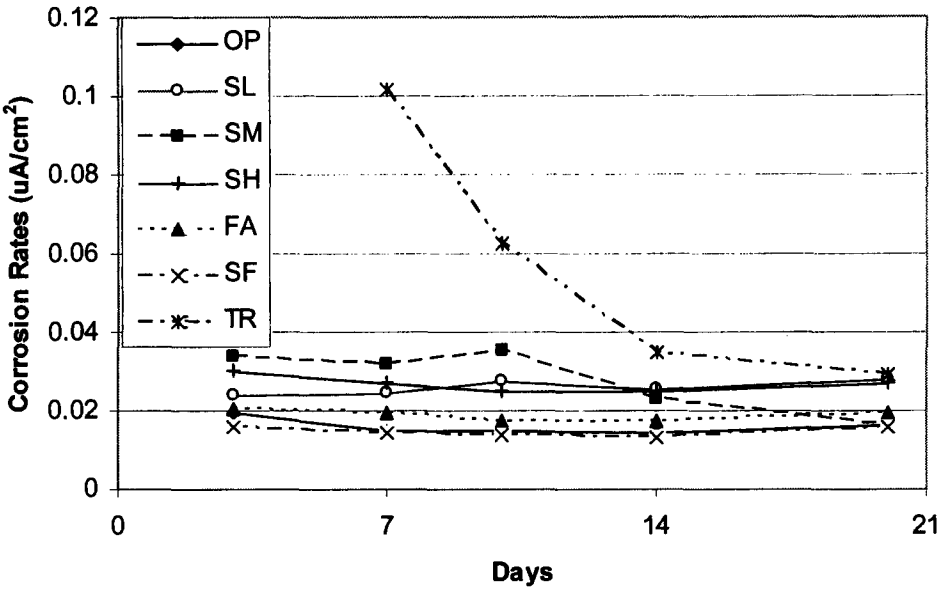

Fig 4.11: Corrosion rates prior to the introduction of chlorides

It is uncertain if a longer initiation period would result in a consistent corrosion rate for all specimens, regardless of the SPS, but from the results distinct differences in corrosion rates were observed during this period of passivity. The higher corrosion rates indicate a passive layer which is somewhat deficient, either as a result of the incorporation of sulphides into the passive layer, the formation of a more porous Fe^{II} layer rather than Fe^{III}, (both discussed in chapter 2), or the continued presence of $S_2O_3^{2-}$ even after the introduction of oxygen. It is likely that once the reducing environment has been neutralized by the removal of S^{2-}, the environment would favour the further passivation and stability of Fe^{III} species. This was observed to some extent by the continuing decrease in corrosion rates of the sulphide bearing SPS but a difference in rates persisted until the introduction of chlorides. This difference in corrosion rates may support the notion of the detrimental effects of incorporating FeS into the passive layer and does not exclude the potentially negative influence of $S_2O_3^{2-}$. The negative impact of sulphides on the passivity of steel is also clearly evident through the lower chloride thresholds as shown in section 4.4.1.

4.6.1 Active Corrosion

The corrosion rates determined after the onset of active corrosion show more stark contrast between sulphide-bearing and sulphide-free SPS. Without exception, the presence of sulphide and thiosulphate during the development of the passive layer in the first 21 days

resulted in a substantial increase in corrosion rate after the addition of chloride which continued over the entire test period ending on day 126. An example of the variation between sulphide bearing and sulphide-free SPS can be seen in Figure 4.12 which shows average corrosion rates for both SM and FA representative SPS. The graphs for individual corrosion rates are found in appendix 4B.

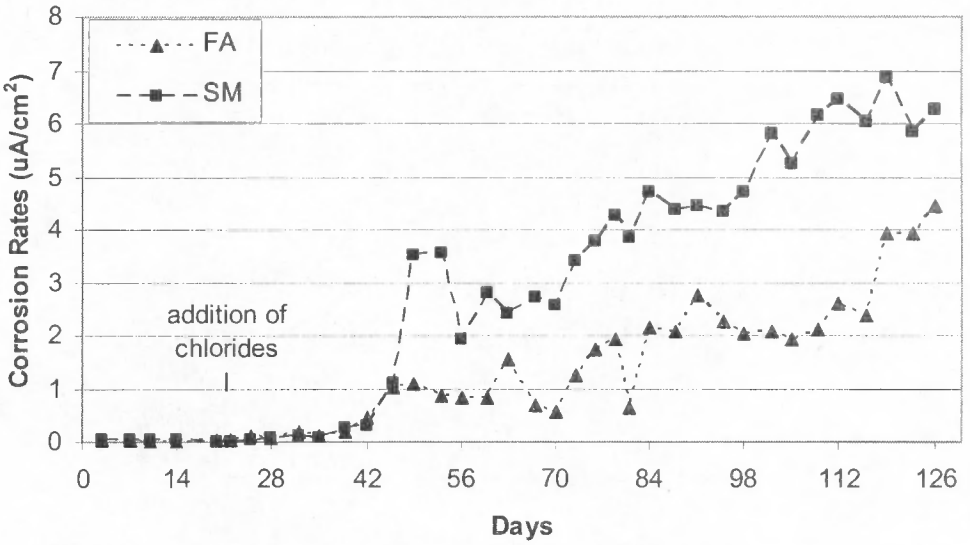

Fig 4.12: Average corrosion rates of mild steel in solutions SM and FA

The onset of corrosion started approximately at the same time for both FA and SM with Cl/OH ratios of 0.60 and 0.51 respectively. Thus, in this particular case, there was apparently little difference in passive properties between these two samples as the passivation rates were also fairly similar at day 14. Once corrosion initiated however the average corrosion rates for FA were generally half those of SM, highlighting the probable effects of sulphides and thiosulphate on the corrosion of steel in concrete and certainly in aqueous conditions. Again the variation in corrosion rates cannot simply be attributed to the variation in the redox potential or oxygen content at the time of passivation, as these differences persisted for only the first 14 days. The DO and redox would certainly affect the passivation of the steel but the higher corrosion rate should be seen primarily as a result of the presence of sulphides and thiosulphate in the SPS. The effects therefore are more than simply a time lag between samples exposed to similar DO and redox and must be explained by a weakened passive layer, with the probable incorporation of FeS into the structure and possible acceleration effects if thiosulphate is present in the SPS.

Average values for corrosion rates taken at chloride concentrations of 0.2, 0.4 and 0.6 M are provided in Table 4.11 and Figure 4.13. The effects of increased corrosion rates associated with the addition of sulphides to the SPS are thus evident, with all sulphide-containing SPS showing considerably higher corrosion rates than their sulphide-free counterparts.

Table 4.11: Corrosion rates ($\mu A/cm^2$) of mild steel for various chloride concentrations and SPS

Days	*(46-70)*	*(73-98)*	*(102-26)*
Cl^- Conc.(M)	*0.20*	*0.40*	*0.60*
PC	0.30	0.32	0.97
SL	1.67	2.19	3.59
SM	2.56	4.32	6.08
SH	8.59	11.94	14.85
FA	0.88	1.95	2.93
SF	16.40	21.50	27.22
TR	25.82	32.86	30.60

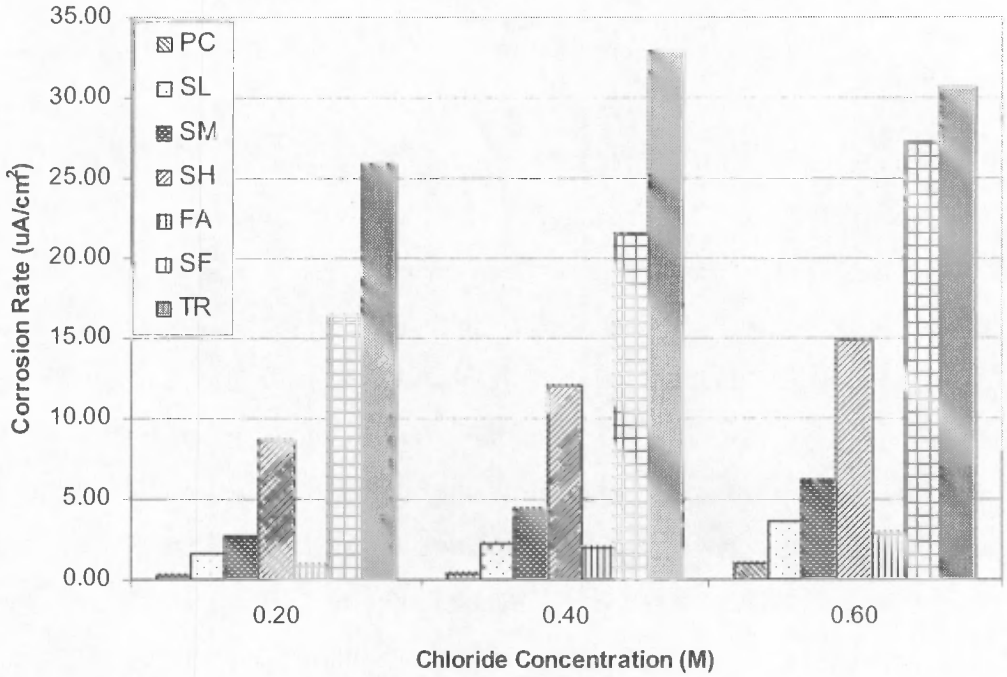

Fig 4.13: Average corrosion rates for various SPS at chloride concentrations of 0.2, 0.4 and 0.6 M

Table 4.11 and Fig 4.13 also show that SL had a higher corrosion than FA which had a lower hydroxyl ion concentration. The effect of sulphides therefore was sufficiently great to reduce the protection afforded the hydroxyl ions resulting in a higher corrosion rate despite a higher concentration of hydroxyl ions.

Table 4.12 shows the effects of increasing chloride concentration, from left to right, and decreasing hydroxyl concentration, from top to bottom, on the factored increase in corrosion rates of sulphide-containing versus sulphide-free SPS. The values are the factor of the corrosion rate of the sulphide-containing samples divided by the corrosion rate of the sulphide-free samples. SM/FA for instance represents the corrosion rate of the sulphide containing SM divided by the corrosion rate of its sullphide-free counterpart FA.

Table 4.12: Increase in corrosion rate versus chloride concentrations

	Chloride Conc. (M)		
Sample	*0.20*	*0.40*	*0.60*
SL/PC	5.55	6.88	3.70
SM/FA	2.90	2.22	2.08
TR/SF	1.57	1.53	1.12

It is interesting to note that the greatest variation in corrosion rate between samples of SPS of the same hydroxyl concentration is generally found at the lower chloride concentrations. As the chloride concentration increases the percentage increase in corrosion rate decreases. Although in the case of SL/PC an increase in this factor was observed at 0.4M Cl, this subsequently decreased again at 0.6 M Cl. The variation in corrosion rate also appears to be affected by changes in hydroxyl concentration, with the greatest variability observed at higher hydroxyl concentrations and a decrease in variability between sulphide-bearing and sulphide-free SPS as hydroxyl ion concentration decreases. Thus the most similar value of 1.12 was observed for TR and SF at a chloride concentration of 0.6 M compared to 5.55 for SL/PC at a chloride concentration of 0.2 M.

The effects of variations in hydroxide content and chloride concentration are even more evident when the relative corrosion rates are compared to chloride and hydroxide concentration as shown in Table 4.13. The first column of 0.2 M chloride, under the rate factor by chlorides, provides the reference factored corrosion rate. The subsequent factored corrosion rates are based on the corrosion rate for the given samples, at their respective

chloride concentrations, divided by the corrosion rate at a chloride concentration of 0.2M for that sample. Similarly the rate factors under the hydroxide component of the table uses the corrosion rate for PC or SL, in the case of sulphide-bearing SPS, as the reference to which the other samples are compared.

Table 4.13: Corrosion rate factor comparison by chloride and relative hydroxyl ions concentration

	Rate factor by chlorides				*Rate factor by hydroxides*		
S^{2-} *Free*	*0.20*	*0.40*	*0.60*	$(OH)^{-1}$ *ratio*	*0.20*	*0.40*	*0.60*
PC	1.00	1.06	3.23	1.00	1.00	1.00	1.00
FA	1.00	2.20	3.31	1.41	2.94	6.12	3.02
SF	1.00	1.31	1.66	4.58	54.55	67.52	28.06
S^{2-}	*0.20*	*0.40*	*0.60*		*0.20*	*0.40*	*0.60*
SL	1.00	1.31	2.15	1.00	1.00	1.00	1.00
SM	1.00	1.69	2.37	1.41	1.54	1.97	1.69
SH	1.00	1.39	1.73	2.12	5.15	5.45	4.14
TR	1.00	1.27	1.19	4.58	15.47	15.00	8.52

A tripling of the chloride concentration in the sulphide-free SPS resulted in a 3.3 times or less increase in the corrosion rate for a given hydroxide concentration. For the sulphide-containing SPS this increase was even lower, approximately 2.4 or less for a given hydroxide concentration. The change in corrosion rate associated with increasing chloride concentrations may be associated with the initial corrosion rate. The sulphide-containing SPS showed higher initial corrosion rates with lower subsequent increase in corrosion rates associated with increased chloride concentration. The effects of a higher initial corrosion rate limiting the subsequent increase in corrosion rate associated with an increase in chloride ions is also shown in the SF sample, though not as effectively as for the sulphide bearing TR sample. An increase in the chloride concentration between 0.2 and 0.6 M can generally be expected to result in a proportionate increase in the corrosion rate. Only TR was shown to have slight decrease in corrosion rate when the chloride concentration was increased from 0.4 to 0.6 M.

The increase in corrosion rate associated with a decrease in hydroxide concentration is however much greater. For non-sulphide samples, a decrease of 1.4 in the hydroxide concentration resulted in at least a 2.9 times increase in corrosion rate for all chloride concentrations and a 4.6 times decrease in hydroxide concentration resulted in a minimum

factored increase of 28, substantially higher than the factored decrease in hydroxide concentration. Changes in the hydroxyl concentration therefore have a greater effect on the corrosion rate than the same relative change in the chloride concentration, *ceteris paribus*.

Sulphide-bearing samples show a similar, though somewhat muted pattern for the effect of absolute hydroxide concentration on the corrosion rate of steel in SPS. The sulphide bearing SPS, as previously stated, showed a higher initial active corrosion rate, yet the effects of either increased chloride concentration or decreased hydroxide concentration were less pronounced.

Due to the substantial contribution of hydroxide concentration to the corrosion process, a relationship based simply on the Cl/OH ratio would be misleading. The absolute value of the hydroxide ion concentration should be taken into account. Figures 4.14 and 4.15, effectively demonstrates this point.

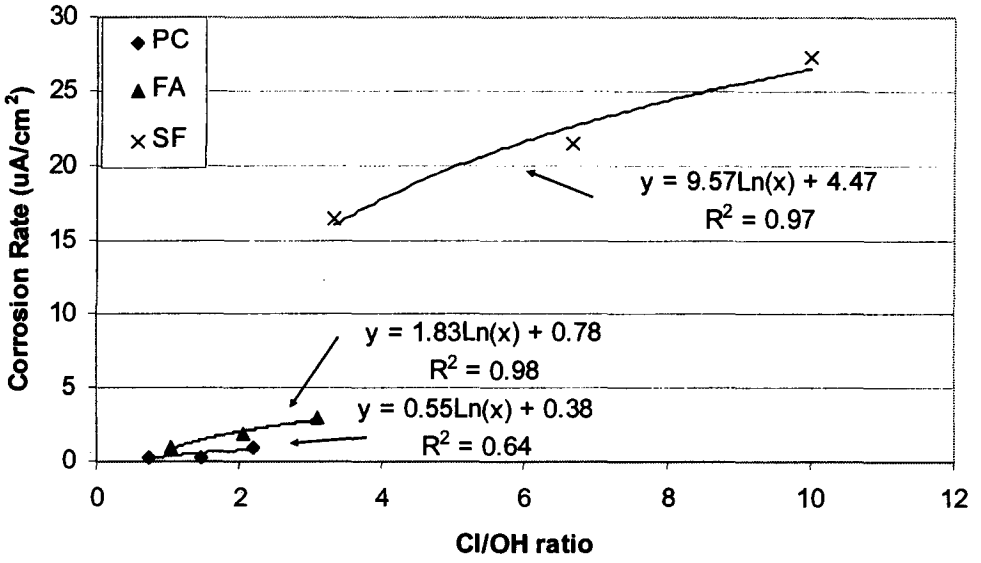

Fig 4.14: Relationship between corrosion rate and Cl/OH ratio for sulphide-free SPS

Figures 4.14 and 4.15 show the change in corrosion rate with Cl/OH ratio for sulphide-free and sulphide-bearing samples respectively. There are essentially a unique set of corrosion rate Cl/OH ratio curves for each of the individual SPS. The change in the starting position for each curve is essentially a function of the absolute hydroxyl concentration and the presence or lack of sulphides.

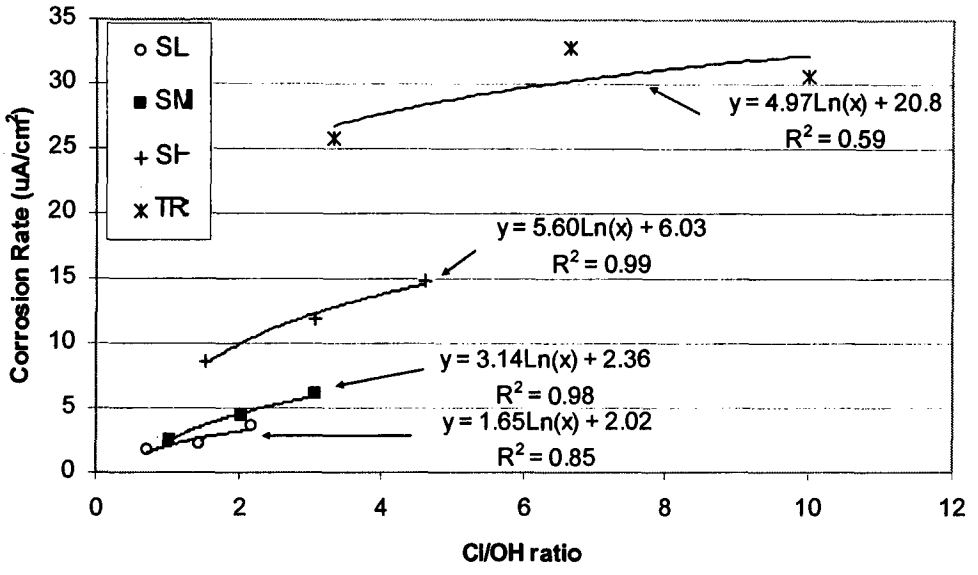

Fig 4.15: Relationship between corrosion rate and Cl/OH ratio for sulphide-bearing SPS

Consider samples SM, SH and TR with Cl/OH ratios of 3.08, 3.08 and 3.33 respectively. The associated corrosion rates are 6.08, 11.94 and 25.82 $\mu A/cm^2$. The corrosion rate of the SH sample is approximately double that of SM for the same Cl/OH ratio and the corrosion rate of TR is approximately 4 times greater than SM for only a minor increase in Cl/OH ratio. Thus the initial absolute hydroxide concentration must be considered in any evaluation of corrosion rates and not simply the Cl/OH ratio. It can be seen that values for PC and FA are fairly similar, though the difference in corrosion rate is still greater than difference in hydroxyl concentration would suggest. It might be reasonable therefore to establish ranges of initial hydroxyl concentration for which a corrosion rate prediction equation could be used. To accurately quantify corrosion rates based on similar initial hydroxides concentrations would require considerable further experimental investigation over the entire range of possible pore solution. For the purposes of the current work and comparison of corrosion rates based on the representative pore solutions, discrete equations as derived from Figures 4.14 and 4.15 will be presented in the following section.

4.6.2 Prediction of Corrosion Rates under Aqueous Conditions

The following equations have been provided as estimates of the corrosion rates ($\mu A/cm^2$) based on Cl/OH ratios for the various SPS with known total initial hydroxide concentrations:

a) PC (OH^- = 0.275 M)

$$I_{corr} = 0.55 \ln\left(\frac{Cl}{OH}\right) + 0.38 \quad \ldots 4.9$$

b) SL (OH^- = 0.275 M)

$$I_{corr} = 1.65 \ln\left(\frac{Cl}{OH}\right) + 2.02 \quad \ldots 4.10$$

c) FA (OH^- = 0.195 M)

$$I_{corr} = 1.83 \ln\left(\frac{Cl}{OH}\right) + 0.78 \quad \ldots 4.11$$

d) SM (OH^- = 0.195 M)

$$I_{corr} = 3.14 \ln\left(\frac{Cl}{OH}\right) + 2.36 \quad \ldots 4.12$$

e) SH (OH^- = 0.130 M)

$$I_{corr} = 5.60 \ln\left(\frac{Cl}{OH}\right) + 6.03 \quad \ldots 4.13$$

f) SF (OH^- = 0.06 M)

$$I_{corr} = 9.57 \ln\left(\frac{Cl}{OH}\right) + 4.47 \quad \ldots 4.14$$

g) TR (OH^- = 0.06 M)

$$I_{corr} = 4.97 \ln\left(\frac{Cl}{OH}\right) + 20.80 \quad \ldots 4.15$$

A logarithmic correlation was chosen which represents decreasing effectiveness with increasing chloride concentration. As previously noted, a decrease in corrosion rate as the chloride concentration increases above approximately 0.5M NaCl might be expected due to reduced DO capacity of the SPS. While this was not observed in the present investigation, further research involving higher concentrations of chlorides might reveal this effect. For the purposes of the current investigation, and most typical chloride levels which would be encountered, the range of values is sufficient.

One limitation of the data pertaining to the PC sample should be noted. Corrosion rates are provided for Cl/OH ratio of 0.73 which is lower than the previously stated critical chloride concentration of 1.21. One of the samples was however actively corroding at this stage and

thus a value for active corrosion was observed. This point highlights the possible variability in corrosion rate and threshold measurements and thus such values need to be seen as likely or representative values, though variation may occur in particular instances.

It may also be argued that the variation in corrosion rate associated with a given Cl/OH ratio is a result of the period over which active corrosion has occurred. If one examines the situation however it is readily apparent that the samples which have been corroding the longest, and showed more fully developed corrosion, had a lower corrosion rate compared to the samples with lower hydroxide concentration and thus shorter periods of exposure to chlorides. For instance, SH displayed an average corrosion rate of 11.94 $\mu A/cm^2$ between days 73 and 98 for 0.4 M Cl (3.08 Cl/OH) compared to an average corrosion rate of 6.08 $\mu A/cm^2$ between days 102 and 126 for 0.6 M Cl (3.08 Cl/OH) for SM which had a higher hydroxide concentration. If anything one would expect an increase in corrosion rate for those samples which had been exposed to active corrosion for a longer period of time. The corrosion values did however show moderate stability for a given level of chlorides, thus the relationship between chloride level, hydroxide concentration and corrosion rate should be valid.

4.7 Chapter Summary

The corrosion of steel in simulated pore solutions was investigated in this chapter. The pore solutions were representative of those determined by pore expression as discussed in chapter three and designed to approximate the seven combinations of materials currently under investigation. The solutions were modified slightly to produce paired samples, one containing sulphides and thiosulphate and one set free from sulphides and thiosulphate but identical in all other ways. The objective was therefore to determine the influence of these anions on the overall corrosion process while still representing the pore solutions characteristic of the specific mixes.

The dissolved oxygen concentration and redox potential of the sulphide bearing solutions was considerably lower than the sulphide free specimens, as expected. The DO levels and redox potentials of the sulphide-bearing solutions moved towards values representative of the sulphide-free samples with time and quite dramatically after the introduction of oxygen. The measurement of sulphides revealed that they were quickly oxidized after the introduction of oxygen as their concentrations fell dramatically and the concentration of thiosulphate increased. Thiosulphate remained present in the solution long after the introduction of oxygen and chlorides and may be partially responsible for the behaviour of steel in the SPS. The steel

was exposed to the reducing environment for a sufficient period of time to influence the development of the passive layer as demonstrated by the elevated corrosion rates and lower potentials of the sulphide-bearing samples prior to the introduction of chlorides

Considerable variability in chloride threshold values exists in the literature, as presented in section 4.1, and this variability was generally observed in the current experiments. The chloride threshold value for initiating corrosion, based on Cl/OH ratio, ranged from 0.51 for SM to 1.39 for SF. Two separate equations, 4.7 and 4.8, for predicting chloride initiation were determined specific to solutions which were either sulphide-free and sulphide-bearing. The inclusion of sulphides was found to lower the chloride threshold for initiating corrosion in all paired samples, though FA had a lower Cl/OH ratio than SH or TR. The variability in the chloride concentration necessary to initiate corrosion is likely inherent to the corrosion process as corrosion initiation by chlorides represents a transition from one form of corrosion to another. Corrosion is an ongoing process of decomposition and repair even under passive conditions and the ability and mechanism by which chlorides disrupt the passive layer quite complex. Those sites on the steel with are defective in someway will provide the first opportunity for a breakdown in passivity. The inclusion of sulphides and thiosulphate has been shown to generally reduce the effectiveness of the passive layer in resisting on the onset of active corrosion due to chloride ions.

It is clear from the results of the aqueous phase investigation that the corrosion of steel is strongly influenced by the nature of the pore solution. The primary factors affecting the corrosion of steel are the hydroxide concentration and the presence of sulphides and thiosulphate during the development of the passive layer and the subsequent role of thiosulphate during active corrosion. The role of the total hydroxide concentration and chloride concentration was determined to be more important than simply the Cl/OH ratio. The corrosion rate increased disproportionately to the change in hydroxyl ion concentration. For example, a 4.8 times decrease in the hydroxyl concentration result in a 15.5 times increase in corrosion rate at a chloride concentration of 0.2 M. Individual corrosion rate equations based on Cl/OH ratios were therefore developed for each mix investigated. The relative performance of the SPS in terms of corrosion rates can be summarized as follows, from highest corrosion rate to lowest: TR>SF>SH>SM>SL>FA>PC.

The pore solution investigation is therefore useful in determining influences of individual aqueous species but does not necessarily describe the situation of steel corrosion in concrete which is subject to additional influences such as relative humidity, porosity and resistivity, to

name a few. The following section on the corrosion of steel in cracked concrete will attempt to address this problem more fully.

4.8 Appendices

4A.1 Linear Polarization Resistance

4A.2 Polarization Curves and the Intersect Method

4A.3 Coulostatic Method

4B.1 Corrosion Potential Plots

4B.2 Corrosion Rate Plots

4A Linear Polarization Resistance Measurements and Coulostat Development

Much of the theory relating to the study and determination of corrosion rates has already been discussed and presented in chapter 2. The general principle of polarization resistance of a metal has provided the basis for most of the current means of assessing corrosion rates. Rodriguez et al. (1994) further stated that all other electro chemical methods are subsidiaries of linear polarization resistance (LPR) techniques and derive their kinetic estimations from the Stern-Geary formula. Some of the general principles and assumptions regarding LPR will be briefly reintroduced, with some description of the chosen methods and their limitations in the current investigation.

4A.1 Linear Polarization Resistance

The term polarization resistance R_p refers to the change in potential over the change in current sufficiently close to corrosion potential. R_p is presented either as Ohms (Ω) or as $\Omega.cm^2$ which is independent of the surface area. The relationship between R_p and the corrosion current is therefore given as (Mansfeld 1970):

$$R_p = \left(\frac{\partial E}{\partial I}\right)_{E_{corr}} \quad \ldots 4A.1$$

with

$$B = \frac{b_a b_c}{2.303(b_a + b_c)} \quad \ldots 4A.2$$

the corrosion current therefore is

$$I_{corr} = \frac{b_a b_c}{2.303(b_a + b_c)}\left(\frac{\partial I}{\partial E}\right)_{E_{corr}} = \frac{B}{R_p} \quad \ldots 4A.3$$

In order to measure R_p, it is generally necessary to measure the polarization curve in the vicinity of E_{corr} for both anodic and cathodic currents (Mansfeld 1970). Stansbury and Buchanan (2000) suggest that the conditions of linearity are generally met for potentials within about 10 mV of E_{corr}. Shreir (1979) states that linearity of the ΔE-ΔI curve is not essential and that Icorr can be determined from the slope of the tangent of non-linear curves. Furthermore, linearity over the range of positive and negative potentials is only achieved when the cathodic and anodic Tafel slopes are equal. Thus the condition of linearity is not essential for estimating R_p and hence I_{corr} but measurements are generally taken within +/- 10 mV of E_{corr}.

Measurements of the polarization curve close to E_{corr} will yield the R_p and hence I_{corr}, provided the Tafel slopes for the material or the constant B are either known or estimated. Figure 4A.1 shows a linear plot of current due to polarization for the superposition of anodic and cathodic current curves. It can be seen that the measured current is zero where I_{corr} anodic = I_{corr} cathodic at E_{corr}. The sweep rate in a potentiodynamic determination of the R_p can have a significant effect on the measured value.

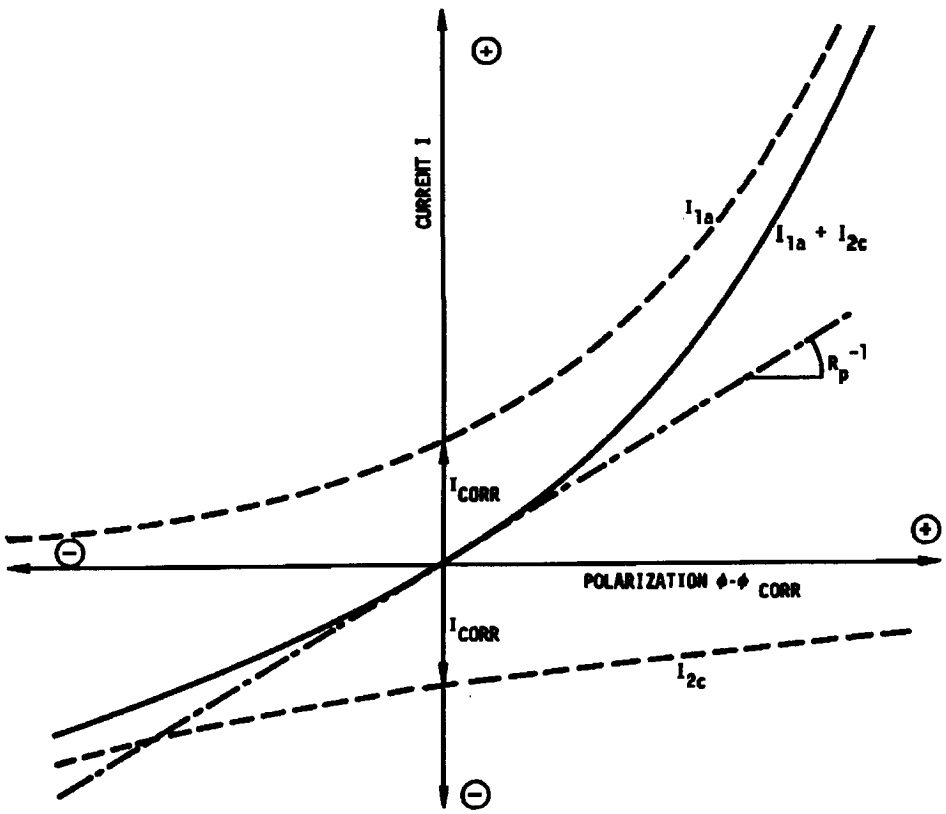

Fig 4A.1: Plot of combined anodic and cathode polarization curves (Mansfeld 1970)

Figure 4A.2 clearly illustrates the change in R_p for passive corrosion associated with sweep rates from 0.1 to 1000 mV/min. The effect of sweep rate on actively corroding samples is however less pronounced.

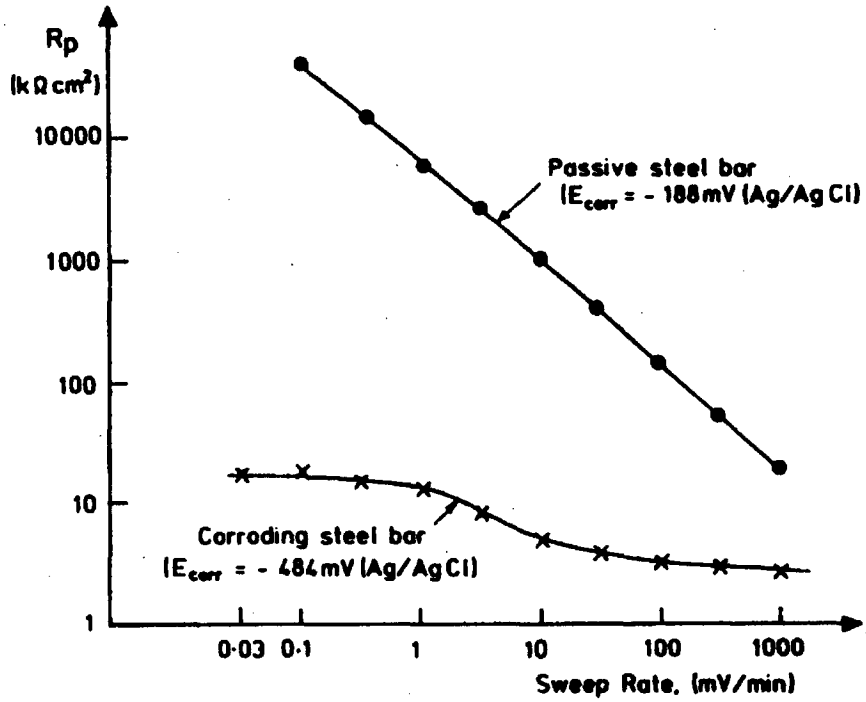

Fig 4A.2: Effects of sweep rate on R_p measurements (Millard et al. 1991)

A standard sweep rate of 10 mV/min has been suggested by Millard et al. (1991) as a reasonable compromise as between practical considerations and accuracy of the measurement.

As shown in chapter 2.6, a chosen B value of 26, without any further knowledge of the Tafel slopes, results in a maximum corrosion rate error of 2 which, given the nature and variability of corrosion, particularly with respect to corrosion in concrete, is quite acceptable. Thus without specific knowledge of the material or the Tafel slopes, a reasonable estimate of corrosion rate can be determined through LPR techniques. One of the greatest benefits of LPR is the non-destructive nature of the test and thus limited damage to the specimen (Rodrigues et al. 1994). Numerous readings can be taken over a period of time without adversely affecting the test specimen.

4A.2 Polarization Curves and the Intersect Method

The theory of polarization curves has been extensively discussed in chapter 2. The corrosion rate is determined from the intersection of the anodic and cathodic polarization curves at E_{corr}. The actual I_{corr} is based on extrapolation of the linear portion of the curves and their intersection at E_{corr}, as seen in Figure 4A.3. The individual curves are therefore determined by measuring the current associated with particular controlled potential. The

curves are generally determined by starting a scan at a certain amount below the E_{corr} and scanning to a given amount above.

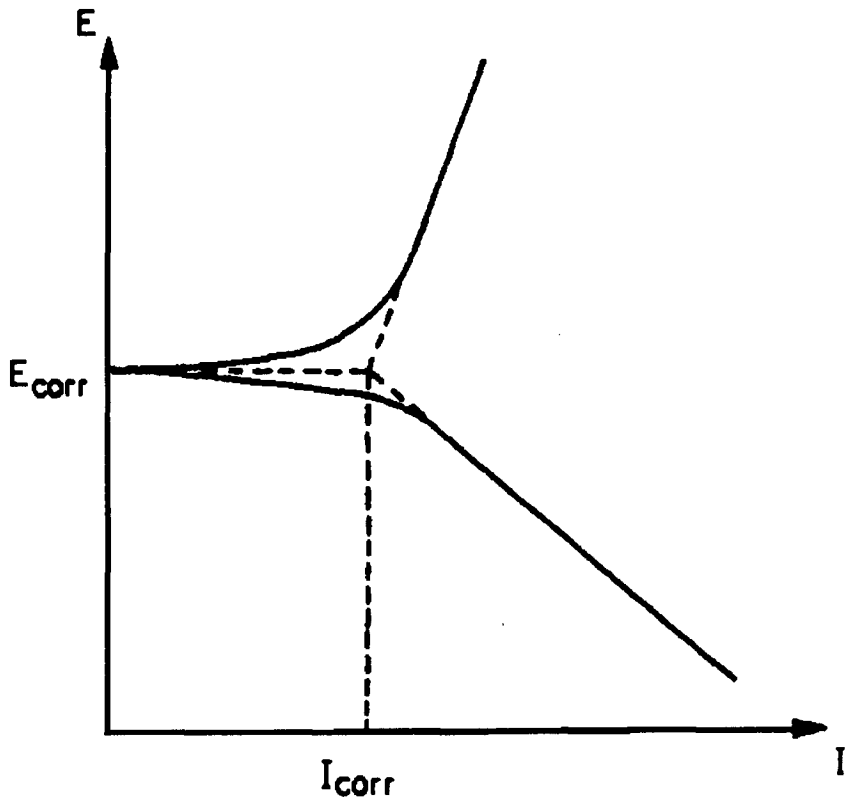

Fig 4A.3: Intersection method based on Tafel curves (Andrade and Alonso 1996)

As Andrade and Alonso (1996) note, the sweep rate is an important parameter which can affect the curves and correction for ohmic drop is also necessary. The impact of sweep rate is clearly seen in Figure 4A.4 which shows the increased range of potentials at which pitting may occur. The particular example given is for the case of stress corrosion cracking but would similarly apply for ordinary corrosion cases as well.

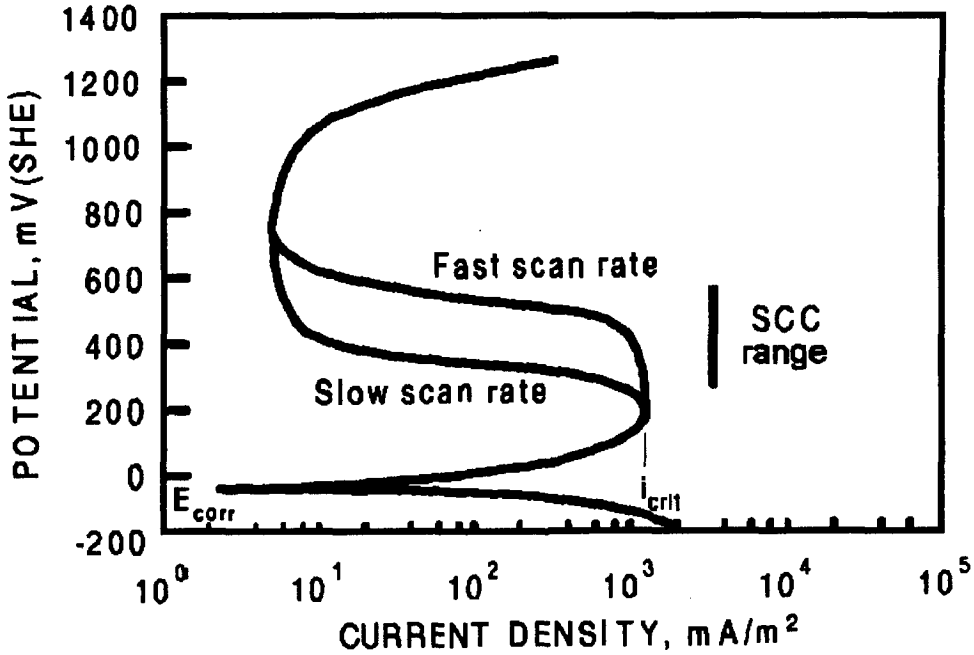

Fig 4A.4: Effects of sweep rate on the pitting potential (Stansbury and Buchanan 2000)

The importance of an appropriate sweep rate is further emphasized in Figure 4A.5, where no passivation is observed for the higher sweep rate.

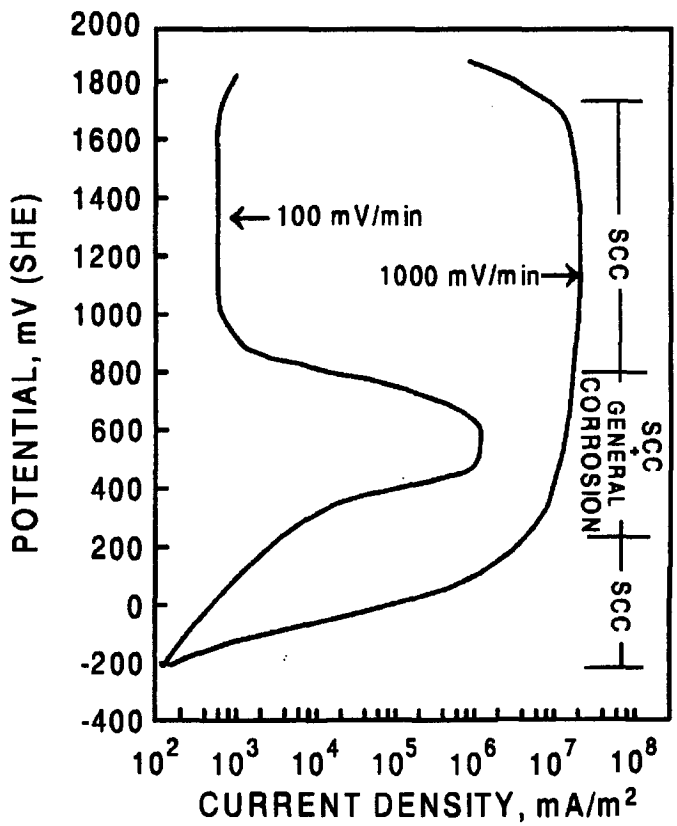

Fig 4A.5: Effects of sweep rate on the anodic polarization curve for carbon steel in boiling $NaNO_3$ (Stansbury and Buchanan 2000)

A balance between practical measuring time and validity of the result must be reached. The sweep rate of 10 mV/min as previously stated, is a reasonable value and is recommended in the ASTM G5 - 94 for potentiodynamic and potentiostatic polarization measurements. In the current investigation a slightly faster scan rate of 24 mV/min was employed to minimize the experimental control time, as chloride measurements surrounding the steel were subsequently taken and chloride migration due to application of an electrical charge would adversely affect these results.

The Tafel extrapolation requires the electrode to be polarized over the whole range of potentials and current to obtain the Tafel lines. According to Mansfeld (1970), anodic polarization results in dissolution of the electrode surface, increase in the roughness factor and formation of corrosion product films. Upon cathodic polarization, the surface film may be reduced contributing additional cathodic currents and variation in the electrolyte. Thus a new specimen is required for each test and complete polarization will essentially destroy the specimen.

The measurement of the entire polarization curve is useful for an in-depth assessment of the material and the determination of Tafel slopes, but generally unwarranted for simple calculation of either R_p or corrosion rate data, which can be determined much quicker from LPR techniques.

4A.3 Coulostatic Method

The coulostatic method of corrosion rate determination is essentially a LPR technique which, unlike the common galvanostatic method which monitors the response of potential to an applied current over a period of minutes, measures the relaxation of the potential after a known charge of duration in the order of milliseconds is applied to the electrode. According to Glass (1995) corrosion rates are related to the time constant describing the potential decay induced by a small charge perturbation as the time constant is related to the polarization resistance through the double layer capacitance. A high corrosion current therefore will lead to a rapid decay of the potential transient whereas with a lower corrosion current the decay of the potential after the perturbation will take some time. A typical potential transient monitored over 30 seconds is shown in Figure 4A.6.

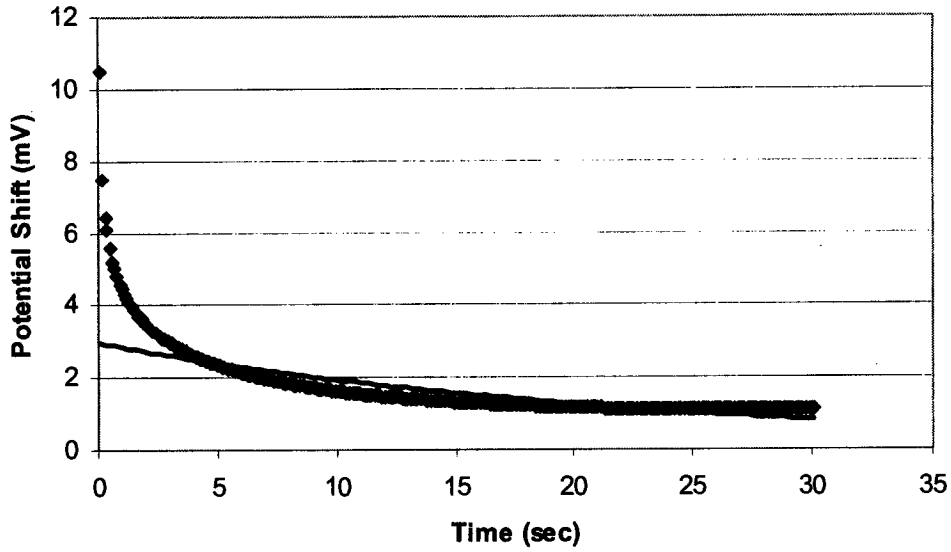

Fig 4A.6: Potential transient of steel electrode after application of small charge

The theoretical development and principles of the coulostatic method have been well presented in a number of sources (Glass et al 1993, Rodriguez and Gonzalez 1994, Hassanein et al 1998). A brief outline of the main features of the method and determination of corrosion rates will be presented at this point. The potential transient is described by the equation (Hassanein et al 1998):

$$n_t = n_o \exp\left(\frac{-t}{\tau_c}\right) \qquad \ldots 4A.4$$

where n_t is the potential shift at time t, n_o is the initial potential shift and τ_c is the time constant. The polarization resistance R_p is then obtained from the time constant and capacitance (C) information, equations 4A.5 and 4A.6, with q_s being the applied charge density.

$$\tau_c = CR_p \qquad \ldots 4A.5$$

$$C = \frac{q_s}{n_o} \qquad \ldots 4A.6$$

Values are obtained by fitting equation 4A.4 to the results for a curve such as that shown in Figure 4A.6. The value of n_o is thus calculated from the fitted equation and not a measured valued. There is an apparent deviation between the fitted curve and the measured potentials shortly after the perturbation as seen in Figure 4A.6. The behaviour of the steel mortar interface is said to be modeled by the Randles equivalent circuit which places a resistor

representing the polarization resistance in parallel with a capacitor which represents the double layer capacitance. Rodriques and Gonzalez (1994) have suggested standard Randles circuit is simplification and that there should be three resistor-capacitor combinations in series accounting for the mortar cover, passivating film and as finally the metal-concrete interface. The first two however are said to discharge almost instantaneously.

Potential measurements are taken 0.1 seconds after the cessation of the charge which allows many of the very earlier to dissipate. The remaining early additional transients are unlikely to significantly effect the corrosion rate measurements as potential readings are taken for at least 30 seconds thus the overall shape of the curve and the resulting equation are still valid.

The length of the charge has been shown by Glass (1995) to have an effect on the shape of the relaxation transient with longer perturbations resulting in progressively flatter relaxation curves as seen in Figure 4A.7. The relaxation curve for perturbations of approximately 35 ms differ only marginally from those of 4.65 ms with perturbations even up to 350 ms showed reasonable agreement.

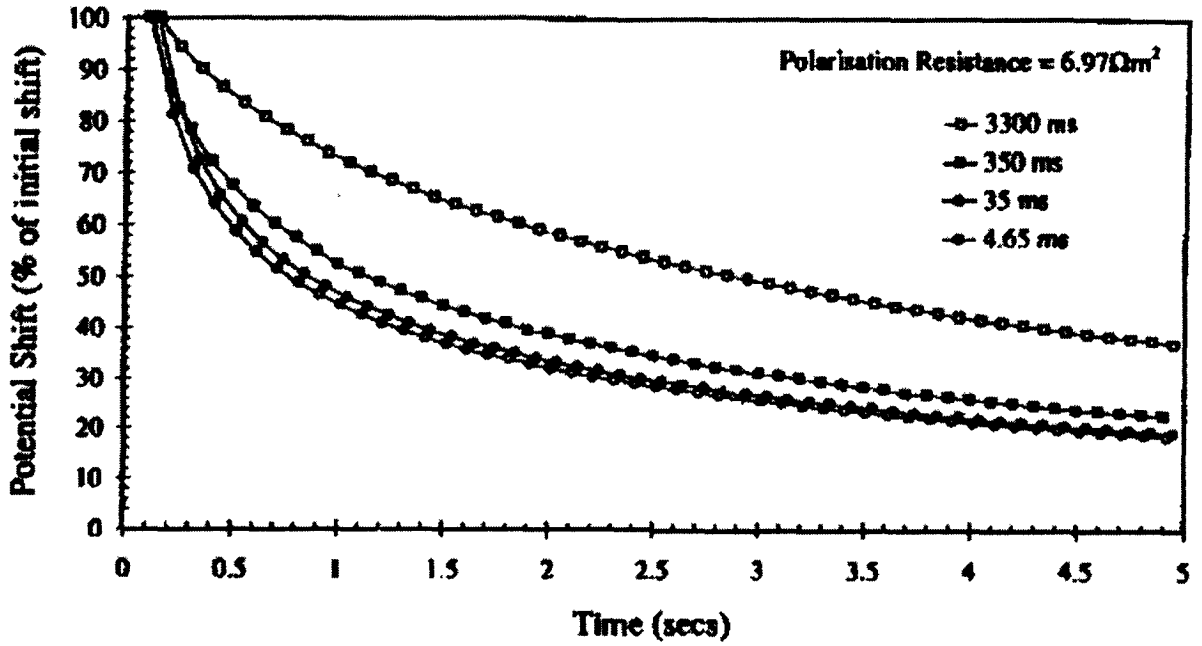

Fig 4A.7: Effect of perturbation length on shape of potential transients (Glass 1995)

The current investigation of corrosion rates employed an HP 34970A data acquisition unit for recording potentials measurements against a Ag/AgCl reference electrode. Measurements were taken at a rate of ten readings per second both before and after the application of the charge. The charge was delivered by means of a purpose built pulse

generator capable of supplying from 1 to 30 mA from 1 to more than 100 ms with most pulses being shorter than approximately 40 ms. The pre-perturbation potential was monitored until reasonable stability was achieved at which point a know charge was sent to the working electrode by means of a stainless steel counter electrode. Any underlying potential trend determined prior to the application of the charge was removed from subsequent value after the perturbation thus ensuring only the true change in potential was used for curve fitting equation 4A.4. Corrosion rates were determined based on the Stern-Geary equation as previously discussed and assuming a B value of 26.

4B.1 Corrosion Potential Plots

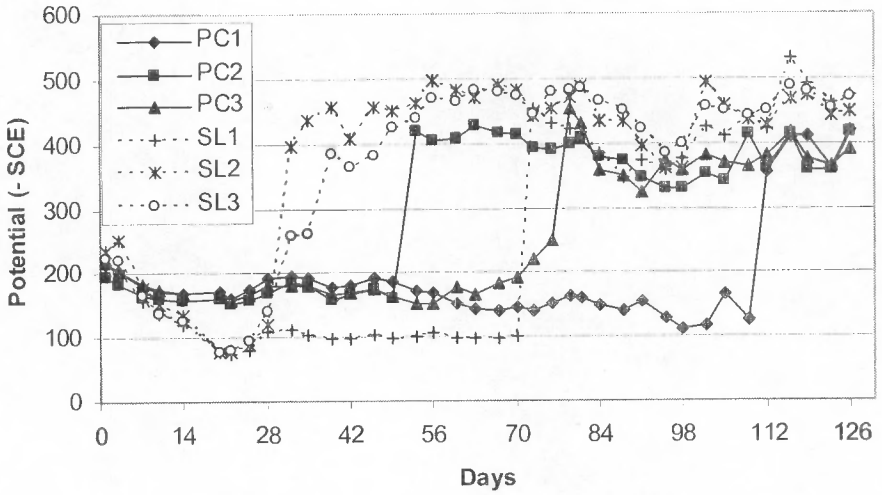

Fig 4B.1: PC and SL potential values

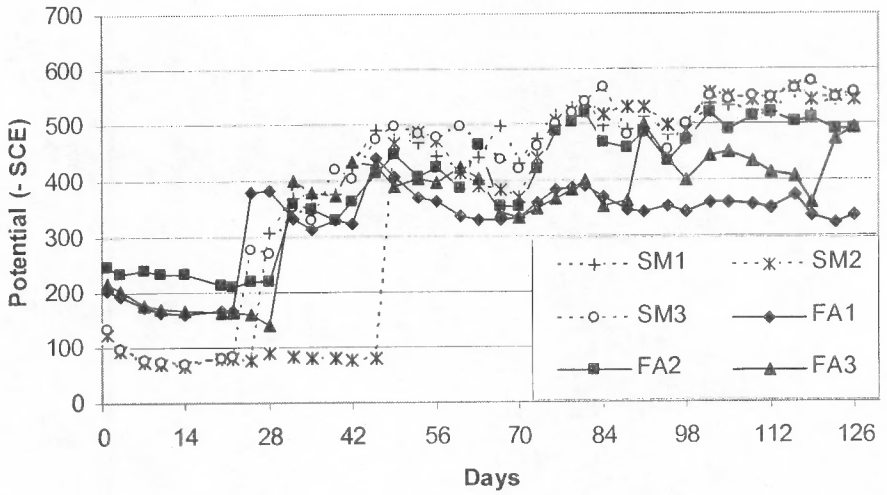

Fig 4B.2: SM and FA potential values

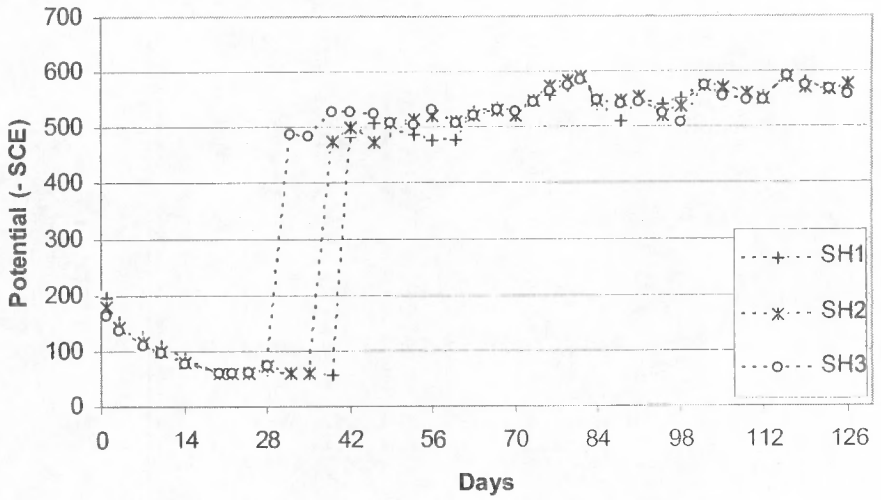

Fig 4B.3: SH potential plots

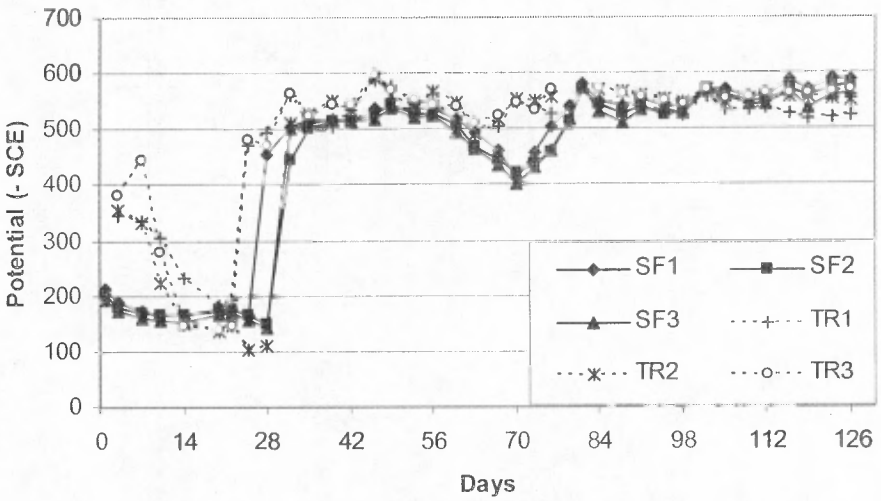

Fig 4B.4: SF and TR potential plots

4B.2 Corrosion Rate Plots

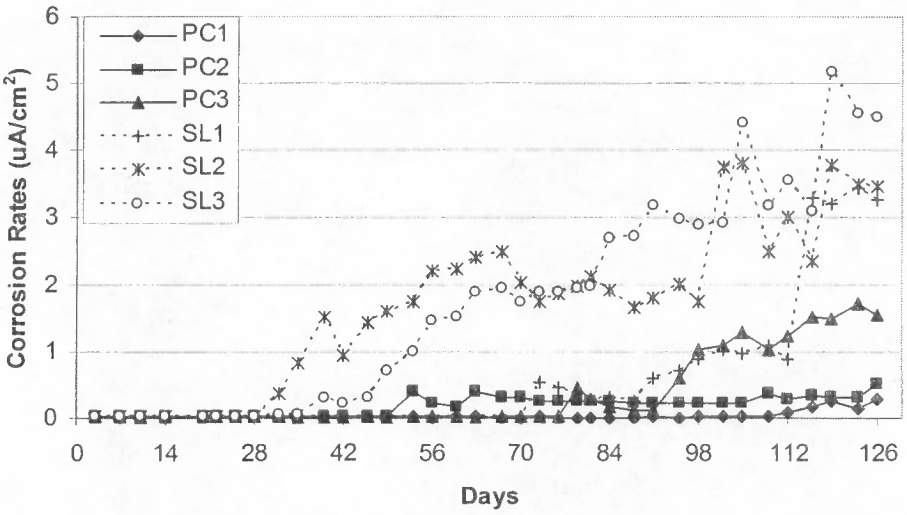

Fig 4B.5: PC and SL corrosion rates

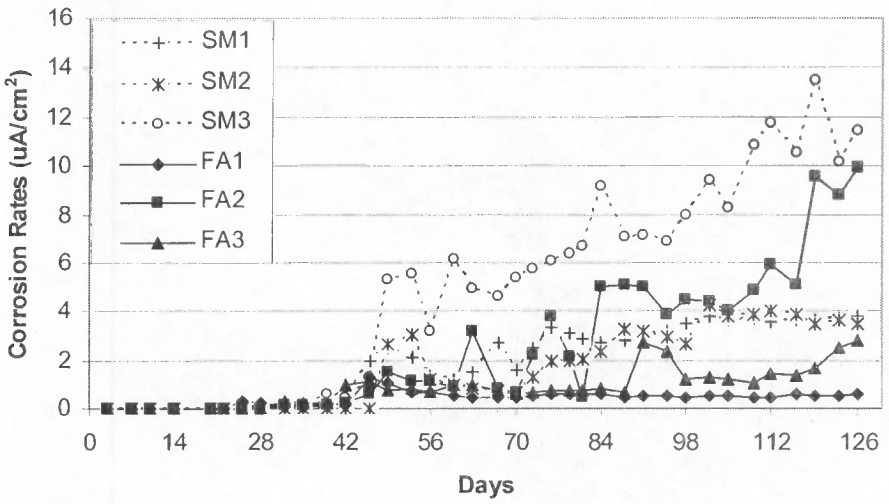

Fig 4B.6: SM and FA corrosion rates

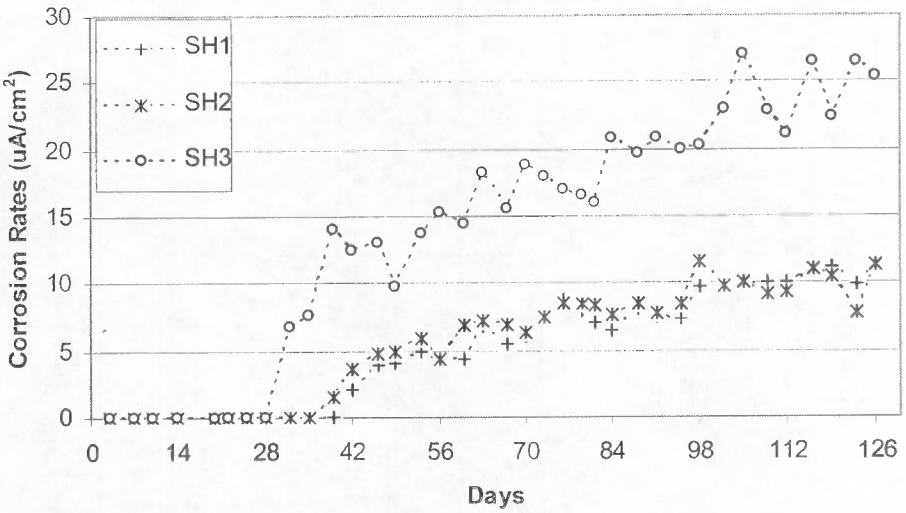

Fig 4B.7: SH corrosion rates

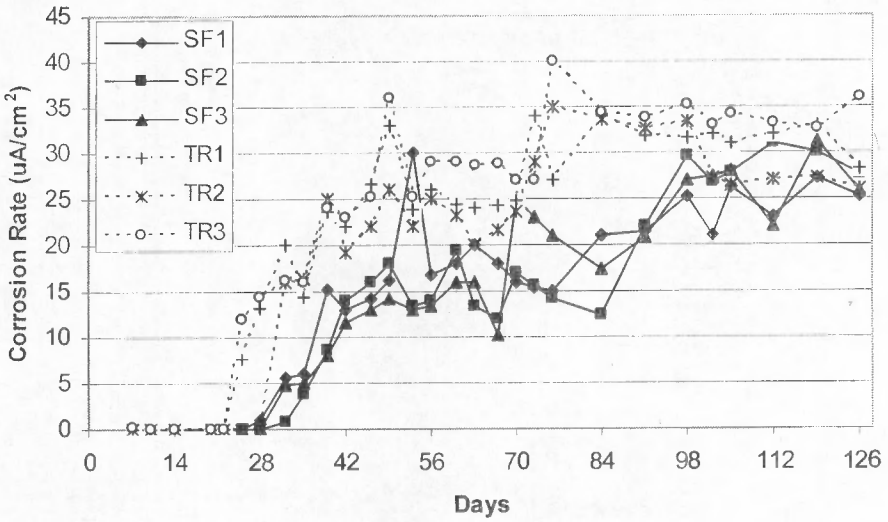

Fig 4B.8: SF and TR corrosion rates

4.9 References

ASTM 1994, *Standard G 5: Standard Reference Test Method for Making Potentiostatic and Potentiaodynamic Polarization Measurements*, **Annual Book of ASTM Standards, Section 3: Metals Test Methods and Analytical Procedures**, Vol 03.02, pp. 48-58.

Andrade, C. and Alonso, C. 1996, *Corrosion Rate Monitoring in the Laboratory and on-Site*, **Construction and Building Materials**, Vol. 10, No. 5, pp. 315-328.

Benjamin, S. and Sykes, J. 1989, *Chloride-Induced Pitting of Swedish Iron in Ordinary Portland Cement Mortars and Alkaline Solutions: The Effect of Temperature*, **Corrosion of Reinforcement in Concrete: Page, C. Treadaway, K. and Bamforth, P. ed.**, Elsevier Applied Sciences: London, pp. 59-64.

Breit, W. 1998, *Corrosion of Steel in Concrete: The Question of Corrosion Initiated by the Critical Chloride Content*, **Betonwerk + Fertigteil-Technik**, Vol. 11, pp. 37-45.

Burstein, G. and Ilevbare, G. 1996, *The Effect of Specimen Size on the Measured Pitting Potential of Stainless Steel*, **Corrosion Science**, Vol. 38, No. 12, pp. 2257-2265.

Cao, H., Baweja, D. and Roper, H. 1990, *Corrosion Characteristics of Steel in Solutions Derived from Cements and Blended Cements*, **Cement and Concrete Research**, Vol. 20, pp. 325-334.

Gillespie, R., Humphreys, D., Baird, N. and Robinson, E. 1989, **Chemistry, 2nd edition**, Allyn and Bacon Inc.: Massachusetts, pp. 876-881.

Glass, G., Page, C., Short, N. and Yu, S. 1993, *An Investigation of Galvanostatic Transient Methods used to Monitor the Corrosion Rate of Steel in Concrete*, **Corrosion Science**, Vol. 35, No 5-8, pp. 1585-1592.

Glass, G. 1995, *An Assessment of the Coulostatic Method Applied to the Corrosion of Steel in Concrete*, **Corrosion Science**, Vol 37, No. 4, pp. 597-605.

Gouda, V. 1970, *Corrosion and Corrosion Inhibition of Reinforcing Steel I: Immersed in Alkaline Solutions*, **British Corrosion Journal**, Vol. 5, pp. 198-203.

Hassanein, A., Glass, G. and Buenfled, N. 1998, *The use of Small Electrochemcial Perturbations to Assess the Corrosion of Steel in Concrete*, **NDT&E International**, Vol. 31, No. 4, pp. 265-272.

Hausmann, D. 1967, *Steel Corrosion in Concrete, How Does it Work?* **Materials Protection**, November, pp. 19-23.

Hinczak, H., Cao, H. and Cook, D. 1989, *Anodic Behavior of Steel in Solutions of Slag Blended Cements, Durability of Concrete, Aspects of Admixtures and Industrial by-Products*, **2nd International Seminar**, Swedish Council for Building Research, pp. 63-76.

Loewenthal, D., Ekama, G. and Marais, G. 1989, *Mixed Weak Acid/Base Systems, Part 1: Mixture Characteristics*, **Water SA**, Vol. 15, No. 1, pp. 3-24.

Mansfeld, F. 1970, *The Polarization Resistance Technique for Measuring Corrosion Currents*, **Advances in Corrosion Science and Technology**, pp. 163-261.

Mammoliti, L., Brown. L., Hansson, C. and Hope, B. 1996, *The Influence of Surface Finish of Reinforcing Steel and pH of the Test Solution on the Chloride Threshold Concentration for Corrosion Initiation in Synthetic Pore Solution*, **Cement and Concrete Research**, Vol. 26, No. 4, pp. 545-550.

Millard, S., Gowers, K. and Gill, J. 1991, *Reinforcement Corrosion Assessment Using Linear Polarization Techniques*, **Evaluation and Rehabilitation of Concrete Structures and Innovations in Design, Proceedings ACI International Conference SP 128-24, Hong Kong**, pp. 373-394.

Morgan, T. 1990, *Some Comments on Reinforcement Corrosion in Stagnating Saline Environments*, **Corrosion of Reinforcement in Concrete: Page, C. Treadaway, K. and Bamforth, P. ed.**, Elsevier Applied Sciences: London, pp. 29-38.

Rodriguez, P. and Gonzalez, J. 1994, *Use of the Coulostatic Method for Measuring Corrosion Rates of Embedded Metal in Concrete*, **Magazine of Concrete Research**, Vol. 45, No 167, pp. 91-97.

Rodriguez, P., Ramirez, E. and Gonzalez, J. 1994, *Methods of Studying Corrosion in Reinforced Concrete*, **Magazine of Concrete Research**, Vol. 46, No. 167, pp. 81-90.

Stansbury, E. and Buchanan, R. 2000, **Fundamentals of Electrochemical Corrosion**, ASM International: Ohio.

Tuutti, K. 1982, **Corrosion of steel in concrete**, Swedish Cement and Concrete Research Institute.

Wheat, H., Kasthurirangan, J., and Kitowski, C. 1997, '*17: Behaviour of Steel in Simulated Concrete Solutions*', **Mechanisms of Chemical Degradation of Cement-based Systems: Scrivener, K. and Young, J. ed.**, E & FN Spon: London. pp. 143-150.

West, J. 1980, **Basic Corrosion and Oxidation**, Ellis Horwood Limited: London.

Yonezawa, T., Ashworth, V. and Procter, R. 1988, *Pore Solution Composition and Chloride Effects on the Corrosion of Steel in Concrete*, **Corrosion Engineering**, Vol. 44, No. 7, pp. 489-499.

CHAPTER 5: EFFECTS OF CEMENT EXTENDERS, CRACKING AND COVER ON THE CORROSION OF STEEL IN CONCRETE

SECTION 1: Review of Literature

The corrosion of steel in aqueous media was discussed in some detail in chapter 4. Knowledge of the chemical processes and the effects of the specific cement extenders on the corrosion process are useful in furthering understanding of the principles of the corrosion mechanisms, but may not adequately represent the true case of corrosion in concrete. In order to make predictions of service life of structures and the impact of cement extenders, it is essential to have representative data. Thus the next set of experiments and discussion will focus on the corrosion of steel in concrete and mortar. Even mortar may not be entirely representative of corrosion in real structures as the inclusion of coarse aggregate may lead to greater voids and discontinuity along or near the steel concrete interface. These voids and points of discontinuity would likely represent preferred corrosion sites compared to a homogenous system. Mortar specimens are likely to present a more uniform consistency throughout the sample and are useful for comparative purposes.

The effects of surface finish and type of the reinforcing on the chloride threshold level were discussed in section 4.1.1. While the environment was a simulated pore solution (SPS), the principle of differing threshold values would still be applicable to the case of steel in concrete though not in absolute terms. The evaluation and comparison of the chloride threshold values must therefore account for these differences. The use of polished surfaces for instance, while not necessarily representing the true picture, allows for comparison within a certain set of experiments.

5.1 Concrete as a Medium for Protection of Steel

Concrete is an ideal medium for the protection of steel. The pore solution provides an environment which results in the formation of a passive layer around the steel due to its high alkalinity (pH usually greater than 12.5), the effectiveness of which has been shown in chapter 4. The concrete cover layer serves to limit the ingress of oxygen and chlorides which are essential for active corrosion. The resistivity of the concrete matrix will also limit the rate of corrosion once it has been initiated. Corrosion of steel in concrete does however occur and can generally be attributed to the transport of aggressive substances from the surface of the concrete to the level of the steel. The transport mechanisms are generally a function of the permeability, including chloride binding, of the concrete which in turn is dependant upon the

total porosity and its distribution. As Brown et al. (1991) state 'porosity of a material is not of interest as an end in itself, rather porosity is of interest because it directly influences both mechanical and transport properties of cementitious materials'.

5.1.1 Porosity and Permeability of Concrete

The heterogeneous nature of concrete results in a number of phases in the material which have specific properties and influence the material as a whole. There are three phases present in concrete: the cement paste, the aggregate, and the aggregate paste interface, also known as the interfacial transition zone (ITZ). In hardened cement paste (HCP) there exist two primary types of pores (excluding intentionally entrained air), capillaries and gel pores, with a possible further subdivision between large and small capillaries and gel pores. Gel pores are inherent in the cement and are a result of the process of hydration. The gel of HCP has a characteristic porosity of approximately 28% (Addis, 1986). Gel pores are small in size (about 2 nm (Brown et al., 1991)), and do not greatly affect the permeability of the concrete. For complete hydration to occur the theoretical minimum water/cement (w/c) ratio by mass is 0.23; this assumes that all of the cement capable of hydrating has done so (Hansson, 1995).

Unlike gel pores, capillary pores are significantly affected by the w/c ratio and the degree of hydration. Capillary pores are formed when there is insufficient gel volume to occupy all the available space. This is associated with an excess of mixing water. Consider the case of limiting space for hydration. If there is an excess of water (w/c > 0.36) there will be more water filled spaces than can be filled by the products of hydration, thus those areas where there is full hydration can expect a gel porosity of approximately 28% and an additional degree of porosity will be added by those areas which have not been filled. It is the interconnection and volume of capillary pores in the cement paste which significantly affect both the durability and strength of the hardened cement. As Neville (1972) has stated, the capillary pores allow for the more rapid diffusion of moisture and various chemicals through the cement mass.

The issue of permeability is complicated by both the presence of aggregates and, more importantly, by the resulting ITZ between the aggregate and HCP. According to Mehta and Monteiro (1993), a typical sedimentary aggregate might have a porosity of 5% compared to 28% for the cement paste. While the porosity of the aggregate is generally much lower, the degree of interconnectivity of the internal pores is much greater thus providing pathways for the movement of fluids or other substances. Table 5.1 shows a comparison of the permeability

of various rock types and the w/c ratio required to produce equivalent permeability of hydrated cement paste.

Table 5.1: Comparison of permeability coefficients between aggregates and cement paste (Base on Perraton et al., 1992)

Type of Rock	*Permeability Coefficient (m/s)*	*w/c ratio of hydrated cement paste of same perm.*
Trap rock	2.47×10^{-14}	0.38
Quartz (Diorite)	8.24×10^{-14}	0.42
Marble	2.39×10^{-10}	0.48
Marble	5.77×10^{-10}	0.66
Gray	1.23×10^{-10}	0.71
Granite	1.56×10^{-10}	0.71

The interface between the aggregate and the cement paste (the ITZ) is generally more porous than the HCP and contains fewer cementitious hydration products, particularly CSH. Mehta and Monteiro (1993) further state that the increase in permeability in concrete is attributed to the presence of micro-cracking of the cement paste in the transition zone during early periods of hydration. The crack widths in the transition zone are generally larger than the capillary cavities found in the cement paste and the interconnected cracks and micro-cracks provide pathways conducive to the transport of water.

5.1.2 Effect of Cement Extenders on Permeability of Concrete

The inclusion of any of the cement extenders (FA, SF or slag) will significantly alter the microstructure of the bulk cement paste and in some cases the ITZ around the aggregate. Slag concretes have been shown to have a similar overall porosity to OPC but with a more refined pore structure characterized by an increase of fine gel pores and a reduction of connectivity of the capillary pores (Parrott, 1995). The permeability of the slag system therefore is lower than OPC despite having essentially the same porosity. Glasser (1991) attributes this to chemical transport away from the slag grains which results in an accumulation of residual porosity at the former grain site. There is therefore a transformation from a system in which permeability occurs as a result of interconnected pores to one in which there are isolated sites distributed throughout the matrix thus effectively reducing the overall permeability.

In one study, the incorporation of 30% Slag was shown to result in an increase in the thickness of the interfacial zone from 37 μm for OPC concrete to 45 μm for an equivalent slag concrete (Nilsen et al., 1992). Although there is an increase in the size of the transition zone,

the relative reduction in the CH concentration compared to OPC at both 7 and 91 days would suggest an increased CSH component and therefore a less permeable transition zone. The primary benefit of Slag in the ITZ is attributed to the nucleation of numerous small and randomly orientated CH crystals on the Slag particles (Nilsen et al., 1992).

The replacement of OPC by FA, similar to slag, results in greater discontinuity of the pore structure and a less permeable material. Berry et al. (1989) have shown that FA pastes have a greater porosity than OPC pastes, particularly with respect to the small void fraction. The inclusion of FA however, tends to block the pore structure possibly through improved nucleation, thus resulting in a less permeable material. It should be noted that at 28 days there appeared to be no net removal of CH from the paste, though there was some slight increase in CSH production. Long periods may be required to evaluate the continued pozzolanic effects. One of the concerns with the use of FA is the perceived requirements for longer curing times to achieve the improved performance. Thomas et al. (1989) however have shown that FA containing concretes were less permeable to both oxygen and water than OPC concretes regardless of the curing period.

The incorporation of SF into concrete has significant benefits to both the microstructure of the bulk cement paste and the ITZ. The ultra fine and highly reactive nature of SF results in the rapid formation of CSH from CH. The CSH in SF concrete however has been shown to have a lower C/S ratio than that of FA. The SF particles surrounding the cement grains serve as nucleation sites for CSH and result in a densified matrix (Roy, 1989). Roy (1989) has shown substantial reduction in the mean pore size distribution with the addition of SF, FA or Slag. The inclusion of SF has been shown to substantially lower the porosity of the ITZ compared to OPC as illustrated in Figure 5.1. The ITZ in the presence of SF is characterized by a considerable reduction in CH though there is little effect on the orientation of the CH crystals (Nilsen et al., 1992). The inclusion of SF does however result in less accumulation of free water at the interface and provides nucleation sites which limit the size of the CH crystals. The importance of the fine filler effects with SF has also been demonstrated by Bentur (1991) through experiments comparing SF with carbon black which revealed the importance of the particle size and shape to its overall effectiveness.

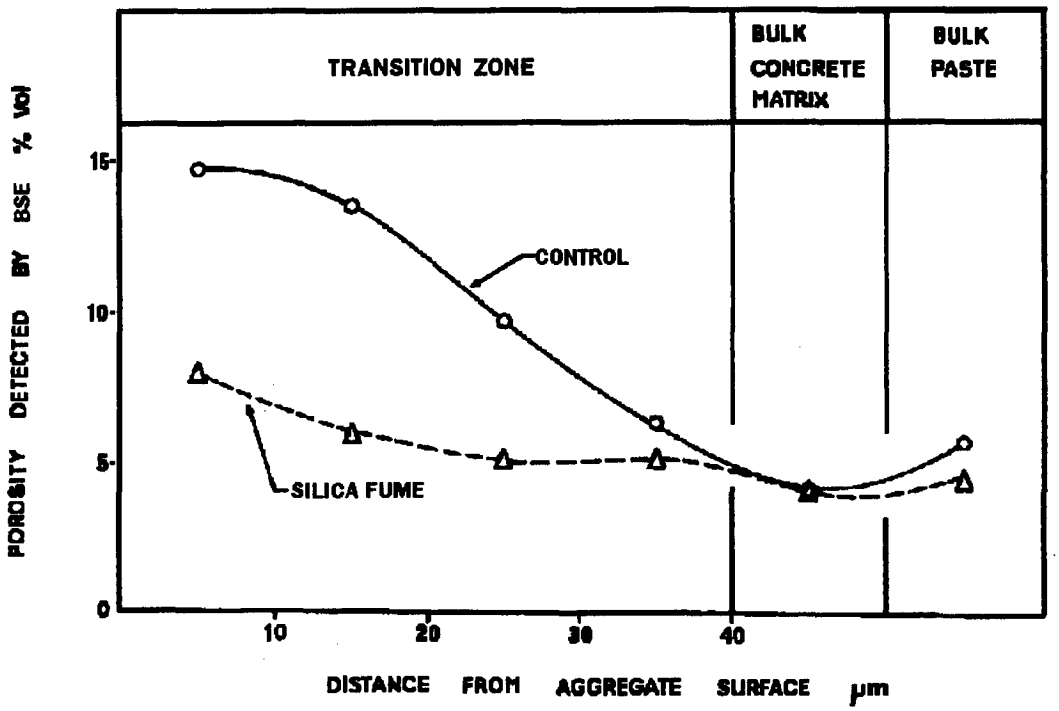

Fig 5.1: Porosity in the ITZ with inclusion of SF (Bentur, 1991)

The inclusion of cement extenders has been shown to generally reduce the permeability of concrete through refinement of pore structure and improved characteristics of the ITZ. The reduction in permeability, thus limiting mobility within the concrete matrix, is likely to result in increased resistivity of the concrete and influence the ingress of both oxygen and chlorides. The improved properties of concrete, made with cement extenders, should help reduce the likelihood of corrosion and the rate of corrosion once initiation has occurred. Parrott (1995) noted however, that concretes made with slag at replacement levels of 25, 50 and 75% had a somewhat greater permeability to air than those made with CEM I after 18 months of drying at 60% RH.

The effects of the pore chemistry on the corrosion of steel were demonstrated in sections 4.5 and 4.6 where PC was shown to provide the best protection to the steel in aqueous solutions through higher threshold values and a subsequent reduction in corrosion rate compared to the other representative standard pore solutions. There must be some competition therefore between the negative chemical influences of the cement extenders and beneficial physical effects associated with the concrete cover that accrue when extenders are used which will be further explored in this chapter.

5.2 Chloride Binding in Concrete

The movement of chlorides through concrete is more than simply a physical phenomenon related to the permeability of the concrete. It has been shown that the movement of chlorides through concrete does not follow exactly the diffusion pattern as given by Fick's second law but there is a time dependence such that the rate of ingress of chlorides decreases with time at a rate greater than Fick's law would predict (Mangat and Molloy, 1994). Zhang and Gjorv (1995) state that the diffusion of chloride in concrete does not follow the Fick's model since electrochemical factors such as ionic interaction and the electrical double layer of the pore walls will interfere with the transport of chloride ions. Chloride binding is essentially the removal of chloride ions from the solution through interaction with the concrete matrix. Chlorides can be bound chemically through a reaction with C_3A to form calcium chloro-aluminates (Boddy et al., 1999). The nature of the concrete chemistry is important in determining the migration of chloride through concrete and thus the level of chloride present at the steel. Chloride binding may further influence chloride transport through partial blocking of pores due to the formation of the calcium chloro-aluminates. It is not the intent of this work to thoroughly review the transport properties and mechanisms of chloride through concrete. As chloride binding affects the level of free chloride in solution it is reasonable to briefly discuss some of the work previously done in this area in as much as it influences the corrosion of steel in concrete.

All mineral cements bind chlorides to some degree and this strongly influences the rate at which chlorides penetrate the concrete when exposed to chlorides from an external source. Chloride binding effectively removes chlorides from the transport process resulting in changes to the pore solution concentration and thus the gradient driving ionic diffusion (Glass et al., 1997). Andrade and Page (1986) investigated the influence of cement type and chloride source (at the time of mixing) on the binding efficiency of cement paste. $CaCl_2$ was shown to yield significantly lower concentration of free chlorides compared to NaCl. The free chloride concentration in the pore solution of a blast furnace cement was approximately half that of the OPC for both NaCl and $CaCl_2$. Arya et al. (1990) showed similar increased binding capacity of slag cements compared to OPC for admixed chlorides but substantially less variation where chlorides migrated into the concrete from an external source. The results from their work are summarized in Table 5.2.

Table 5.2: Effect of binder type on chloride binding (Arya et al., 1990)

Binder Type	*Total Cl*	*Free Cl*	*Bound Cl*	*% bound*
PC	1.635	0.831	0.804	50
30% FA	1.887	0.818	1.069	57
70% slag	1.750	0.830	0.920	53
10% SF	1.265	0.684	0.581	46
SRPC	1.659	0.885	0.774	47

Glass et al. (1997) noted a variation in the order of binder binding efficiency with 65% slag resulting in the greatest degree of chloride binding, in contrast to the work of Arya et al. (1990) who showed 30% FA having greater binding capacity compared with 70% slag. The effects of cement extenders are graphically shown in Figure 5.2 which also includes equations for the Langmuir binding isotherms. The effects of variations in total chloride content are also evident.

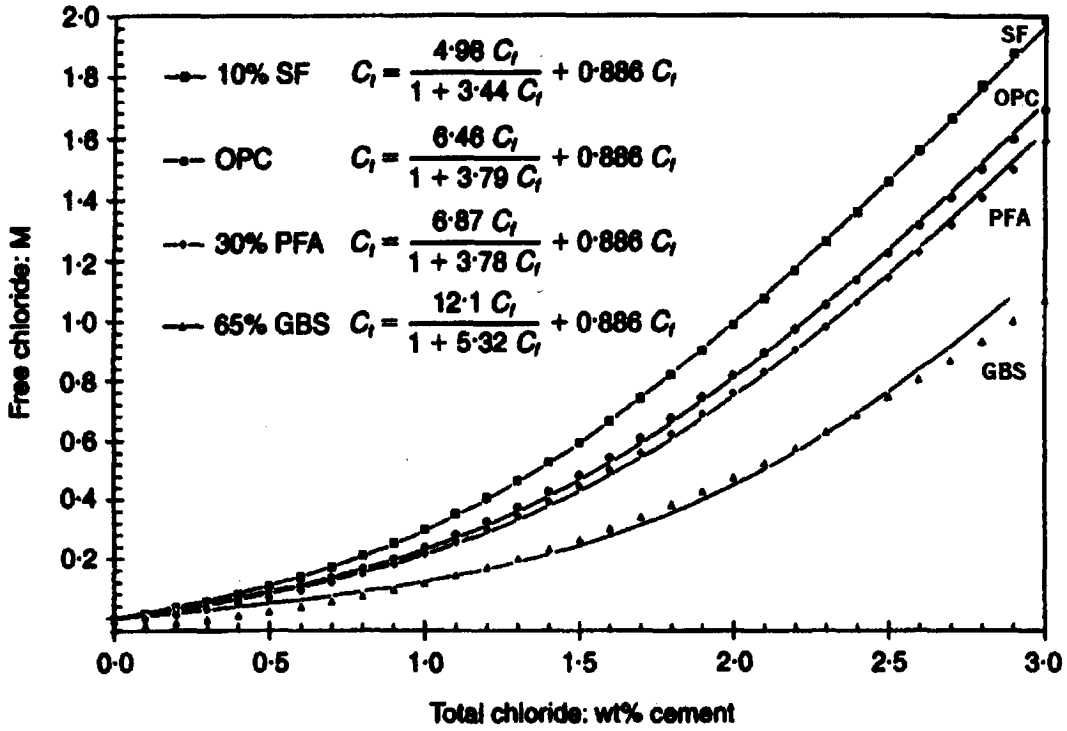

Fig 5.2: Chloride binding relationships dependant on binder type and total chloride concentration (Glass et al., 1997).

Binding of chlorides results in a substantial lengthening of the time to corrosion initiation. Martin-Perez et al. (2000) show that diffusion coefficients based on Freundlich binding isotherms can increase the time to depassivation from 44 years, without binding, to

199 years with binding, ceteris paribus, in their particular example. The effects of cement extenders, and by inference chloride binding, on limiting the ingress of chlorides are provided by Tarek et al. (2002) in their examination of concrete after 15 years of exposure in tidal zones. For an assumed cover depth of 70 mm and a threshold value of 0.4% water soluble chlorides by mass of cement, the time to initiation is 22, 65 and 150 years for OPC, FA (10-20%), slag (60-70%) respectively. The effects of binder type and chloride binding clearly influence the time required for chlorides to attain sufficient concentration to initiate corrosion. Even if corrosion has started, the rate of corrosion will continue to be affected by the binding as there is a much slower increase in chloride level which will in turn limit the increase in corrosion rate.

5.3 Critical Chloride Threshold Levels

There has been much debate surrounding the issue of chloride threshold levels required to initiate corrosion. Much of this debate has focused on the presentation of the chloride level, whether it should be expressed as the ratio of Cl/OH with Cl representing the free chlorides available in the solution or for instance water or acid (total) soluble chlorides by mass of cement. It is generally stated that only the free chlorides ions are able to depassivate the steel and are thus critical in the assessment of reinforcing corrosion (Alonso et al., 2000, Pettersson, 1994, Hansson and Sorensen, 1990).

Glass and Buenfeld (1997) suggest that bound chlorides do in fact pose a substantial risk and that chloride threshold values are best presented as total chloride content relative to mass of cement. In the assessment of available literature, Glass and Buenfeld note a greater range in values for presenting free chloride concentration compared to total chloride concentration. For instance, in one case the lowest total chloride content is 38% of the highest while the lowest free chloride content is only 15% of the highest. One would expect that if only free chloride ions participated for any given total chloride concentration there would be a smaller range of possible chloride threshold levels. The observed effect of a smaller range of total critical chloride concentrations suggests that bound chlorides do present a risk and chloride concentrations are best expressed as such. Furthermore, the highest concentration of free chlorides in which steel has been examined is 4M which is only twice the concentration of the highest critical chloride level require to initiate corrosion compared to values for total chloride concentration which are more than 5 times the highest reported value required to induce corrosion. Thus, there is both a smaller variability in chloride concentrations for total chlorides and a greater overall range in which steel in concrete has been evaluated.

The measurement and reporting of chloride levels in the current investigation is therefore based on the total chloride concentration. Both the practical issues related to ease of measurements and the suggestions by Glass and Buenfeld, which indicate presentation of total chlorides as a more sound and reliable method of analysis, led to the total chloride concentration being adopted.

The critical chloride threshold value of 0.4% by mass of cement had been suggested for some time as stated in code BS 8110 (Pettersson and Sandberg, 1997). Table 5.3 provides a summary of some of the work for establishing the critical chloride content for the corrosion of steel in concrete. All the work listed in Table 5.3 allowed for the diffusion of chloride through the concrete or mortar to the steel and chlorides were not incorporated into the concrete at the time of mixing. There are many further works which used chloride inclusion at the time of mixing but these have not been presented in this list as there is no allowance for the proper development of the passive layer and the availability of chloride would be affected by the early hydration mechanisms.

Breit (1998) investigated a number of cement types including, PC, Slag cement, FA, Rapid Hardening and SF with a steel electrode embedded in mortar and exposed to 1% chloride solution. The critical chloride threshold ranged from 0.25 to 0.75% by mass of binder with 0.25% representing a 10% probability and 0.80%, 100% probability of corrosion. No distinction was stated between the cement types. An examination of the data however shows that the SF containing samples generally had a lower chloride threshold in the range of 0.25 to 0.4% which is also consistent with the work of Hansson and Sorensen (1990).

Pettersson (1992) showed an increase in chloride threshold value for the FA sample compared to OPC. One explanation was that the reduction in porosity caused by the inclusion of FA resulted in a lower availability of oxygen at the steel surface. The pH of the FA mix was also quite high at 13.5, which was not dissimilar to the pH of 13.7 for the OPC sample.

Table 5.3: Chloride threshold levels for corrosion initiation

	Total Cl % Cem.	*Free Cl mg/l*
Hansson and Sorensen (1990)		
Plain carbon steel w/c 0.5 mortar		
Exposure 1M NaCl after 30 days		
OPC - Danish	0.85	
Rapid hardening	0.95	
Sulphate resisting (low C_3A)	0.85	
FA (22%)	0.56	
OPC -Swedish	1.01	
Micro Silica (10%)	0.39	
Breit (1998)		
Steel electrode w/c 0.5 & 0.6 mortar		
Exposure 1% Cl		
PC, Slag cement, FA, Rapid hardening		
min, max	0.25-0.75	
SF (10% added), w/c 0.55	0.25-0.40	
Pettersson (1992)		
Steel electrode, w/c 0.6, mortar		
Exposure 1M NaCl at 30 days		
OPC	1.3	37000
Silica oxide (10%)	0.5	12900
FA (25%)	1.7	36500
Thomas (1996)		
Mild steel bars, w/c variable		
Uniform strength, marine exposure after 28 days		
OPC	0.70	
FA 15%	0.65	
FA 30%	0.50	
FA 50%	0.20	

The effects of the addition of microsilica were again shown to significantly reduce the chloride threshold value to less than half that of the OPC sample. The effects of w/b ratio on the chloride concentration were investigated by Pettersson and Sandberg (1997) and can be seen in Figure 5.3. An increase in water/binder (w/b) ratio generally results in a lowering of the required chloride level. An increase in w/b ratio from 0.4 to 0.6 resulted in approximately a 40% reduction in the critical chloride concentration.

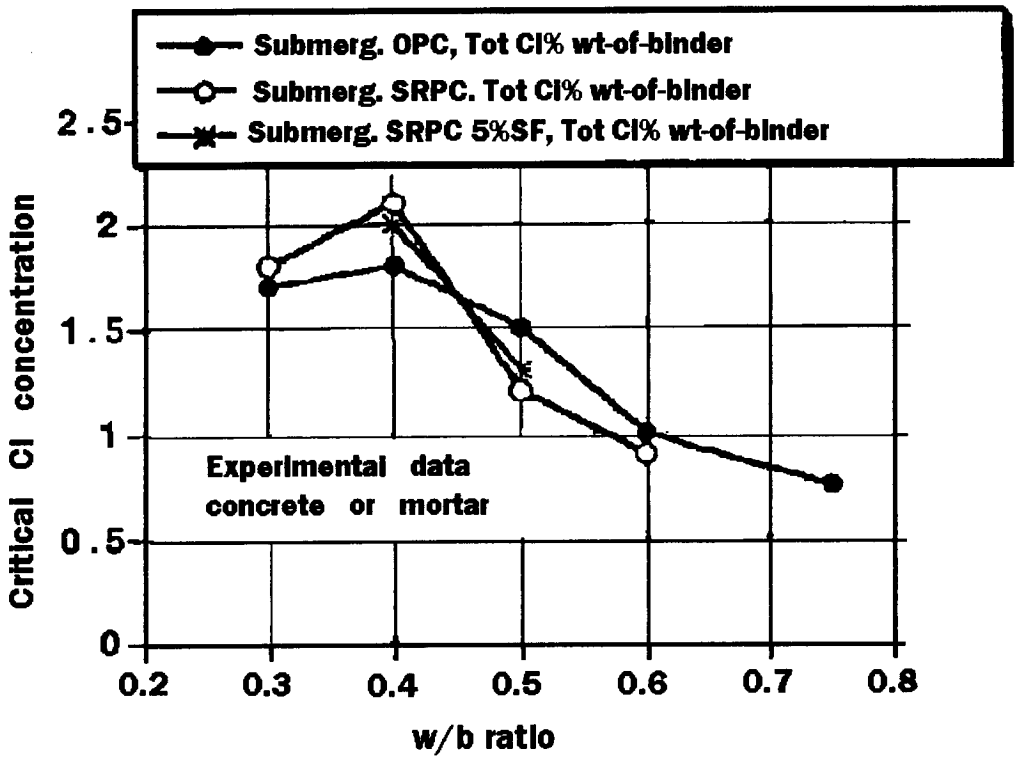

Fig 5.3: Effect of w/b ratio on the critical chloride concentration (Pettersson and Sandberg, 1997)

The influence of FA on the chloride threshold is also the subject of some debate with Thomas (1996) showing a significant reduction in chloride threshold level with the addition of FA compared to Pettersson (1992) who showed a modest increase. The effects of FA on the pore solution generally result in a reduction of the hydroxide concentration and it would be expected that in most cases the inclusion of FA would result in a lower chloride content to initiate corrosion as demonstrated by Thomas. The relationship between total chloride concentration and the Cl/OH ratio for OPC and FA (30%) is shown in Table 5.4. Thomas notes that despite FA having a lower chloride threshold the overall effects of FA are beneficial due to the increased resistance to chloride penetration.

Table 5.4: Relationship between total chlorides and Cl/OH ratio (Thomas, 1996)

Cl content	*Cl/OH in pore solution*	
(% wt. of cement)	*OPC*	*FA 30%*
0.5	0.44	0.61
1.0	1.34	2.03
2.0	4.02	5.36

The results from the literature, as given by Pettersson and Sandberg (1997), generally indicate that the inclusion of slag has little effect on the chloride threshold level though Macphee and Cao suggest the presence of sulphide should have some negative effect on the threshold level. There appeared to be relatively little difference in chloride thresholds shown in the work of Breit (1998) where a slag cement was employed. Glass and Buenfeld (1995) also state that there is no evidence that slag influences the chloride threshold. The inclusion of sulphide ions was shown to have some small effects on the chloride threshold level as demonstrated in the aqueous phase work presented in section 4.5, though the hydroxyl content and hence Cl/OH ratio was more influential. The conflicting views on the role of sulphide and the clear acceleration of the corrosion rate therefore required further investigation of the chloride threshold, particularly with the use of South African materials.

Alonso et al. (2000) have shown the dependence of chloride concentration on potential for the initiation of steel corrosion as seen in Figure 5.4.

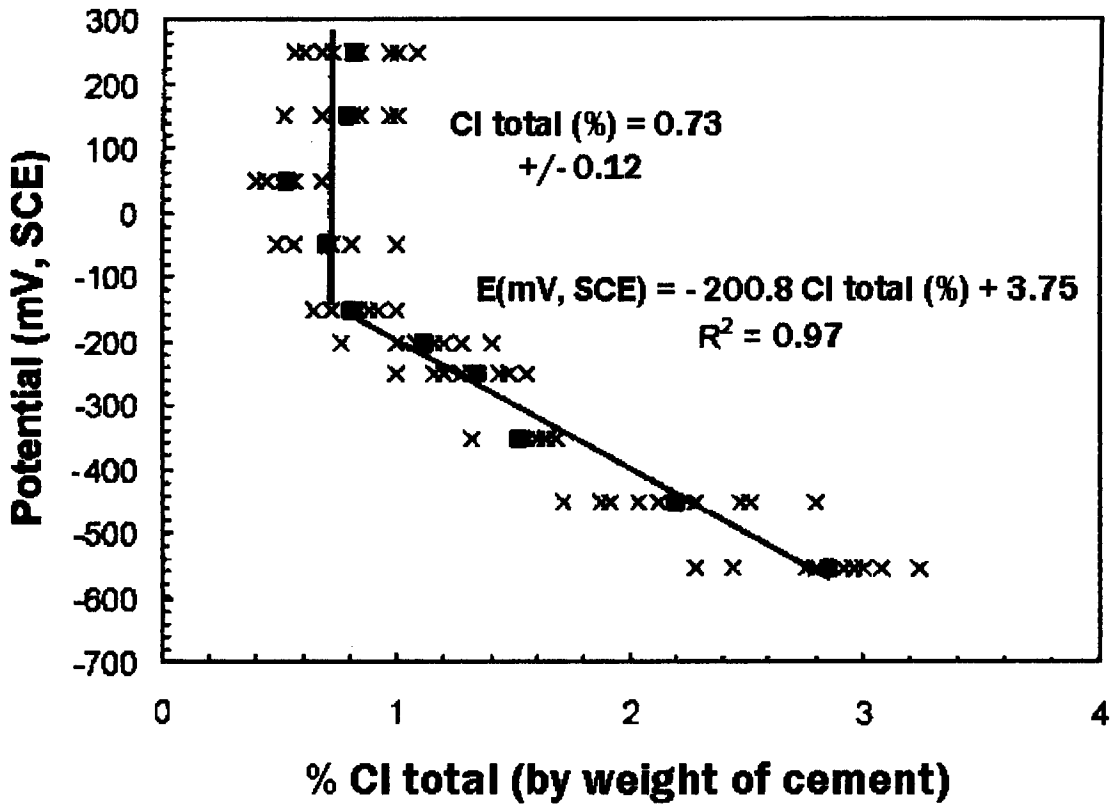

Fig 5.4: Relationship between potential and chloride threshold (Alonso et al., 2000)

A critical chloride concentration, by mass of cement, of approximately 0.73 % was determined for ribbed bar in PC mortar specimens for potentials more positive than –200 mV. For potentials more negative than -200 mV, the critical chloride concentration was shown to vary according to:

$$E_{pot} = -200.8 \bullet (\%Cl^{-}total) + 3.75 \qquad \ldots 5.1$$

where E_{pot} is the potential of the rebar relative to a SCE.

A decrease in rebar potential therefore implies an increase in the chloride content necessary to induce corrosion. This is of particular interest to the current investigation as the inclusion of slag will be shown, later in this chapter, to have a significant impact upon the 'passive potential' of the steel, and, by extension from the work of Alonso et al., to affect the chloride concentration necessary to induce corrosion.

It is not the purpose of this work to present a comprehensive evaluation of all the research into the critical chloride contents as a number of papers including Glass and Buenfeld (1997), have adequately addressed this topic. It is sufficient to show that disagreement with respect to the role of cement extenders, particularly FA and Slag, exists. Within the context of this work aimed at evaluating the impact of cement extenders on the corrosion rates of steel in concrete, it is desirable to have chloride threshold information regarding the specific material under investigation.

5.4 Corrosion Rates

There are a great number of variables which will affect the corrosion rate of steel in concrete. Tuutti (1982) has listed some of them as: cement type, cement content, water/cement ratio, workmanship and environment, moisture, temperature, carbonation, cracking and cover thickness. Mangat and Molloy (1992) suggest that the factors controlling reinforcement corrosion can be summarized by the alkalinity and permeability of the concrete matrix, with the latter controlling the diffusion of Cl^{-}, O_2 and moisture to the steel. They note in their investigation however, that alkalinity is of secondary concern with the w/c ratio being the primary controlling factor.

The fundamental electrochemical processes in reinforcement corrosion have been shown to be governed by anodic control, that is the dissolution of iron, rather than access of oxygen. Alonso et al. (1988) state that cathodic control, the availability of oxygen, is only an issue when the concrete is under water or soil, or the cover is sufficiently thick to ensure the pores remain saturated. The nature of the corrosion reaction requires both a flow of electrons and

ions to complete the circuit. The electrical resistivity and hence resistance of the concrete to the flow of ions therefore will also affect the corrosion rate as demonstrated by Alonso et al. (1988).

A number of the factors affecting the corrosion rate of steel in concrete will now be presented. It is difficult to fully isolate the individual effects and state that the observed corrosion rate is a function of a specific variable. For instance, the inclusion of a cement extender such as FA will affect the permeability of the concrete in addition to resistivity and pore solution composition. Permeability is essentially a physical parameter which affects the mobility of water and other substances (O_2 for instance) around the steel and is significantly affected by the w/c ratio. Conductivity however is not greatly influenced by either the w/c ratio or porosity of the material (Tuutti 1982). It is necessary therefore to examine a variety of effects such as w/c ratio, resistivity, cover and cracking in order to more fully understand the nature of the corrosion process and ultimately be able to make predictions about the likely corrosion rates and remaining useful life in a particular structure.

5.4.1 Water/Cement Ratio and Cement Content

The w/c ratio is expected to affect the corrosion characteristics of the concrete primarily through densification of the pore structure which would limit the ingress of O_2 and increase the resisitivity of the concrete. Corrosion rates for 12 mm deformed rebar cast in concrete, with a cover depth of 10 mm, and three different w/c ratios and cement contents, were examined by Mangat and Molloy (1992). The specimens were exposed to cyclic periods of wetting and drying after 14 days air curing. The results are provided in Table 5.5.

Table 5.5: Influence of w/c and cement content on corrosion rates (Mangat and Molloy, 1992)

w/c	*Cement* kg/m^3	i_{corr} uA/cm^2	Cl^- *% mass cem*
0.45	430	0.13	1.4
0.58	430	0.65	2.0
0.76	430	2.16	2.3
0.58	330	0.62	1.73
0.58	530	0.52	1.21

It is evident that w/c ratio had a significant impact upon the corrosion rate of steel in concrete with the total cement content less so. The highest corrosion rate was observed in the 0.76 w/c

ratio with the accompanying highest chloride concentration. The lowest corrosion rate of 0.13 $\mu A/cm^2$ was found to occur in the w/c 0.45 sample despite having a higher chloride content than the 0.58 w/c with 530 kg cement. The effect of the w/c ratio is considerable, such that the lower w/c ratio resulted in a lower corrosion rate with a higher chloride concentration compared to the higher w/c ratio which had a lower chloride content. The effects of the material are thus more significant than simply limiting the chloride ingress. The cement content was shown not to significantly affect the corrosion rate which ranged from 0.52 to 0.65 $\mu A/cm^2$ for cement contents between 330 and 530 kg/m^3. This is also supported by (Rasheeduzzafar et al., 1990). The effects of w/c ratio and hence permeability on corrosion characteristics are even more stark when it is considered that 530 kg of cement resulted in a Cl/OH ratio of 6 compared to 11 for the 0.45 w/c ratio with 430 kg cement. Thus the physical effects of the concrete appear to dominate the chemical contributions of the hydroxyl ions in the pore water.

A similar reduction in corrosion current from 59 μA to 25 μA with decrease in w/c ratio from 0.6 to 0.5 was noted by Schiessl and Raupach (1990). The decrease in corrosion current is attributed to lower permeability of the concrete at w/c ratio 0.5.

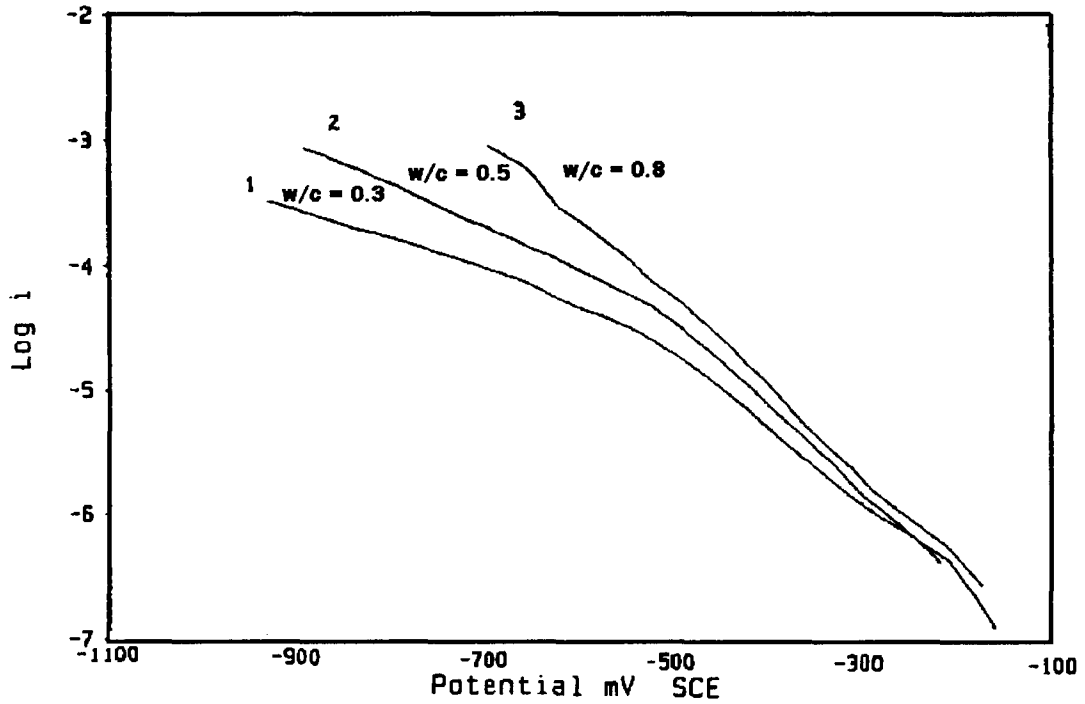

Fig 5.5: Influence of w/c ratio on cathodic reduction of oxygen (Sykes, 1995)

The effects of a lower w/c ratio on the permeability of the material to O_2 can be seen indirectly in Figure 5.5 for the cathodic reduction curve of mild steel in chloride-free mortar

specimens. The decreasing current *i* for a given potential is observed as the w/c ratio decreases from 0.8, curve 3, 0.5, curve 2, to 0.3, curve 1 thus limiting the availability of oxygen. The reduction in the cathodic current curve will therefore result in a smaller corrosion current even in the absence of any other contribution from the w/c ratio such as increased resistivity.

5.4.2 Effect of Cover

The effects of cover on the corrosion rate of steel in concrete have been effectively demonstrated by a number of authors (Lambert et al., 1991, Balabanic et al., 1996, and Raupach, 1996). Lambert et al. (1993) investigated the corrosion rate of 3 mm diameter mild steel rods in cement pastes (w/c 0.5) at cover depths of 10, 20, 30 and 40 mm. The specimens were exposed to monthly wet/dry cycles with 5% NaCl over a period of 2 years. After the initiation period and the onset of active corrosion, relatively stable corrosion rates were observed. It is likely that chloride levels at the various depths continued to increase, but an effective maximum corrosion rate (approximate) was observed for various cover depths as follows:

10 mm	= 20 $\mu A/cm^2$
20 mm	= 0.2 $\mu A/cm^2$
30 and 40 mm	= 0.04 $\mu A/cm^2$

The maximum corrosion current may be explained by the progressively decreasing availability of oxygen at greater cover depths. The 30 and 40 mm cover depths exhibited essentially the same corrosion rate. The corrosion rate of 0.04 $\mu A/cm^2$ appears low but was considered to represent active corrosion as there was a noticeable increase from the previous passive conditions.

There appear to be two main inter-related mechanisms for controlling the corrosion rate of steel, both dependant upon the relative humidity of the concrete. The movement of O_2 from the atmosphere to the surface of steel is a function of the diffusion coefficient (the ease with which O_2 can move through concrete) and the depth of the steel. The diffusion coefficient is in turn affected by both the w/c ratio, through the permeability of the concrete, and the relative humidity of the concrete. The movement of O_2 through concrete is significantly reduced by an increase in the proportion of water-filled voids. The O_2 diffusion coefficients for two w/c ratios of cement paste at various RH are provided in Figure 5.6. The substantial impact of RH on the diffusion coefficient is evident with an increase in RH from 60 to 80% resulting in approximately an order of magnitude decrease in diffusion coefficient.

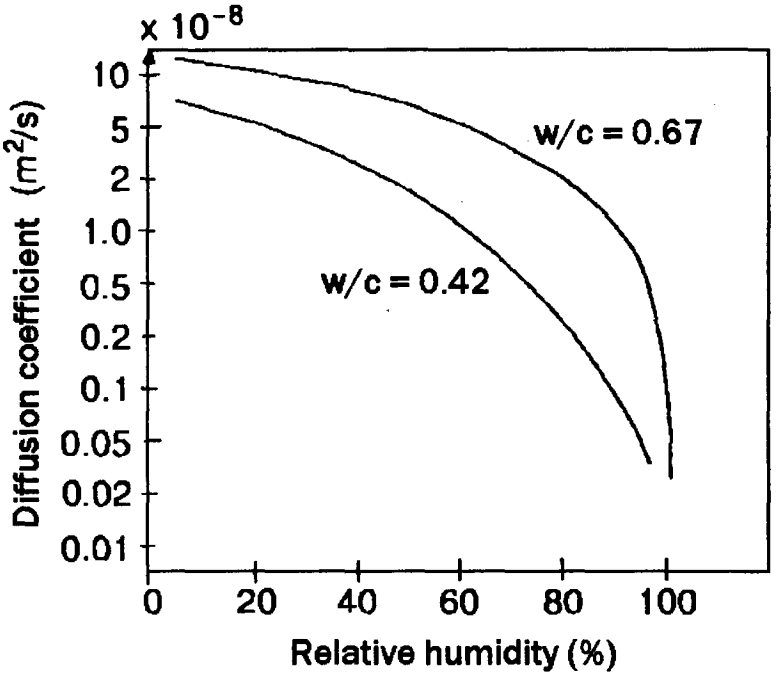

Fig 5.6: Influence of w/c ratio and RH on the diffusion coefficient for O_2 (Bentur et al., 1997)

The effects of cover on the diffusion of O_2 are illustrated in Figure 5.7. An increase in cover depth from 20 to 50 mm would result in an order of magnitude reduction in the availability of O_2 at 60% RH.

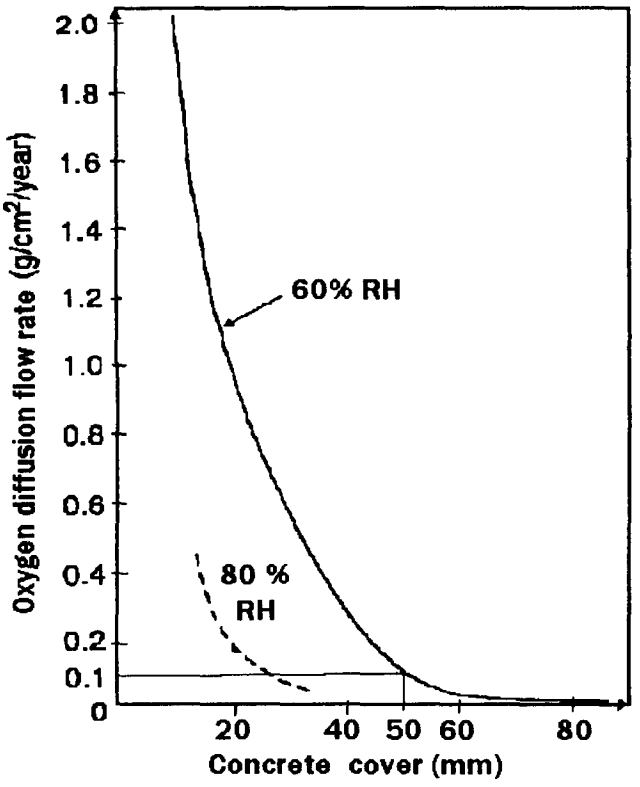

Fig 5.7: Effect of concrete cover on the diffusion of O_2 (Bentur et al., 1997)

Thus the coupled effect of an increasing cover depth and a shift in RH from 60 to 80% would result in almost two orders of magnitude decrease in the availability of O_2. The increased cover depth is also likely to minimize the influence of the external drying at the depth of the steel thus sustaining a fairly high RH.

The influence of O_2 diffusion and cover depth on the macro-cell corrosion current has been demonstrated by Raupach (1996). The influence of RH and cover on the movement of O_2 through concrete is clearly significant. The corrosion reaction will consume O_2 at a given rate depending upon certain electrochemical conditions such as Cl concentration, and resistivity. If O_2 is supplied in greater concentration than is required, there will be little or no change to the corrosion rate. Thus an order of magnitude change in supply of O_2 may not significantly affect the underlying corrosion of steel in concrete. Figure 5.8 provides a theoretical description of the influence of cover and diffusion coefficient on the macro-cell corrosion current.

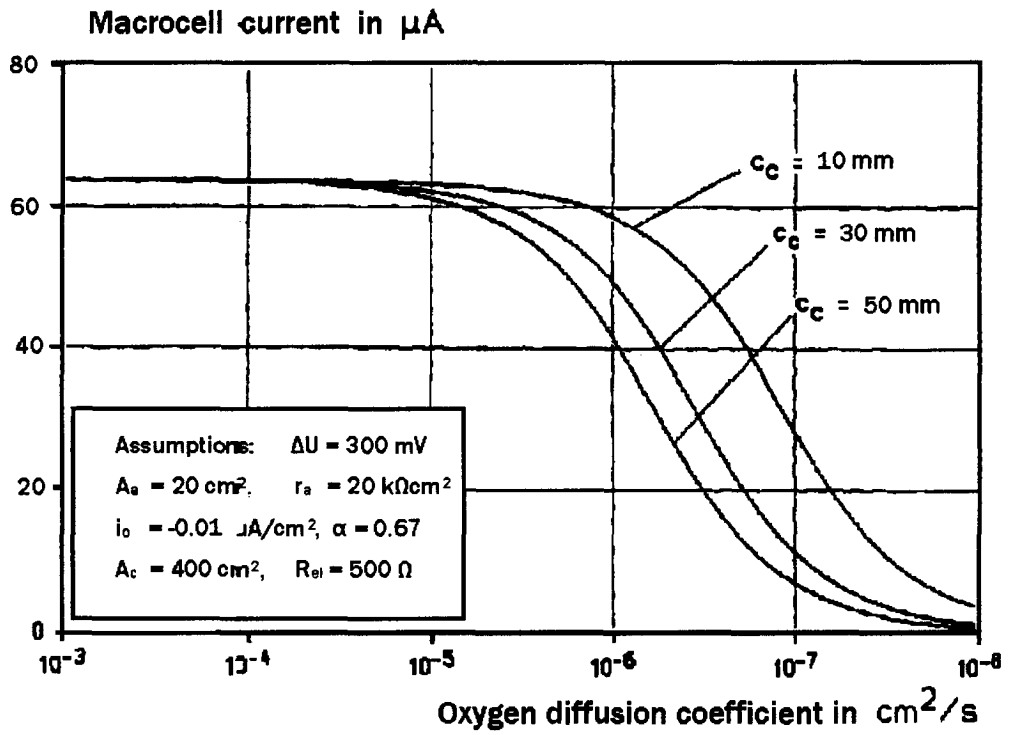

Fig 5.8: Implications of cover (C_c) and diffusion coefficient on macrocell corrosion current (Raupach, 1996).

It can be seen that for diffusion coefficients above 10^{-5} cm^2/s there is no appreciable change in corrosion current. At a diffusion coefficient of 10^{-6} cm^2/s an increase in cover from 10 to 50 mm results in a reduction of the corrosion current by one third.

5.4.3 Influence of Resistivity and Relative Humidity

Alonso et al. (1988) have noted, where O_2 is relatively free to penetrate to the depth of the steel, the corrosion reaction is no longer limited by the cathodic reaction. Anodic control or resistivity considerations must therefore be the principle factors controlling the rate of corrosion. Since anodic control is unlikely to be significant, except for the case of passive corrosion, the resistivity of the system must be the controlling factor under most non or semi-saturated situations. Resistivity of the concrete is affected only moderately by the w/c ratio, thickness or chloride content of the concrete (Tuutti, 1982). The resistivity of the concrete only changes by a factor of two when the w/c ratio is reduced from 0.7 to 0.4, or when $CaCl_2$ is added in concentrations up to 4% by mass of cement. The relatively minor reduction in resistivity associated with the inclusion of Cl^- is attributed to the already highly conductive properties of the very alkaline pore solution.

A change in the RH of the concrete from 100% to 50% however results in a substantial decrease in the conductivity of the concrete by several orders of magnitude as shown in Figure 5.9.

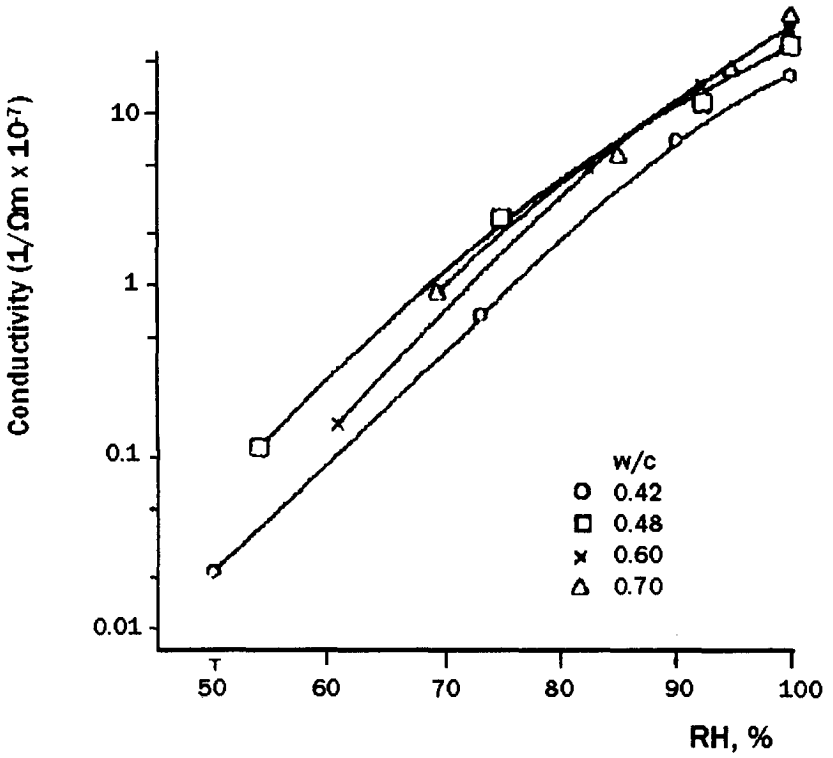

Fig 5.9: Effect of RH on conductivity of concrete (Tuutti, 1982)

The relationship between the resisitivity of the concrete, as measured in kOhm.cm, and corrosion risk is summarized by Andrade and Alonso (1996) in Table 5.6. The assessment is

based on an evaluation of real structures where corrosion rates of below 0.1 $\mu A/cm^2$ are considered negligible, 0.1-1.0 $\mu A/cm^2$ low to moderate and above 1.0 $\mu A/cm^2$ high.

Table 5.6: Relationship between resisitivity and corrosion risk (Andrade and Alonso, 1996)

Resistivity (kOhm.cm)	*Risk Level*
> 100 - 200	Corrosion values will be very low even if chloride contaminated
10 - 100	Low to high corrosion rate
< 10	Resistivity is not the controlling parameter

Increasing the RH of concrete results in a lowering of the resistivity of the concrete which facilitates corrosion, yet at the same time the increased RH tends to limit the ingress of O_2 needed for the cathodic reaction. Enevoldsen et al. (1993) suggest a RH 'threshold' for promoting corrosion to be approximately 85%, below which corrosion rate is rather limited. Tuutti (1982) states that cathodic control becomes effective at RH above approximately 90%, thus the maximum expected corrosion rate would occur where the RH of the concrete is between about 85 and 90%.

It was stated earlier in this section that w/c ratio and cover have only a minor influence on the resistivity of concrete. While this is true where the concrete is in a controlled environment and conditioned for a sufficiently long period of time, the effects of w/c and cover are quite profound in maintaining the RH of the concrete where there are seasonal fluctuations or periods of cyclic wetting and drying such as concrete exposed to tidal action or sea spray. Cover and w/c ratio are therefore important parameters through their effect on controlling the RH, and, by extension resistivity, of the concrete in the vicinity of the steel.

5.4.4 Influence of Temperature

The general principle of temperature affecting reaction rates was discussed in section 4.23 with the presentation of the Arrhenius equation. It was noted however that the corrosion rate of steel in concrete is unlikely to follow the equation directly due to factors such as the reduction in the solubility of dissolved oxygen, and accelerated drying of the concrete. Schiessl and Raupach (1990) determined that a 5°C increase in temperature resulted in an acceleration of the corrosion rate by a factor of 1.4 (approximately 2 x greater for a 10 degree rise in temperature).

A relationship between temperature and corrosion current is given by equation 5.2 (Liu, 1996):

$$i_1 = i_2 e^{2283\left(\frac{1}{T_2}-\frac{1}{T_1}\right)} \quad \ldots 5.2$$

where i_1 = corrosion current density at T_1

i_2 = corrosion current density at T_2

T_1 = temperature of concrete measured (degree K)

T_2 = desired temperature (degree K)

A change in temperature from 293 K to 303K results in a 1.3 factor increase in corrosion rate, which is less than the 2 times increase suggested by Schiessl and Raupach (1990). As Lopez et al. (1993) have noted, the effects of temperature should never be considered in isolation of the availability of electrolyte. If there is a constant supply of electrolyte, such as under saturated conditions, the temperature effects will be more pronounced (and the estimate by Schiessl and Raupach more reasonable) as the specimen will not experience drying and the associated increase in resistivity. Situations with cyclic wetting and drying, and those used in the current investigation, are more likely to follow equation 5.2 and thus will be used as a basis of comparison of corrosion rates across various temperatures.

5.4.5 Inclusion of Cement Extenders

The use of cement extenders has been shown in sections 5.2 and 5.3 to have a significant impact upon the pore structure of concrete and its ability to bind chloride ions. Furthermore, the nature of the pore solution has also been investigated in chapter 4 and the effects on the corrosion rate of steel in simulated pore solutions were determined. The changes in both the chemical properties of the pore solution and physical properties of the cover layer therefore are likely to significantly impact upon the corrosion rate of steel in concrete.

Sirivivatnanon et al. (1994) investigated the impact of three cement extenders, at various replacement levels, on the corrosion rate of steel in mortars. The steel was machined and polished and provided with a 10 mm cover. After an initial curing period, the samples were exposed to 3% NaCl. The corrosion rates may be affected by variations in the chloride content at the level of the steel since the diffusion characteristics of blended cements differ substantially from PC. The chloride concentrations in the first 10 mm however are generally not significantly different, thus it reasonable to compare the corrosion rates under these conditions. The effects of cement extenders on macrocell corrosion are evident in Figure 5.10.

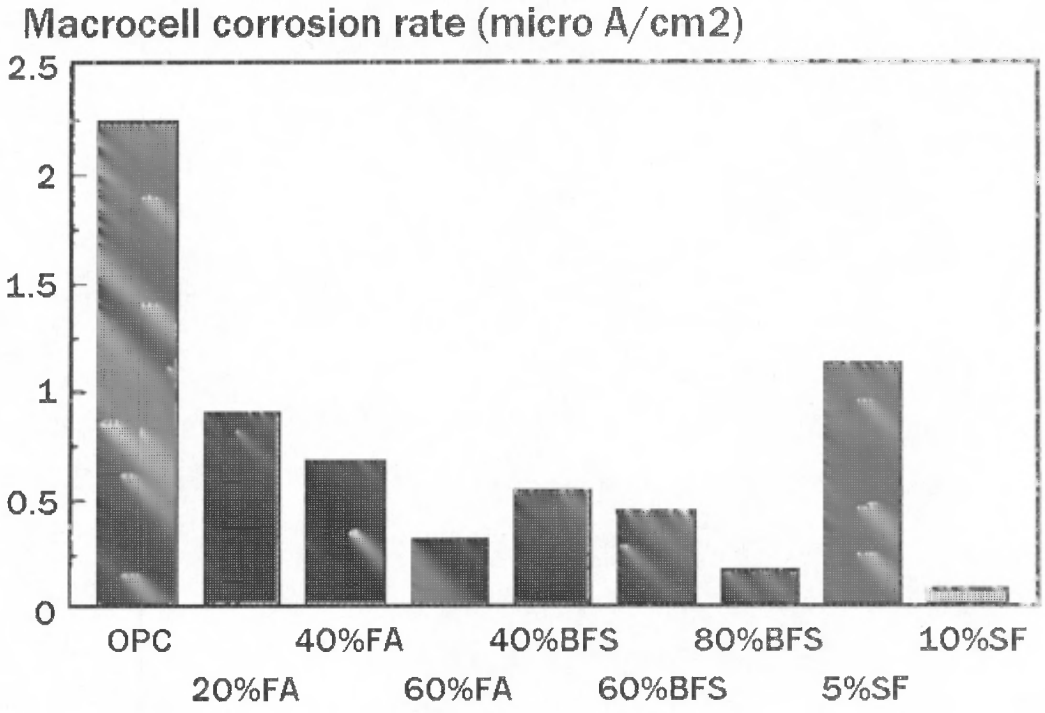

Fig 5.10: Effect of cement extenders on macrocell corrosion of steel (Sirivivatnanon et al., 1994)

The results from the macrocell corrosion test provide a useful ranking of the effectiveness of cement extenders in reducing the corrosion rate in the order of decreasing corrosion rate: PC > 5% SF > 20% FA > 40% FA > 40% BFS > 60% BFS > 60% FA > 80% BFS > 10% SF. Increasing concentrations of any of the cement extenders were shown to consistently reduce the measured corrosion rate. These effects were also noted by Thomas et al. (1990) for increased replacement levels of FA at cover depths of 10 and 20 mm resulting in progressively lower metal loss. Variations in chloride level would be more pronounced for the greater cover depth of 20 mm and there would be some difficulty in making a direct comparison between the various replacement levels.

The polished nature of the steel, and limited cover used by Sirivivatnanon et al. (1994) however, make the direct application to representative rates somewhat difficult. Regardless of the limitations, the information provides a valuable source for comparison and highlights the likely effects of the various cement extenders. Schiessl and Raupach (1990) indicate a similar reduction in macrocell corrosion in concrete for the addition of cement extenders made with 2% chlorides by mass of cement. The ranking order was somewhat different with PC > 20% Slag > 10% SF > 26% FA > 42% Slag at 100 days though there were relatively small

differences in corrosion rates between the various cement extenders. Most of the research, including Pettersson (1992) and Page et al. (1986), shows similar trends with some variability in the exact ranking order. Arya and Xu (1995) however state that for a 3% addition of chlorides at the time of mixing, FA had a higher corrosion current than PC which in turn was greater than the slag or SF samples. At 1% chlorides, the effects are even more contrary to the prevailing view and show PC having lower corrosion rates compared to any of the cement extenders. Mangat et al. (1994) provided similar results to Arya and Xu for their 3% chloride contaminated samples, with FA having a higher corrosion rate than PC at a cover of 10 mm. The specimens were exposed to marine cycle conditions in a spray chamber. It was noted that the chloride concentration of the pore fluid was higher in the FA samples compared to the control and would likely account for the increased corrosion rate. At depths beyond 30 mm, FA was shown to reduce the chloride concentration. The importance of adequate cover depth and curing, neither of which was provided in this case, are clearly shown. The somewhat contradictory nature of the information on the influence of cement extenders therefore requires further investigation to more properly understand both the chemical and physical processes at work.

The inclusion of slag in particular has been shown to have rather unique effects on the early age development of the passive layer. These effects have been noted in the discussion of aqueous work in chapter 4, and are also evident to some degree in the work of Valentini et al. (1990) with steel in mortar specimens as given in Figure 5.11. The corrosion potential of steel in mortar was initially more negative in the slag bearing concretes but these tended to reduce over time particularly when stored at 50% RH. It is interesting to note that 75% slag replacement had the most negative initial potential but quickly rose to values comparable to the PC control though little mention of this is made in their discussion. The current densities after 28 days of curing were approximately 10 times greater for the slag bearing material than those made without slag. The corrosion currents quickly dropped with time to approach values closer to the PC samples. It was noted that the current densities for the slag bearing material decreased as the replacement level of slag increased from 20 to 75%, which was also consistent with the reduction in electrical conductance associated with an increasing proportion of slag.

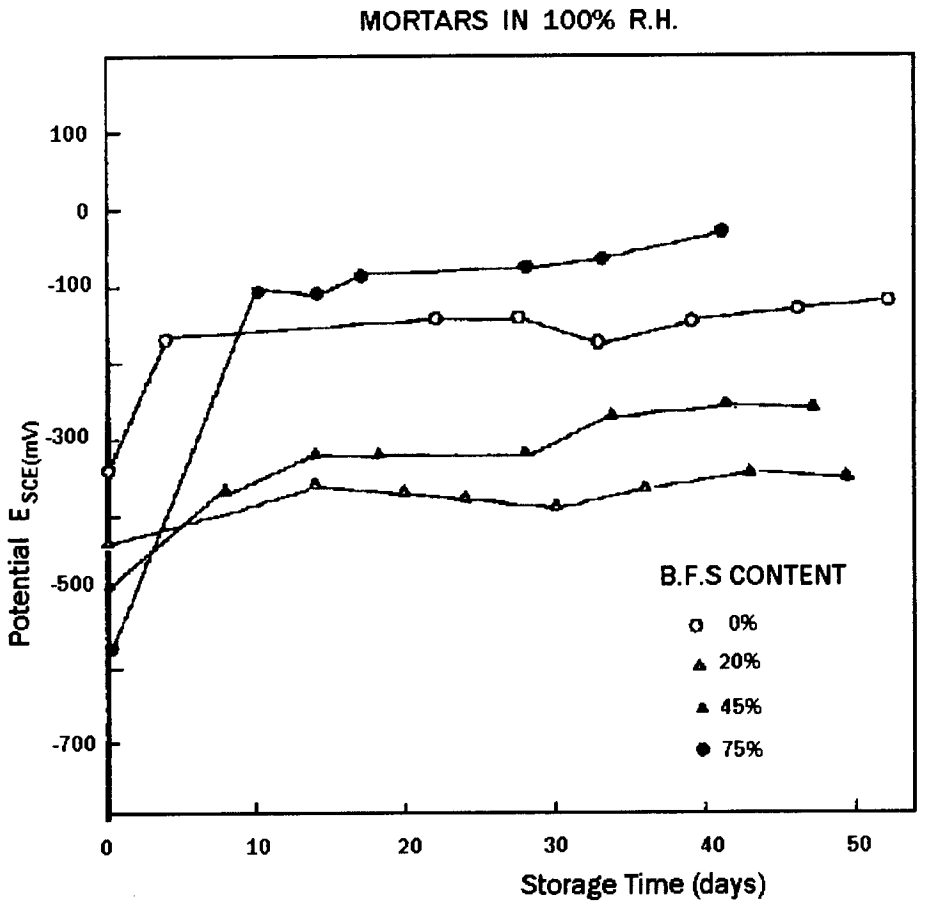

Fig 5.11: Potential measurements for steel in mortar made with various replacement levels of slag, stored at 100% RH (Valentini et al., 1990)

The values are provided over a period of approximately 50 days. Further information on the longer term effects of the addition of slag could be interesting. As Valentini et al. rightly note, steel corrosion can be affected by not only the aggressiveness of the solution but also oxygen availability and medium conductance.

5.4.6 Influence of Cracking

The question of the effect of cracks on the corrosion rate of steel in concrete and service life of a structure has been the subject of much debate. Beeby (1978) and Arya and Wood (1995) suggest that there is no direct relationship between crack width and corrosion rate. They refute other claims of a correlation by stating that the cracks may accelerate corrosion initiation, but not necessarily the propagation rate. Assuming two cracks A and B, which become active at 1 and 2 years, after 3 years there is 100% more corrosion at crack A, this falls to 50% at 4 years and 5% after 20 years. Thus the time at which the measurements are

taken will affect the comparison. The more important considerations are: 1) crack properties, for instance whether the crack is active or dormant, 2) concrete-steel properties, whereby low permeability of the concrete will limit ionic transport, high moisture limits oxygen ingress and increased strength leads to better bond and less slip at the steel-concrete interface, and 3) service environment. Controlling the environment around the steel-concrete interface is therefore more important than the presence of the crack itself and, while cracks may accelerate the initiation of corrosion, the subsequent rate of corrosion is minimal for intersecting cracks (Arya and Wood, 1995). Arya and Wood also note that the type of reinforcing may have an effect with plain bars corroding slightly more than deformed bars. The minor improvement in deformed bars has been attributed to the improved bond strength which reduces the slip zone where anodic activity usually occurs.

Suzuki et al (1990) also support the argument of limited effect of crack width on corrosion rate, though they note some early-age differences in corrosion rate based on crack width, but these decreased with time. The w/c ratio was found to have a more significant impact on corrosion rate than crack width. Pettersson et al. (1996) examined a number of crack width and cover combinations using both OPC and SF concrete. For a w/b ratio of 0.3 the cover had an effect on corrosion rates for crack widths of 0.4 mm, but above this crack width, the cover was shown to have a negligible effect on corrosion as seen in Figure 5.12. The smaller crack widths would be more likely to benefit from autogenous healing and thus limit the effect of the crack. Hwang et al. (1994) suggest that crack widths should be limited to 0.3 mm as crack self-healing in sea water is impaired above this width. The corrosion rate determined by Pettersson et al. (1996) varied with the addition of microsilica from a value of 10 μm/year for OPC, 5 μm/year for 5% replacement and approximately 2.3 μm/year for 10 and 15% replacements at 300 days. Crack widths therefore impact upon corrosion rate by limiting the effectiveness of concrete. An increase in cover from 15 to 30 mm resulted in a substantial reduction of corrosion rate for 0.4 mm cracked specimens but had little effect on the wide cracks (0.8 mm).

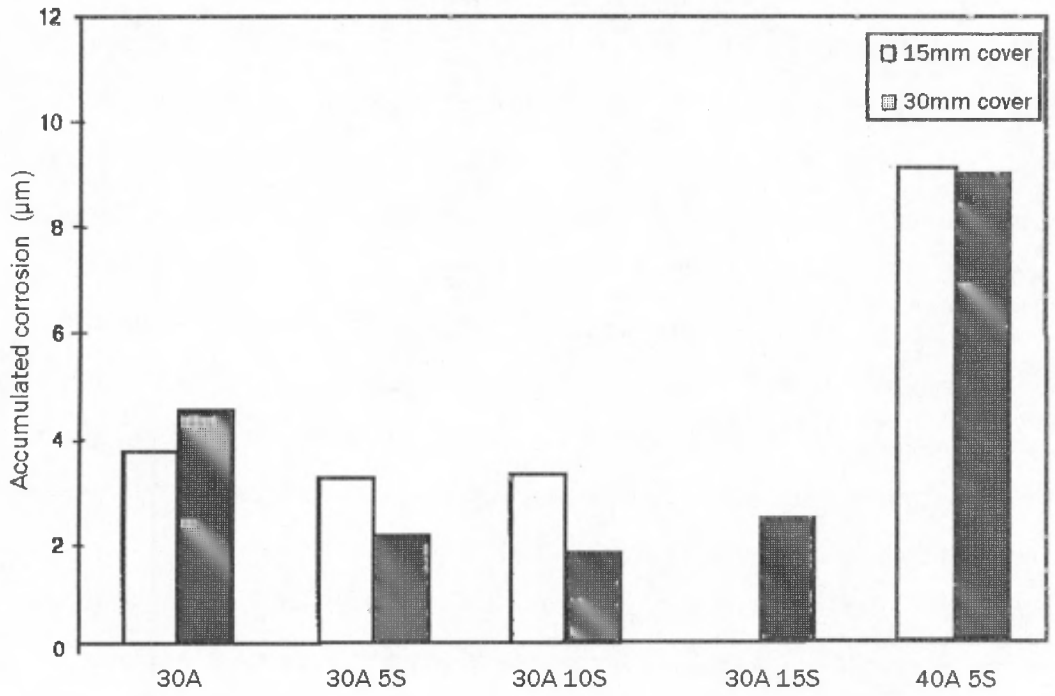

Fig 5.12: Effect of cover on corrosion rates of steel in concrete with a 0.8 mm crack, 30A represents w/c = 0.3 for Swedish SRPC and 5S represents 5% SF
(Pettersson et al., 1996)

The prevailing view on cracks has been reasonably summarized by Tuutti (1982) who states that cracked structures can often be regarded as though they were non-cracked since cracks usually have very little negative effect. He does however provide a number of exceptions where this may not be the case including:

- structures with cracks larger than 0.3 mm in liquids containing chlorides
- structures in which concrete cover is less than 20 mm, and particularly porous structures
- structures having major movement where cracks widths will vary

The noted exceptions for concern due to cracking are quite significant and would apply to most coastal structures. Further investigations in this area are necessary particularly where cement extenders are to be employed. The results from the use of extenders are varied, as noted in the previous section and, coupled with the issue of cracking, a more detailed and systematic approach to understanding this problem is necessary.

covering. Research into the influence of crack widths and the presence of crack themselves has shown varied results on the overall rate of corrosion.

There is therefore considerable disagreement as to the influence of binder type and cracking on the corrosion rate of steel in concrete. The contradictory nature of the literature under review necessitates further investigation particularly for its relevance to South African conditions and materials. These are the two main research areas therefore which have been examined and will be presented in section 2.

5.5 Summary of Current Literature

The corrosion of steel in concrete and the specific influence of cement extenders has been the subject of much debate and research. Concrete provides an ideal medium for protection provided harmful anions are prevented from penetrating the concrete to the steel in sufficient concentrations to initiate the corrosion process. Cement extenders have been shown to generally reduce the permeability of concrete through reduction in porosity, the degree of interconnected voids and improvements to the ITZ. Chloride binding is a further phenomenon which is determined by the nature of the binder. Chloride binding essentially limits the rate of chloride penetration by immobilizing the chloride ions and thus limiting the availability of free-chlorides which can drive the diffusion process and ultimately depassivate the steel. Slags and FA have been shown to result in the greatest degree of chloride binding.

The concentration of chlorides necessary to initiate corrosion cannot adequately be described by a single value. A brief examination of a few studies indicates a range of 0.25 to 1.7 % total chlorides by mass of cement. Factors such as surface finish of the rebar, type of steel, and differences in mix design make direct comparisons of previous research difficult. The inclusion of cement extenders has been shown by some to result in a lowering of the chloride threshold while others state there is no evidence to suggest that extenders, slag in particular, result in a reduction of the chloride threshold. The same variability in chloride threshold values associated with the use of cement extenders is also evident in corrosion rate studies. The inclusion of cement extenders generally results in a lower corrosion rate but there is considerable contradictory research in this regard.

The rate at which steel corrodes in concrete is dependant upon a number of interrelated factors: w/c ratio, cover, RH and resistivity, binder type, temperature and cracking. The w/c ratio for instance affects the permeability of the concrete and thus a reduction in concrete permeability will limit the availability of oxygen to the cathode and the maximum possible corrosion rate. Cathodic control however is normally only an issue at high RH, greater than 90%. At RH below approximately 85% the resistivity of the concrete increases substantially and limits the ionic flow and possible corrosion rate. The two opposing RH requirements of oxygen availability and resistivity result in a maximum corrosion rate when RH is the range between 85% and 90%. Any factor which affects the RH of the system will therefore have an impact upon the corrosion rate.

Cracking has generally been shown to substantially shorten the initiation period by providing for a direct access of chlorides to the steel, bypassing the protective concrete

Table 5.7: Summary of experimental investigation

Series	*Cover (mm)*	*Chloride Threshold*	*Corrosion type (uncracked)*	*Corrosion type (cracked)*	*Durability Index*	*Rebar*
I Concrete	40	X	passive			R 16 mm
II Concrete	20	X	active / passive	active	X	S / R 16 mm
	40			active		S 16 mm
Mortar	15	X				S 12 mm

Where: S - smooth mild steel bar, R - ribbed reinforcing steel

Note: an additional set of PC specimens was cast using 16 mm smooth mild steel with a cover of 20 mm according to concrete series II for the purpose of investigating the influence of rebar slipping on corrosion rates and chloride threshold concentrations.

Table 5.8: Relative percentages of binder type for mortar and concrete series I and II

Mixtures	*Cement*	*Slag*	*Fly Ash*	*Silica Fume*
PC	100	0	0	0
SL	75	25	0	0
SM	50	50	0	0
SH	25	75	0	0
FA	70	0	30	0
SF	93	0	0	7
TR	50	43	0	7

As a result of the problems associated with the movement of chlorides in concrete series I only passive corrosion conditions and chloride threshold concentrations were determined from the specimens in this set of mixes. There was insufficient active corrosion rate data to provide a reasonable comparison of results. The uncracked 20 mm cover specimens from concrete series II faced a similar problem of the slow movement of chlorides through the concrete cover but did provide additional information including: some chloride threshold concentrations, passive and some active corrosion conditions, and a comparison of both smooth and deformed rebar types. The cracked concrete and durability index specimens were also cast using the same mix design as concrete series II. The mortar mix was used solely for the purpose of providing additional information about the critical chloride threshold concentration.

SECTION 2: Experimental Investigation and Discussion

5.6 Experimental Objectives and Procedures

The influence of cement extenders on the pore solution chemistry has been discussed in chapter 3. Aqueous phase testing of steel in simulated pore solutions (SPS) was conducted, as discussed in chapter 4, to determine the specific chemical influences the cement extenders would have on corrosion threshold and rates. It was shown that the inclusion of cement extenders reduced the hydroxyl content of the pore solution and, in the case of slags, resulted in a significant presence of sulphides. The combined effects of reduced hydroxyl concentration and elevated sulphide levels resulted in substantially higher corrosion rates for slags compared to the control case of PC.

To determine the actual influence of cement extenders on the corrosion rate and chloride threshold concentration, representative concrete and mortar samples containing steel at appropriate cover depths were cast. Prior to the main investigation it was necessary to characterize the materials, the details of which are provided in section 5.6.1. There were two primary components to the investigation into the performance of cement extenders:

1) evaluation of the passive corrosion characteristics of deformed steel rebar embedded in concrete.

2) effect of cracking and crack width on the corrosion rates

A secondary component in the overall investigation was the determination of critical chloride threshold concentrations for the individual binder type.

An initial attempt was also made to examine corroding steel under uncracked conditions. The principle guiding the research was that the experiments should, so far as possible, represent the true nature of corrosion as observed in practice. In particular the passive layer needs an opportunity to develop prior to the introduction of chlorides. As such, it was decided that a ponding regime of 3 days in 5% NaCl solution and 4 days drying at a constant temperature of 30°C would be used. A 40 mm cover depth for 16 mm diameter deformed bar was chosen with a nominal aggregate size of 19 mm. It was quickly determined that, even under the accelerated conditions, the movement of chlorides through the concrete would be too slow and a lower cover depth of 20 mm would also be needed, for which a smaller 9 mm aggregate was chosen to prevent short circuiting of the cover. One further mortar mix was also included which was used for determination of chloride threshold values. The experimental investigation, with respect to mix design and properties to be studied, is summarized in Table 5.7 and the relative proportion of binder type in Table 5.8

10b) Concrete mix design Series II (w/c = 0.58, 14 days wet curing)

Material	*PC*	*SL (25%)*	*SM (50%)*	*SH (75%)*	*FA (30%)*	*SF (7%)*	*TR (50:43:7)*
Water	175	175	175	175	175	175	175
CEM I	302	227	151	75	211	281	151
Slag		75	151	227			130
FA					91		
SF						21	21
Sand	750	750	750	750	750	750	750
Stone (9 mm)	1050	1050	1050	1050	1050	1050	1050
S.P. (Sika 163)						1.5	1.5

10c) Mix design for mortar threshold samples (w/c = 0.58, 14 days wet curing)

Material	*OT*	*LT (25%)*	*MT (50%)*	*HT (75%)*	*FT (30%)*	*ST (7%)*	*TT (50:43:7)*
Water	258	258	258	258	258	258	258
CEM I	444	333	222	111	311	413	222
Slag		111	222	333			191
FA					133		
SF						31	31
Sand	1598	1598	1598	1598	1598	1598	1598
S.P. (Sika 163)						2.2	2.2

Strength tests were performed on 100 mm cube at ages of 28, 56 and 90 days based on mix design series I and II. The samples were vibrated to ensure adequate compaction, stripped after 24 hours and cured in water at 23°C until tested. The samples were loaded at a rate of 15 MPa/min and the maximum load noted.

5.6.2 Durability Index Measurements

The durability index measurements comprise a suite of three tests developed by the University of Cape Town in collaboration with the University of the Witwatersrand, which can be used to rapidly assess the transportation characteristics of a given concrete with respect to oxygen, water and chlorides. The philosophy behind the tests was that they should be sufficiently sensitive to account for variations in material characteristics such as binder type, w/c ratio, and curing among others. The values obtained from these tests may not be entirely representative of the fundamental characteristics of the materials but can be used to provide indexes which are correlated against material performance both in the lab and on site and used to predict likely material performance.

Durability indexes of oxygen permeability, water sorptivity and chloride conductivity were measured for mix design series II at ages 28, 56 and 90 days. A number of 100 mm

5.6.1 Material characterization

Four binder types, resulting in seven mix designs as previously shown in Table 5.8, representing the primary materials used in practice throughout South Africa, were selected for evaluation. The oxide and mineral analysis of the materials are provided in Table 5.9. The two concrete and one mortar mix design are shown in Table 5.10.

Table 5.9: Oxide and Mineralogical analysis of binders used

Oxide	*PC*	*Slag*	*FA*	*SF*	*Mineralogical (OPC)*	*%*
SiO_2	21.5	35.7	53.1	91.9	C_3S	74.7
CaO	65.9	34.3	4.2	0.0	C_2S	5.3
Al_2O_3	3.7	13.6	33.7	0.7	C_3A	3.8
Fe_2O_3	3.6	0.7	3.6	0.8	C_4AF	10.9
Mn_2O_3	0.06	1.10	0.05	0.09		
TiO_2	0.18	0.60	1.77	0.11		
MgO	0.88	10.20	1.02	0.26		
SO_3	3.28	2.86	0.30	0.46		
K_2O	0.54	0.80	0.75	1.33		
Na_2O	0.19	0.20	0.40	0.42		

A Klipheuwel sand (natural pit sand) with a finess modulus of 1.86 was used. The detailed grading analysis may be found in Appendix 5A.1. The sand was first oven dried prior to use to remove moisture. Standard tap water was used for the production of the specimens.

Table 5.10: Details of mixture designs (all units in kg/m^3, except SP in Litres)

10a) Concrete mix design Series I (w/c = 0.58, 16 hours curing)

Material	*PC*	*SL (25%)*	*SM (50%)*	*SH (75%)*	*FA (30%)*	*SF (7%)*	*TR (50:43:7)*
Water	160	160	160	160	160	160	160
CEM I	277	208	139	69	194	257	139
Slag		69	139	208			118
FA					83		
SF						20	20
Sand	770	770	770	770	770	770	770
Stone (19 mm)	1050	1050	1050	1050	1050	1050	1050
S.P. (Sika 163)						1.4	1.4

down in a 5% NaCl solution leaving the opposite face exposed to the air. After one week at ambient temperature (approximately 20 - 25°C) the samples were transferred to a climate control room set at 30°C where they were cycled with 3 days ponding in 5% NaCl solution and 4 days drying.

The decision to expose the samples to a salt solution at an early age was an attempt to reconcile the need for passive layer development in an environment free from chlorides, coupled with the need to obtain activation of corrosion over a reasonable period of time. It was considered that 40 mm would provide sufficient cover to permit the material properties of the concrete to fully develop in a manner representative of the particular binder type employed. The early age ponding would allow for an initial rapid movement of chlorides without having to reduce the cover of the concrete. Particular care in handling was required for the 75% slag specimens as they were very weak at this early stage of development.

The samples were initially monitored bi-weekly, approximately 2 days after commencement of drying, for corrosion potential and rate, and resistivity. Corrosion rates and potential were initially determined by means of GECOR 6, which uses a linear polarization technique, the details and development of which are provided in numerous publications (Broomfield, 1996, Feliu et al., 1996, Flis et al., 1995). Once the coulostatic system, described in Appendix 4A.3, and built at the University of Cape Town was operational and tested, it became the primary method of corrosion rate and potential monitoring. Resistivity measurements were taken by means of a four probe Wenner technique (Gowers and Millard, 1999).

Active corrosion was considered to have begun once the potential showed a significant movement to more negative values, around -200 mV Ag/AgCl, and the corrosion rates shifted from previously passive levels, usually less than 0.05 $\mu A/cm^2$, toward larger currents of approximately 0.1 $\mu A/cm^2$. Normally two successive increasing measurements would be considered sufficient to determine the end of the passivation period. Once an initial increase in rate of potential was noted, those samples were monitored on a weekly basis. It could be argued that the waiting period would result in an overestimation of the required chloride level for initiating corrosion. The relative time between activation and its observation and measurement however will be shown to be quite small compared with the overall exposure period, thus any change in chloride level would be practically insignificant.

Once the chloride threshold level was deemed to have been reached, the point of the most negative potential along the bar was marked and the sample cored with a 68mm diameter core barrel. Minimal water was used to prevent leaching of the chlorides. The sample was then cut

cubes were cast, for each of the seven individual mix designs, demoulded after 24 hours and cured in 23°C water until the time of testing. A 68 mm diameter core was taken from the sample and sliced, with a continuous wet diamond blade, to remove the surface cover concrete (5 mm) and provide 25mm thick samples for testing. The precise methods employed for conducting the experiments are described in detail in the following references: Alexander et al. (1999[a,b,c]). A brief summary of test design and principles are provided in Appendix 5B and typical values are provided in the discussion section of this chapter.

5.6.3 Threshold values

Three sets of samples comprising concrete mix design series I and II and the mortar specimens were used in the investigation of chloride threshold values. The series I and II specimens contained one central deformed 16 mm rebar cut to a length of 220 mm while the mortar specimens used a 12 mm diameter round mild steel bar cut to 95 mm. A further set of specimens containing a 16 mm round mild steel bar of 355 mm length were also cast to determine if slipping of rebar would influence chloride threshold concentration. The details of the experimental procedures for 16 mm round bar samples are provided in section 5.6.4. All sets of steel bars were wire brushed, to remove any mill scale, and then cleaned with acetone. An electrical connection was made by a copper wire attached to the steel at one end for the series I and II specimens and brass threaded rod was screwed into the end of the mortar specimen bars. Once the electrical connection was made the ends were shrink wrapped and epoxied to leave a central exposed area of 90 cm^2 for series I samples and 25 cm^2 for the mortar bars. The threaded brass rod of the mortar specimens and copper wire of the series I specimens were also coated leaving only the end exposed to prevent any bimetallic corrosion. Just prior to casting, the steel was again cleaned and carefully placed to avoid any contamination of the surface.

Concrete Series I Samples

The dimensions of the cast specimens were 100 x 100 x 240 mm with a 40 mm cover for the steel. The concrete was poured in one continuous layer and vibrated for approximately one minute, to ensure adequate compaction and removal of entrapped air. After 16 hours the specimens were demoulded and the two opposite sides and ends sealed with epoxy, leaving 40 mm cover and the opposite face exposed. The purpose of the epoxy was an attempt to ensure uniaxial movement of chlorides through the sample and prevent wicking near the sides and subsequent preferential movement along the bar. The samples were then placed face

leaving a section of concrete approximately 5mm above and below the steel and a width of 20 mm. The specimen was then sliced along the length of the steel to produce a top (exposed face) and bottom concrete section which could be independently analyzed for chloride content.

The top and bottom sections of the steel samples were dried at 100°C for 3 days to remove the evaporable water content. The specimens were then individually ground. The aggregate and other mix constituents were assumed to be uniformly distributed throughout, even around the rebar. This assumption may not be entirely accurate but, for the purposes of comparison between the mixes, it is a reasonable assumption.

Chloride concentration was determined by potentiometric titration of 0.1M $AgNO_3$ against a silver / potassium chloride reference electrode until the equivalence point was reached. A Mettler titrator was used for this work. A known quantity of powder sample was first measured and the chlorides dissolved with 2 ml of 1:1 diluted Nitric acid for at least 45 minutes prior to buffering with 2.5 ml of 50g/l Sodium Acetate and then titrated. The results were expressed as chloride by mass of binder.

Concrete Series II Samples

The specimens cast using concrete design series II, were virtually identical to those of concrete series II except the specimens in series II had a cover of 20 mm, stone size of 9 mm and were permitted to cure in water for 14 days prior to ponding with salt solution. The rest of the procedures for determining chloride threshold concentrations remained the same. The slow rate of chloride penetration however meant that only the PC and a few other specimens had displayed signs of active corrosion before the end of the study period. Results from the threshold series II specimens therefore have not been provided in the discussion on chloride threshold concentrations but those specimens that were measured showed good agreement with the results from series I.

Mortar Samples

The mortar samples were cast face down, for each of the seven mix designs, in plastic cylinders of 105 mm diameter, providing 15mm of cover over the top and bottom of the steel as shown in Figure 5.13. The samples were vibrated to remove entrapped air. After 24 hours the samples were placed in water at 23°C for 14 days. The sides of the samples were coated with epoxy, once removed from the plastic moulds, to restrict the movement of chlorides. A

plastic cylinder formed a container for ponding on the top face with 5% NaCl. The samples were exposed to continuous wetting on the one face and drying on the other at 30°C.

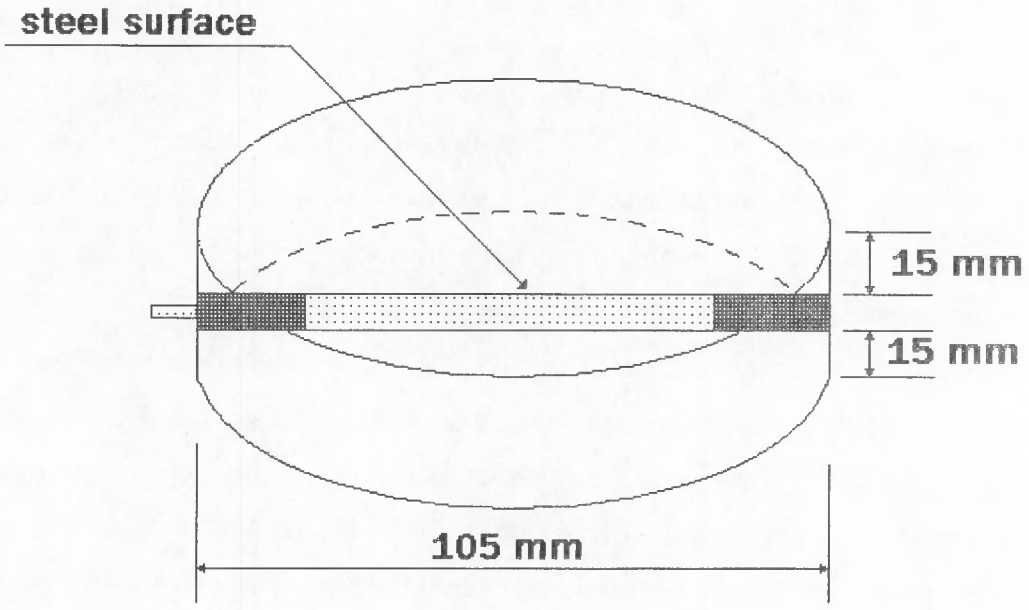

Fig 5.13: Mortar threshold samples with embedded 12 mm round steel rebar

Measurements of corrosion potentials and rates were taken bi-weekly using the coulostatic technique as described in appendix 4A.3. The same principles for determining the initiation of corrosion as described for the series I samples were also applied to the mortar specimens. The geometry of the specimens resulted in a slightly different procedure being used for obtaining the mortar specimens to be analyzed. The sides of the samples were cut to leave a 20 mm strip containing the steel electrode. The 10 mm of the top and bottom of the specimen were removed leaving 5mm of mortar above and below the steel. A central section of approximately 50 mm in length was then taken for chloride analysis in the same manner as described for the series I samples. The top and bottom sections of mortar were analyzed separately. Since no coarse aggregates were present the reliability of the chloride measurements, with respect to material proportions, were improved.

5.6.4 Corrosion Rate Measurements

One set of specimens containing deformed rebar and two sets of specimens containing mild steel round bar were cast in concrete, according to concrete design series II, for the evaluation of both active and passive corrosion rates. All the samples were prepared from the same moulds producing concrete specimens 375 mm in length with a cross section of 120 x

120 mm. The individual steel bars of 16 mm diameter, both mild and deformed, were cut to a length of 355 mm, from the same respective production run, and cleaned and prepared in the manner as described in section 5.6.3, leaving an exposed surface area of 158 cm^2. The samples were cast face down with the steel cover provided from the base of the mould.

Sample preparation

The first set of specimens contained deformed rebar with a cover depth of 20 mm. Three samples for each binder type were cast and vibrated to ensure adequate compaction and removal of entrapped air. After 24 hours the samples were stripped and coated with epoxy on the two opposite sides and ends to limit wicking on the sides and ensure unidirectional chloride movement. It was initially envisaged that samples would periodically be cored next to the steel to check chloride levels, thus the need for a uniform chloride concentration along the cross section of the sample. The samples were water cured at 23°C for 14 days at which point they were moved to a climate control room set at 30°C and cycled with 3 days ponding in 5% NaCl solution and 4 days drying.

A second set of 12 PC specimens were cast using smooth mild steel bars at a cover depth of 20 mm. The specimens were again demoulded after 24 hours and cured at 23°C for 14 days. A longitudinal load was then applied to the steel bars of six samples, as shown in Figure 5.14, to produce a slip of approximately 0.7 mm. The other six samples remained unslipped and the ends of all the samples were sealed with epoxy. A rectangular bath was placed on the top surface to allow for ponding with 5% NaCl under the same exposure conditions described for the other samples. The objective of this experiment was to compare corrosion rates between deformed bars previously cast and mild steel bars, in addition to any effects that slipping of the bar might have on corrosion rates. Three each of the slipped and unslipped specimens were also used to determine chloride threshold concentrations in the same manner described in section 5.6.3.

The final set of specimens was cast using smooth mild steel bar at cover depths of 20 and 40 mm. Eight specimens for each binder type and cover depth were cast. The samples were again cured for 14 days in 23°C water at which point one central transverse crack was produced by three point bending. The samples were cracked to produce crack width of approximately 0.2 mm and 0.7 mm in different specimens. The three most representative specimens for each crack width and combination of cover and crack width were selected. The crack width was measured on the top surface of the crack. The sides of the cracks were sealed and the samples placed in the climate control room for ponding with 5% NaCl solution.

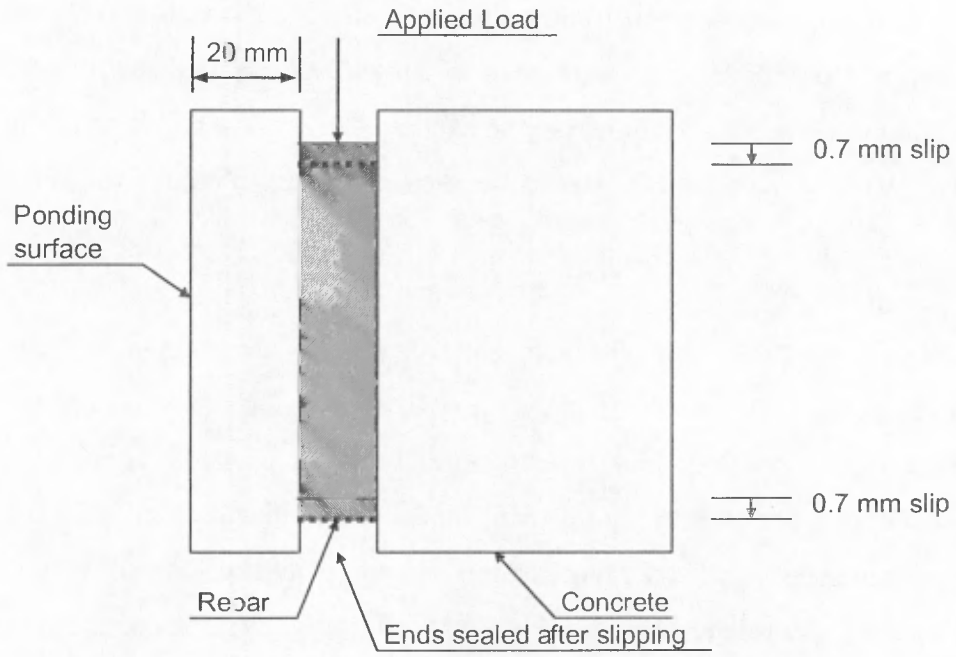

Fig 5.14: Cross section of sample with longitudinal slipping of round bar (not to scale)

The use of deformed rebar is preferable for investigating corrosion as it more closely resembles that which is used in practice. The formation of the cracks however was dependant upon slipping of the bar. Attempts to produce cracks with ribbed bars were unsuccessful as the movement of the bar relative to the concrete resulted in not only the desired transverse but also longitudinal cracking which would have dramatically changed the nature of the investigation.

Sample monitoring

The samples were monitored bi-weekly for corrosion rate, potential and resistivity. Corrosion rate data was obtained by means of the coulostatic method and potentials were measured relative to Ag/AgCl electrode. Resistivity measurements were taken using the four probe Wenner technique.

5.7 Results and Discussion for Compressive Strength and Durability Index Values

Durability index (DI) values for oxygen permeability, water sorptivity and chloride conductivity, in addition to cube strength, were measured for each binder type concrete mix designs in series II at ages 28, 56 and 90 days. The strength results are presented in Table 5.11.

Table 5.11: Strength (MPa) results for 100 mm cubes, Series II

Binder Type	*Ages (days)*		
	28	*56*	*90*
PC	46.5	52.7	59.5
SL	43.2	51.1	52.5
SM	42.7	47.4	48.1
SH	28.2	32.6	35.1
FA	42.2	51.3	56.9
SF	49.7	52.3	56.1
TR	46.5	51.6	56.6

It is evident from the strength results that SF had the most rapid strength development but then slowed with time with PC having the highest 90 day strength. The PC and TR blends displayed very similar trends over the entire period having the same 28 day values with TR being only slightly less than PC at 90 days. The delayed hydration and strength gains normally associated with the inclusion of 43% slag were clearly offset by the incorporation of 7% SF. There was a relatively small difference between the 25 and 50% slag mixes (SL and SM respectively), though the 50% slag content mix had a somewhat lower strength even after 90 days. The long time needed for the maturing of FA mixes is evident with the second lowest strength at 28 days but showing continued strength gain over time and equal to the TR blend at 90 days. Only the SH blend of 75% slag performed poorly with a strength of 28 MPa at 28 days, increasing to only 35 MPa after 90 days. All other mix designs therefore provide a satisfactory level and rate of strength gain which could be used in regular construction applications. Strength results, while giving a general assessment of concrete quality, do not provide sufficient specific information needed for assessing the long term durability of concrete.

Considerable work has been done to determine the DI values for various South African concretes. Table 5.12 contains typical values associated for PC, FA, SF and slag bearing concretes with a w/b ratio of 0.6 and 28 days wet curing.

Table 5.12: Typical DI values for various types of concrete (based on Alexander et al. 1999[a])

Binder type	*OPI*	*Water sorptivity(mm/√h)*	*Chloride conductivity(mS/cm)*
PC	9.87	8.9	1.83
30% FA	9.87	9.7	1.25
50% Slag	9.58	8.6	0.75
10% SF	10.29	5.0	0.63

These values can be taken to represent the normal range of concretes produced in South Africa and help to place the values presented in this section in perspective. The meaning of these values are discussed both in Appendix 5B and within this section.

Sorptivity is essentially the movement of a wetting front through a porus medium due to capillary action (Alexander et al. 1999[a]). The degree to which the wetting front moves through the concrete, as measured by the accumulation of mass with time, provides information on the general pore structure of the material. The lower the sorptivity 'S' the more resistant the concrete to the movement of water. The results for water sorptivity are provided in Figure 5.15. According to the durability classification described by Alexander et al. 1999[a], a sorptivity value of less than 6 mm/√h is considered to be excellent, between 6 and 10 mm/√h good and greater than 10 mm/√h poor. All the measurements, including the SH mix design, are considered to be at least good with a highest 90 day value of 6.8 mm/√h. The strength results showed PC strength to be almost double SH yet the water sorptivity results are virtually the same at 6.5 and 6.8 mm/√h respectively after 90 days. All of the other mix designs showed improvement over the PC control sample and had sorptivity values less than 6 mm/√h, with TR the lowest at 4.5 mm/√h after 90 days.

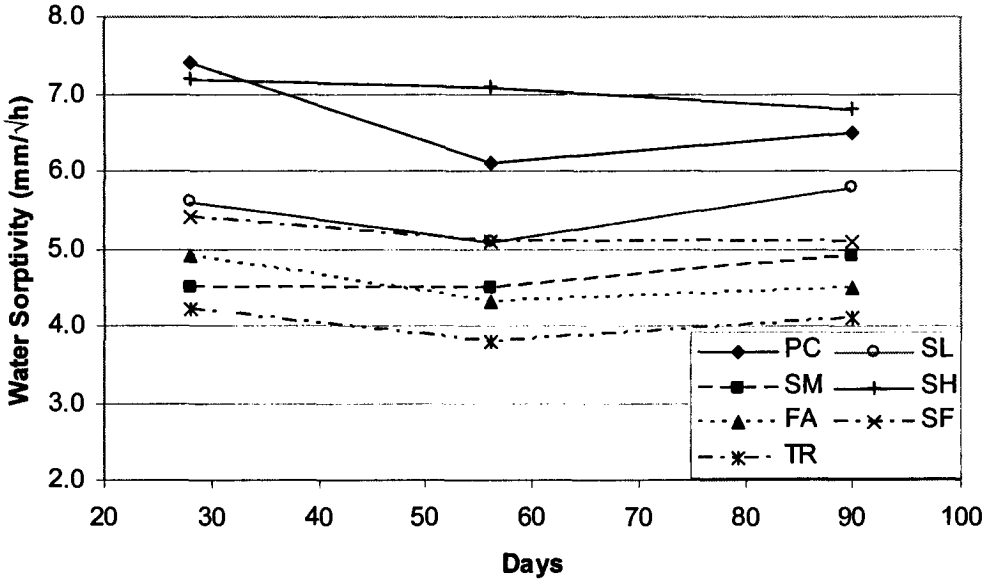

Fig 5.15: Water sorptivity values for mix design series II.

Most of the samples had a lower 56 day sorptivity value compared to 90 days, although in practical terms the difference is negligible. This result is somewhat unusual in that continued

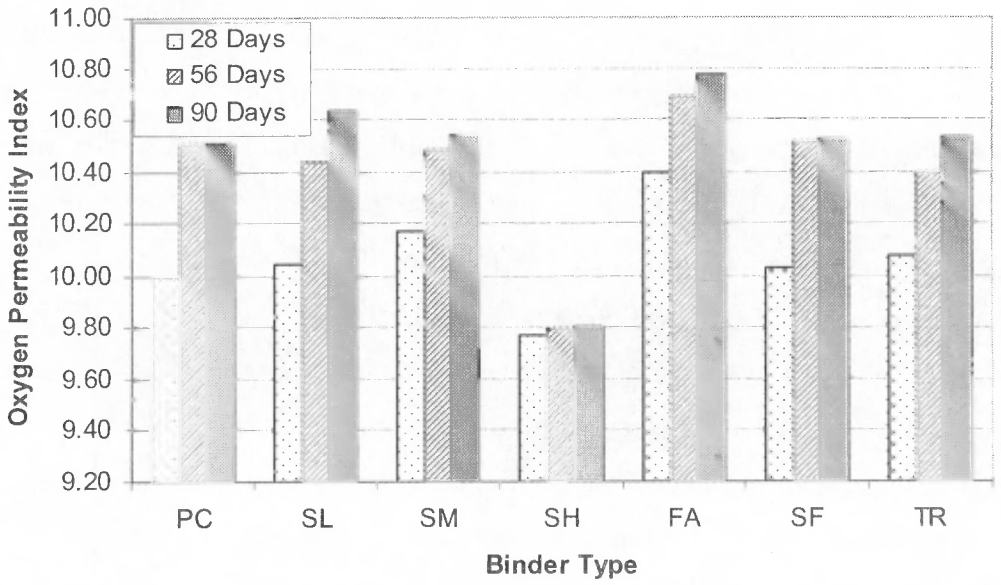

Fig 5.16: Oxygen permeability index values at 28, 56 and 90 days

An OPI value greater than 10 is considered to provide excellent overall durability, with 9.5 to 10 good, and 9 to 9.5 poor (Alexander et al. 1999[a]). The SH samples showed "good" performance indicators for all ages with very little development between 28 and 90 days. The remaining samples all indicated "excellent" durability performance with considerable gain between 28 and 56 days and generally some further improvement between 56 and 90 days. The OPI samples did not appear to suffer from the same phenomenon as the water sorptivity values which occasionally show a decrease in performance from 56 to 90 days. The relative permeabilities of the concretes, at 90 days, can be ranked as follows: FA < SL < SM < TR < SF < PC < SH. FA provided the best resistance to oxygen flow with a coefficient almost half that of PC. The permeability coefficient for SL was approximately 25% lower than PC with SM, TR, SF and PC being similar. SH however was 5 times more permeable than PC to the movement of oxygen. The OPI results again emphasize the differences between durability and strength with FA being considerably less permeable than PC despite having a somewhat lower strength at 90 days. These differences are further highlighted by the 28 day results where FA had the second lowest strength and greatest resistance to oxygen permeability, 40% lower than the next closest and less than half the permeability of PC. Based on the oxygen permeability results FA would be expected to provide the greatest protection to the steel with SH the least.

hydration of the concrete would normally lead to a further resistance in penetration. Care was taken in the drying of the samples at 50°C to limit possible cracking. The continued densification of the material may however make the material susceptible to thermal cracking. Changes between the 56 and 90 day values may not be that significant as the ranking order among the samples was not altered from 56 to 90 days. The greatest change in value was associated with SL which increased 14% from 56 to 90 days.

Oxygen permeability index (OPI) represents the negative log of the coefficient of permeability (m/s) of oxygen through a concrete sample. A poor concrete with connectivity of the pores will therefore have a high coefficient of permeability which would allow easy access of oxygen to the steel. Concretes with very low coefficients of permeability (high OPI) would impede the access of oxygen to the steel and limit the maximum corrosion rate given sufficient cover. The interaction between cover and permeability of the concrete is therefore important in controlling the availability of oxygen. A more permeable concrete would require a greater cover depth to obtain the same degree of oxygen reduction at the level of the steel as a less permeable mix, *ceteris paribus*. The results for the oxygen permeability coefficients are given in Table 5.13 with the OPI values being provided in Fig 5.16.

Table 5.13: Oxygen permeability coefficients ($x10^{-10}$) m/s

Binder Type	*Age (days)*		
	28	*56*	*90*
PC	1.000	0.309	0.314
SL	0.898	0.363	0.234
SM	0.671	0.331	0.291
SH	1.680	1.610	1.570
FA	0.401	0.206	0.170
SF	0.940	0.304	0.302
TR	0.838	0.401	0.297

The final durability index parameter which was examined was the chloride conductivity. Chloride conductivity can serve as a durability prediction parameter in two ways. Firstly, it is a direct measure of the resistance of the material to the movement of a charge. As corrosion is dependant upon ionic movement through concrete to complete the circuit, a decrease in the conductivity (increase in resistance/resistivity) would therefore reduce or limit the corrosion rate. The second function of the chloride conductivity is a measure of the susceptibility of the concrete to the diffusion of chlorides. The relationship between diffusion and conductivity and the development of the test are briefly discussed in Appendix 5B.3. Results for the chloride conductivity test can be found in Figure 5.17.

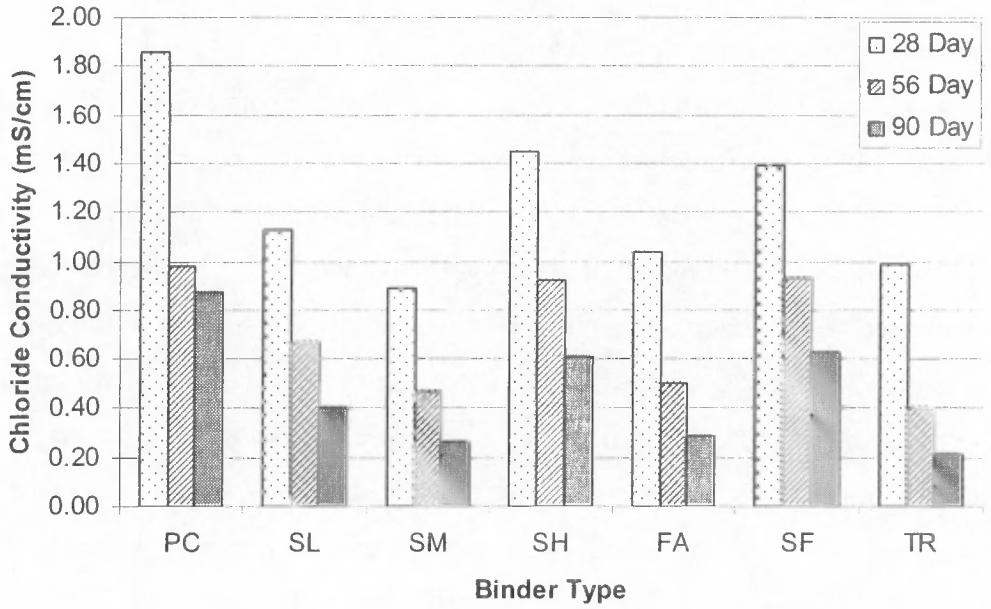

Fig 5.17: Chloride conductivity measurements

There is a significant reduction in the chloride conductivity readings with time which is evident in all samples. The chloride conductivity values for TR in particular were approximately 80% lower at 90 days than at 28 days. A chloride conductivity value less than 0.75 mS/cm is considered to be indicative of concrete with excellent durability potential. All the samples except for PC (0.87 mS/cm) had values less than this at 90 days. The PC sample also performed well and would be considered in the good classification. TR, FA and SM all performed very well with conductivity values less than 0.3 mS/cm. The SH sample, which performed relatively poorly with respect to the other durability indexes, showed similar values to the SF and better than PC.

Each of the three durability index tests reveals particular characteristics of the material. An assessment of the likely corrosion resistance of a material should be a function of these characteristics. The SH sample, for instance, performed relatively poorly for the sorptivity and OPI tests but showed reasonable values in the case of chloride conductivity. The material's resistance to the movement of a charge may therefore have a significant impact upon the possible corrosion rate and may result in a reduction in corrosion rate despite the two other durability indexes being worse than the PC control sample. The durability index values will be correlated with the corrosion rates measurements discussed in section 5.9 and their use as a predictive tool for assessing future life of a structure in chapter 6.

5.8 Results and Discussion for Chloride Thresholds

The results for the determination of the critical chloride concentration to initiate corrosion of steel in concrete create somewhat of a confusing picture and lead to questions about some of the existing views on chloride thresholds. A general trend of lower chloride threshold concentrations with reductions in hydroxide concentration and the presence of sulphides was noted in the aqueous phase work of chapter 4. The impact of reductions in hydroxide concentration and the presence of sulphides was however less evident in the chloride threshold values compared to the very significant effects on corrosion rates, as determined in the aqueous phase investigation. It was suggested that breakdown of the passive film is not easily quantifiable and subject to considerable variability. It is possible that what would appear to be a minor influence may significantly impact upon the overall process thus affecting the chloride threshold value. The results from the more representative cases of steel in mortar and concrete are no exception.

There were a number of problems with the threshold specimens cast from concrete mix design series I and II and the mortar series. In particular, the connections on a few of the specimens deteriorated over the evaluation period and as such the number of specimens available for determining chloride threshold concentrations decreased. In the case of SH and SF (concrete series I), only one specimen from each was analyzed for chloride threshold concentration. The average chloride threshold concentration of concrete mix series I, together with the number of specimens analyzed and the range of values for each binder type is provided in Table 5.14. The chloride threshold concentrations were determined after the potentials showed a significant movement to more negative values, around -200 mV Ag/AgCl, and the corrosion rates shifted from previously passive levels, usually less than 0.05 $\mu A/cm^2$, toward larger currents of approximately 0.1 $\mu A/cm^2$.

Table 5.14: Chloride threshold concentrations (expressed as % mass of binder) for concrete series I specimens

Binder Type	*Average chloride threshold concentration (%)*	*Range of values*	*Number of samples measured*
PC	0.53	0.29 - 0.87	3
SL	0.41	0.22 - 0.61	2
SM	0.08	0.06 - 0.11	2
SH	0.2	N.A.	1
FA	0.36	0.29 - 0.43	2
SF	0.51	0.51 - 0.71*	1 (3)
TR	0.08	0.07 - 0.09	2

Note: the stated range of values for SF includes measurements taken from concrete mix design series II and includes a total of three measurements. The chloride concentration is the single reported values from the concrete series I mix.

5.8.1 Comparison of Chloride Threshold Results from Mortar and Concrete Samples

Chloride threshold values were obtained for both mortar and concrete samples. Figure 5.18 provides the chloride threshold concentration for the first specimen to show signs of corrosion for each binder type of concrete series I and mortar series. The reported chloride threshold represents the lowest critical chloride threshold observed, not the average.

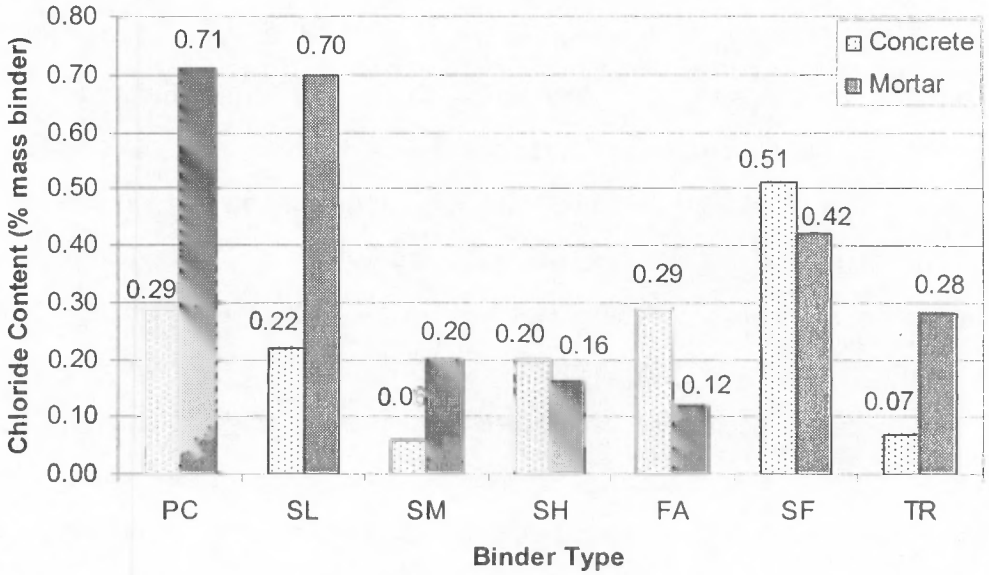

Fig 5.18: Lowest chloride threshold concentration (% mass of binder) for concrete series I and mortar specimens

The concrete samples generally showed a lower chloride threshold level than the mortar specimens. On average the concrete samples showed chloride threshold values which were 37% lower than the corresponding mortar specimens. There was a greater absolute range in measured chloride threshold concentrations for the mortar specimens which should allow for greater differentiation of results compared to the concrete series. The lowest measured chloride value for any of the concrete specimens was 21% that of the concrete PC specimen which was comparable to the mortar series where the lowest measure threshold was 17% that of the mortar PC specimen.

There were a number of important differences between the two sets of samples which may explain some of these discrepancies. The coarse aggregate contained in the concrete samples would likely result in a less homogeneous material with large aggregate particles in close contact with the rebar. The coarse aggregate would result in greater entrapped air and bleed water around the aggregates which may result in areas with less dense matrix bonded to the steel reinforcing. Voids on the surface of the steel would act as a preferential site for the initiation of corrosion, and thus reduce the overall chloride threshold. The mortar samples with the more uniform matrix would not suffer from this problem to the same degree and would therefore be expected to have a slightly higher chloride threshold value. The increase in cement content coupled with the degree and ease of compaction associated with the mortar specimens would further improve their resistance to corrosion initiation.

The mortar samples also contained smooth round mild steel compared to the deformed bar used in the concrete samples. The presence of discontinuities on the steel surface may act as preferred sites for the initiation of corrosion thus reducing its ability to resist the onset of corrosion. A comparison between ribbed and mild round bar however has shown relatively little difference in chloride threshold values and is discussed in greater detail in section 5.8.2.

One further influence which must be considered is the cover of 40 mm for the concrete samples compared to 15 mm for the mortar samples. At lower cover depths there is a faster increase in chloride concentrations compared to greater depths. Any delay in detecting the initiation of corrosion and subsequent preparation of the sample would result in an elevated chloride threshold level. The change in chloride concentration with depth is greatest near the surface and the inclusion of portions of mortar closer to the surface would result in higher chloride values compared to those taken in the concrete at greater depths.

Regardless of the reasons for variations in the results of the mortar and concrete specimens the differences are substantial. Chloride threshold results from mortar specimens therefore should not be used as a prediction for the initiation of the corrosion of steel in real

structural concrete. The mortar specimens are of value if used as an indication of the relative performance of a particular binder type

5.8.2 Effect of Reinforcing Type, Cover Depth and Bar Slip on the Chloride Threshold Concentration

The comparison of reinforcing bar type and slip conditions was based on three sets of PC specimens cast according to concrete mix design II at a cover depth of 20 mm. Two sets of smooth round bar under slipped and non-slipped conditions were compared in addition to one set of ribbed reinforcing steel. There are some differences between mild steel round bar and deformed reinforcing bar including the presence of discontinuities on the deformed bar and slightly higher yield strength. A somewhat higher average chloride threshold concentration of 0.88 % chloride by mass of cement was observed for the ribbed bar compared to an average of 0.73% for the two sets of round bar. This difference in average chloride threshold value however is fairly small given the range of values, 0.47% to 0.92% for smooth bar and 0.31% to 1.46% for ribbed bar. A summary of the chloride threshold results from the comparison of rebar type and slipping conditions is provided in Table 5.15.

Table 5.15: Chloride threshold concentrations (as a percentage mass of binder) for deformed bar, smooth bar and slipped conditions.

Rebar type and interface condition	*Chloride Threshold concentration (%)*	*Range of values*	*Number of samples measured*
ribbed steel unslipped	0.88	0.31 - 1.46	3
smooth steel unslipped	0.66	0.47 - 0.83	3
smooth steel slipped	0.83	0.75 - 0.92	2

The un-slipped bar had an average chloride threshold value of 0.66% compared to the slipped bar which was 0.83% by mass of cement. The unslipped bars showed a greater range of threshold values from 0.47% to 0.83% compared to the slipped bars which were limited to 0.75% to 0.92%. The difference in variation is primarily explained by a reduction in the samples size of the slipped bars for which only two measurements were available compared to three for the unslipped specimens. The difference in chloride threshold concentration between the slipped and unslipped bars was small and no negative impact, such as elevated chloride

thresholds due to damage of the bar concrete interface, was associated with slipping of the bar.

The bar slip was introduced at 14 days thus there would still be considerable time for continued hydration to repair some of the damage that might have occurred, particularly since the first bar did not start to corrode until 18 weeks later. The movement of the bar would have disrupted some of the hydration products directly bonded to the steel but would not change the overall environment to which the steel was exposed. If voids were present at the steel surface before the slip they would also remain afterwards, though re-positioned a distance 0.7 mm relative to the steel. Similarly if voids were not present it is unlikely that more would form, though some degree of microcracking is likely in the concrete near the surface of the steel. The microcracking and the bond between the steel and concrete would have been healed through further hydration after the slip was introduced. This experiment was primarily conducted to validate the use of bar slip for crack formation in the corrosion rate study discussed in section 5.10. Since no negative effects were observed in the slipped bars and there was relatively small difference between ribbed and round bar, it was reasonable to proceed with this approach.

The use of lower covers has resulted in an elevation of the chloride threshold levels. An average chloride concentration of 0.53% was noted for the PC samples (concrete mix design I) with a cover depth of 40 mm compared to 0.88% for PC (concrete mix design II) at a cover of 20 mm. Both sets of samples were produced with ribbed reinforcing steel. As two slightly different mix designs and curing conditions were used it is difficult to make an absolute statement regarding cover and the difference in average values is relatively small compared to the possible range of chloride threshold values for both sets of samples. Furthermore the differences in chloride threshold values, as noted in section 5.8.1, may in part be a result of a more rapidly changing concentration gradient at the lower cover depths. Further study would be required to make definitive statements regarding the influence of cover on chloride threshold values and the differences in chloride threshold values between nominally identical samples, shown in the current work, highlight the variability associated with chloride threshold measurements.

5.8.3 Influence of Binder Type on Chloride Threshold Concentration

The chloride threshold concentrations, measured as a percentage of mass of cement, for various binder types were presented in Table 5.14 and Figure 5.18. It was noted in section 5.8.1 that it is inappropriate to use mortar specimens for determining the absolute chloride

threshold concentrations as these differ from the case of steel in concrete. The mortar specimens are useful however in examining the relative impact of binder type on chloride threshold concentration. Table 5.16 provides the relative values for the average chloride threshold concentration for concrete specimens, the initial measured chloride threshold for mortar specimens and the predicted values based on the aqueous phase investigation. The first specimen of each binder type to shown active corrosion is presented for the mortar series in Table 5.16 as there were a number of specimens which had not yet reached activation at the conclusion of the investigation and it would not be appropriate to state an average value.

Table 5.16: Relative concentration of: hydroxide ions, predicted chloride thresholds, average chloride thresholds for concrete and initial thresholds for mortar specimens

Binder Type	*Measured OH^-*	*Predicted Cl^-*	*Average Measured Cl^- (Concrete)*	*Initial Measured Cl^- (Mortar)*
PC	1	1	1	1
SL	0.86	0.54	0.78	0.99
SM	0.61	0.46	0.16	0.28
SH	0.39	0.38	0.38	0.23
FA	0.52	0.60	0.68	0.17
SF	0.20	0.29	0.95	0.59
TR	0.20	0.29	0.15	0.39

The relative proportion of average measured chloride threshold concentrations for concrete series I, compared to the predicted values based on the aqueous phase investigation can be seen graphically in Figure 5.19.

An examination of Figure 5.19 reveals generally good agreement between the relative predicted chloride threshold concentrations, based on the investigation of steel in simulated pore solutions, and those found in the measured concrete specimens (concrete series I) with two notable exceptions being SF and SM. Since corrosion initiation is essentially a thermodynamic issue, the study of corrosion thresholds in aqueous solution should provide a reasonable estimate of the tendency for steel to corrode in concrete with similar pore solutions. The corrosion rates, which are a function of various kinetic parameters, determined from aqueous phase work would not be directly comparable to those obtained from steel in concrete, but could provide some useful qualitative data as will be discussed in section 5.10. The relative chloride threshold level at which corrosion was first detected, for the specific binder types in the mortar series, is also in general agreement with the average measured concrete values.

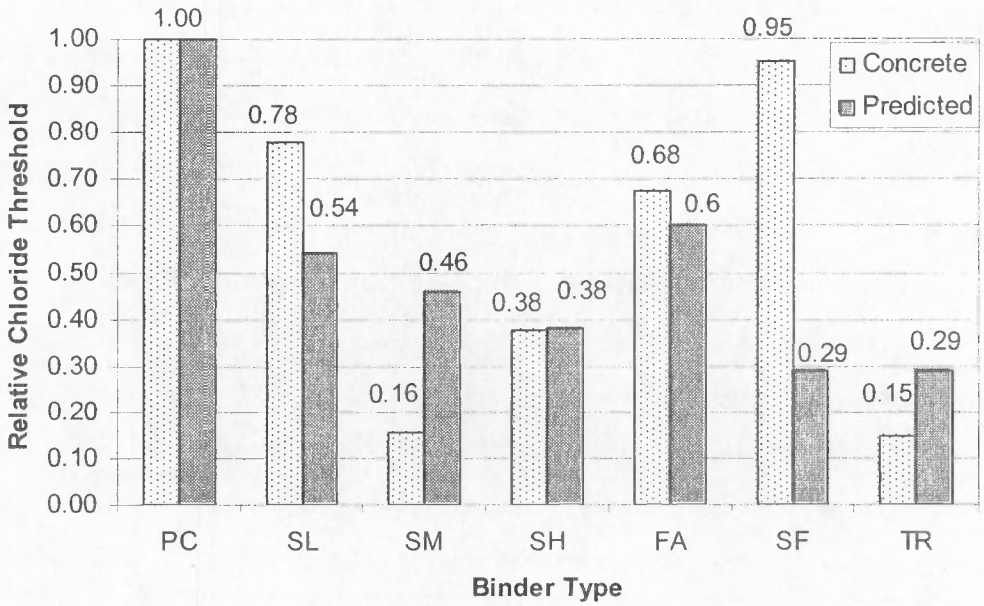

Fig 5.19: Relative chloride threshold concentrations for aqueous phase predicted values and average concrete measured values

The inclusion of any of the cement extenders results in a lowering of the chloride threshold concentration. For both the mortar and concrete series, binder types PC, SL and SF were shown to provide the greatest resistance to corrosion initiation. The relative performance between the mortar and concrete specimens differed most notably in the case of FA where the concrete specimens showed a relative average of 0.68 compared to the relative initial value 0.17 for the mortar specimens.

The inclusion of SF results in a significant decrease in the hydroxyl ion concentration of the pore fluid. It was shown in chapter 3 that both SF and TR had hydroxyl ion concentrations approximately 20% those of PC. From the results of the aqueous phase work, a similar reduction of 25% of the chloride threshold concentration was also observed. The predicted relative chloride threshold value for both TR and SF was given as 0.29. The inclusion of SF in actual concrete specimens however resulted in a chloride threshold concentration similar to that of the PC control sample. The almost identical chloride threshold concentration for SF compared to PC runs contrary to the prevailing view as given by Frederiksen (2000).

This departure of the SF specimens is difficult to explain particularly since the TR specimens, which had the same concentration of silica fume, resulted in a relative chloride threshold concentration very similar to the predicted value and significantly lower than the PC control. It appears therefore that the characteristics of the TR specimens were dominated by

the slag component rather than the SF component with respect to the initiation of corrosion due to chloride ions. All of the remaining samples generally followed the conventional trend of lower chloride threshold value associated with reduction in hydroxyl ion concentration as shown in Table 5.16.

It was considered that the use of a superplasticizer may have impeded the corrosion initiation but results from TR, which also employed a superplasticizer, were approximately 30% those of the SF specimens. The superplasticizer may contribute by ensuring better distribution of the SF throughout the matrix and ensuring sufficient flow of the concrete and mortar around the rebar. The chloride threshold value will depend on the degree of porosity or voids immediately around the steel. If the mix is more flowable and ensures adequate coverage of the steel with hydration products, there would be fewer areas which may be deficient in hydroxides and thus lead to an overall higher chloride threshold. SF has another important benefit, and that is densification of the ITZ. The same principle of improving the zone around aggregate also applies to steel which could simply be viewed as a larger and smoother aggregate. A densification of the interface immediately around the steel would help to counter possible defects on the steel surface and limit the exposed area initially available for corrosion. The improved material characteristics at the steel concrete interface thus appear to have offset the overall reduction in hydroxide concentration resulting in a chloride threshold value very similar to the PC control.

The TR sample did not appear to benefit to the same degree as the SF from the inclusion of a superplasticizer. The major difference between the two samples is the inclusion of 43% slag. The TR samples more closely approximated the relative chloride threshold levels of SM which had similar concentration of slag (50%). As the sulphides and thiosulphates were shown in chapter 4 to generally impact negatively upon the chloride threshold value, the combined effect of lower hydroxide concentration coupled with the presence of sulphides has overcome the benefits associated with the SF.

The expected effects of the inclusion of slag are shown in Table 5.16 with the relative predicted chloride threshold level being lower than the relative hydroxyl ion concentration. The measured chloride concentrations of the concrete samples generally seem to support this argument with all slag bearing materials having a lower relative chloride concentration than the corresponding relative hydroxyl ion concentration. The measured chloride threshold for SL and SH were both equal or somewhat greater than the predicted values while the SM specimens showed a substantial reduction in the chloride threshold concentration compared to both the predicted value and the PC control. The large decrease in chloride threshold is

observed for both SM with a slag replacement of 50% and TR with a 43% replacement. It appears that moderate replacement levels (50%) of slag have a greater impact upon the chloride threshold concentration than either low (25%) or high (75%) replacement levels. At low levels of replacement by slag (SL) the behaviour is more akin to PC. The somewhat muted effects of the high replacement levels (SH) are likely a result of the more open pore structure, as demonstrated by the durability index values presented in section 5.7, which would allow for the rapid oxidation of the sulphides. SM, with its denser pore structure, would limit the oxidation of sulphides and ensure their presence for a longer period of time. If complete oxidation of the sulphides, at the level of the steel, occurred prior to chlorides reaching the steel it is possible that some of the damage to the passive layer, associated with the sulphides, may be repaired and the chloride threshold concentration may increase somewhat. The very low chloride threshold concentration determined for SM and TR may be a cause for concern, as they would offset much of the gains normally associated with the reduced permeability of the cover concrete. More directed research is needed to accurately quantify the chloride threshold for slag bearing material particularly at replacement levels in the range of 50% and to determine if long term healing of the passive layer is possible after the sulphides have been oxidized.

5.8.4 Selection of Chloride Threshold Concentration

The breakdown of the passive layer is a complex mechanism dependant upon numerous variables. It is not possible therefore to state a simple or single chloride threshold value. The chloride threshold concentration for the PC specimens, for instance, ranged from 0.29 % to 0.87 % mass of chlorides by mass of binder. The effects of the SF in particular show that variables beyond simply the pore solution chemistry must be considered. The reduction of the hydroxide concentration by the inclusion of cement extenders generally reduces the corrosion threshold, as does the presence of sulphides. The reduction in chloride threshold concentration does not vary uniformly with the level of slag replacement. SM, at a 50% replacement by slag, had a substantially lower chloride threshold than either SL or SH.

In the case of SF it is considered that the densification of the interfacial zone around the steel resulted in a chloride threshold concentration similar to that of PC despite a significant reduction in the hydroxyl ion concentration. At times one of the processes may dominate as was seen in the dramatic difference between TR and SF.

The use of mortar specimens as a means of determining chloride threshold concentrations for steel in concrete is not advisable. The chloride threshold concentrations for the concrete

specimens were on average 37% lower than the corresponding mortar specimens. The mortar specimens may however be useful for determining the relative performance of various binder types and showed similarities with the concrete specimens.

The use of smooth steel resulted in a slight decrease in the average chloride threshold concentration compared to ribbed reinforcing. There was considerable overlap in the range of observed values for both the smooth and ribbed steel. The effects of slipping of the rebar were also investigated and the slipped PC concrete specimens were found to have somewhat higher chloride threshold concentrations compared to the unslipped bars. Since there were no deleterious effects of slipping, the use of smooth bars in cracked concrete, where the crack is sustained through slipping of the bar, should not unduly influence the initiation process and will provide results comparable to case of ribbed reinforcing steel in concrete.

Further refined investigation would be necessary to more accurately determine the influences of the individual factors. The results from the current investigation show a significant and varied dependence of the chloride threshold level associated with the inclusion of cement extenders. The traditionally accepted value of 0.4% is therefore inappropriate for blended cements, and binder-specific chloride threshold values should be used. The results of the chloride threshold investigation are summarized in Table 5.17.

Table 5.17: Summary of factors influencing chloride threshold concentrations

Factors	*Results*
mortar specimens	The use of mortar results in an increase in the chloride threshold concentration compared to concrete.
ribbed and smooth steel	There is little difference between ribbed and smooth steel, although the ribbed steel did have a slightly higher chloride threshold concentration.
slipping of steel rebar	Slipping of the rebar resulted a minor increase in the chloride threshold concentration compared to unslipped bars. Slipping of the rebar did not appear to harm the specimens.
binder type	The use of any of the cement extenders results in a reduction of the chloride threshold concentration. SM and TR showed the greatest reduction of the chloride threshold concentration with the inclusion of SF resulting in almost no change compared to PC

5.9 Results and Discussion for Passive Corrosion Conditions

The corrosion rates and potentials of steel embedded in concrete were studied in both the passive and active state for concrete mix design series II (w/b ratio 0.58 with 9 mm aggregate). The cracked specimens allowed for the investigation of active corrosion for two crack widths of 0.2 mm and 0.7 mm and two cover depths of 20 mm and 40 mm while the uncracked specimens provide information on the passivity of the steel. Concrete resistivity measurements were also taken for each of the samples.

The general relationship between the probability of corrosion and the potential ($Cu/CuSO_4$), as stated in ASTM C876, is provided in Table 5.18. The potential in mV, relative to Ag/AgCl, was determined assuming it to be 70 mV positive to the $Cu/CuSO_4$. While potential measurements provide a reasonable indication of thermodynamic activity they do not provide any kinetic information as to the rate of corrosion. The direct determination of the corrosion rate is therefore necessary. The relationship between corrosion current density ($\mu A/cm^2$) and degree of corrosion is provided in Table 5.19.

Table 5.18: Relationship between potential and probability of corrosion (ASTM C 876)

Probability of Corrosion	*mV ($Cu/CuSO_4$) ASTM C 876*	*mV (Ag/AgCl)*
90% no corrosion occurring	< -200	< -130
uncertain	-200 to -350	-130 to -280
90% corrosion occurring	> -350	> -280

Table 5.19: Degree of corrosion and current density, $\mu A/cm^2$ (Broomfield et al., 1994)

Corrosion current density ($\mu A/cm^2$)	*Degree of corrosion*
< 0.1	passive conditions
0.1 to 0.5	low to moderate
0.5 to 1	moderate to high
> 1	high

The assessment of the influence of cement extenders on the corrosion characteristics of steel in concrete, prior to the initiation of chloride induced corrosion, was performed on uncracked samples cured in water for a period of two weeks. The aqueous phase work showed that both the corrosion potential and rate were strongly influenced by the presence of sulphides, which in concrete would be attributed to the presence of slag. The first portion of the investigation, using concrete, therefore focused on verifying these observations. A moving average of three potentials for all the samples, over the first 110 weeks, is provided in Figure

5.20. It should be noted that for the purposes of this discussion all potential values are measured against a Ag/AgCl reference electrode unless explicitly stated.

The initial readings for all the slag bearing materials showed very negative potentials: -636, -638, -593 and -593 mV for SL, SM, SH, and TR respectively, compared to -209, -150 and -190 mV for PC, FA and SF. The highly negative potentials are indicative of reducing potentials associated with the sulphides and thiosulphates which are liberated during the hydration of the slag bearing materials, as demonstrated from the pore solution results presented in Chapter 3. The non-slag bearing materials all showed more positive, oxidizing potentials. The early internal environmental differences are likely responsible for the long term changes in the passive corrosion rate due to the formation of an imperfect protective layer of ferric and ferrous oxides associated with the more reducing slag bearing materials. FeS is also readily precipitated and likely further compromises the protective nature of the oxide layer being formed around the steel.

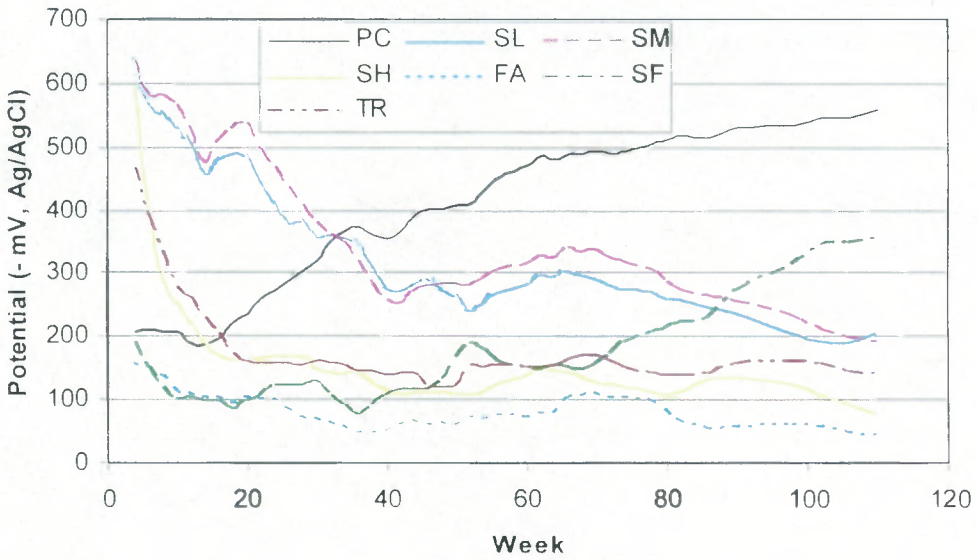

Fig 5.20: Results for moving average of potentials for first 110 weeks

It is apparent from Figure 5.20 that while it took over 100 weeks for the potentials of SL and SM to reduce to what would be considered passive potentials, the results for SH and TR very quickly fell to values more similar to the other non slag bearing samples. The rapid reduction in potential of the SH sample is a result of both the fairly open nature of the pore structure which would permit the ingress of O_2 from the environment and the low hydroxide concentration which would reduce the stability of the sulphide ion and accelerate the oxidation process. The OPI for SH was 9.78 compared to 10.08 for TR and 10.05 for SL at 28

days. The OPI for TR however showed a reduced permeability compared to both SM and SL for which the potentials were very slow to reduce. The ease of oxygen ingress therefore could not have been a factor in the resulting oxidation of sulphides for the TR samples. The low concentration of sulphide and thiosulphate, 8 and 10 mg/l for TR compared to 59 and 75 mg/l for SL at 28 days, coupled with the reduced hydroxide concentration, would account for the rapid oxidation of sulphides and subsequent change in potential to more positive values.

5.9.1 Early Age Results

Active corrosion initiated fairly quickly in the PC samples starting at approximately week 18, which is indicated by the move to more negative potentials as shown in Figure 5.20 and the dramatic increase in corrosion rate as shown in Figure 5.21. The early age results for potential, corrosion rate and resistivity are provided in Table 5.20. The results are based on the readings averaged over the first 16 weeks. Average values for the first 16 weeks are presented, because subsequent to this time the PC samples showed initiation of active corrosion and would have to be excluded from further comparison of passive values.

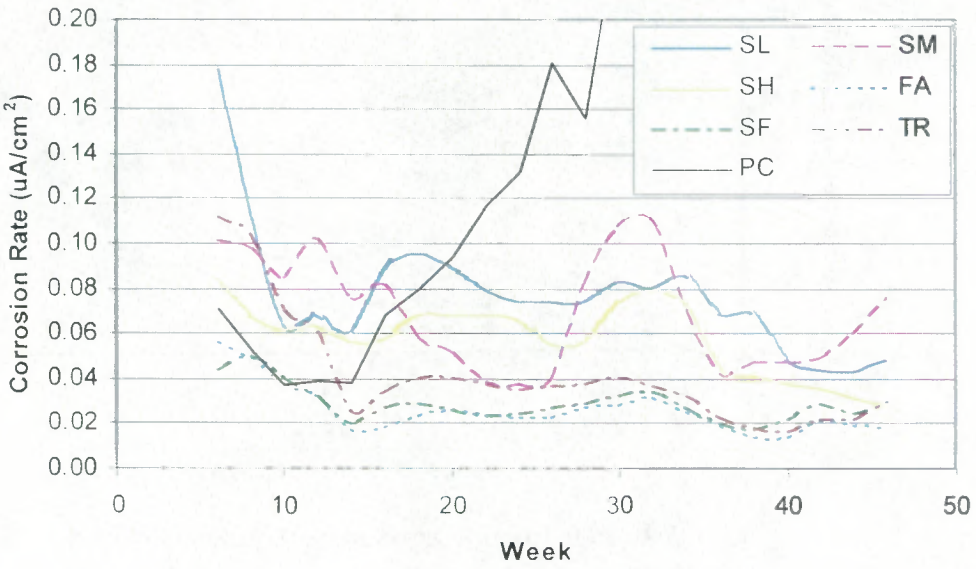

Fig 5.21: Moving average of early age corrosion rates

Note: The corrosion rates for the PC specimens continued to increase with time and for the purpose of differentiating between the other specimens only the PC values up to week 30 are included in this graph.

Table 5.20: Values averaged over first 16 weeks

Material type	*Potential (- mV)*	*Rate ($\mu A/cm^2$)*	*Resistivity ($k\Omega cm$)*
PC	199	0.045	8
SL	524	0.086	18
SM	542	0.086	35
SH	288	0.063	56
FA	126	0.033	27
SF	119	0.035	24
TR	307	0.064	67

The averaged potential and corrosion rate values presented in Table 5.18 show three distinct groups:

a) The first group are those with slag bearing material SL and SM having similar pore solutions characterized by high hydroxide and sulphide concentrations, and a well developed pore structure as shown by OPI values indicating better performance than PC at 28 days. The early age potential values are highly negative with similarly high corrosion rates, considering chlorides have not penetrated to the depth of the steel. The corrosion rates for SL and SM are approaching the active level and almost double that of PC, despite having resistivity values 2 to 4 times higher than PC.

b) The second group of samples (SH and TR) are also slag bearing, at similar or greater replacement levels, yet display more positive potentials and have lower corrosion rates than SL and SM. The potentials are still in what is normally considered the region indicating active corrosion as stated in Table 5.18. The impact of the slag component of the second group however is minimized by a combination of reduced hydroxide concentration, lower initial sulphide and thiosulphate concentrations or open pore structure which permits the rapid movement of oxygen to the depth of the steel and oxidation of the various sulphur species. The resistivity values of the second group of samples are at least seven times greater than PC with corrosion rates 1.5 times higher.

c) The final group are those which do not contain slag and show potential values and corrosion rates indicative of normal passive conditions. PC, FA and SF all had corrosion rates between 0.33 and 0.45 $\mu A/cm^2$ suggesting passive corrosion conditions. It should be noted that the sulphide concentration of PC sample was measurable though low, 15 mg/l at 90 days, compared to FA, 6 mg/l, or SF, 2 mg/l. The highest corrosion rate again corresponded to the samples with highest sulphide concentration even among the samples in this final group. The

relationship between average passive corrosion rates over the first 16 weeks and sulphide concentration can be seen in Figure 5.22.

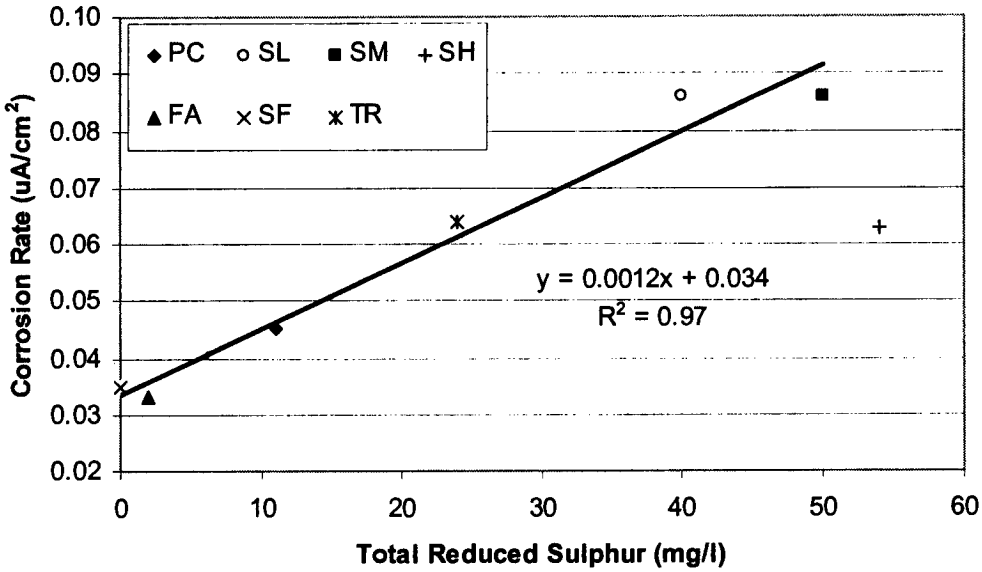

Fig 5.22: Dependence of passive corrosion rate (average of first 16 weeks) on 7 day sulphide concentration

The trend line shown in Figure 5.22 excludes SH which was found to have the highest sulphide concentration at 7 days. The behaviour of SH is rather unusual in that it has a high sulphide concentration and very negative potential. The material undergoes a substantial transformation however when exposed to the atmosphere due to the open pore structure which permits the rapid oxidation of the sulphides and shift of the corrosion potentials to more noble values. The rapid changes in the pore solution make a comparison of SH with the other samples difficult.

An examination of the remaining samples, excluding SH, shows a clear relationship between the early age passive corrosion rates and the sulphide concentration of the pore solution of cement paste measured at 7 days. The 7 day sulphide results were chosen as they would be more representative than the 28 day or 90 day results of the pore solution chemistry during the initial formation of the passive layer. The impact of sulphides on the passive layer development was demonstrated in Chapter 4, such that those samples which were initially exposed to sulphides had higher corrosion rates than the sulphide free samples, even after all the sulphides were oxidized. The comparison of corrosion rates at later periods, such as over the first 16 weeks, to early age pore solution composition is therefore reasonable.

The results from the resistivity measurements do not fall into the same groups as those provided by potential or corrosion rate. A moving average of resistivity values over the study period is provided in Figure 5.23

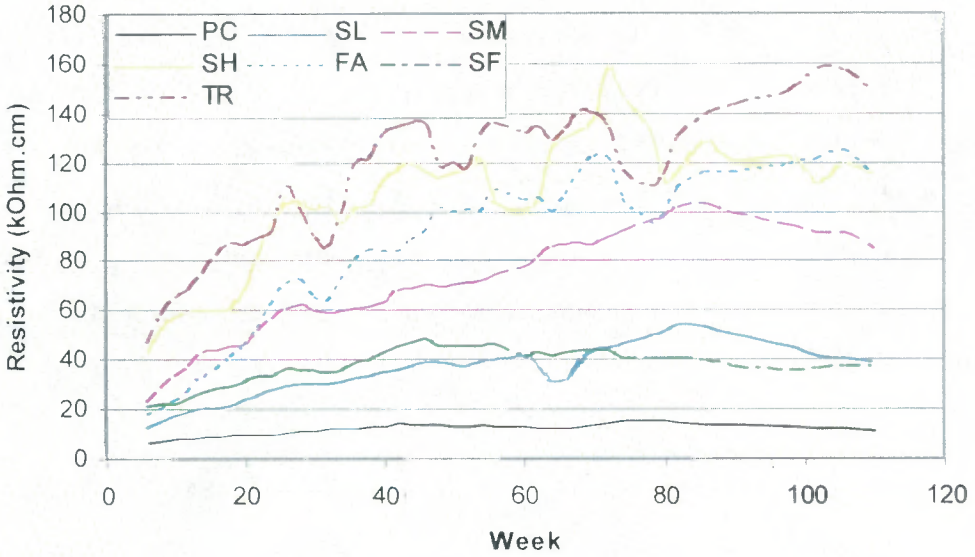

Fig 5.23: Moving average of resistivity over study period

It can be seen from Figure 5.23 that there are three groups of resistivity results. The PC sample showed the lowest results with time. SF and SL resulted in a moderate increase in resisistivity while FA, SM, SH and TR all showed appreciable gains. The inclusion of slag does not provide for a unique resistivity value though its inclusion does result in an increased resistivity compared to PC. The resistivity of the concrete does not appear to be a controlling factor in the early age passivation of steel, rather the presence of sulphides, from the inclusion of slag, appears to determine early age passive corrosion rate. SM, SH and TR all contained appreciable quantities of slag and had resisivity values greater than SF and FA, yet showed corrosion rates almost double those of FA and SF.

The resistivity of the samples generally showed increasing trends with continued hydration and partial drying. Over time however the ingress of chlorides would tend to increase the conductivity of the pore solution and thus lower the overall resistivity. A peak resistivity value was observed for most samples though TR showed signs of a continuing increase in resistivity which would be consistent with its dense pore structure and slow rate of chloride ion penetration.

5.9.2 Later Development

The passive potentials and passive corrosion rates of all the samples reduced and stabilized with time, but those containing slag continued to show more negative potentials and higher corrosion rates over the entire study period than the slag-free samples. A moving average of corrosion rates for the study period starting at week 34 is provided in Figure 5.24. It should be noted that once PC started to corrode actively it could no longer be compared to the other samples with respect to the passive corrosion case and is therefore not shown in Figure 5.24. The potential, corrosion rate and resistivity values for all samples over the entire study period are provided in Appendix 5D.1. At approximately week 72, as seen in Figure 5.24, the SF samples began to corrode actively and were excluded from further comparison of passive conditions.

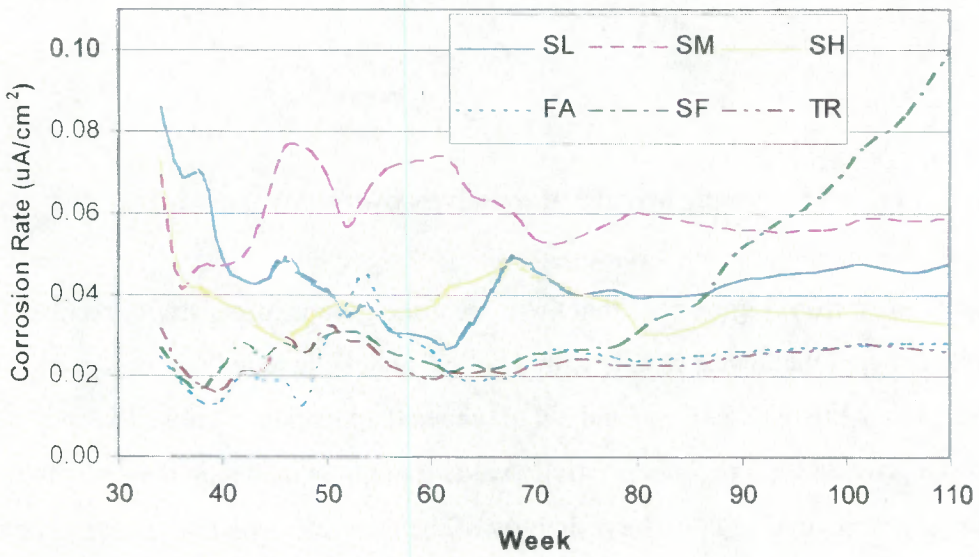

Fig 5.24: Moving average corrosion rates for SL, SM, SH, FA SF and TR from week 34 to 110

A comparison of passive corrosion conditions therefore is possible between weeks 40 and 70 for all samples except PC. Average values of corrosion potential, rate and resistivity over the period of week 40 to week 70 are provided in Table 5.21.

Table 5.21: Average values from weeks 40 to 70

Sample	*Potential (- mV, Ag/AgCl)*	*Rate ($\mu A/cm^2$)*	*Resistivity ($k\Omega cm$)*
PC	436	0.662	13
SL	279	0.041	38
SM	297	0.064	75
SH	125	0.039	118
FA	75	0.024	101
SF	145	0.026	44
TR	146	0.023	132

The results indicate that the trend of slag bearing materials giving higher corrosion rates and more negative potentials continues well beyond the first few weeks. After one year the potentials of SL and SM would normally be associated with a corroding state but as can be seen from the corrosion rates some form of passivity, though deficient compared to FA and SF, exists. The potential and corrosion rate for SH and TR in particular have reduced considerably from their initial high values to values more representative of non-slag bearing material. The decrease in corrosion rate of the TR samples can be attributed to the low initial concentrations and subsequent oxidation of the sulphides together with a high resistivity. SH would have experience similar changes though not as dramatic as is evident by the still elevated corrosion rate.

The observed passive corrosion rates associated with what is normally considered to be active corrosion potentials for the SL and SM highlight the need for reliable corrosion rate information when examining the conditions of structures. Assumptions of the state of corrosion based on potential measurements can clearly be misleading in the case of concrete containing cement extenders such as slags.

5.9.3 Relationship Betwee: Potential, Chloride Concentration and Passivity

The concrete chloride threshold concentrations, determined in section 5.8, and measured chloride concentrations at the end of the study period are provided in Table 5.22. The chloride concentrations of the PC samples are well above that required to initiate corrosion and are confirmed by both the measured potential and corrosion rate values.

Table 5.22: Average concrete Cl^- threshold values, section 5.8, and measured Cl^- concentrations at end of study period (as % mass of cement)

Binder Type	*Average Cl^- threshold*	*Range of values*	*meaured Cl^- (week 110)*
PC	0.53	0.29 - 0.87	2.49
SL	0.41	0.22 - 0.61	0.71
SM	0.08	0.06 - 0.11	0.19
SH	0.2	N.A.	0.15
FA	0.36	0.29 - 0.43	0.21
SF	0.51	0.51 - 0.71*	0.96
TR	0.08	0.07 - 0.09	0.18

Note: the stated range of values for SF includes measurements taken from concrete mix design series II and includes a total of three measurements. The chloride concentration is the single reported values from the concrete series I mix.

The potential and corrosion rates of SF moved from a passive to active state after approximately 72 weeks which agrees with the measured chloride concentration, at the end of the study period (110 weeks after casting), of 0.96 % which is well above the 0.51, % Cl^- by mass of cement, indicated as a threshold concentration. SH, and FA showed chloride concentrations, at the end of the study period, approaching activating concentrations while SL, SM and TR had chloride concentrations above that which would be considered necessary for inducing corrosion. Despite the elevated chloride concentrations of SL, SM and TR there was no indication of a significant increase in corrosion rate though SL did increase somewhat after approximately week 52. The potentials of SL, SM and TR continued to move to more noble values over this period despite the increase in chloride concentration.

The work of Alonso et al. (2000) relating chloride threshold values to corrosion potential is of considerable interest when applied to the problem of more negative potentials associated with slag bearing materials. Their work shows a dependence of chloride threshold values on potential of the steel such that the more negative the potential the greater the chloride threshold value, as seen in Figure 5.25. For potentials more negative than -150 mV (SCE) there appears to be a linear relationship between potential and chloride threshold. A decrease in potentials from -150 mV to -350 mV (SCE) would result in approximate doubling of the chloride threshold concentration.

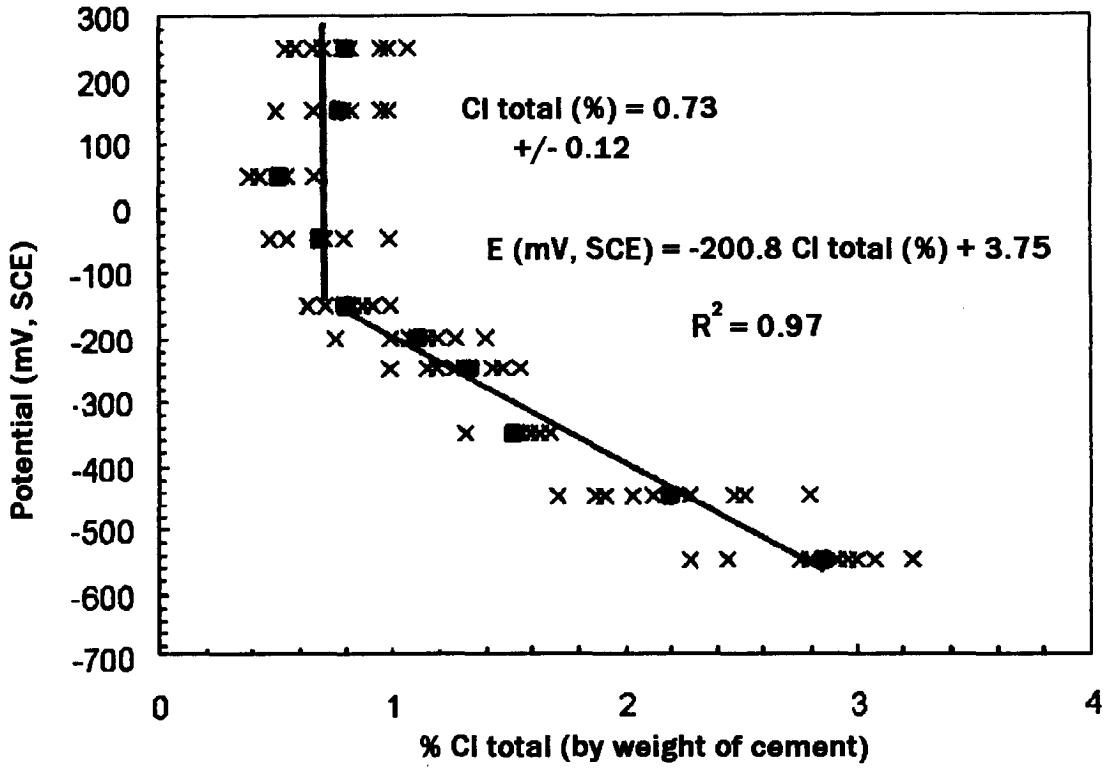

Fig 5.25: Dependence of Cl^- threshold level on potential (Alonso et al., 2000)

The current examination of the cement extenders and chloride threshold, section 5.8, showed lower chloride thresholds particularly for the slag bearing materials. The values of the potentials for the threshold slag specimens were similar to those of the PC samples and significantly more positive than those used in the study on passivation characteristics as shown in Table 5.23.

Table 5.23: Comparison of potential values from non-active chloride threshold specimens and passive corrosion study specimens

Binder Type	*Passive study potential (- mV, Ag/AgCl)*	*Non-active Chloride threshold potentials (- mV, Ag/AgCl)*
PC	436	62
SL	279	54
SM	297	25
SH	125	50
FA	75	63
SF	145	102
TR	146	55

The non-active chloride threshold potentials reported in Table 5.23 are typical average values, for the specific binder type, prior to the initiation of corrosion for concrete series I as described in section 5.8. The reported potentials for the passivation study the average values for week 40 to 70. The PC specimens are already actively corroding during this period and cannot be compared to the non-active threshold specimens. The more rapid decrease in potential was attributed to the very early ponding and exposure to the atmosphere of the threshold samples in mix design I compared to those of mix design II. If the potentials were held at more negative values for a prolonged period of time as demonstrated in Figure 5.20, the low threshold values reported for the SL and SM in section 5.8 would likely have to be raised. The effect of more negative potentials increasing the chloride threshold level may explain why SL did not show signs of corrosion despite having a chloride concentration well in excess of the previously observed threshold value at low potentials. Sulphides therefore have two competing effects on the passivation of steel and its ability to resist chloride ions; firstly the sulphides limit the effectiveness of the passive layer and allow for lower chloride threshold concentrations; secondly the sulphides also lower the potential to more negative values which has the effect of raising the chloride threshold concentration while the potentials are suppressed.

There is in effect a competition between chlorides reaching the steel and the shift in potential. So long as the potential remains significantly negative the chloride threshold value is likely to be greater and thus limiting increases in the corrosion rate for a given chloride concentration. With the progression of time the level of chloride will increase and the chloride threshold level decrease with the move to more noble potentials until a state of active corrosion is reached. Further research will be required to more accurate define chloride thresholds which are dependant upon potential and sulphide.

The lack of active corrosion observed in the TR samples cannot be explained by the same process as the potential values were less than -150 mV and should not affect the chloride threshold value. It is probable that the measured chloride values, at the end of the study period, are simply approaching the upper limit of chloride threshold concentrations. Chloride thresholds concentrations have been shown in section 5.8 to be highly variable and TR specimens from the passive corrosion study may be representative of that variability.

The inclusion of slag as a cement extender has been shown to adversely affect the formation of the passive layer due to the observed increase in passive corrosion rate over the period of investigation. The elevated corrosion rate, almost double the rate compared to other extenders, still remains below what is considered the active - passive transition of 0.1 $\mu A/cm^2$.

The values did reduce somewhat from their initial levels but the corrosion rates appear fairly stable from week 80 until the end of the study period (week 110) emphasizing the long term effects of the sulphides in the slag concrete. The other cement extenders of FA and SF showed improved performance compared to the PC control even at the very early stage of less than 16 weeks. The samples continued to show reduction in both the potential and corrosion rate from week 40 until week 70 with average corrosion rates of 0.24 and 0.26 $\mu A/cm^2$ for FA and SF respectively. The ternary blend of sample TR showed a mixed behaviour between the slag bearing samples and SF. The very early results showed highly negative potentials (-307 mV over the first 16 weeks) and higher corrosion rates. These values decrease over time and the sample showed characteristics more similar to SF. The effects of the inclusion of slag in this case were tempered by the lower hydroxide concentrations associated with SF and did not appear to have a lasting effect. All the samples exhibited what would be considered passive corrosion rates which would be of no structural consequence. The real test of the performance of the material is in their resistance to the active corrosion associated with the ingress of chlorides, particularly where service cracking has short circuited the normal service life period.

5.10 Active Corrosion Characteristics

The influence of cement extenders on the active corrosion of steel in concrete was observed through an examination of cracked concrete. Crack surface widths of approximately 0.2 and 0.7 mm were obtained by three-point bending of the specimen and maintained by some slipping of the bar. Slipping was shown in section 5.8.2 not to have any detrimental effects on the chloride threshold value. The movement of chloride along a slipped bar compared to an unslipped bar is briefly studied as discussed in Appendix 5C.2. There was no substantial difference in movement of chlorides along the slipped bar compared to the unslipped bar. (The term "unslipped" refers to the control specimens which were not subject to an axial load on the steel and thus did not experience any differential movement between the rebar and the concrete.)

5.10.1 Effects of Bar Type and Concrete Steel Interface

The difference in corrosion rates between slipped and unslipped bars was reasonably small compared to the possible range of values exhibited for either the slipped or unslipped bars. The maximum observed corrosion rate for a PC concrete series II specimen with ribbed reinforcing was approximately 1.4 $\mu A/cm^2$, which is substantially greater than the 0.12

$\mu A/cm^2$ difference between the slipped and unslipped specimens. The average corrosion rates between week 66 and 86 was 0.35 $\mu A/cm^2$ for the unslipped and 0.47 $\mu A/cm^2$ for the slipped bars. It is interesting to note however that while the chloride threshold value was higher for the slipped bars, the time at which corrosion initiated was much earlier, approximately week 36 compared to week 66 for the unslipped. The chlorides appeared to have penetrated through the cover concrete of the slipped samples faster than the unslipped which would explain the elevated corrosion rates. At the end of the study period the slipped samples had an average chloride concentration of 1.7% by mass of cement compared to the unslipped bars of 1.5%. The differences between the two sets are minor and further more directed research would be required to determine if real differences did exist. For the purposes of the current investigation on the influence of cement extenders on the corrosion of steel in cracked concrete, the use of slipping to maintain crack widths appears reasonable and should not excessively influence the outcome of the results or compromise the comparison of values.

A further deviation in the experimental investigation from real structures was the use of smooth round mild steel bar compared to deformed rebar. The differences in corrosion rates between ribbed reinforcing bars and smooth round bar was investigated using PC samples corresponding to mix design series II at a cover depth of 20 mm. The average corrosion rates after initiation for ribbed and smooth bar are shown in Figure 5.26. The ribbed bars showed a greater degree of variability compared to the smooth bars but the general trend between the two sets of samples appear similar. The average corrosion rates for the first 20 weeks of active corrosion were 0.32 $\mu A/cm^2$ for the deformed bars compared to 0.35 $\mu A/cm^2$ for the smooth bars. The maximum corrosion rate for the deformed bars was somewhat higher at 0.57 compared to 0.41 $\mu A/cm^2$ for the smooth bars. The differences between the two types of bars are again small and with the variation between the two on average less than 10%, the use of smooth bars in the experiment should not preclude the application of the data in modeling the service life for real structures. Smooth bar was needed to prevent longitudinal cracking of the concrete specimen, due to movement of the bar, during three point bending to induce a transverse crack.

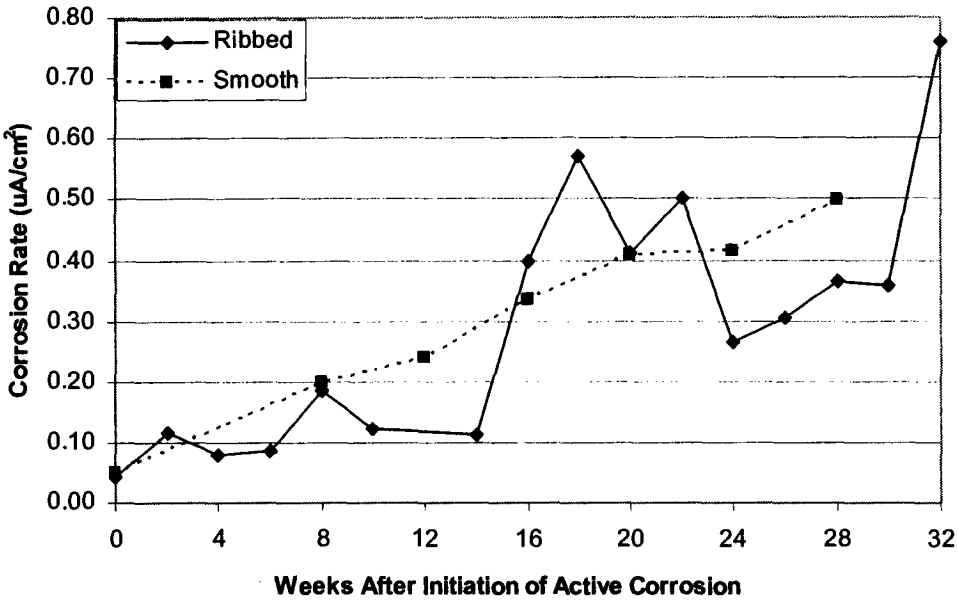

Fig 5.26: Corrosion rates ($\mu A/cm^2$) of smooth round bar and deformed ribbed reinforcing in OPC concrete after initiation of active corrosion

5.10.2 Values of Corrosion Potential

The impact of slag on the corrosion potential of the steel and the likely relationship between sulphides and oxygen is again highlighted by the very rapid reduction in potential immediately after cracking and before exposure to chloride solutions. The potential of SL was shown to reduce very gradually over time in sound concrete such that the potential was still more negative than -250 mV even after 80 weeks. By contrast this same reduction in potential was achieved in less than 50 minutes after cracking of the specimen as shown in Figure 5.27. The cracking of the concrete allowed rapid access of oxygen to the steel which would result in oxidation of the sulphides and shift from a reducing environment to a more oxidizing one. A process which in uncracked concrete would have taken years was thus accomplished in a matter of hours. The same result occurred in the aqueous phase work with introduction of oxygen to the system. Although the potentials in the aqueous phase work moved to more 'normal' levels, the effects of the sulphides remained present as was seen with the elevated corrosion rates even under passive conditions (section 4.6.1). It is not necessary therefore that the reducing environment be maintained for the sulphides to affect the corrosion process.

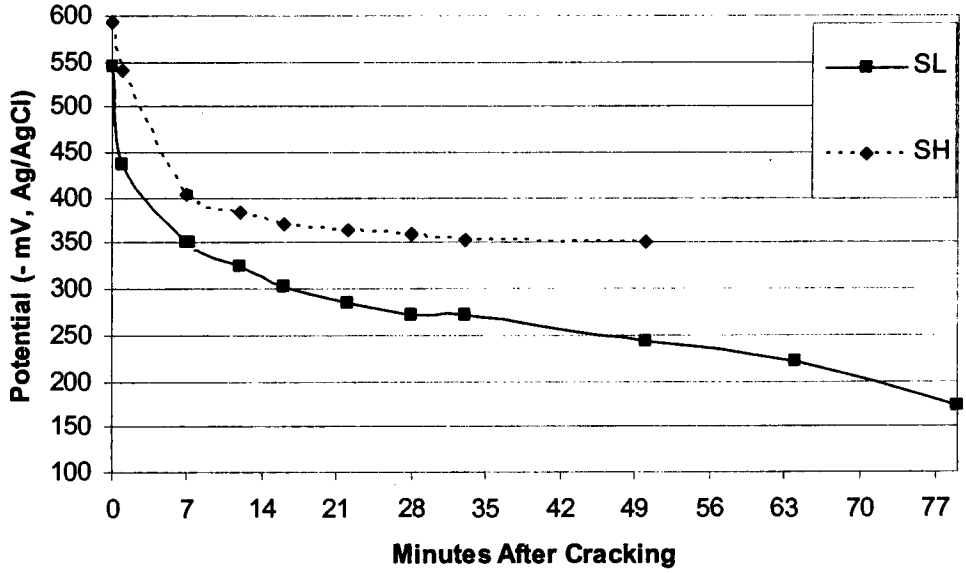

Fig 5.27: Potential of steel immediately after cracking

Their mere presence at the time of casting, due to the hydration of slag, ensures some form of lasting impact. The ongoing impact of the sulphides is likely evident in the form of a defective passive layer, due to the precipitation of FeS on the steel surface as described by Salvarezza et al. (1982).

Once the specimens were cracked, the potentials generally settled to those indicative of a passive corrosion state prior to the initiation of active corrosion due to chloride ion ingress. The cracked specimens were allowed to remain in air for approximately two days after cracking and prior to the initiation of ponding with salt solution. Very early age potential readings (less than 1 day after cracking) were only taken on a limited number of samples. For a more comprehensive review of the mechanisms and to perform quantitative predictions, more research would be required.

The dramatic impact of cracking on the corrosion potential can be clearly seen in Figure 5.28 which shows a comparison of PC and SM for cracked (0.2 mm) and uncracked concrete with cover depths of 20 mm. Active corrosion, is considered to have commenced with a substantial shift in potentials to more negative values as defined in Table 5.18. The potentials of the cracked PC specimens moved into the region indicating active corrosion less than two weeks after ponding, which is also supported by the corrosion rate measurements taken at that time as will be discussed in the following section. The uncracked PC samples did not reach

comparable negative potentials of -490 mV until week 70. The potentials for the cracked SM samples showed a similar rapid move towards negative potentials.

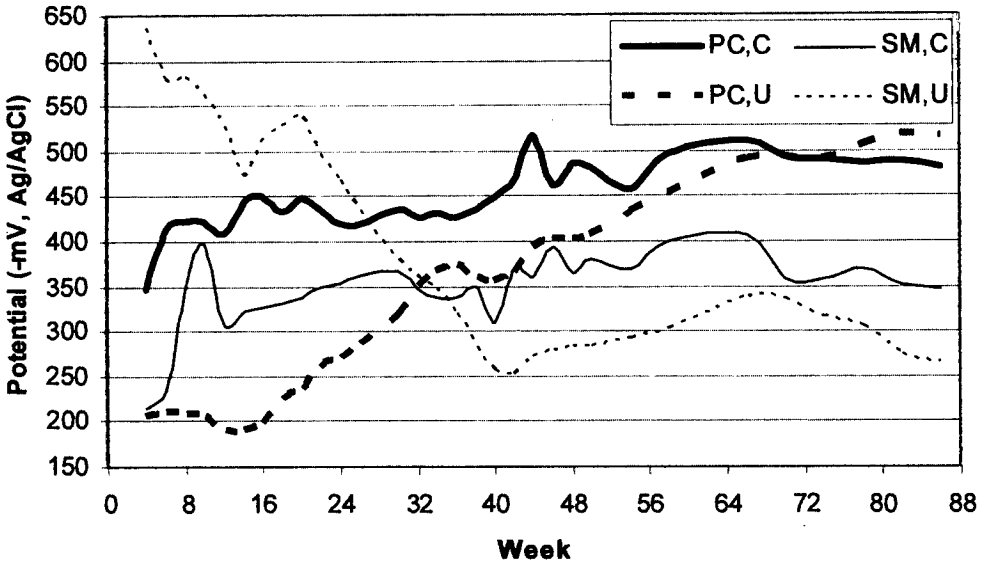

Fig 5.28: Moving average of potentials for PC and SM, 0.2 mm cracked and uncracked specimens (C - cracked, U - uncracked)

The uncracked SM samples however displayed more negative potential values than the cracked samples until week 36 despite the uncracked samples having a lower passive corrosion rate than the active cracked samples, 0.07 $\mu A/cm^2$ for the uncracked samples and 0.33 $\mu A/cm^2$ for the cracked samples over the same period. The negative potentials of SM in uncracked concrete are again attributed to presence of sulphides in the pore solution.

The moving average of potentials for steel at depths 20 mm and 40 mm in 0.2 mm cracked concrete are provided in Figures 5.29 and 5.30 respectively. Figure 5.29 and 5.30 show a rapid onset of corrosion after ponding (week 2). In most cases corrosion initiated within two to four weeks of exposure to salt water. The moving averages for the various binder types are generally determined from the potentials from three individual specimens and combined over three successive periods to form a moving average.

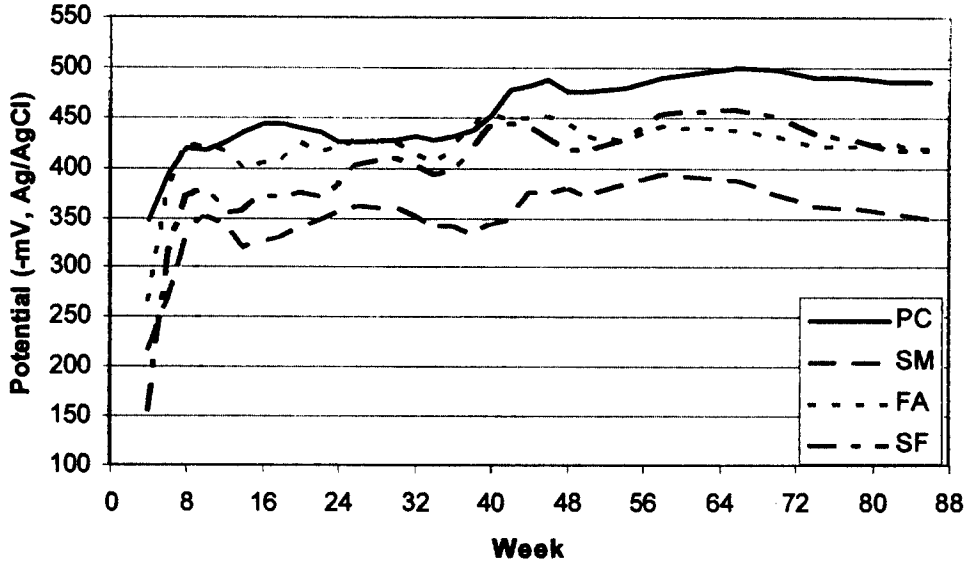

Fig 5.29: Moving average of potentials for steel at 20 mm cover and 0.2 mm cracking

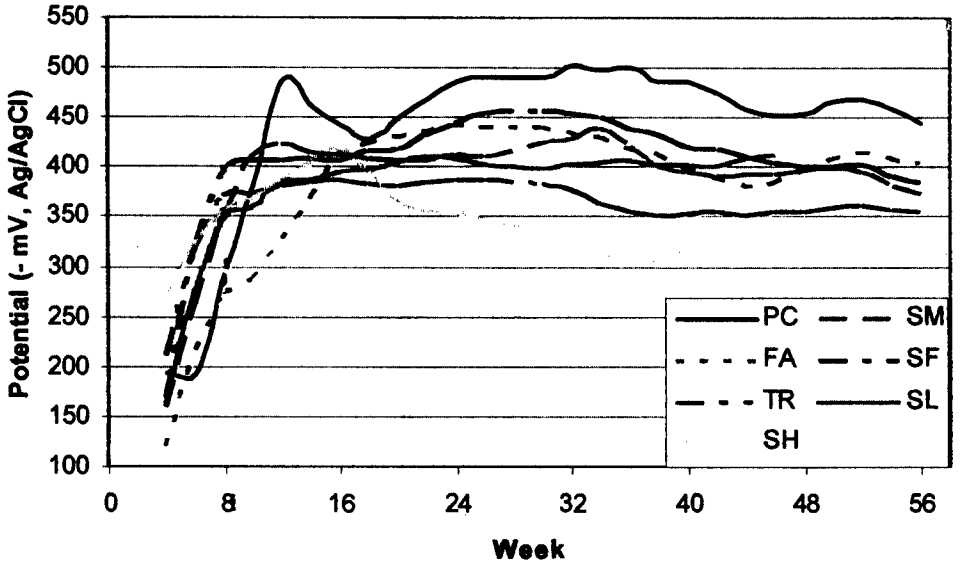

Fig 5.30: Moving average of potentials for steel at 40 mm cover and 0.2 mm cracking

Two PC specimens with a cover of 40 mm and crack width 0.2 mm and one SL specimen of the same series however did not show signs of corrosion until weeks 40 and 42 respectively. The delayed onset of corrosion was attributed to the autogenous healing of the crack. The deep cover and small crack width allowed for the delayed effects. These specimens were not included in the overall assessment of active corrosion rates and are not represented in Figure

5.30 where the potentials for PC are determined from only 1 specimen and SL from 2 specimens. The average potentials for all the cracked specimens may be found in Appendix 5D.2.

The slag bearing samples were shown in section 5.9 to have the most negative potentials in the passive state. It is interesting to note that once activation occurred the change in potential for the slag bearing samples was much smaller and resulted in more positive potential values than the PC control samples. In the case of 20 mm cover and 0.2 mm crack width, the slag bearing samples had a more positive corrosion potential than any of the other mixes (PC, SF and FA). This trend is generally repeated in with cover depths of 40 mm and 0.2 mm crack widths providing more positive potentials for SH, TR, SL and SM than FA, SF or PC. The true determination of the concrete's ability to resist corrosion of the steel is not solely a function of the steel's potential but rather the actual corrosion rate as will be discussed in the following section.

5.10.3 Stability of Corrosion Rates over Time

The results from the current investigation allow for the comparison of a number of factors which would influence corrosion rate: cover depth (20 mm and 40 mm), crack with (0.2 mm and 0.7 mm) and inclusion of cement extenders for each combination of cover and cracking. The general trend which is typical of the corrosion specimens is illustrated in Figure 5.31 for 20 mm cover and 0.2 mm crack widths. The PC samples showed a continuous increase in corrosion rate over the first 48 weeks before stabilizing. An examination of the resistivity values of the samples over the same period reveals a similar stability after approximately week 50 as shown in Figure 5.32. The resistivitiy of the PC samples reached a value of 16 kOhm.cm after 54 weeks after which there was little change. The FA samples were shown to have a substantially higher resistivity which reached a point of apparent relative stability after 26 weeks though some further increases were noted. Any further substantial shift in resistivity would be unlikely unless the environmental conditions changed.

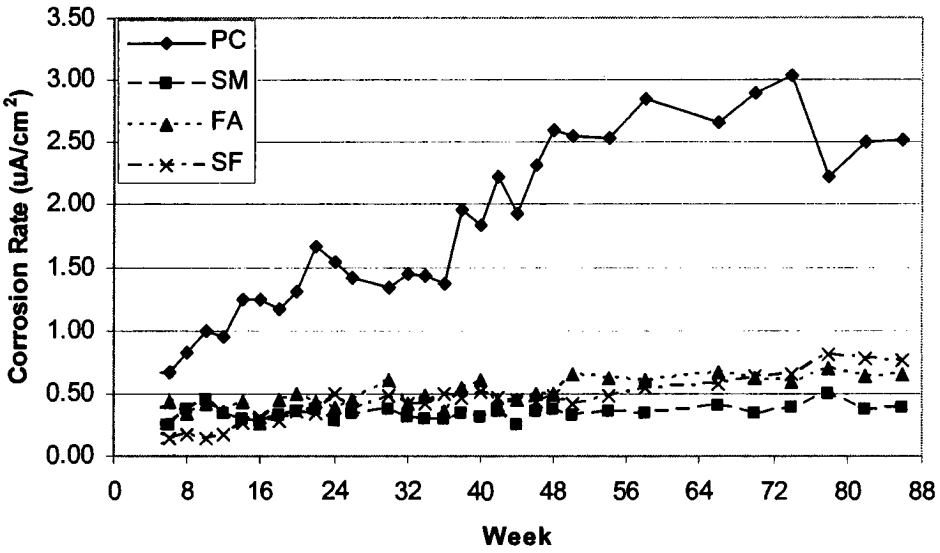

Fig 5.31: Corrosion rates for 20 mm cover and 0.2 mm crack width

The chloride concentration however is likely to continue to rise but this may not necessarily lead to a steady increase in corrosion rates. The resistivity of the concrete and availability of oxygen (coupled with the reduced solubility of oxygen in chloride contaminated solution) will place an effective ceiling on the observed corrosion rate. The relative stability of the corrosion rates after week 50 suggests that this is probably the maximum expected corrosion rate under the existing conditions. The relationship between chloride concentration and corrosion rates will be discussed in greater detail in section 5.10.4.

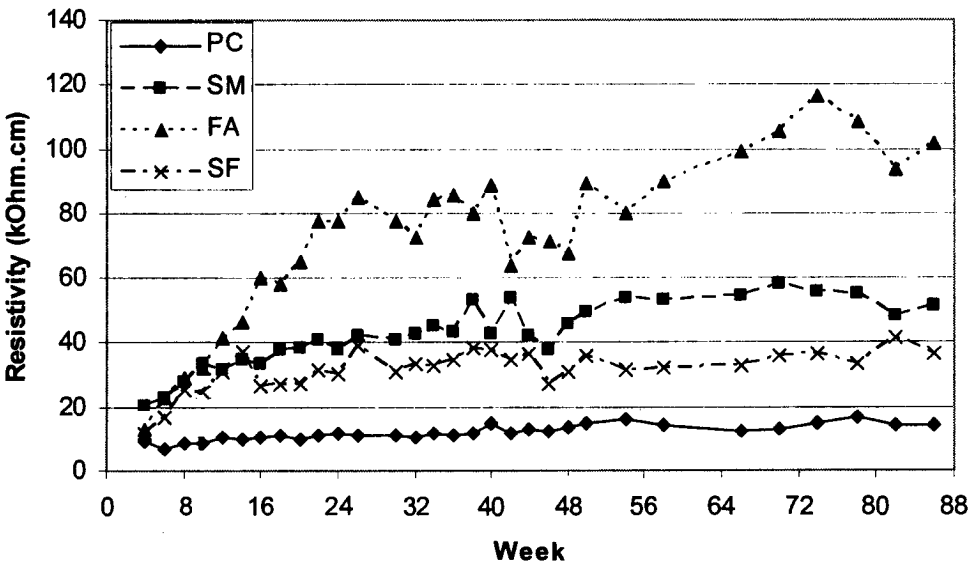

Fig 5.32: Average resistivity values for 20 mm cover 0.2 mm cracked samples

The build up of corrosion products around the steel however will cause expansive pressure and while most of these expansive pressures can probably be released through transverse cracking, corrosion further along the bar will likely lead to longitudinal cracking allowing greater ingress of oxygen and leading to accelerated corrosion at a future point. The effects of limiting the availability of oxygen and resistivity of the material are evident in the samples containing cement extenders which showed a much slower rise in corrosion rates and appeared reasonably stable even before 50 weeks. The relative increase in corrosion rates for PC, SM and FA from week 8 to week 86 are provided in Table 5.24.

Table 5.24: Corrosion rates ($\mu A/cm^2$) and change in rates between week 8 and 86 for 20 mm cover and 0.2 mm crack width.

Sample	*Week 8*	*Week 50*	*Week 86*	*% change (8 - 50)*	*% Change (50 - 86)*
PC	0.83	2.56	2.57	+ 210	+ 0.6
SM	0.37	0.32	0.39	- 13	+ 20
FA	0.34	0.64	0.65	+ 88	+ 1.4

The increase in corrosion rate of 210% for PC between week 8 and 50 is considerably higher than the 88% increase found in the FA samples. This general trend of increasing initial corrosion rate followed by a subsequent stabilizing of the rates is found in virtually all samples regardless of cover depth or crack width. The SM specimens showed a slight reduction in corrosion rate between week 8 and 50, but the rates remained stable over the study period such that at week 86 there was only 5% increase over the corrosion rate at week 8.

The 40 mm cover samples generally reached their maximum stable corrosion rate much earlier than those with 20 mm cover. The maximum corrosion rates for the 40 mm samples were lower than those with 20 mm cover depth and in the case of PC samples doubling the cover depth resulted in more than a 50% reduction in corrosion rate. The increase in cover would limit the availability of oxygen so that the stabilization of the corrosion rate at lower maximum value, compared to the 20 mm cover, was reached at a much earlier point, generally between week 16 and 20 as shown in Figure 5.33.

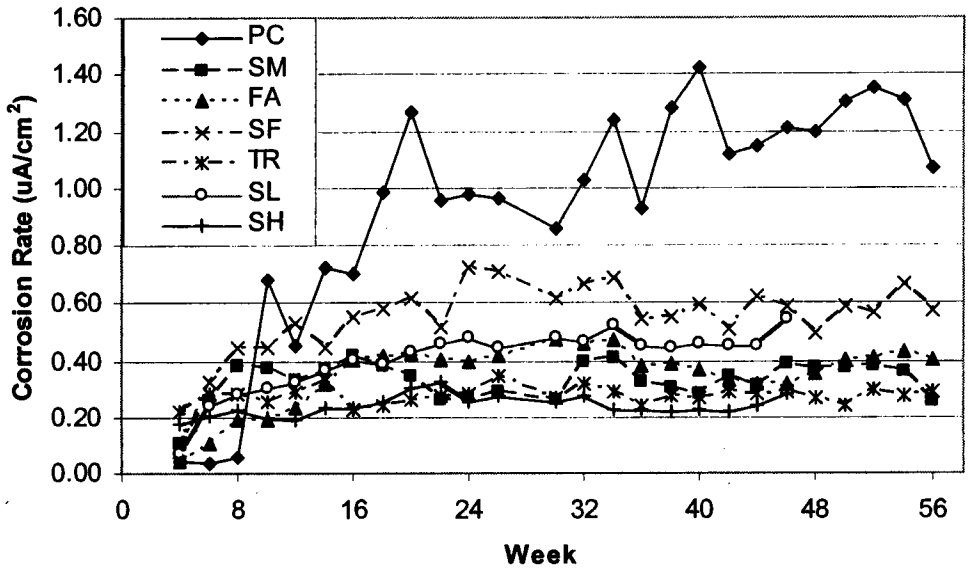

Fig 5.33: Corrosion rates for 40 mm cover and 0.2 mm crack samples

A more complete discussion on the factors influencing corrosion rates will be presented in the following sections The purpose of this discussion was to show that stability of the corrosion rates was obtained and that further substantial changes, within the scope of this investigation, are unlikely. The measured values for the stabilized corrosion rates, potentials and resistivities can therefore be used with reasonable confidence in the following sections.

5.10.4 Chloride Concentration and Corrosion Rates Stability

The stabilizing of corrosion rates as seen in the concrete samples was not observed in the aqueous phase work, section 4.6. Consider the aqueous FA sample in which corrosion initiated at a chloride concentration of 0.12 M and the corrosion rates continued to increase steadily up to the maximum observed chloride concentration of 0.6 M (a 5 time increase). The maximum chloride level measured for concrete SF, with 40 mm cover and 0.2 mm crack, was 1.7 % by mass of cement, which was only 3.3 times higher than the chloride threshold value. If the increase in chloride concentration resulted in a continual increase in corrosion rate, as suggested by the aqueous phase investigation, the stabilization of corrosion rates as observed in Figure 5.31 and 5.33, for the SF 40 mm cover 0.2 mm crack width should not have occurred. In the aqueous phase samples, oxygen was continually supplied and the resistivity of the solution was very low. Stability of corrosion rates in the concrete samples therefore

occurred well before the limiting effects of the chloride ions, due to the reduced solubility of oxygen in solution as discussed in section 2.8.

The chloride concentrations, expressed as % mass of cement, provided in Tables 5.25 and 5.26 indicate that all the specimens were well above their respective threshold values in the vicinity of the crack. The chloride concentrations were determined at two locations: 30 mm along the steel on either side of the crack, and from 30 mm to 90 mm from the crack at one side along the steel. The individual chloride concentrations for either the near crack or remote from crack sections therefore are determined over a 60 mm length of the steel bar.

There is a substantial difference in chloride concentration in the vicinity of the crack between those concretes made with PC and those which used a cement extender regardless of the crack width of cover depth. The chloride concentration at the crack for SM was less than half that of PC.

Table 5.25: Chloride concentrations (% mass of cement) for near crack and remote from crack section of samples taken at end of study period (week 86) for 20 mm cover depth

Sample	*Cl⁻ Threshold*	*Near crack*		*Remote from crack*		*Near crack increase over threshold* (x)	
		0.2 mm	*0.7 mm*	*0.2 mm*	*0.7 mm*	*0.2 mm*	*0.7 mm*
PC	0.53	4.36	4.15	1.78	1.73	8.2	7.8
SM	0.08	1.86	2.25	0.22	0.28	23.3	28.1
FA	0.36	1.91	2.05	0.25	0.21	5.3	5.7
SF	0.51	2.47	2.92	0.39	0.92	4.8	5.7

Table 5.26: Chloride concentrations (% mass of cement) for near crack and remote from crack section of samples taken at end of study period (week 56 for all expect SL and SH taken at week 46) for 40 mm cover depth

Sample	*Cl⁻ Threshold*	*Near crack*		*Remote from crack*		*Near crack increase over threshold* (x)	
		0.2 mm	*0.7 mm*	*0.2 mm*	*0.7 mm*	*0.2 mm*	*0.7 mm*
PC	0.53	2.63	3.14	0.35	0.36	5.0	5.9
SL	0.41	1.83	2.24	0.08	0.16	4.5	5.5
SM	0.08	1.24	1.81	0.01	0.02	15.5	22.6
SH	0.2	0.84	1.37	0.27	0.20	4.2	6.9
FA	0.36	1.38	1.70	0.02	0.03	3.8	4.7
SF	0.51	1.73	2.48	0.02	0.02	3.4	4.9
TR	0.08	1.06	1.40	0.15	0.09	13.3	17.5

The crack conditions were nominally the same for all samples so that the chloride concentration of the solution where the crack intersected the steel should have been very similar. The subsequent differences in chloride concentrations are then a function of the movement of chlorides through the concrete and along the bar. The resistance of the concrete made with cement extenders to the movement of chlorides is much greater than that of the PC samples. The differences in chloride concentrations between the various binder types are further enhanced when examining the concentrations away from the crack. The chloride concentration of PC for 20 mm cover and 0.2 mm crack was 2.3 times greater than SM at the crack, while away from the crack the difference in chloride concentrations increased to 8 times greater for the PC samples.

An increase in crack width generally resulted in an overall increase in the chloride concentration but the differences between the samples decreased. The 2.3 times increase in chloride concentration of PC over SM at a crack width of 0.2 mm reduced to a 1.8 times increase at a crack width of 0.7 mm. These results are typical of the samples as shown in Tables 5.25 and 5.26. The chloride concentrations away from the crack, at 20 mm cover, were generally greater than the measured chloride threshold concentrations. At the end of the study period, the samples were broken open and the steel examined. The corrosion products were limited to the vicinity of the crack, with no corrosion evident in the area from 30 to 90 mm away from the crack. The amount of corrosion product closely matched that of the measured corrosion rates by qualitative examination.

The presence of cracks resulted in the rapid ingress of chlorides to the steel in sufficient concentrations to initiate and sustain corrosion for both 20 and 40 mm covers. The chloride concentrations were measured at the end of the study period which was 86 weeks for the 20 mm samples and 56 weeks for the 40 mm cover samples (note that values for SL and SH were determined at week 46). A direct quantitative comparison of total chloride concentrations between the two cover depths is difficult. The difference in time between the two sets is 30 weeks and linearly proportional increase in chloride concentrations would result in higher concentrations for the 40 mm cover as shown in Table 5.27. Such a simplified adjustment would overestimate the actual chloride concentration. It is reasonable to say however that the differences between the chloride concentrations at 20 mm and 40 mm cover are small (less than 12%) and that the ingress of chloride concentration with time in the vicinity of the crack would likely be similar. The differences in chloride concentrations away from the crack however remain significant as the depth of concrete through which the chlorides must travel is considerable.

Table 5.27: Chloride concentrations (% mass of cement) at location of the crack for 0.2 mm crack width with 40 mm samples adjusted to 86 weeks

	0.2 Cracked		
Sample	*20 mm*	*40 mm*	*% difference*
PC	4.36	4.05	-7
SM	1.86	1.91	3
FA	1.91	2.13	12
SF	2.47	2.66	8

Assuming a similar development of chloride concentrations with time in the vicinity of the crack for cover depths of 20 and 40 mm, the much earlier stabilization of corrosion rates at a lower level for the 40 mm cover, as stated in section 5.10.3, implies that a maximum representative corrosion rate was reached at a lower chloride concentration for the 40 mm cover samples compared to the 20 mm. The continuing increase in chloride concentration of the 40 mm samples did not result in the same increase in corrosion rate as experienced by the 20 mm samples for a given chloride concentration.

The two general effects of limiting oxygen to the cathode and resistivity of the concrete matrix are responsible for the observed stabilization, as previously shown in Figure 5.31 and Figure 5.33, and result in a representative corrosion rate. The long term active corrosion rates therefore are not dependant upon the chloride concentration in cracked concrete. Where chloride concentration may be a longer term issue is in its tendency to reduce the resistivity of the concrete, but these effects were not explicitly noted during the time frame of this investigation and further research would be required to determine more long term results. Based on the observations of this investigation it is therefore possible to determine a characteristic corrosion rate for each concrete matrix, including the various cement extenders, which will be a function of limiting oxygen ingress and resistance of the material to ionic movement in addition to the chemistry of the pore solution as demonstrated in the aqueous phase work and the role of slag in the passivation of the steel in concrete.

5.10.5 Influence of Crack Width on Corrosion Rates

The corrosion rate of steel in concrete was shown to increase with size of the surface crack from 0.2 mm to 0.7 mm. It was established in section 5.10.1 that the induced bar slip had a minor (increase of 0.12 $\mu A/cm^2$) effect on the corrosion rate with the slipped bar specimens having a corrosion rate 0.12 $\mu A/cm^2$ higher than the unslipped specimens. It is

reasonable that any difference in corrosion rate associated with the slip required to induce a 0.2 mm crack compared to a 0.7 mm crack would be even smaller. The difference in corrosion rate between the 0.2 mm and 0.7 mm cracks is likely to be primarily a function of the size of the crack rather than the slip required to produce the crack. A comparison of corrosion rates for 0.2 mm and 0.7 mm cracks are provided in Table 5.28 and illustrated in Figure 5.34 for 20 mm cover. The corrosion rates are averages from 32 to 46 weeks for SL and SH and from 32 to 56 weeks for the remainder for the 40 mm cover samples and 58 to 86 weeks for the 20 mm cover samples.

Table 5.28 Influence of crack width on corrosion rate ($\mu A/cm^2$)

40 mm cover			
	0.2 mm	*0.7 mm*	*Percentage change*
PC	1.20	1.48	+ 23
SL	0.47	0.55	+ 17
SM	0.35	0.53	+ 51
SH	0.24	0.34	+ 42
FA	0.39	0.50	+ 28
SF	0.59	1.03	+ 75
TR	0.28	0.42	+ 50
20 mm cover			
	0.2 mm	*0.7 mm*	*Percentage change*
PC	2.65	3.23	+ 22
SM	0.39	0.51	+ 31
FA	0.64	0.71	+ 11
SF	0.67	1.12	+ 67

The increase in crack width has three primary effects: firstly the larger cracks allow for the easier movement of chloride solution to the steel and provide larger reservoirs of chlorides after the solution is initially removed and until the crack has an opportunity to dry; secondly the larger cracks provide a greater area of exposed steel; finally and perhaps most importantly, the larger crack widths prevent autogenous healing of the concrete or the corrosion products from sealing the crack and thus limiting the ingress of chlorides to the steel.

The corrosion rates of steel did increase with crack width but these increases were generally minor compared to the change associated with cover or use of cement extenders as shown in Figure 5.34. The use of any of the cement extenders results in at least a 50% reduction in corrosion rate compared to PC for the 40 mm samples and a 75% reduction for the 20 mm cover samples at 0.2 mm crack width. In both the 20 mm and 40 mm cover

specimens, SF was shown to have the greatest increase in corrosion rate from a crack width of 0.2 mm to 0.7 mm. SF specimens complete their hydration process very quickly and there is very little subsequent development of the microstructure compared to PC or the other cement extenders. Since the cracks were induced at 14 days any repair to the cracks or the steel concrete interface which may have occurred with other binder types would have been less likely to occur in the SF specimens.

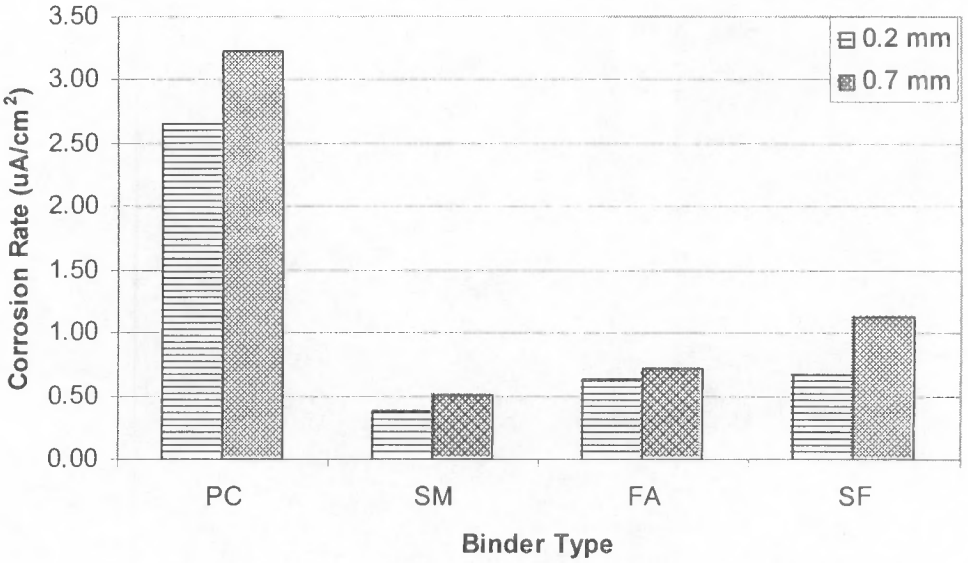

Fig 5.34: Average corrosion rates for 20 mm cover with 0.2 and 0.7 mm crack widths

The subsequent discussion on corrosion rates will use an average value taken from the 0.2 mm and 0.7 mm crack widths. In practice it is very difficult to accurately quantify a crack width and these widths can change substantially over the length of crack. The use of single corrosion rate representative of the cracks ranging between 0.2 mm and 0.7 mm is more reasonable for the purposes of comparing the influence of cement extenders and cover than trying to define unique rates for each crack width.

5.10.6 Corrosion Rates, Resistivities and Cement Extenders

The effect of the inclusion of cement extenders on chloride-induced corrosion of steel in concrete is significant and in the case of slag somewhat surprising. The passivation study and aqueous phase work suggested that slag-bearing materials would perform poorly, on the basis of the elevated corrosion rates compared to the PC samples. The durability index values however generally showed improved characteristics of slag-containing samples compared to PC, with exception of SH, though SH did have an improved chloride conductivity value. The

effects of the inclusion of cement extenders can be seen in Figures 5.35 and 5.36, presented as the average corrosion rates of 0.2 and 0.7 mm cracked specimens at a cover depth of 40 mm, from week 32 to the end of the study period (week 46 for SL and SH and week 56 for the remainder), and for a cover depth of 20 mm from week 58 to 86.

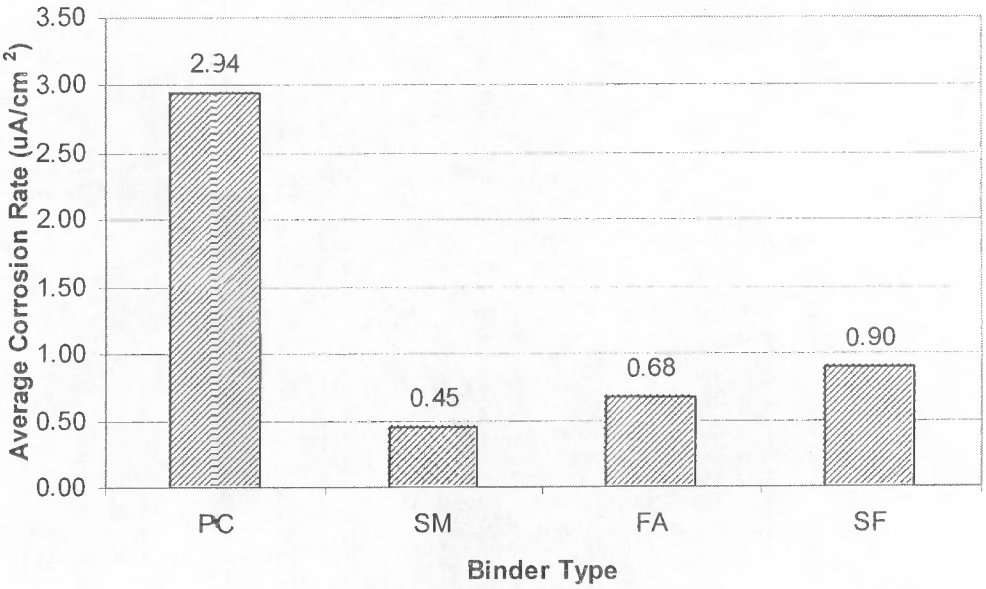

Fig 5.35: Average corrosion rates for specimens with 0.2 mm and 0.7 mm crack widths at 20 mm cover from week 58 to 86

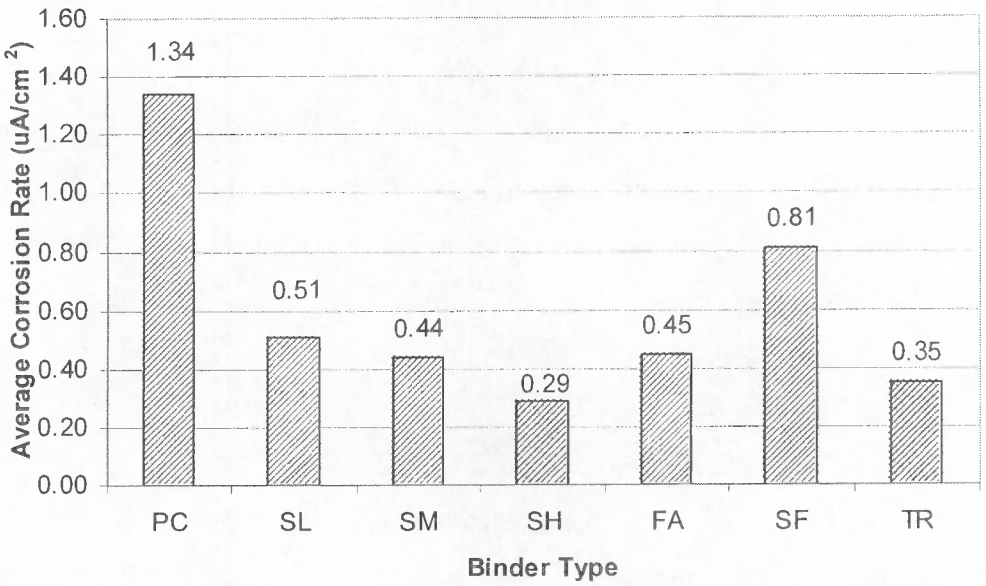

Fig 5.36: Average corrosion rates for specimens with 0.2 mm and 0.7 mm crack widths at 40 mm cover from week 32 to 56 (32 to 46 for SL and SH)

The corrosion rates reveal that instead of the slag concretes performing poorly they significantly reduced the corrosion rate in all cases. Surprisingly, SH which had the worst durability indexes (except for chloride conductivity) displayed the lowest average corrosion rate, one fifth that of PC. SL, SM, FA and TR, for 40 mm cover, all displayed active corrosion rates in the range of 0.35 to 0.51 $\mu A/cm^2$, which is less than half that of PC (1.34 $\mu A/cm^2$). The inclusion of SF resulted in a reduction in the corrosion rate of approximately 40%. The relative performance of the various binder types compared to PC is provided in Table 5.29.

Table 5.29: Actual and relative corrosion rate ($\mu A/cm^2$) compared to PC various for binder types

40 mm cover	*Rate*	*Percentage of PC*
PC	1.34	100%
SL	0.51	38%
SM	0.44	33%
SH	0.29	22%
FA	0.45	33%
SF	0.81	60%
TR	0.35	26%

20 mm cover	*Rate*	*Percentage of PC*
PC	2.94	100%
SM	0.45	15%
FA	0.68	23%
SF	0.90	31%

The results from the passivation and aqueous phase study are both indicative of the influences of the binders on the chemical aspects of the corrosion process. It was shown in Chapter 4 and section 5.9 that those samples containing appreciable levels of sulphides and thiosulphate (greater than 50 mg/l of total sulphur) had elevated corrosion rates compared to those with very low levels (FA, SF and PC). A linear relationship between corrosion rate and sulphide concentration was also shown in Figure 5.22. The pore solution chemistry is therefore of importance in the consideration of chloride threshold concentrations and passive corrosion rates but appears to offer little insight when viewed in the context of active corrosion. Once active corrosion in concrete begins, the corrosion rates increase beyond those which can be sustained in the absence of chlorides. The system moves from a situation where

it is either controlled or previously influenced by the presence of sulphides to one where the chloride interaction is dominant. In the aqueous phase investigation, there were no physical or resistivity limits to the phenomena. The corrosion of steel in concrete is dependent upon not only the chemical characteristics of the pore solution and ingress of chlorides but also the resistivity of the concrete which limits the ionic flow between the anode and cathode, and the availability of oxygen. The corrosion rate of the steel under passive conditions was sufficiently low as to not be governed by resistivity, or oxygen availability considerations. At elevated active corrosion rates these factors now become dominant.

The resistivity of the concrete was found to increase with the use of cement extenders. Any of the cement extenders resulted in at least a doubling of the resistivity compared to PC as shown in Figure 5.37. SH, FA and TR all had concrete resistivity values in excess of 100 kOhm.cm. It is interesting to note that the resistivities for SM and SF were 63 and 44 kOhm.cm respectively, yet when combined to form the ternary blend the resulting resistivity was significantly higher (112 kOhm.cm). The presence of SF would provide sites for the nucleation of the pozzolanic reaction products thus reducing the permeability of the concrete. The subsequent reactions associated with the hydration slag would be confined to a micro structure with an already reduced permeability and thus the remaining hydration products would significantly reduce the overall permeability of the concrete. The micro structure of the concrete was not specifically studied in the present investigation and would need to be confirmed by further research.

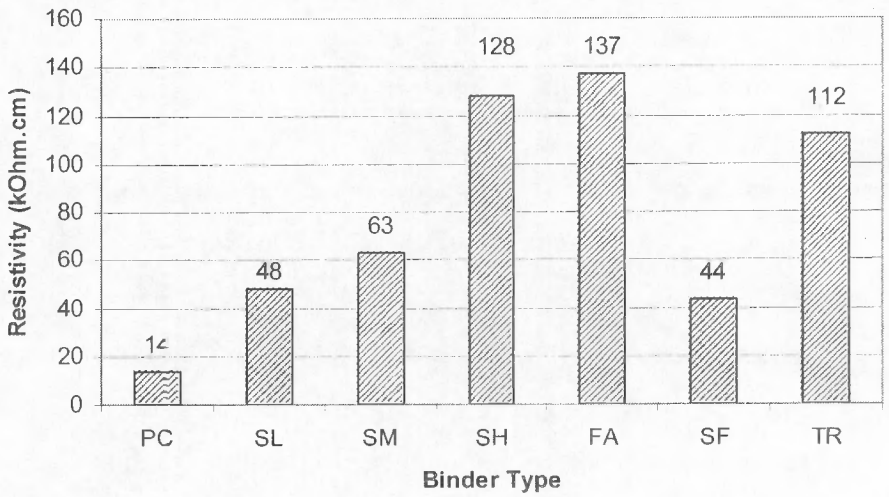

Fig 5.37: Average resistivity values for 40 mm cover samples from week 32 to 56 (32 to 46 for SL and SH)

The elevated resistivity of the FA and TR concrete would be expected from the durability index values which showed improved material characteristics with respect to PC for TR and FA. The durability index values however did not entirely predict the performance of all the binder types. Table 5.30 shows the relative resistivity values together with the relative performance of durability index values compared to PC. PC is taken to be 1 with the other values ratios or fractions. The relative chloride conductivity performance (the inverse of chloride conductivity ratios) of SL for instance is 2.2 which indicates it had a chloride conductivity value 0.45 times lower than PC. The measured resistivity values over time for all samples can be found in Appendix 5D.4.

Table 5.30: Relative material performance characteristics of binder types, based on 90 day durability index values, and average resistivity values

Mix Design	*Resistivity*	*Water Sorptivity*	*Oxygen perm. coef.*	*Chloride Conductivity*
PC	1.0	1.0	1.0	1.0
SL	3.4	1.1	1.3	2.2
SM	4.5	1.3	1.1	3.3
SH	9.1	1.0	0.2	1.4
FA	9.8	1.4	1.8	3.0
SF	3.1	1.3	1.0	1.4
TR	8.0	1.6	1.1	4.2

The inverse of the chloride conductivity values should be an indication of resistivity of the concrete yet there is a substantial deviation with respect to FA, SF, TR and in particular SH. The chloride conductivity values of SH would indicate a resistivity similar to that of SF, not second highest as was observed. The very high resistivity values and thus low corrosion rate may be partially explained by the open pore structure. As resistivity measurements were taken at least one day after drying, the open pore structure of the SH would allow more rapid drying thereby increasing the measured resistance of the concrete. This idea of an open pore structure is further validated by the elevated chloride concentrations found away from the crack, second only to PC as previously provided in Table 5.26. In the case of SH the high resistivity of the concrete is not achieved through densification of the pore structure but rather through a more permeable one which allows for rapid drying. The low measured corrosion rates of SH were corroborated by a qualitative visual examination of the steel at the end of the examination period for the 20 mm and 40 mm cover cracked samples.

An examination of the resistivity values will reveal a general correlation between resistivity and corrosion rate. The correlation is not entirely consistent as the highest average resistivity value of 137 kOhm.cm was found in FA which had a higher corrosion rate than SH, TR and similar to SM which had resistivity approximately half that of FA. The general inversely proportional relationship between corrosion rate and concrete resistivity can be seen in Figure 5.38.

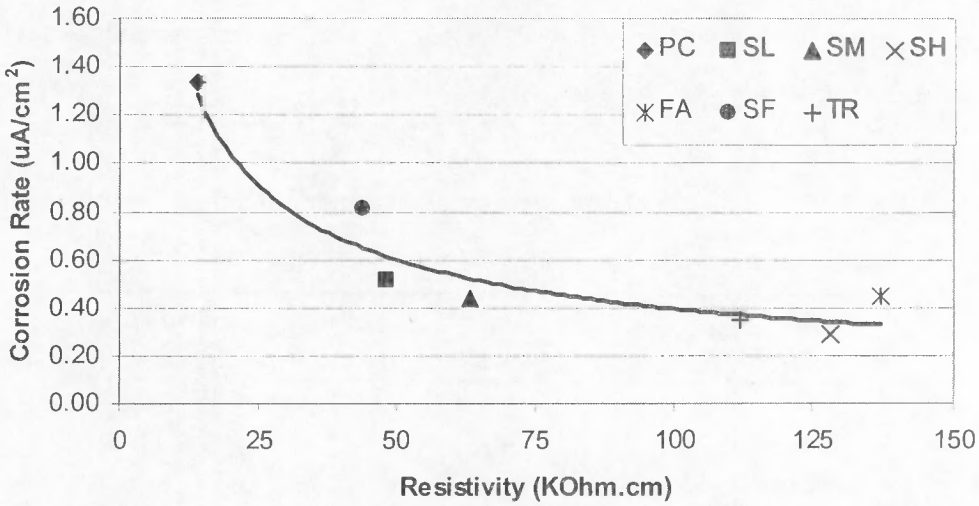

Fig 5.38: Relationship between average corrosion rate ($\mu A/cm^2$) of 0.2 mm and 0.7 mm cracked specimens with cover depths of 40 mm and resistivity

It is apparent from Figure 5.38 that as the resistivity of the concrete increased the average measured corrosion rate decreased. The response of the corrosion rate to resistivity is clearly non-linear such that a small initial increase in resistivity resulted in a significant decrease in corrosion rate whereas a subsequent increase of the same magnitude has a smaller impact upon the reduction in corrosion rate.

The resistivity values alone are not sufficient to account for the differences in corrosion rates between the various specimens. FA had the highest resistivity value yet SM had a resistivity value half that of FA with the same corrosion rate. With respect to the durability indexes, FA was shown to have the lowest permeability to oxygen, the second lowest water sorptivity, and chloride conductivity values similar to SM and TR and significantly better than SH yet displayed higher corrosion rates. The correlation between corrosion rates and the measured durability index, pore solution composition and resistivity values will be discussed in greater detail in Chapter 6. A more comprehensive evaluation of the relationship among the

various factors will be used to form a predictive corrosion rate model based on the results presented in this chapter.

5.10.7 Effects of Cover on Corrosion Rates

The effects of cover on the corrosion rate of steel in concrete are similar to those of crack width. An increase in cover from 20 mm to 40 mm was found to significantly reduce the corrosion rate in PC samples for both 0.2 and 0.7 mm cracks widths as shown in Figure 5.39.

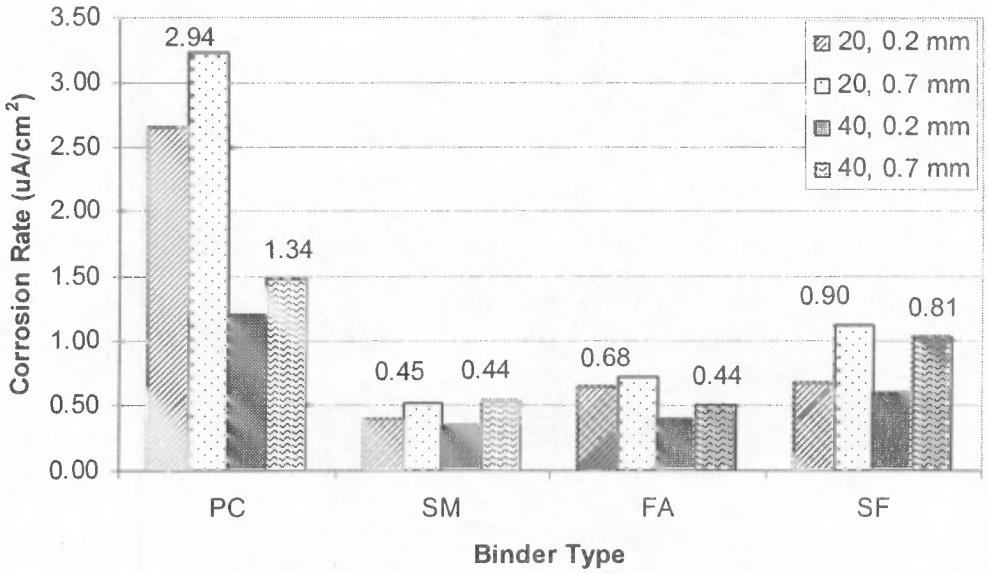

Fig 5.39: Effect of cover on corrosion rates

Note: the values to the left are average corrosion rates for 0.2 and 0.7 mm crack widths of the 20 mm cover depths while the values to the right are averages for the 40 mm cover depth for each set of specimens

The same dramatic reduction in corrosion rate observed in PC was not found in the other samples. The increase in cover had little effect on the corrosion rate of the concrete containing cement extenders. The increase in cover would have reduced the availability of oxygen by increasing the depth through which the oxygen must travel, in addition to delaying the drying action at the depth of the steel. All the samples would have experienced a similar effect but the PC samples would be particularly affected due to their elevated corrosion rates and thus higher oxygen requirement. It is likely that the concrete containing cement extenders already

had suppressed levels of oxygen or a sufficiently high resistivity that a further increase in cover had little effect.

There was little real difference in measured resistivity between the 20 mm and 40 mm cover specimens as shown in Table 5.31 compared to the range of possible values for the various binder types. The 20 mm cover depths generally had lower observed resistivity values which may partially be explained by the closer proximity of steel rebar to the probes used for measuring the samples. Again the differences in resistivity values between the cover depths are much smaller than those which are binder dependent. There would be some differences however, in resistivity of the concrete at the depth of the steel due to different drying environments as the 40 mm cover specimens would take longer to dry than the 20 mm cover specimens. Additionally, the effect of improved curing at greater cover depths would result in a less permeable material and somewhat higher resistivity ceteris paribus. The presence of the crack however would accelerate the drying process in the vicinity of the crack and tend to minimize the differences directly associated with cover.

Table 5.31: Average resistivity (kOhm.cm) values for 20 mm and 40 mm cover depths specimens

Binder Type	*20 mm*	*40 mm*
PC	16	14
SM	53	63
FA	90	137
SF	36	44

The high resistivity values associated with the use of cement extenders therefore tends to control the maximum observed corrosion rate to a depth of 40 mm cover as measured in this investigation. If greater cover depths of steel were investigated for all the binder types there may come a point where the availability of oxygen controls the corrosion rate. This principle is demonstrated in the example shown in Figure 5.40.

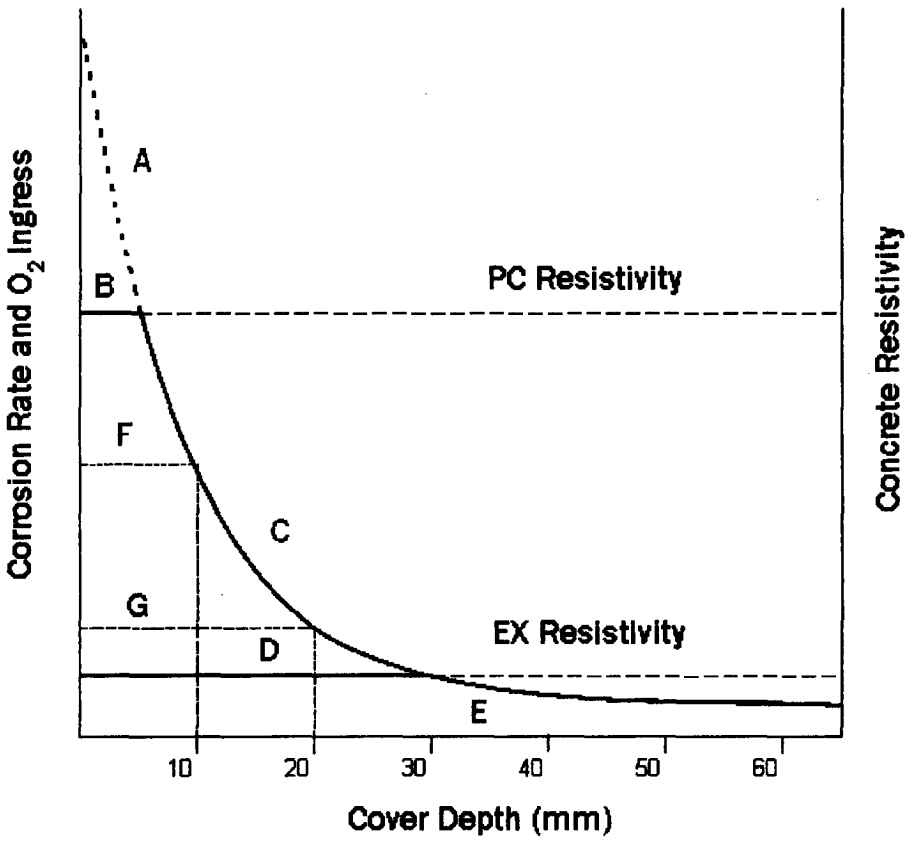

Fig 5.40: Relationship between corrosion rate, O_2 and resistivity

Fig 5.40 illustrates a general example of the interaction between corrosion rate, resistivity and availability of oxygen. The controlling nature of oxygen on the corrosion rate was presented in chapter 2 and section 5.4.2 and well documented by Raupach (1996). In the current example the availability of oxygen at a given cover depth is defined by curve ACE. The same curve is also used as a representation of the corrosion rate since oxygen is required for the cathodic reaction ($H_2O + \frac{1}{2}O_2 + 2e^- \rightarrow 2OH^-$). The resistivity of the concrete however results in a maximum possible corrosion rate even if there is sufficient oxygen to support a higher reaction rate. The resistivity controls are shown as horizontal lines PC and EX, where PC would representative of the OPC concrete and EX of the concrete produced with cement extenders. The lines would likely be sloped somewhat to account for the variation in resistivity with cover depth. More research would be required to accurately define the slope of these curves, but for the purposes of the current discussion a horizontal resistivity line is sufficient. Consider a sample with a resistivity given by PC. The maximum possible corrosion rate curve is given by the combined line BCE. At a cover depth of 10 mm the

hypothetical corrosion rate (oxygen availability) is given by line F and similarly the corrosion rate at a depth of 20 mm is given by line G. If another sample EX is considered, the maximum corrosion rate curve is given by the combined line DE. At a cover depth of 10 mm the corrosion rate is given as D. At a depth of 20 mm the corrosion rate is again controlled by the resistivity, and D is the resultant. Only at depths greater than 30 mm does it revert to oxygen controlled. The same oxygen availability curve was used in this example for both types of concrete. Macphee and Cao (1993) have suggested that the cathodic curve would vary for slag concretes so as to reduce the oxygen concentration at each depth. The inclusion of any of the cement extenders would have a similar effect of shifting the oxygen availability curve and hence change the corrosion rates.

It is important to emphasize that no direct measurements of oxygen were made at the depth of the steel and the supposition of the limiting effect of oxygen are based on measured corrosion rates, resistivity values and the assumption that the cathodic process is based purely on the reduction of oxygen as provided in chapter 2 in the discussion on electrochemical corrosion.

The increase in cover, while dramatic and necessary for the reduction of corrosion rates in PC samples, does not produce the same benefit in concretes made with cement extenders. A concrete structure with a 20 mm cover depth, but containing FA, has a corrosion rate half that of PC with twice the cover. The inclusion of cement extenders is therefore essential for minimizing corrosion damage once active corrosion has initiated.

5.11 Chapter Summary

The influence of cement extenders on the corrosion characteristics of steel in concrete has been investigated in this chapter. The inclusion of cement extenders generally results in a lowering of the chloride threshold concentration, though SF which has one of the lowest hydroxide concentrations displayed threshold levels comparable to PC. The inclusion of slag in samples SM, SH and TR resulted in chloride thresholds approximately $1/3^{rd}$ that of PC. The chloride threshold for SL however was only moderately less than PC. The relative performance of the materials can be ranked from highest threshold to lowest in the order: PC > SF > SL > FA > SH > TR > SM with chloride threshold concentrations provided in Table 5.32.

Table 5.32: Chloride threshold values expressed as percentage chloride by mass of cement (binder)

Binder Type	*Concrete*
PC	0.53
SL	0.41
SM	0.08
SH	0.20
FA	0.36
SF	0.51
TR	0.08
Average	0.31

The relatively poor performance of the cement extenders is attributed to the reduction in alkalinity and the presence of sulphide ions in the slag bearing materials. A similar pattern of reduced performance with respect to chloride threshold concentration was also observed in the aqueous phase investigation though the SF pore solution sample showed a chloride threshold concentration ¼ that of PC which was more consistent with its hydroxide concentration. The relatively good performance of SF in the concrete and mortar samples may be a result of a denser pore structure in the interfacial transition zone between the bulk cement past and the steel reinforcing thus limiting the availability of steel not strongly bonded to the products of hydration.

The mortar specimens were shown to generally have improved threshold values compared to the concrete samples. Greater uniformity of the mix and fewer voids associated with the presence of large aggregate may account for the differences. It should also be noted that the cover of the mortar samples was 15 mm compared to the 40 mm of the concrete samples. The difference in chloride threshold concentrations between the mortar and concrete specimens implies, that while mortar specimens may be useful to give an indication of relative performance of binder type or mix design, they should not be used an indication of the chloride threshold concentration of steel in concrete.

Corrosion rates prior to activation by chlorides revealed somewhat similar performance trends with the inclusion of slag resulting in elevated passive corrosion rates and very negative potentials. The corrosion rates of the slag bearing materials were higher than the PC or other extended samples despite generally having higher resitivity values. The inclusion of FA and SF results in a more refined pore structure as shown by the durability indices and coupled with higher resistivity values had lower passive corrosion rates than PC. The average

corrosion rates under passive conditions can be ranked from lowest to highest: FA < SF < PC < SH < TR < SL & SM as indicated by Table 5.33.

Table 5.33: Average corrosion rates over the first 16 weeks

Binder type	*Corrosion Rate ($\mu A/cm^2$)*
PC	0.045
SL	0.086
SM	0.086
SH	0.063
FA	0.033
SF	0.035
TR	0.064

The higher corrosion rates associated with slag bearing materials is again attributed to the presence of sulphides, and thiosulphate, the effects of which extend well beyond the first weeks and even after the sulphides have been oxidized as demonstrated in the aqueous phase work. The higher corrosion rates in the slag bearing specimens, despite the elevated resistivities of the concrete, demonstrates that the corrosion rates associated with passive levels of corrosion were not controlled by the resistance of the concrete and that the chemical nature of the pore solution and the interaction with the rebar were more important factors under passive conditions.

The very negative corrosion potentials of the slag bearing materials, SL and SH, -546 and -593 mV respectively at age 14 days, where shown to rapidly move to more noble potentials similar to PC, FA or SF once the rebar was exposed to the atmosphere by means of cracking. The rapid change in potential was attributed to oxidation of the sulphides in the region of the steel.

The generally negative trend of incorporating slags was not observed under active corrosion conditions. SH which by all accounts should not perform well was shown to have the lowest average corrosion rate. The inclusion of any of the cement extenders resulted in at least a 40% reduction in corrosion rate compared to PC, with 5 out of 6 of the extender mix designs showing more than 60% reduction in corrosion rates. The lower corrosion rates are not simply a function of one variable such as resistivity, although this will have a major impact. The reduction in corrosion rates is also dependant upon factors such as limiting the availability of oxygen. The chemical indicators such as pores solution composition, chloride threshold concentration and even passive corrosion rates appear to offer little guidance on

predicting the corrosion rate after initiation. The nature of the corrosion process has therefore changed from one dominated by the chemical properties under passive conditions to one in which the physical properties of the concrete surrounding the rebar are of paramount importance. That is not to suggest that the sulphides, chlorides or hydroxyl ions do not have an impact but rather once chloride have reached the steel in sufficient concentration the resistivity of the material and control of oxygen ingress are more significant. Average corrosion rates for 0.2 mm and 0.7 mm cracked concrete with steel at cover depths of 20 mm and 40 mm are provided in Table 5.34.

Table 5.34: Average corrosion rates ($\mu A/cm^2$) for 0.2 mm and 0.7 mm crack widths at covers of 20 mm and 40 mm

40 mm cover		
Binder Type	*0.2 mm*	*0.7 mm*
PC	1.20	1.48
SL	0.47	0.55
SM	0.35	0.53
SH	0.24	0.34
FA	0.39	0.50
SF	0.59	1.03
TR	0.28	0.42
20 mm cover		
Binder Type	*0.2 mm*	*0.7 mm*
PC	2.65	3.23
SM	0.39	0.51
FA	0.64	0.71
SF	0.67	1.12

The presentation of a single corrosion rate for the particular binder types and crack widths is reasonable given the stability of the corrosion rates with time despite constantly increasing chloride concentrations. The stated values provide a reasonable estimate of the likely maximum corrosion rate experienced by the various binder types under the conditions of transverse cracking. Subsequent longitudinal cracking causing by expansive pressures of the corrosion products would likely increase the observed rates but were not part of this investigation.

An increase in cover depth from 20 to 40 mm was shown to have substantial benefits to PC, reducing the corrosion rate by more than half. The same benefits of increased cover were not observed in the other samples. The extended concretes already had reduced corrosion

rates due to lower permeability and higher resistivities. The corrosion rates of the concrete made with cement extenders were already at their maximum given the resistivity of the concrete and further limitations on oxygen availability due to increased cover depth had little impact. The inclusion of any of the cement extenders had a much greater effect than doubling the cover.

Increase in crack width was also shown to elevate the corrosion rate in all cases. An increase in crack width from 0.2 mm and 0.7 mm resulted in an increase in corrosion rate between 11 and 75%. While an increase of 75% is significant for that particular specimen, the change in crack width had little effect on the relative order of performance and did not significantly distort the results. It is again interesting to note that SF showed the greatest variation in corrosion rate associated with an increase in crack width. The rapid hydration of SF may have limited subsequent healing of the steel-concrete interface once the crack was obtained through slipping of the reinforcing steel. Damage to the interface would not have been repaired to the same extent as that of the slag or FA specimens which require longer periods to reach 'full' hydration. The comparison of slipped mild steel round bar and unslipped bar in uncracked PC concrete however revealed a difference in average corrosion rate, between week 66 and 86, of less than 0.12 $\mu A/cm^2$ which suggests that slipping of the bar had a noticeable though small effect. The presence of cement extenders had a much greater effect than crack width itself.

The following chapter will use the information derived from the study of corrosion characteristics to present a preliminary model which can be used to assist in the evaluation of service life of reinforced concrete made with cement extenders. Durability index values will also be employed in a further attempt to quantify material such that the model would be applicable to other mix designs not specifically studied during this investigation.

5.12 Appendices

5A.1 Sand grading analysis

5B.1 Oxygen Permeability

5B.2 Water Sorptivity

5B.3 Chloride Conductivity

5B.4 Durability Index Test Results

5C.1 Chloride Threshold Values

5C.2 Effects of Bar Slipping on Chloride Movement

5D.1 Corrosion Characteristics for Mix Design Series II Passivation Study

5D.2 Corrosion Potentials for Cracked Concrete Study

5D.3 Corrosion Rates for Cracked Concrete Study

5D.4 Resistivty Values for Cracked Concrete Study

5A Materials Characterization

5A.1 Sand Grading Analysis

Trial 1 *Sieve Size*	*Mass Retained (g)*	*% Retained*	*Cumulative % Retained*
4750	0.0	0	0
2360	5.1	1	1
1180	71.5	14	15
600	86.3	17	33
300	99.1	20	52
150	176.4	35	88
150+	61.8	12	100
Total	500.2		189
FM			***1.89***

Trial 2 *Sieve Size*	*Mass Retained (g)*	*% Retained*	*Cumulative % Retained*
4750	0.0	0	0
2360	5.6	1	1
1180	64.8	13	14
600	82.0	16	30
300	102.0	20	51
150	176.5	35	86
150+	68.9	14	100
Total	499.8		183
FM			***1.83***

Trial 3 *Sieve Size*	*Mass Retained (g)*	*% Retained*	*Cumulative % Retained*
4750	0.0	0	0
2360	5.3	1	1
1180	72.4	14	16
600	85.4	17	33
300	99.5	20	53
150	167.5	33	86
150+	70.0	14	100
Total	500.1		188
FM			***1.88***

Average FM	***1.86***

5B Summary of Durability Index Tests

5B.1 Oxygen Permeability

Permeability is a measure of the ability of concrete to transfer a fluid through the pore structure of the material under an applied pressure while the pores are saturated with that particular fluid. The principle behind most permeability measurements revolves around an attempt to determine the Darcy coefficient of permeability. The falling head permeameter, developed at the University of Witwatersrand, applies an initial pressure to one side of a concrete specimen with the other side at normal atmospheric pressure and then measures the decrease in pressure with time as permeation occurs. From the slope of the log of pressure head versus time the permeability coefficient may be determined as follows (Alexander et al 1999[1]):

$$k = \frac{\omega V g d}{R A \theta t} \ln \frac{P_o}{p} \qquad \ldots 5B.1$$

Where:

- k - coefficient of permeability (m/s)
- ω - molecular mass of permeating gas (kg/mol)
- V - volume of the pressure cylinder (m^3)
- g - acceleration due to gravity (m/s^2)
- d - sample thickness (m)
- R - universal gas constant (Nm/Kmol)
- A - cross sectional area of specimen (m^2)
- θ - absolute temperature (K)
- t - time (s)
- P_o - pressure at start of test (kPa)
- P - pressure at time t (kPa)

The coefficient of permeability is then transformed into the oxygen permeability index (OPI) by taking the negative log.

$$OPI = -\log_{10} k \qquad \ldots 5B.2$$

The oxygen permeability test therefore provides a rapid estimation of the resistance of a particular concrete to the transport of gas. The values obtained for the various concretes can provide a basis of comparison and a means of estimating the degree of influence on the microstructure of the cement extenders under consideration. The movement of oxygen

through concrete is also one of the fundamental parameters governing the rate of corrosion and is therefore essential in any attempt to meaningfully study the corrosion of steel in concrete.

5B.2 Water Sorptivity

Another useful measure of the pore structure of concrete, including dimensional effects, is the degree to which the material absorbs water. Absorption is a process where fluid is drawn into a porous unsaturated material by capillary suction. Capillary suction is significantly dependant upon the orientation and connectivity of the pores. Capillary suction is significant near the surface of the concrete but tend to decrease with depth thus. The test therefore is a useful measure of the near surface characteristics of the material (Alexander et al. 1999[1]).

Concrete samples of 68 mm diameter and 25 mm thickness are initially preconditioned at 50°C to ensure uniform moisture content. The sides of the specimens are also sealed to ensure unidirectional movement. The concrete samples are then placed in a few millimeters of water and weighed at regular intervals to determine the mass of water absorbed. Prior to saturation the test is stopped and the samples are vacuum saturated to determine the porosity (Alexander et al. 1999[1]). The sorptivity, S, of the concrete is taken from the slope of the straight line of mass of water absorbed versus the square root of time,

$$S = \frac{\Delta M_t}{t^{1/2}} \cdot \frac{d}{M_{sat} - M_o} \qquad \ldots 5B.3$$

Where:

ΔM_t - change in mass with respect to the dry mass (g)

M_{sat} - saturated mass of concrete (g)

M_o - dry mass of concrete (g)

d - sample thickness (mm)

t - period of absorption (hr)

5B.3 Chloride Conductivity

The diffusion of gas, liquids or ions through concrete under a concentration gradient is perhaps one of the most useful individual pieces of information pertaining to the structure of the material under investigation. Chlorides in particular represent the single biggest threat to the long term durability of concrete under numerous environmental conditions and their movement is often by means of diffusion as the steel is normally at depths greater than would

be substantially affected by capillary suction. Diffusion rates in concrete are dependant upon temperature, moisture content, type of diffusant, and inherent diffusivity of the material with further complications arising from chemical interactions (chloride binding), defects such as cracks and possible presence of stray currents (Alexander et al 1999[1]).

The diffusion coefficient D, as previously noted, is equal to the ionic flux under a unit concentration gradient. Each ion has a characteristic diffusivity at a constant temperature and low concentration but the presence of other ions and higher concentrations affect this value. Conduction is the movement of ions under an electrical field and is related to diffusion through Einstein's relationship (Streicher 1997):

$$u = zF\frac{D}{RT} \qquad \ldots 5B.4$$

Where

μ - mobility of an ion.

z - charge of ion

F - Faraday's constant

D - diffusion of ion

R - gas constant

T - absolute temperature

There is a further relationship between conductance and diffusivity incorporating transport coefficients through the material and in water, which holds at high concentrations and is less sensitive to many of the non-ideal effects (Streicher 1997). The diffusion coefficient therefore can be calculated from a simple conductance test.

The test as developed by Streicher involves measuring the ionic flux (current) across a sample due to a 10 V potential difference as shown in Figure 5B.1. The concrete disc sample is oven dried at 50°C followed by vacuum saturation in a 5M NaCl solution for 24 hours prior to testing.

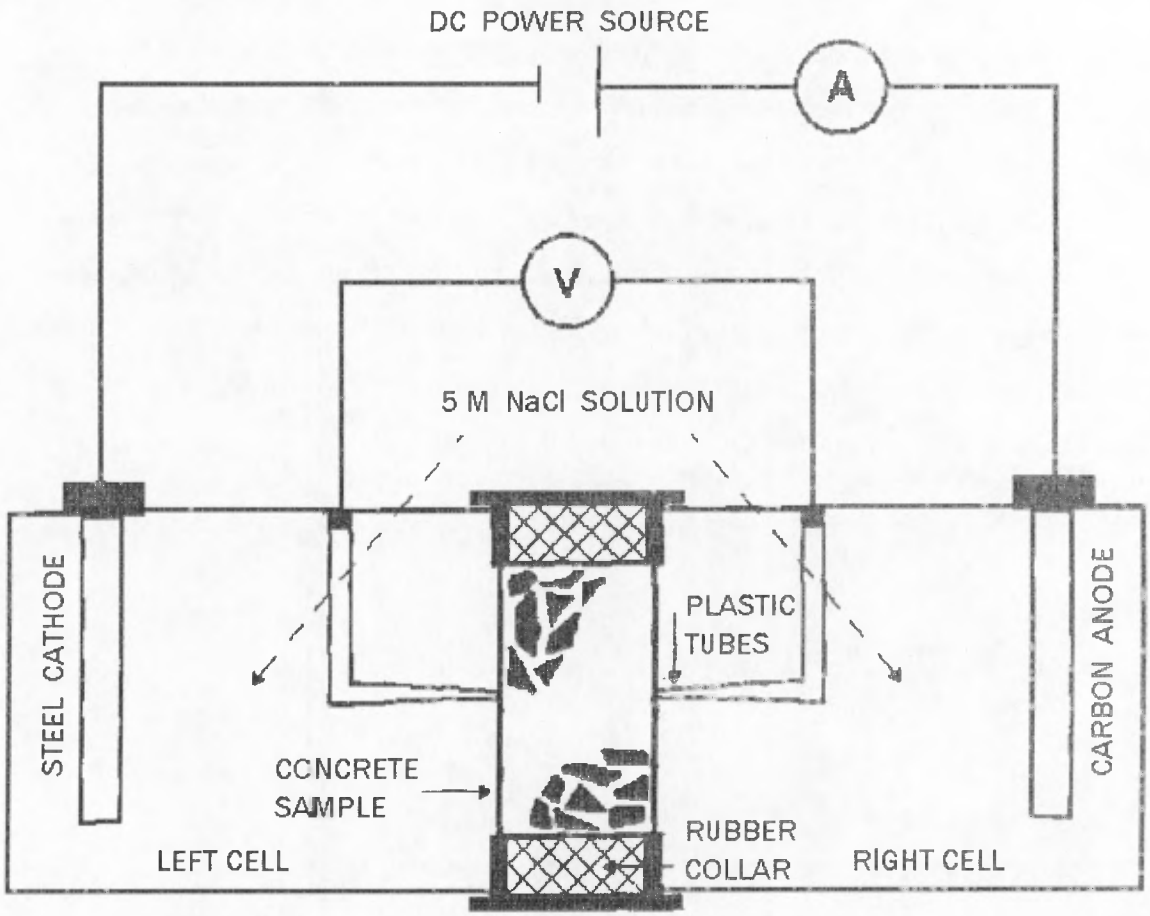

Fig 5B.1: Schematic of chloride conductivity test (Alexander et al. 1999[2])

The apparatus allows for a very rapid determination of the chloride conductivity value which can be defined as (Alexander et al 1999[b]):

$$\sigma = \frac{it}{VA} \qquad \ldots 5B.5$$

Where:

σ - chloride conductivity (ms/cm)

i - current (mA)

V - voltage (v)

t - specimen thickness (cm)

A - cross-sectional area (cm^2)

5B.4 Durability Index Test Results

Water Sorptivity Values (mm/√h)

Mix Design	*Age (days)*		
	28	*56*	*90*
PC	7.4	6.1	6.5
SL	5.6	5.1	5.8
SM	4.5	4.5	4.9
SH	7.2	7.1	6.8
FA	4.9	4.3	4.5
SF	5.4	5.1	5.1
TR	4.2	3.8	4.1

Oxygen Permeability Index (log scale)

Mix Design	*Age (days)*		
	28	*56*	*90*
PC	10.00	10.51	10.50
SL	10.05	10.44	10.63
SM	10.17	10.48	10.54
SH	9.78	9.79	9.80
FA	10.40	10.69	10.77
SF	10.03	10.52	10.52
TR	10.08	10.40	10.53

Chloride Conductivity (mS/cm)

Mix Design	*Age (days)*		
	28	*56*	*90*
PC	1.86	0.98	0.87
SL	1.13	0.66	0.40
SM	0.89	0.47	0.26
SH	1.45	0.92	0.61
FA	1.04	0.50	0.29
SF	1.39	0.93	0.62
TR	0.99	0.41	0.21

Appendix 5C

5C.1 Chloride Threshold Values

A) Chloride threshold values for concrete specimens
(total chloride as a percentage mass of binder)

Binder Type	*Concrete*
PC	0.53
SL	0.41
SM	0.08
SH	0.20
FA	0.36
SF	0.51
TR	0.08
Average	***0.31***

B) Chloride threshold concentration of first specimen to show signs of active corrosion for each binder type in concrete series I and mortar series

Binder Type	Concrete	Mortar
PC	0.29	0.71
SL	0.22	0.70
SM	0.06	0.20
SH	0.20	0.16
FA	0.29	0.12
SF	0.51	0.42
TR	0.07	0.28

5C.2 Effects of Bar Slippage on Chloride Movement

One set of samples was prepared using a PC mix as described by mix design II. The rebar had an electrical connection on either end of the bar with a total length of sample of 375 mm. After two weeks the samples were sawn in half, the bar in one half of sample was then slipped approximately 0.7 mm The samples were then placed in a bath with the cut surface exposed to a 5% NaCl solution. After one month the samples were cut longitudinally and the depth of chloride penetration observed through application of 0.1M solution of $AgNO_3$ on the surface and subject to ultraviolet light. The principles behind the method are explained in greater detail by Schoppel et al. (1988). The area which contained chlorides, at a concentration of

approximately 0.4% by mass of cement, showed up as purple with the uncontaminated area remaining brown.

Preferential movement of chlorides was observed along the bars compared to the bulk matrix for both the slipped and unslipped bars and no appreciable difference was observed between the two sets of measurements. It should be noted that the purpose of this fairly quick investigation was not to comprehensively address the issue of chloride movement along slipped and unslipped bars, but to provide some assurance that the approach taken to maintain crack widths would not unduly influence the environment around the steel and make the comparison of observed corrosion rates meaningless from a practical perspective.

Appendix 5D: Corrosion Characteristics

5D.1 Corrosion Characteristics for Mix Design Series II Passivation Study

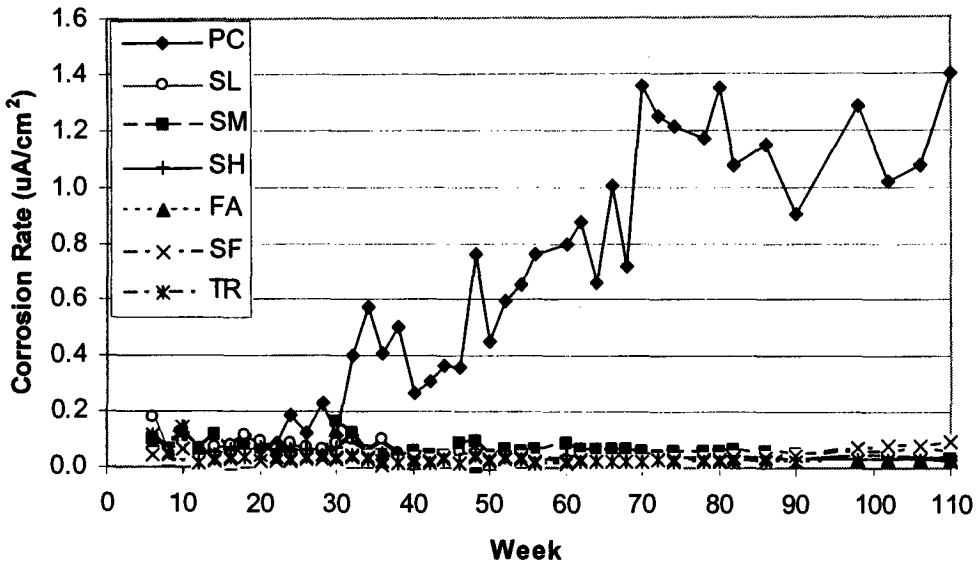

Fig 5D.1: Corrosion rates for all specimens

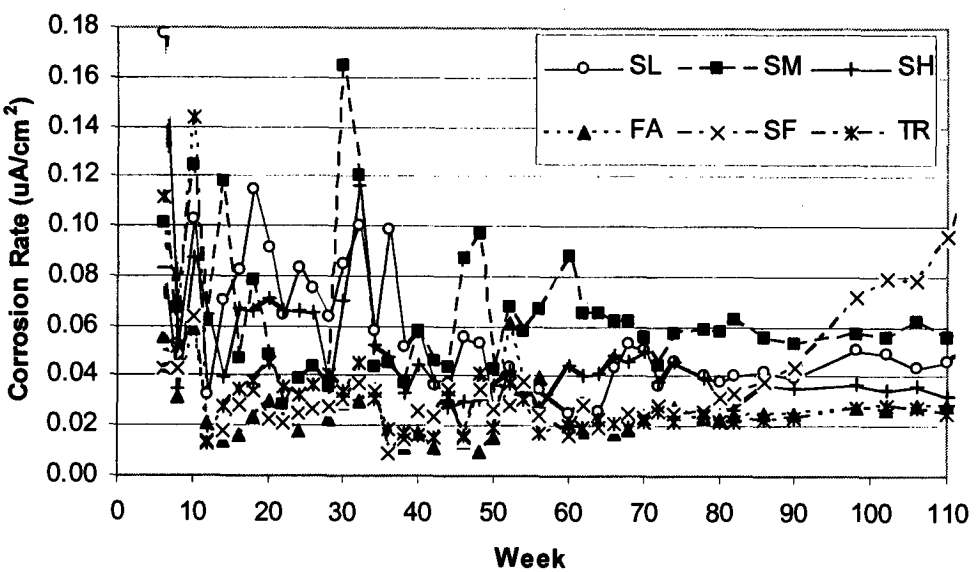

Fig 5D.2: Corrosion rates excluding PC

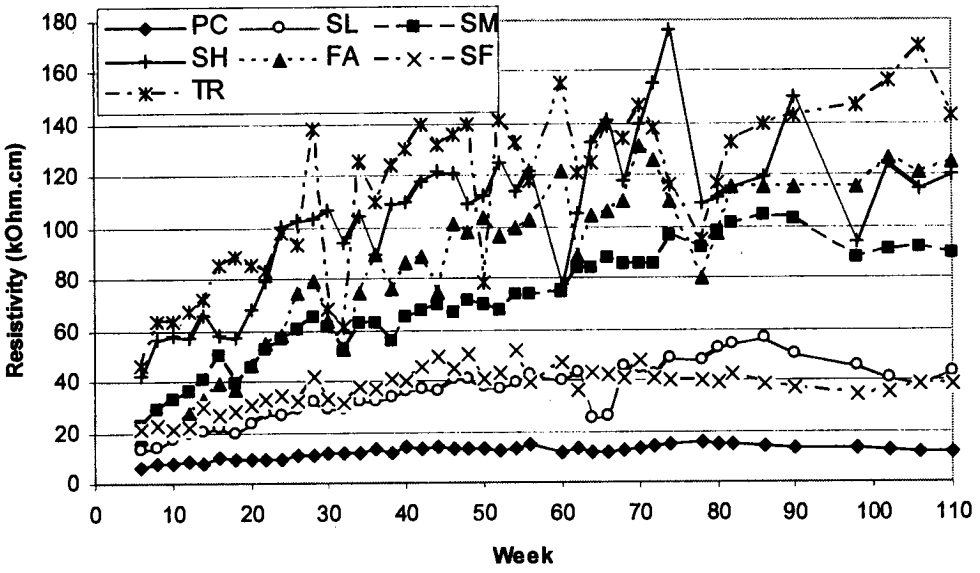

Fig 5D.3: Resistivity values for all samples

5D.2 Corrosion Potentials for Cracked Concrete Study

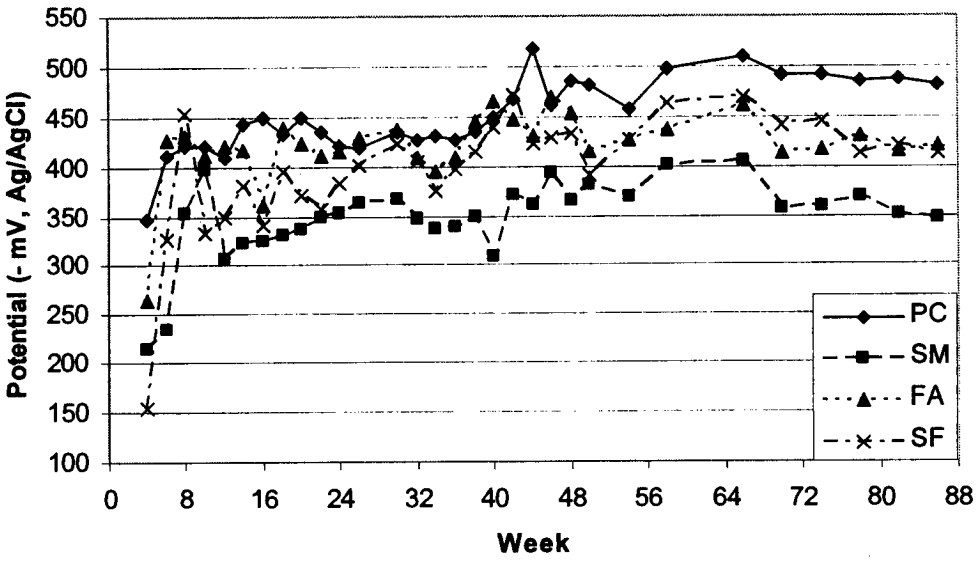

Fig 5D.4: Potentials for 20 mm cover and 0.2 mm crack width

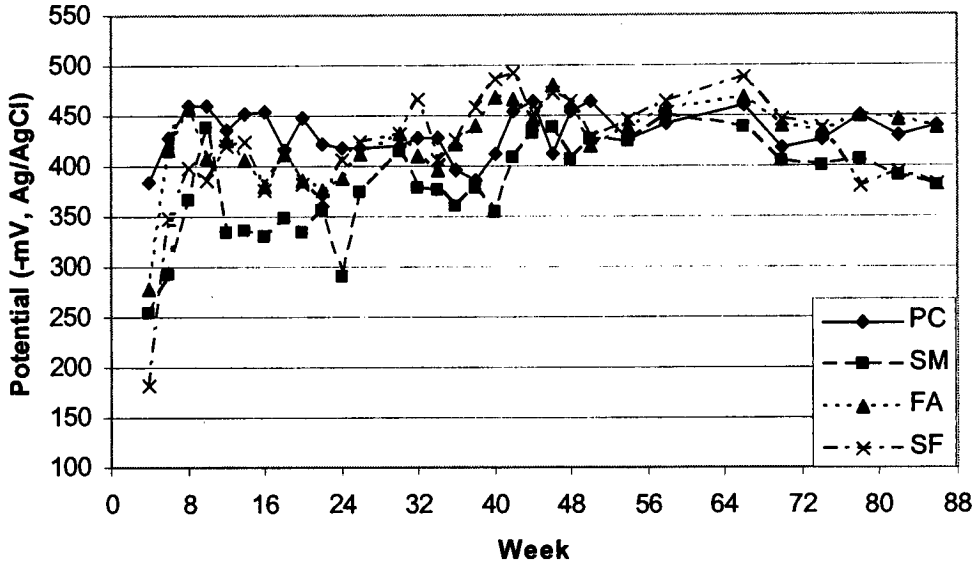

Fig 5D.5: Potentials for 20 mm cover and 0.7 mm crack width

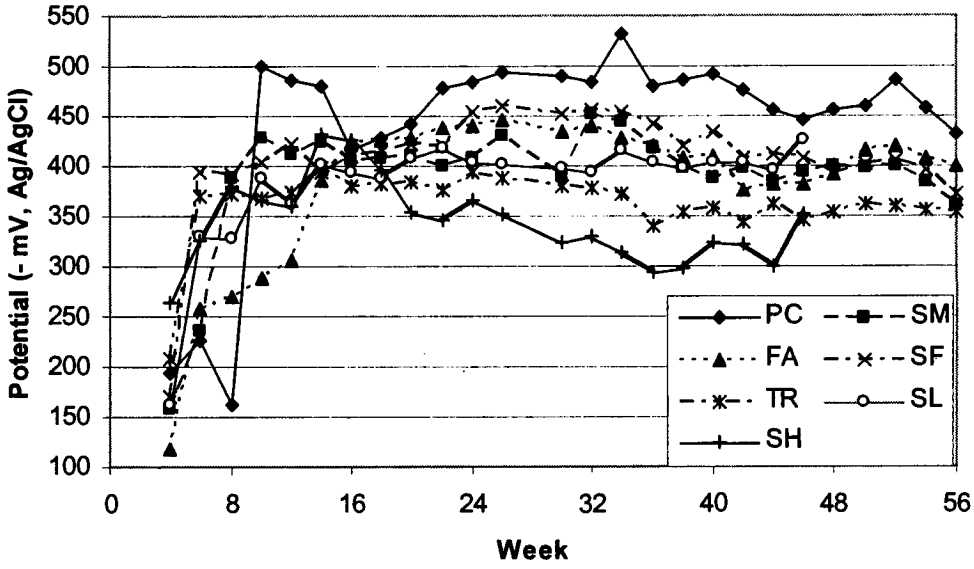

Fig 5D.6: Potentials for 40 mm cover and 0.2 mm crack width

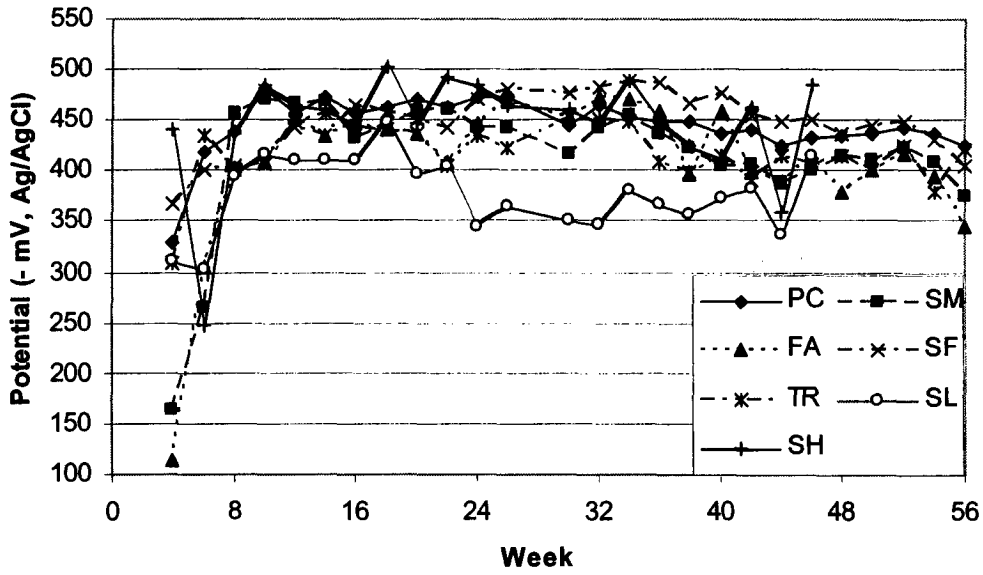

Fig 5D.7: Potentials for 40 mm cover and 0.7 mm crack width

5D.3 Corrosion Rates for Cracked Concrete Study

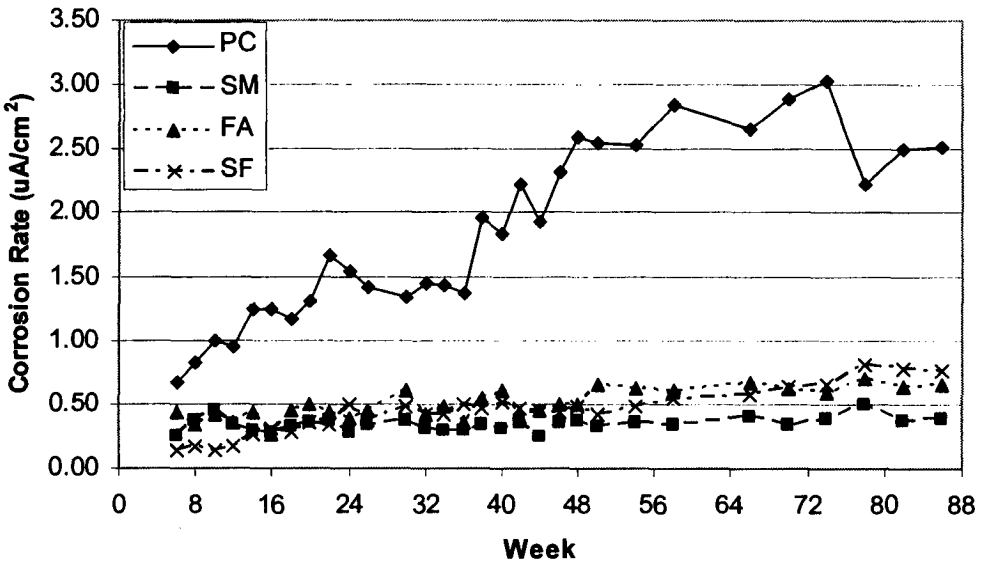

Fig 5D.8: Corrosion rates for 20 mm cover and 0.2 mm crack width

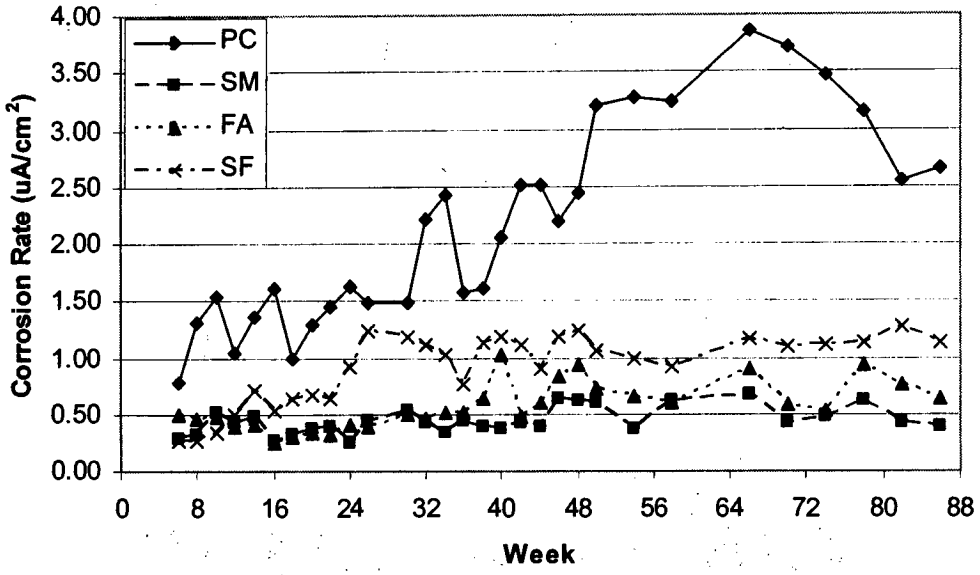

Fig 5D.9: Corrosion rates for 20 mm cover and 0.7 mm crack width

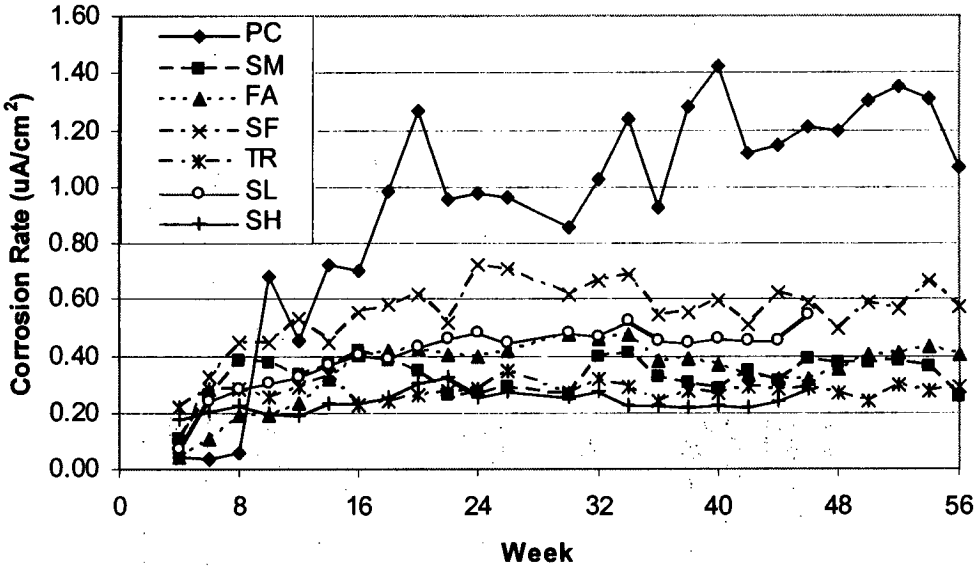

Fig 5D.10: Corrosion rates for 40 mm cover and 0.2 mm crack width

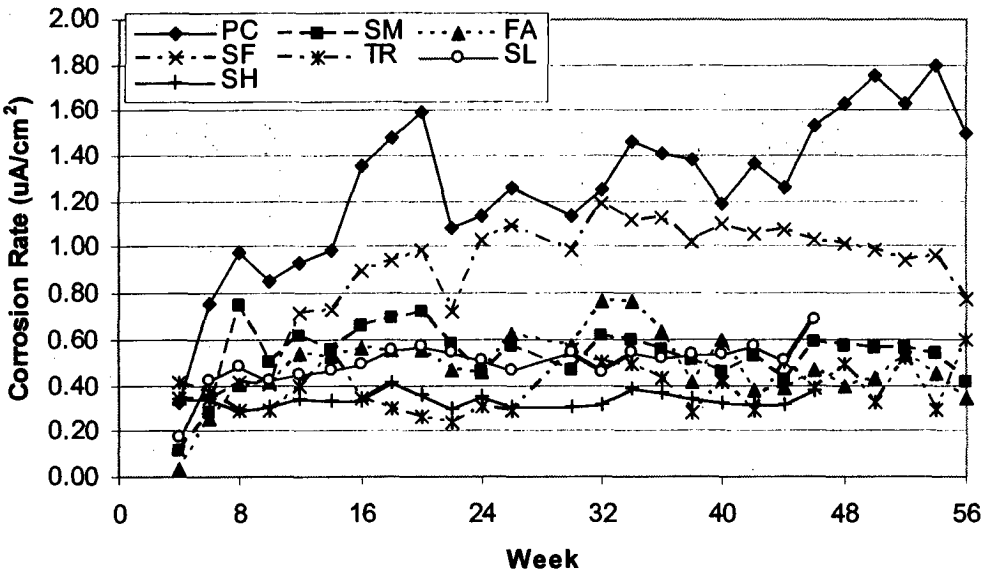

Fig 5D.11: Corrosion rates for 40 mm cover and 0.7 mm crack width

5D.4 Resistivty Values for Cracked Concrete Study

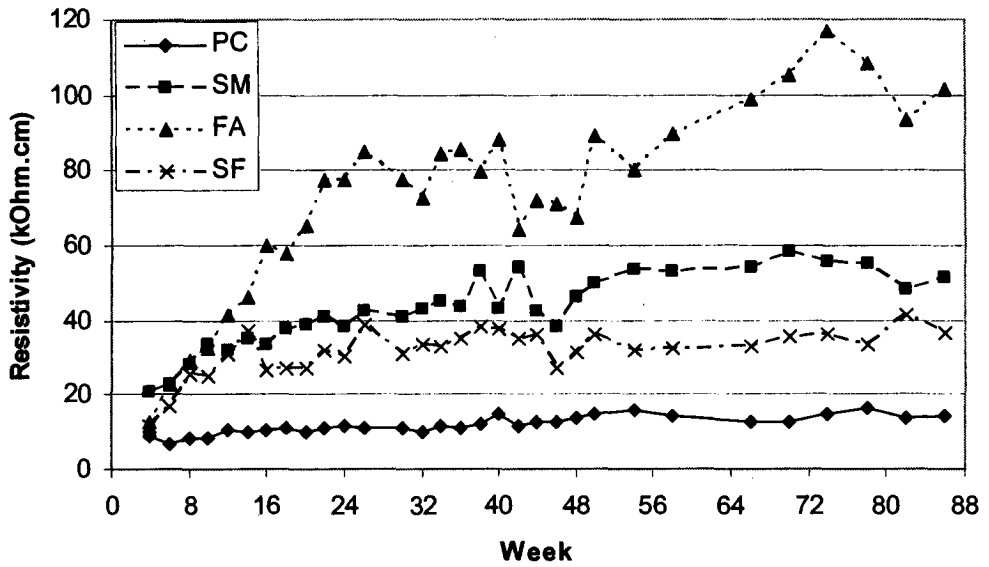

Fig 5D.12: Resistivity for 20 mm cover and 0.2 mm crack width

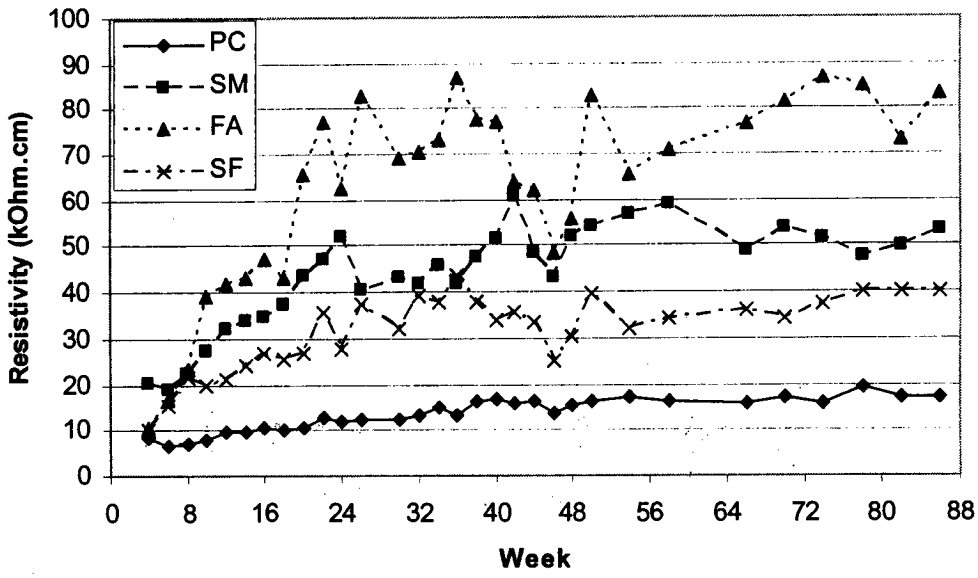

Fig 5D.13: Resistivity for 20 mm cover and 0.7 mm crack width

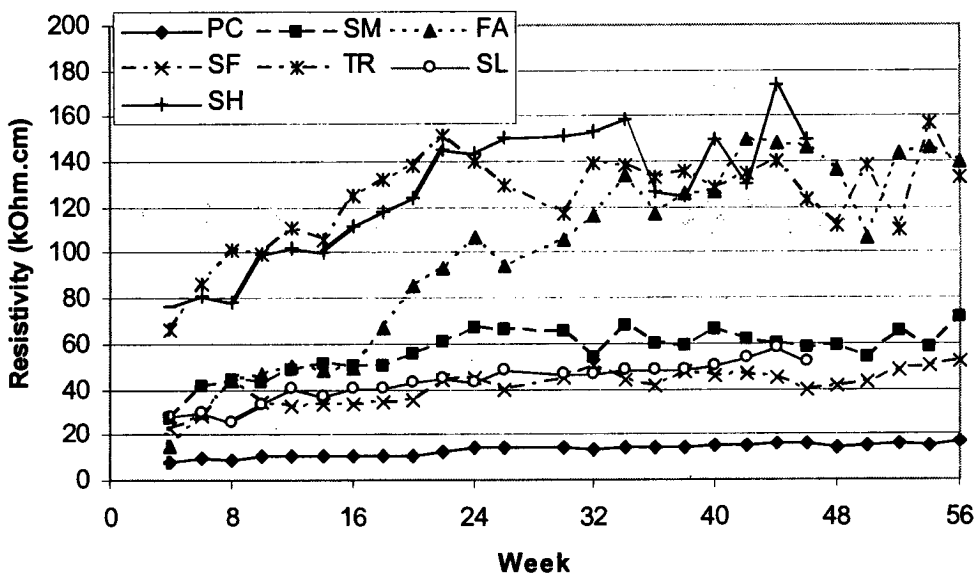

Fig 5D.14: Resistivity for 40 mm cover and 0.2 mm crack width

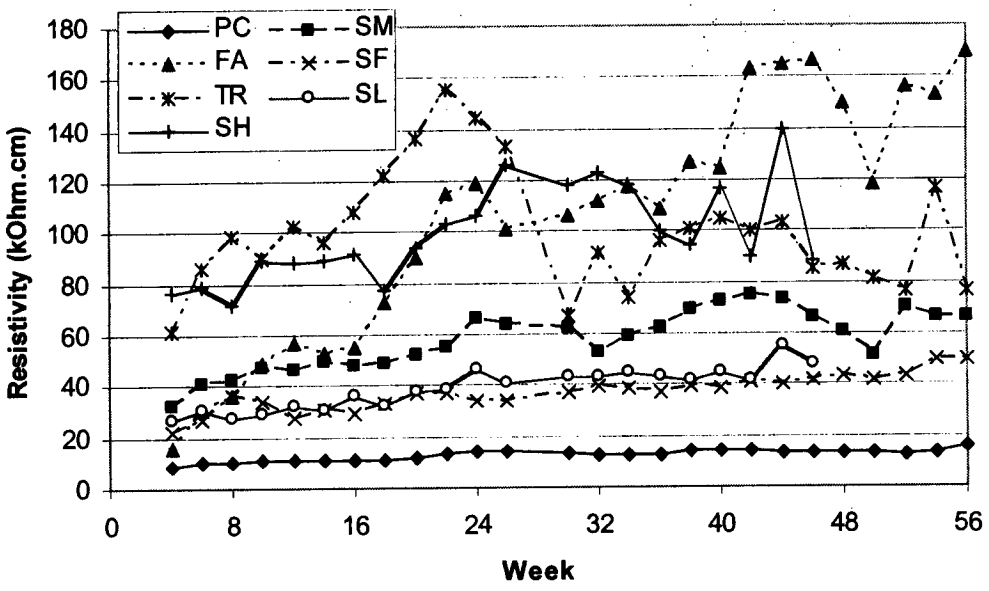

Fig 5D.15: Moving average of resistivity, 40 mm cover and 0.7 mm crack width

5.13 References

Addis, B. J. ed. (1986), **Fulton's Concrete Technology 6th edition**, Portland Cement Institute.

Alexander, M., Mackechnie, J. and Ballim, Y. 1999[a], **Guide to the use of Durability Indexes for Achieving Durability in Concrete Structures, Research Monograph No. 2,** Department of Civil Engineering University of Cape Town and University of the Witwatersrand.

Alexander, M., Steicher, P. and Mackechnie, J. 1999[b], **Rapid Conductivity Testing of Concrete, Research Monograph No. 3**, Department of Civil Engineering University of Cape Town.

Alexander, M., Ballim, Y. and Mackechnie, J. 1999[c], **Concrete Durability Index Testing Manual, Research Monograph No. 4**, Department of Civil Engineering University of Cape Town and University of the Witwatersrand.

Alonso, C., Andrade, C. and Gonzalez, J. 1988, *Relationship between Resistivity and Corrosion Rate of Reinforcements in Carbonated Mortars Made with Several Cement Types*, **Cement and Concrete Research**, Vol. 8, pp. 687-698.

Alonso, C., Castellote, M. and Andrade, C. 2000, *Dependence of Chloride Threshold with the Electrical Potential of Reinforcement*, **Second International Rilem Workshop on Testing and Modeling the Chloride Ingress into Concrete, France**, p 11.

Andrade, C. and Alonso, C. 1996, *Corrosion Rate Monitoring in the Laboratory and on-Site*, **Construction and Building Materials**, Vol. 10, No. 5, pp. 315-328.

Andrade, C. and Page, C. 1986, *Pore Solution Chemistry and Corrosion in Hydrated Cement Systems Containing Chloride Salts: A Study of Cation Specific Effects*, **British Corrosion Journal**, Vol. 21, No. 1, pp. 49-53

Arya, C., Buenfeld, N. and Newman, J. 1990, *Factors Influencing Chloride-Binding in Concrete*, **Cement and Concrete Research**, Vol. 20, pp. 291-300.

Arya, C. and Wood, L. 1995, **The Relevance of Cracking in Concrete to Corrosion of Reinforcing**, Concrete Society Technical Report No. 44.

Arya, C. and Xu, Y. 1995, *Effect of Cement Type and Chloride Binding and Corrosion of Steel in Concrete*, **Cement and Concrete Research**, Vol. 25, No. 4, pp. 893-902.

Balabanic, G., Bicanic, N. and Durekovic, A. 1996, *The Influence of w/c Ratio, Concrete Cover Thickness and Degree of Water Saturation on the Corrosion Rate of Reinforcing Steel in Concrete*, **Cement and Concrete Research**, Vol. 26, No. 5, pp. 761-769.

Beeby, A. 1978, **Concrete in the Oceans, Cracking and Corrosion, Technical Report No. 1**, Slough: Cement and Concrete Association.

Berry, E., Hemmings, R., Langley, W. and Carette, G. 1989, *Beneficiated Fly Ash: Hydration, Microstructure, and Strength Development in Portland Cement Systems*, **Fly Ash, Silica Fume, Slag, and Natural Pozzolans in Concrete, Proceedings Third International Conference Trondheim, Norway**, ACI, SP 114, vol. 1, pp. 241-273.

Bentur, A., Diamond, S. and Berke, N. 1997, **Steel Corrosion in Concrete, Fundamentals and Civil Engineering Practice**, London: E & FN Spon, pp. 41-43.

Bentur, A. 1991, *Microstructure, Interfacial Effects and Micromechanics of Cementitious Composites*, **Ceramic Transactions Vol. 16, Advances in Cementitious Materials**, pp. 523-49.

Boddy, A., Bentz, E., Thomas, M. and Hooton, R. 1999, An **Overview and Sensitivity Study of a Multimechanistic Chloride Transport Model**, *Cement and Concrete Research*, Vol 29, pp. 827-837.

Breit, W. 1998, *Corrosion of Steel in Concrete, the Question of Corrosion Initiated by the Critical Chloride Content*, **Betonwerk and Fertigteil Technik**, Vol. 11, pp. 37-45.

Broomfield, J., Rodriguez, J., Ortega, L. and Garcia, A. 1994, *Corrosion Rate Measurements in Reinforced Concrete Structures by a Linear Polarization Device*, **Concrete Bridges in Aggressive Environments, ACI SP-151**, pp. 163-181.

Broomfield, J. 1996, *Field Measurements of the Corrosion Rate of Steel in Concrete using Microprocessor Controlled Unit with a Monitored Guard Ring for Signal Confinement*, **Techniques to Assess the Corrosion Activity of Steel Reinforced Concrete Structures, ASTM STP 1276**, pp. 91-106.

Brown, P., Shi, D. and Skalny, W. 1991, *Porosity/Permeability Relationships*, **Materials Science of Concrete II, Mindess and Skalany (ed.)**, American Ceramic Society, pp. 83-109.

Enevoldsen, J., Hansson, C. and Hope, B. 1993, *The Influence of Relative Humidity on the Corrosion Rates of Steel Embedded in Mortar and Concrete*, **Proceedings of the Third Canadian Symposium on Cement and Concrete**, National Research Council, pp. 342-350.

Feliu, S., Gonzalex, J. and Andrade, C. 1996, *Electrochemical Methods for On-Site Determinations of Corrosion Rates of Rebar*, **Techniques to Assess the Corrosion Activity of Steel Reinforced Concrete Structures, ASTM STP 1276**, pp. 107-118.

Flis, J., Pickering, H. and Osseo-Asare, K. 1995, *Assessment of Data from Three Electrochemical Instruments for Evaluation of Reinforcement Corrosion Rates in Concrete Bridge Components*, **Corrosion Science**, August, pp. 602-609.

Frederiksen, J. 2000, *Chloride Threshold Values for Service Life Design*, **Second International Rilem Workshop on Testing and Modeling the Chloride Ingress into Concrete, France**, p. 18.

Glass, G. and Buenfeld, N. 1995, *Chloride Threshold Levels for Corrosion Induced Deterioration of Steel in Concrete*, **Chloride Penetration into Concrete: Proceeding of Rilem Workshop, France, Ed. Nilsson, L. and Ollivier, J.**, pp. 429-440.

Glass, G. and Buenfled, N. 1997, *The Presentation of the Chloride Threshold Level for Corrosion of Steel in Concrete*, **Corrosion Science**, Vol. 39, No. 5, pp. 1001-1013.

Glass, G., Hassanein, N. and Buenfeld, N. 1997, *Neural Network Modeling of Chloride Binding*, **Magazine of Concrete Research**, Vol. 49, No. 181, pp. 323-335.

Gowers, K. and Millard, S. 1999, *Measurement of Concrete Resistivity for Assessment of Corrosion Severity of Steel Using Wenner Technique*, ACI **Materials Journal**, Vol. 96, No. 5, pp. 536-541.

Hansson, C. (1995), *Concrete: The Advanced Industrial Material of the 21st Century*, **Metallurgical and Materials Transactions**, Vol 26A, June, pp.1321-1341.

Hansson, C. and Sorensen, B. 1990, *The Threshold Concentration of Chloride in Concrete for the Initiation of Reinforced Corrosion*, **Corrosion Rates of Steel in Concrete, ASTM STP 1065, American Society for Testing and Materials**: Philadelphia, pp. 3-16.

Hwang, C., Chen, J. and Chiou, I. 1994, *Concrete Cracking and Corrosion of Steel Bar*, **Corrosion and Corrosion Protection of Steel in Concrete, Proceedings of International Conference, University of Sheffield ed. Swammy**, Vol. 1, pp. 310-323.

Lambert, P., Page, C. and Vassie, P. 1991, *Investigations of Reinforcing Corrosion. 2. Electrochemical Monitoring of Steel in Chloride-Contaminated Concrete*, **Materials and Structures**, Vol. 24, pp. 351-358.

Liu, Y. 1996, *Modeling the Time to Corrosion Cracking of the Cover Concrete in Chloride Contaminated Reinforced Concrete Structures*, **Dissertation for Doctor of Philosophy**, Virginia Polytechnic Institute and State University.

Lopez, W., Gonzalez, J. and Andrade, C. 1993, *Influence of Temperature on the Service Life of Rebars*, **Cement and Concrete Research**, Vol. 23, pp. 1130-1140.

Machphee, D. and Cao, H. 1993, *Theoretical Description of Impact of Bast Furnace Slag (BFS) on Steel Passivation in Concrete*, **Magazine of Concrete Research**, Vol. 45, No. 162, pp. 63-69.

Mangat, P., Khatib, J. and Molloy, B. 1994, *Microstructure, Chloride Diffusion and Reinforcement Corrosion in Blended Cement Paste and Concrete*, **Cement and Concrete Composites**, Vol. 16, pp. 73-81.

Mangat, P. and Molloy, E. 1994, **Prediction of Long Term Chloride Concentration in Concrete**, *Materials and Structures*, Vol. 27, pp. 338-346.

Mangat, P. and Molloy, E. 1992, *Factors Influencing Chloride-Induced Corrosion of Reinforcement in Concrete*, **Materials and Structures**, Vol. 25, pp. 404-411.

Martin-Perez, B., Zibara, H., Hooton, R. and Thomas, M. 2000, *A Study on the Effect of Chloride Binding on Service Life Predictions*, **Cement and Concrete Research**, Vol. 30, pp. 1215-1223.

Mehta, P. and Monteiro, J. 1993, **Concrete Structure, Properties and Materials**, New Jersey: Prentice Hall.

Neville, A. 1972, **Properties of Concrete**, London: Pitman Publishing.

Nilsen, U., Sandberg, P. and Folliard, K. 1992, *Influence of Mineral Admixtures on the Transition Zone in Concrete*, **Interfaces in Cementitious Composites, Proceedings of the Rilem International Conference**, London: E & FN Spon, pp. 65-70.

Page, C., Short, N. and Holden, W. 1986, *The Influence of Different Cements on the Chloride-Induced Corrosion of Reinforcing Steel*, **Cement and Concrete Research**, Vol. 16, pp. 79-86.

Parrott, L. 1995, *The Influence of Cement Type and Curing on the Drying and Air Permeability of Cover Concrete*, **Magazine of Concrete Research**, June, No. 171, pp. 103-111.

Perraton, D., Aitcin, P. and Carles-Gibergues, A. 1992, *Permeability, As Seen by the Researcher*, **High Performance Concrete, From Materials to Structure**, London: E & FN SPON, pp. 252-275.

Pettersson, K. 1994, *Chloride Threshold Value and the Corrosion Rate in Reinforced Concrete*, **Corrosion and Corrosion Protection of Steel in Concrete: Proceedings of International Conference held at the University of Sheffield, ed. Swamy R.**, Vol. 1, pp. 461-471.

Pettersson, K. 1992, *Chloride Threshold Value and Corrosion Rate in Reinforced Concrete,* CBI report 2.92, Swedish Cement and Concrete Research Institute, p 43.

Pettersson, K., Jorgensen, O. and Fidjestol, P. 1996, *The Effect of Cracks on Reinforcement Corrosion in High-Performance Concrete in a Marine Environment*, **Concrete in Marine Environment, Proceedings Third CANMET/ACI International Conference SP-163, Ed. Malhotra**, pp. 185-200.

Pettersson, K. and Sandberg, P. 1997, *Chloride Threshold Levels, Corrosion Rates and Service Life for Cracked High-Performance Concrete*, **Durability of Concrete: Proceeding Fourth CANMET/ACI International Conference, Australia, ed. Malhotra**, pp. 451-472.

Rasheeduzzafar, Al-Saadoun, S., Dakhil, F. and Al-Gahtani, A. 1990, *Effect of Cement Composition on Corrosion of Reinforcing Steel in Concrete*, **Corrosion of Reinforcement in Concrete, Ed. Page, C., Treadaway, K. and Bramforth, P.**, London: Society of Chemical Industry, pp. 213-226.

Raupach, M. 1996, *Investigations on the Influence of Oxygen on Corrosion of Steel in Concrete - Part 2*, **Materials and Structures**, Vol. 29, pp. 226-232.

Roy, D. 1989, *Fly Ash and Silica Fume Chemistry and Hydration*, **Fly Ash, Silica Fume, Slag, and Natural Pozzolans in Concrete, Proceedings Third International Conference Trondheim, Norway**, ACI, SP 114, vol. 1, pp. 117-138.

Salvarezza, R., Videla, H and Arvia, A. 1982, *The Electrodissolution and Passivation of Mild Steel in Alkaline Sulphide Solutions*, **Corrosion Science**, Vol. 22, No. 9, pp. 815-829.

Schiessl, P. and Raupach, M. 1990, *Influence of Concrete Composition and Microclimate on the Critical Chloride Content in Concrete*, **Corrosion of Reinforcement in Concrete, Ed. Page, C., Treadaway, K. and Bramforth, P.**, London: Society of Chemical Industry, pp. 49-58.

Schoppel, K., Dorner, H. and Letsch, R. 1988, *Indication of Free Chlorine Ions on Concrete Surfaces by the UV-Test*, **Betonwerk and Fertigteil Technik**, Vol. 11, pp. 80-85.

Sirivivatnanon, V., Bucea, L., Meck, E., Yozghatlian, S. and Cao, H. 1994, *Influence of Fly Ash, Ground Granulated Blast Furnace Slag and Silica Fume on Chloride Induced Corrosion of Steel Reinforcement*, **2nd International Symposium on Blended Cements**, Malaysia, pp. 114-120.

Suzuki, K., Ohno, Y., Praparntanatorn, S. and Tamura, H. 1990, *Mechanism of Steel Corrosion in Cracked Concrete*, **Corrosion of Reinforcement in Concrete, Ed. Page, C., Treadaway, K. and Bramforth, P.**, London: Society of Chemical Industry, pp. 19-28.

Sykes, J. 1995, *Electrochemical Studies on Steel in Concrete*, **Materials Science Forum, Electrochemical Methods in Corrosion Research V**, Vol. 192-194, pp. 833-842.

Tarek, U., Toru, Y. and Hidenori, H. 2002, *Chloride Diffusion, Microstructure and Mineralogy of Concrete after 15 years of Exposure in Tidal Environment*, **ACI Materials Journal**, Vol. 99, No. 3, pp. 256-263.

Thomas, M. 1996, *Chloride Thresholds in Marine Concrete*, **Cement and Concrete Research**, Vol. 26, No. 4, pp. 513-519.

Thomas, M., Matthews, J. and Haynes, C. 1990, *Chloride Diffusion and Reinforcement Corrosion in Marine Exposed Concretes Containing Pulverized-Fuel Ash*, **Corrosion of Reinforcement in Concrete, Ed. Page, C., Treadaway, K. and Bramforth, P.**, London: Society of Chemical Industry, pp. 198-212.

Thomas, M., Matthews, J. and Haynes, C. 1989, *The Effect of Curing on the Strength and Permeability of PFA Concrete*, **Fly Ash, Silica Fume, Slag, and Natural Pozzolans in Concrete, Proceedings Third International Conference Trondheim, Norway**, ACI, SP 114, vol. 1, pp. 191-217.

Tuutti, K. 1982, **Corrosion of Steel in Concrete**, Swedish Cement and Concrete Research Institute: Stockholm

Valentini, C., Berardo, L. and Alanis, I. 1990, *Influence of Blast Furnace Slags on the Corrosion of Steel in Concrete*, **Corrosion of Steel in Concrete, ASTM STP 1065**, Philidephia, pp. 17-28.

CHAPTER 6: CONCLUSIONS FROM EXPERIMENTAL WORK AND SERVICE LIFE PREDICTIONS

The inclusion of cement extenders has been shown to dramatically lower the active corrosion rate of steel in concrete. Steel in the passive state, prior to the introduction of chlorides, was also significantly affected by the use of cement extenders. Notably, slag resulted in a considerable increase in the passive corrosion rate but still below the conventionally held threshold value of 0.1 $\mu A/cm^2$. Cement extenders yield real overall corrosion rate benefits despite the negative chemical impact associated with the inclusion of slag. The negative chemical impact of the cement extenders was demonstrated in the aqueous phase investigation which showed higher corrosion rates and lower chloride threshold values for all of the cement extenders, and the passivation study revealed higher corrosion rates associated with the slag-bearing material despite higher resistivity values.

One issue which is still somewhat debatable is the impact, and more specifically the ability to accurately quantify the impact, of cement extenders on the chloride threshold. The issue of uncertainty with respect to the chloride threshold concentrations will be further discussed in section 6.4.

Knowledge of corrosion rates and their values is of importance in trying to rank the influence of cement extenders in a general context of durability. Quantification of the time to cracking and the extension in service life associated with the inclusion of cement extenders provides practical and valuable information to the engineer and allows for meaningful predictions and comparisons based on life cycle costing. It was not within the scope of the current work to investigate or model the time to cracking associated with the corrosion of reinforcing steel in concrete. There have been numerous papers written on the various approaches used to model the propagation period. Some of these models will be briefly discussed in this chapter. The data and knowledge of the influence of cement extenders on the corrosion of steel in concrete gained in this investigation can then be used in conjunction with one of the existing mechanical cracking approaches to form a propagation period service life model of relevance to the engineer.

6.1 Conclusions from Experimental Investigations

The influence of cement extenders on various characteristics of the corrosion of steel in concrete has been extensively examined in this investigation. The chemical composition of the various binder types and their influence on the pore water was determined. Once the

aspects of the chemical composition were known, an aqueous phase investigation commenced which allowed for the examination of specific aspects of the pore solution, in particular sulphides and thiosulphate and their role in promoting or controlling the corrosion of mild steel. Aqueous chemistry represents only one component of the corrosion process and any attempt to ultimately provide useful information to engineers on service life and design guides should ultimately be validated by insitu data or at least initially by representative laboratory environments. In this regard, the corrosion of steel embedded in cracked concrete was studied to determine the effects of specific binder types and combinations. The separate but coordinated investigations of aqueous and solid phase work allowed for the determination of chemical and physical aspects which influence the corrosion process. The results from the cracking investigation were then used to form a predictive model, based on early age chloride conductivity results, for estimating future corrosion rates and ultimately time to cracking and loss of serviceability.

6.1.1 Pore Solution Composition

The study of pore water derived from pastes of the various mix designs revealed distinctive characteristics which were dependant upon the binder type. The inclusion of any of the cement extenders resulted in a lowering of the hydroxyl ion concentration relative to the PC control sample. The inclusion of slag had a moderate impact on the relative hydroxyl ion concentration with FA and ultimately SF leading to greater reductions. The relative concentrations of hydroxyl ions are provided in Figure 6.1.

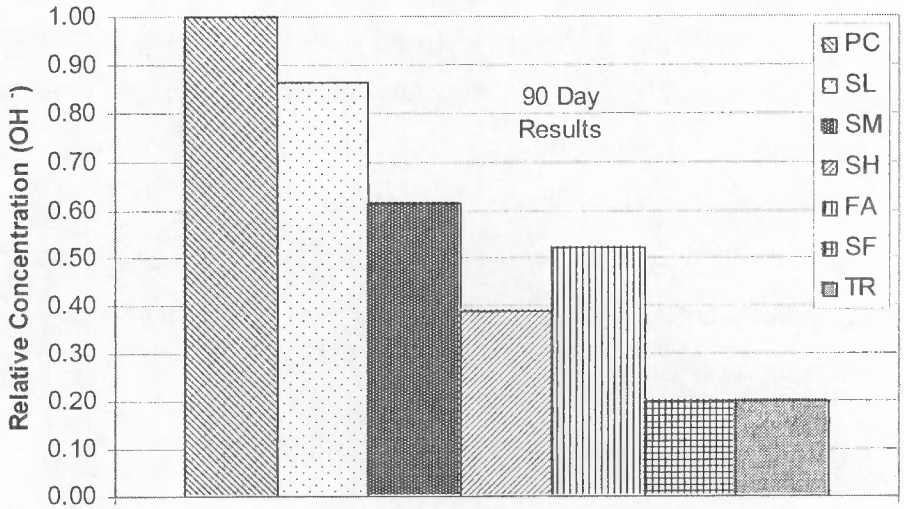

Fig 6.1: Relative concentration of hydroxyl ions compared to PC

The ternary blend (TR) of PC, SF and slag was dominated by the SF component and showed hydroxyl ion levels almost identical to the SF sample.

One of the greatest observed differences between the binder types was the significant presences of sulphides and thiosulphate in the slag bearing materials. SL, SM and SH had a total reducing sulphur (TRS) concentration, given as combined concentration of sulphide plus thiosulphate, of at least 70 mg/l compared to 17 mg/l for PC. The TR samples again showed their heavy dependence upon the SF chemistry with a TRS of 15 mg/l compared to 70 mg/l for SM. TR did however have a TRS concentration approximately 5 times that of SF. Sulphides had a number of impacts on the pore solution:

1) reducing the redox potentials to less than –465 mV for SL, SM and SH, compared to –346 mV for PC.

2) decreasing the dissolved oxygen content, through the conversion of sulphide to thiosulphate and ultimately sulphate, to approximately 0.1 mg/l for SL, SM and SH at 90 days compared to 2.1 mg/l for PC. The relationship between total reducing sulphur and DO was provided in equation 3.1.

The TR blend showed DO levels of 0.4 mg/l which were significantly below those of both SF and PC. The impact of reduced DO content and redox potential on the corrosion characteristics were determined in the aqueous phase investigation where it was shown that the lower DO levels and more negative redox potentials resulted in elevated 'passive' corrosion rates compared to those samples with higher DO levels and redox potentials. It should be noted that the low DO levels and redox potentials were associated with the sulphide-bearing simulated pore solutions and that the presence of sulphides would also have affected the corrosion characteristics. The lower DO levels of the sulphide-bearing pore solutions may have been insufficient to provide complete passivation of the rebar and thus permitted higher corrosion rates.

6.1.2 Aqueous Phase Investigation

The chloride threshold level for the initiation of corrosion was generally found to vary proportionately to the hydroxyl ion concentration. The Cl/OH ratio for the non-sulphide containing samples ranged from 0.6 for FA to 1.39 for SF. The corrosion rates of steel in simulated solutions were more strongly dependant upon the change in hydroxyl ion concentration than chloride concentration. As the chloride concentration increased from 0.2 M to 0.6 M, the corrosion rate increased by a modest factor of 1.7 for SF and approximately 3.3 for FA and PC. A decrease in the hydroxyl ion concentration by a factor of 1.4 and 4.6

resulted in an increase in corrosion rate by a factor of 3 and 28 respectively for FA and SF, for a fixed chloride concentration of 0.6M. The corrosion rate therefore was found to be strongly dependant upon the hydroxyl ion concentration of the solution.

The presence of sulphides in the pore solution was shown to have detrimental effects on the corrosion characteristics of steel in simulated pore solutions. All the sulphide containing samples showed higher passive corrosion rates over the first 14 days prior to the introduction of oxygen or chlorides. Once chlorides were added at 21 days the sulphide bearing samples showed significantly higher corrosion rates compared to the control samples. It should be noted that once oxygen was introduced to the system most, if not all the sulphides, were converted to thiosulphate or possibly sulphate before the chlorides were introduced. The effect of sulphides on the corrosion characteristics persisted long after their disappearance from the simulated pore solution. The sulphides suppress the development of the passive layer, through reducing the availability of oxygen, and provide inclusion points of sulphides (FeS) in the passive layer, which would reduce its effectiveness in protecting the steel.

The required chloride threshold levels for inducing corrosion generally decreased with the presence of sulphides, though SH had higher Cl/OH ratio than FA which contained no sulphides. There was generally greater variability associated with the determination of chloride threshold levels compared to corrosion rate measurements. Some caution should be taken in trying to precisely define a critical chloride concentration. If there is variability in the carefully controlled aqueous phase environment, there is likely to be more variability in the case of reinforced concrete structures subject to numerous additional influences.

6.1.3 Chloride Threshold Values in Concrete

The inclusion of cement extenders generally results in a lowering of the chloride threshold, though SF which has one of the lowest hydroxide concentrations displayed threshold levels comparable to PC. The inclusion of slag in samples SM, SH and TR resulted in chloride thresholds approximately one-third those of PC. The chloride threshold for SL however was only moderately less than PC. The relative performance of the materials can be ranked from highest threshold to lowest in the order: SF > PC > SL > FA > SH > TR > SM with the values given in Table 6.1. The different performance of the cement extenders is attributed to the reduction in alkalinity and the presence of sulphides in the slag bearing materials.

Table 6.1: Binder specific chloride threshold concentrations expressed as % chloride by mass of cementitious material for concrete samples

Binder Type	*Chloride Threshold (%)*
PC	0.53
SL	0.41
SM	0.08
SH	0.20
FA	0.36
SF	0.51
TR	0.08

The unusual performance of SF having a chloride threshold similar to PC despite having a hydroxyl ions concentration approximately one-fifth that of PC presents an anomaly. The aqueous phase investigation would suggest that SF should have a much lower chloride threshold level. The improved performance was attributed in part to the densification of the ITZ around the steel concrete interface. The fact that TR did not show the same effects is likely a result of the sulphides in the solution which would impede the development of the passive layer. In the case of SF the expected chloride threshold based on the chemistry of the pore solution was not realized and the improved effects must be a result of the physical properties of the material. In the case of TR the physical benefits of SF did not negate the deleterious chemical effects of the sulphides or the reduction in hydroxyl ion concentration.

6.1.4 Corrosion Rates

Passive corrosion rates prior to activation by chlorides revealed similar performance trends to the threshold values with the inclusion of slag resulting in elevated passive corrosion rates and very negative potentials. The highly negative potentials of the slag bearing specimens is consistent with the aqueous phase work and are a result of the reducing nature of the sulphide ions. The oxidation of the sulphides, as measured in the aqueous phase work, resulted in an increase of the potential measurements to more positive values. These effects were confirmed in the concrete specimens when cracking resulted in a sudden and rapid positive movement in potential. The slag corrosion rates in uncracked concrete were still higher than the PC or other extended samples despite having higher resistivity values. The inclusion of FA and SF results in a more refined pore structure as shown by the durability indices and coupled with higher resistivity values had lower passive corrosion rates than PC.

The average corrosion rates under passive conditions can be ranked from lowest to highest: FA < SF < PC < SH < TR < SL & SM as shown in Figure 6.2.

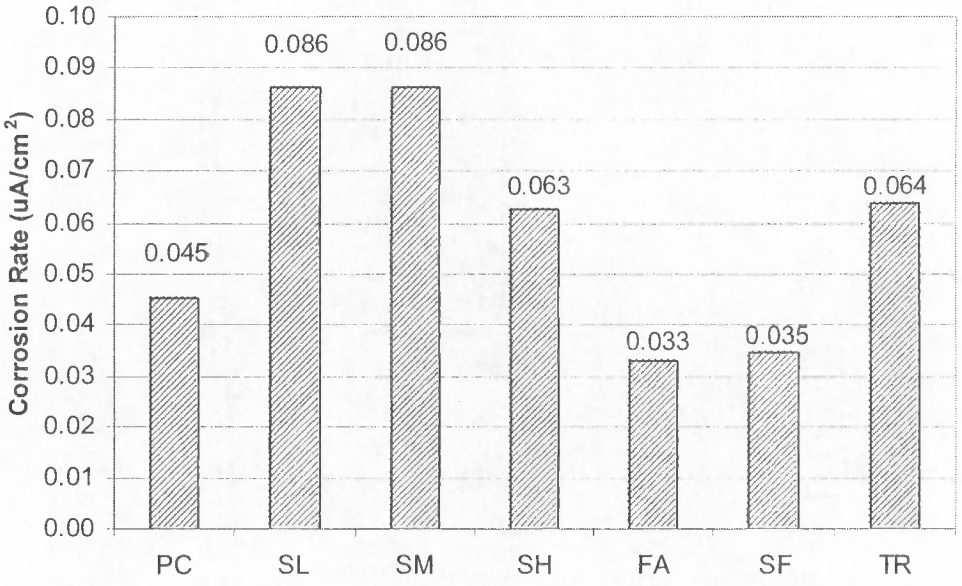

Fig 6.2: Average corrosion rate over first 16 weeks prior to activation

The higher corrosion rates associated with slag bearing materials is again attributed to the presence of sulphides and thiosulphate, the effects of which extend well beyond the first weeks and even after the sulphides had been oxidized as demonstrated in the aqueous phase work.

The generally negative trend of incorporating slags was reversed when it came to their performance under active corrosion conditions. SH, which by all accounts should not perform well, was shown to have the lowest average corrosion rate. The inclusion of any of the cement extenders resulted in at least a 40% reduction in corrosion rate compared to PC, with 5 out of 6 of the extender mixes showing more than 60% reduction in corrosion rates. The lower corrosion rates are not simply a function of one variable such as resistivity, although this will have a major impact. The reduction in corrosion rates is also dependant upon limiting the availability of oxygen at low rates of corrosion and the enhanced chloride binding effects of slag concrete. The negative impact of the sulphides has not disappeared but has simply been dominated by the other characteristics of slag such as generally improved microstructure and chloride binding, thus immobilizing the chlorides. The corrosion rates from lowest to highest are provided as follows: SH < TR < SM < FA < SL < SF < PC.

The impact of oxygen availability on controlling the corrosion rate was put into question as there was little correlation between OPI and corrosion rate, and the decrease of cover depth from 40 mm to 20 mm was shown to have a fairly minor impact upon corrosion rates for the blended materials. The decrease in cover depth however resulted in a significant increase in corrosion rate for the PC control sample. The different response of the materials to the change in cover was a result of drying and the availability of oxygen at the lower cover depths coupled with the resistivity. The low resistivity, and associated chloride conductivity, of the PC samples permitted a moderate to high corrosion rate at cover depths of 40 mm. A decrease in the cover resulted in faster drying near the steel and the availability of oxygen increased. Due to the low resisitivity even in moderately dry concrete, the corrosion rate likely increased in accordance with the availability of oxygen. The blended cements had corrosion rates which were limited by the resisitivity of the concrete such that increases in the availability of oxygen at the lower depth had little impact upon the corrosion rate. The PC samples were controlled by the diffusion of oxygen while the resistivity of the remaining blended samples primarily determined the corrosion rates.

6.2 Predictions of Corrosion Rates

This section will explore the possibility of using the information derived from the study of corrosion characteristics to present a preliminary model which can be used to assist in the evaluation of service life of reinforced concrete structures made with cement extenders. Durability index values will be employed in an attempt to quantify the material such that the model may be applicable to other mix designs not specifically studied during this investigation.

Cement extenders were shown to strongly influence the active corrosion rate of steel in concrete in order from lowest to highest: SH < TR < SM < FA < SL < SF < PC. Since cement extenders were also shown to significantly affect the various durability indexes, as measured at 28, 56 and 90 days, it is reasonable that some relationship should exist between the material characteristics of the concrete and the corrosion rate of the steel. The durability index tests assess various aspects of the material characteristics of the concrete, such as the permeability of the microstructure and conductivity, which would affect the corrosion rate. A correlation between durability index value and corrosion rates would allow different concrete mixes to be quantifiably ranked and their service life more accurately assessed prior to construction.

The correlation between durability index values and corrosion rates will be based on average corrosion rates taken between weeks 32 and 56 for all samples except SL and SH, for

which values are taken between weeks 32 and 46. The corrosion rates are combined averages from 40 mm cover depths and 0.2 mm and 0.7 mm crack widths. It was shown in chapter 5 that there was little change in corrosion rate over this period and the value can be considered the representative expected corrosion rates for the various cement extenders. Corrosion rates were also shown in chapter 5 to be more dependent on binder type than crack width. As there was relatively little difference between the 0.2 mm and 0.7 mm crack compared to binder type, an average value for the crack widths was chosen for comparative purposes. Furthermore the precise quantification of crack widths is difficult as they vary along the length of the crack and for practical considerations of comparing corrosion rates it is reasonable to consider the presence of a visible transverse crack sufficient without trying to compare the width of the crack.

6.2.1 Oxygen Permeability Index

The first of the durability indexes to be examined is the OPI which provides a representation for the mobility of oxygen through the concrete. As oxygen is essential for corrosion it would be expected that this is a useful parameter for comparison. The relationship between corrosion rates and 90 day OPI is shown in Figure 6.3.

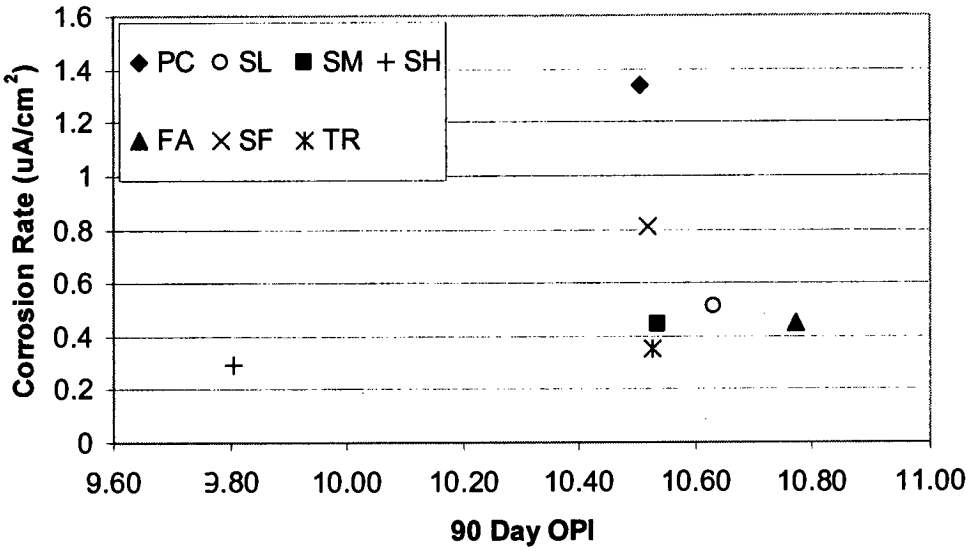

Fig 6.3: Plot of 90 day OPI and average 40mm cover corrosion rates

It can be seen from Figure 6.1 that there is no apparent correlation between corrosion rate and OPI as measured at 90 days. The drying period was sufficiently long to allow the diffusion of oxygen through the concrete such that the available oxygen at the steel was greater than that

required to sustain the reaction. There is effectively a surplus of oxygen under the given exposure conditions regardless of the use of extenders. If the concrete were subject to more saturated conditions, for instance RH above 95%, the permeability of the concrete to oxygen, as determined by the moisture state of the concrete, would likely become a dominant factor controlling the corrosion rate. The statement on the availability of oxygen is further supported by the limited effect of increasing cover on reducing the corrosion rate. In the case of the blended cements, the corrosion rates at a cover depth of 20 mm were already low due to the resistivity of the concrete. An increase in cover, while decreasing the availability of oxygen, had little effect on the corrosion rate. The availability of oxygen at either 20 or 40 mm cover depth was therefore greater than that which was required based on the corrosion rate.

By contrast, the corrosion rates in the PC samples showed a dependence of corrosion rate on cover depth which can be ascribed to the low resisitivity of the concrete. The corrosion rate of the PC samples was sufficiently high as to be affected by a reduction in the availability of oxygen, but this was not true for the other binder types. The SF sample showed a 4% improvement in the performance of the concrete, with respect to limiting the ingress of oxygen, which would not account for the almost 40% reduction in corrosion rates. OPI values may be of use in a comparison of PC samples with different w/c ratios which would affect the microstructure of the concrete. The purpose of the present investigation however was the study of binder type at a fixed w/c ratio and as such no further attempt was made to correlate corrosion rate values with the oxygen permeability of the concrete. That is not to say that the OPI has no value, as it clearly indicates the generally beneficial effect of including cement extenders on the permeability of the concrete. The OPI also clearly demonstrated the relatively open pore structure of SH and its susceptibility to the ingress of oxygen and infers the potential for rapid drying of this concrete.

6.2.2 Water Sorptivity

The water sorptivity test provides information on the general pore geometry of the material by assessing the movement of a wetting front through the concrete due to capillary suction. The water sorptivity values again demonstrated the improvement in material properties associated with using a cement extender for all but the SH sample. The relationship between average corrosion rates and 90 day water sorptivity values are shown in Figure 6.4.

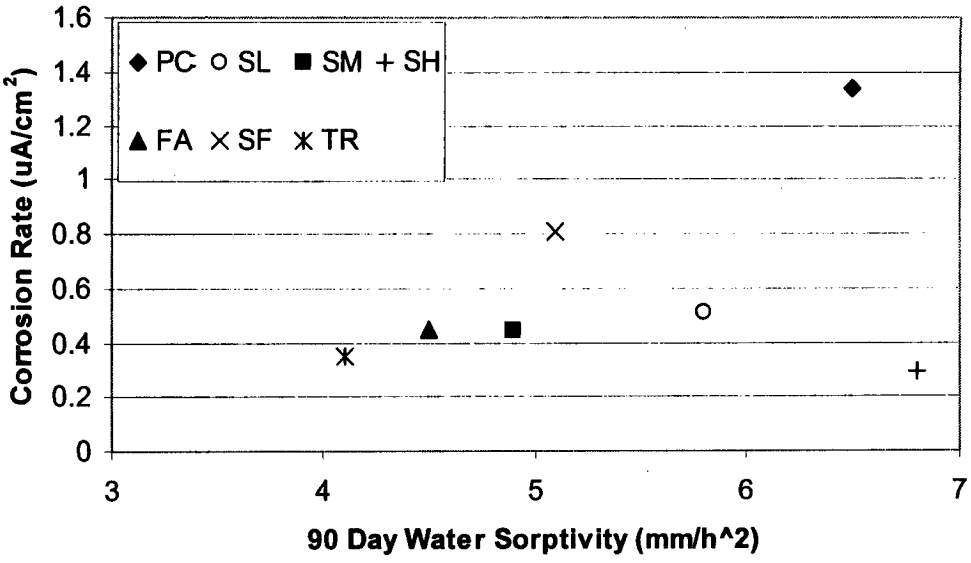

Fig 6.4: Relationship between water sorptivity and corrosion rate

It can be seen from Figure 6.4 that there appears to be only a poor correlation between water sorptivity and corrosion rate. Removing SH from the set results in a correlation coefficient of 0.66 which is still rather poor.

The water sorptivity values again highlight the poor performance of SH and provide further evidence of an open pore structure which appears to contradict the observed performance. As with the OPI values they provide little value as a direct means for assessing the corrosion resistance of concrete.

6.2.3 Resistivity

The resistivity values provide a useful snapshot of the material at a given point in time. Differences in pore structure and permeability will significantly affect rate of drying of the concrete and thus the measured resisitivity. Resistivity values were observed to vary from the start of the drying period to the end of the drying period with the SH samples showing the greatest increase in resistivity over the drying period. The range in observed resistivity values associated with SH is due to the relatively open pore structure which was shown by the measured OPI and water sorptivity values. SH would be more susceptible to drying effects which would account for the increase in resistivity from the start of the drying period to the end. The resistivity values were usually taken at the time of corrosion rate determination but would still be susceptible to factors such as surface carbonation or surface drying compared to more moist conditions at a greater depth near the steel.

The restivity values, as measured at the time of corrosion rate measurements, are not fundamental indicators of material properties as a material with an open pore structure which is susceptible to rapid drying could have the same value as one with a much denser pore structure. A high resistivity value therefore can be obtained either by a material with an open pore structure subject to rapid drying or one with a much denser composition, depending on its moisture state. Regardless of the cause of the high resistivity the effect on corrosion rate is very similar as demonstrated in Figure 6.5. If however the exposure conditions were different, such that the relative humidity of the concrete remained higher, the open microstructure of concrete, such as SH, would result in a lower resistivity and thus permit a higher degree of corrosion until the reaction became oxygen deprived. A concrete where the resistivity was due to a dense microstructure would not be as significantly affected by the moisture content, and the resistivity would continue to limit the corrosion rate. For resistivity values to be used as a general indicator of material characteristics they should ideally be tested at the same moisture content or degree of saturation. The chloride conductivity test is a form of resistivity measurement as will be discussed in the following section.

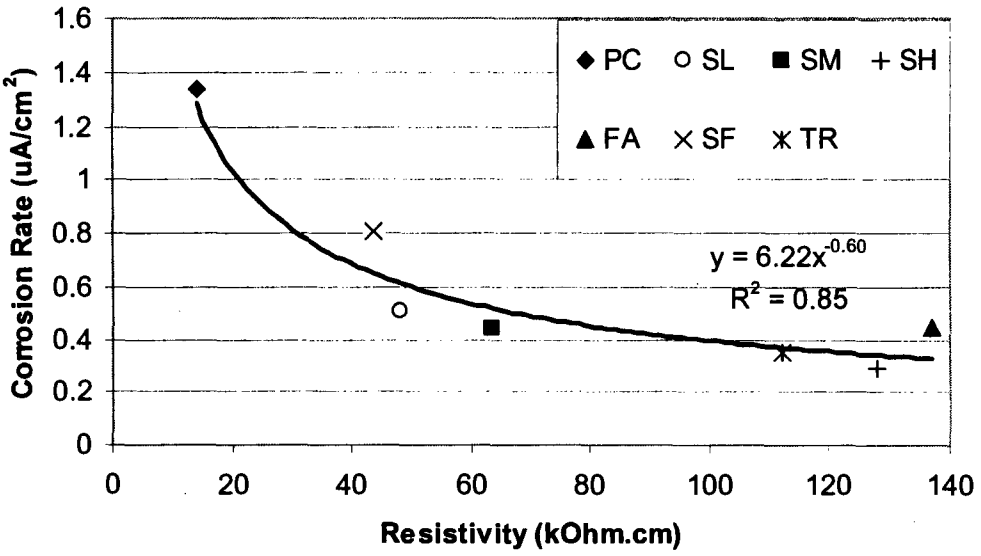

Fig 6.5: Average resistivity and corrosion rate measurements for 40 mm cover from week 32 to 56 (week 32 to 46 for SL and SH)

Figure 6.5 shows a clear dependence of corrosion rate on the resistivity of the concrete. The correlation coefficient of 0.85 suggests a reasonable dependence of corrosion rate on resistivity of the concrete and certainly more so than the availability of oxygen. There is a 50% reduction in corrosion rate as the resistivitiy increases from 20 to 60 kOhm.cm but only

a 25% reduction as the resistivity increase from 60 to 100 kOhm.cm. Beyond approximately 60 kOhm.cm there is a substantial reduction in the effectiveness of increasing resistivity. The corrosion rate has moved from a case of oxygen control to resistivity control and further increases have diminishing effects. Problems in measurements such as edge effects, size of the sample, and preferential current travel along the steel, limit the accuracy. The results from the chloride conductivity will be shown to overcome some of these difficulties.

The importance of oxygen transport, as derived from changes in cover depth, are only apparent where the resistivities are low and the corrosion rates are high as demonstrated in Figure 6.6. At resistivity of approximately 40 kOhm.cm or above there is relatively little change in corrosion rate for an increase in cover depth and the corrosion rate remains strongly correlated with the resistivity.

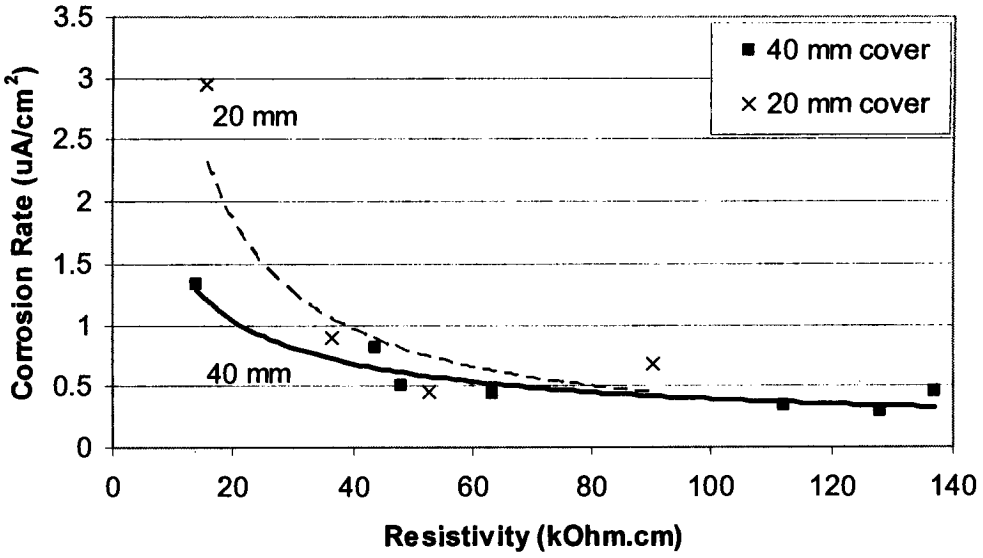

Fig 6.6: Relationship between corrosion rate, resistivity and cover depth

The resistivity of the concrete therefore should provide a reasonable estimate of corrosion rate for cover depths between 20 and 40 mm where cement extenders are used. Above a resistivity of 40 kOhm.cm variations in cover appear to have little effect. If concrete is produced with PC only then other considerations such as cover depth must be included for a reasonable estimate of corrosion rate to be determined.

6.2.4 Chloride Conductivity

The chloride conductivity experiments were performed at 28, 56 and 90 days and the preconditioning of the samples ensured adequate and uniform conditioning prior to testing.

The preconditioning does not always result in uniform penetration particularly in concrete with a dense microstructure. Where uniform penetration is not obtained, the chloride conductivity value would be lower than it should have been. The test tends to overstate the resistance of the concrete to ionic movement but only for concretes which already have an appreciably low conductivity (i.e. < 0.3 mS/cm). The error associated with non-uniform penetration of the solution should not seriously limit the effectiveness of the chloride conductivity results as an indicator of the fundamental material performance of the concrete. The relationship between chloride conductivity and corrosion rates is shown in Figure 6.7.

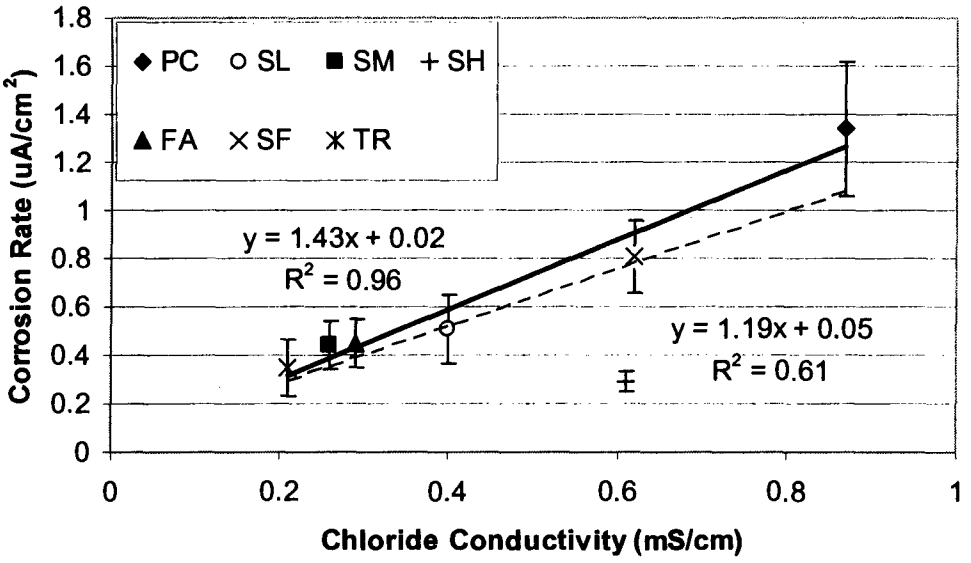

Fig 6.7: Relationship between chloride conductivity and corrosion rate

The dashed trend line is based on all the samples and shows only a moderate degree of correlation between corrosion rate and chloride conductivity. If the SH sample is excluded however then there is very good agreement (correlation coefficient = 0.96) between the corrosion rate and chloride conductivity. The error bars representing one standard deviation for each binder type are also shown in Figure 6.7. The average standard deviation, expressed as a percentage of the corrosion rate, was ± 23%. There is therefore reasonable confidence in the accuracy of this relationship between corrosion rate and chloride conductivity. It is therefore possible to make predictions not only about the initiation period as determined by diffusion of the chlorides but also the propagation period with knowledge of corrosion rates coupled with an appropriate damage model.

Conductivity is the inverse of resistivity. The differences between the chloride conductivity and measured resistivity values are due to conditioning and age of the samples.

The chloride conductivity results were obtained after they were continuously water cured, dried and then vacuum saturated with a NaCl solution. The resistivity measurements were taken on the actual corrosion specimens and after a period of drying. It was noted in section 6.2.3 that with the resistivity measurements a dense concrete and porous concrete could both show the same resistivity under certain environmental conditions. Preconditioning of the samples for use in chloride conductivity measurements prevents this and provides a better representation of the micro-structural properties of the material. Other limitations of the specimen resistivity values, as determined in this investigation, include: edge effects, size of the sample and the preferential movement of current along the steel. The chloride conductivity samples suffer from none of these defects. The use of 5M NaCl in the preconditioning does however result in an artificial environment but all the samples are subject to the same environment and this provides a reasonable means of comparison. Furthermore the attempt to correlate the influence of cement extenders on corrosion rates with durability index and resistivity values has been based on empirical observations.

The inclusion of slag at replacement levels of 25% and 50% showed consistent improvements over the PC control sample with respect to chloride conductivity, resistivity and corrosion rate. A 75% slag replacement resulted in a substantial increase in the chloride conductivity value similar to SF despite having a corrosion rate almost 1/3 that of SF. The decrease in corrosion rate continued with increasing slag concentrations but the chloride conductivity did not follow this same trend. The water sorptivity and oxygen permeability values reveal a more open microstructure compared to PC and thus a higher chloride conductivity value would have been expected rather than one lower than PC or SF. The known ability of slag concrete to bind chloride ions, as shown by Glass et al. (1997), may account for the improved performance in the chloride conductivity test. The bound chlorides would have resulted in some degree of pore blockage thus lowering the overall conductivity of the samples. The chloride binding effects coupled with high resistivity of SH concrete during the drying period would have resulted in the observed low corrosion rates despite the generally poor performance characterization of the material.

The following section will further develop the relationship between chloride conductivity and corrosion rate to form the basis of an overall corrosion prediction model.

6.2.5 Corrosion Rate Prediction Model

The basic relationship between corrosion rate and chloride conductivity shown in Figure 6.7 has been modified to account for increase in chloride conductivity value with the inclusion

of slag between replacement levels of 50% and 75%, equation 6.1. As was noted in section 6.2.4, the average standard deviation of the corrosion rate upon which equation 6.1 is based is ±23%. The equation is applicable, through the slag correction factor (*f*), for the range of slag replacement from 25% to 75% as studied in this investigation. The exact point at which chloride conductivity starts to increase with increasing slag concentration has not been determined. The chloride conductivity values were therefore assumed to vary linearly between the 50% and 75% replacement levels to produce an overall corrosion rate consistent with observed data.

$$i_{corr} = 1.43\frac{C_{c,90}}{f} + 0.02 \qquad \ldots 6.1$$

where:

f - slag correction factor $= 10^{(|0.5-S|-0.5+S)}$

i_{corr} - corrosion rate $\mu A/cm^2$

$C_{c,90}$ - chloride conductivity value (mS/cm) at 90 days

S - slag concentration expressed as a decimal percentage (ie 0.75 for 75%)

The chloride conductivity values themselves have not been corrected but rather the numerical relationship between corrosion rate and chloride conductivity is modified to account for the change in material properties associated with increasing the slag concentration above 50%. These changes, as noted in this chapter, result in a lower corrosion rate despite a higher chloride conductivity value and more open structure. The equation provides a correlation coefficient of 0.96 and should be representative for samples with replacement levels of extenders up to those measured: Slag up to 75%, FA to 30%, SF to 7% and a ternary blend of PC:Slag:SF corresponding to 50:43:7. The slag concentration of the FA, SF and PC samples is zero and would be entered as such into equation 6.1. Equation 6.1 is a representation of a linear relationship between chloride conductivity measured at 90 days and the average corrosion rates for 40 mm cover with crack widths between 0.2 and 0.7 mm.

The decrease of cover depth from 40 to 20 mm was shown to have a minor impact upon corrosion rates for the blended materials. The decrease in cover depth however resulted in a significant increase in corrosion for the PC control sample. It was suggested in chapter 5 and here in chapter 6 that different response of the materials to the decrease in cover was partially a result of drying and the availability of oxygen at the lower cover depths. The low resistivity, and associated chloride conductivity, permitted a moderate to high corrosion rate at cover

depths of 40 mm. A decrease in the cover permitted faster drying near the steel and the availability of oxygen increased. Due to the low resistivity even in moderately dry concrete the corrosion rate increased in accordance with the availability of oxygen. The blended cement concretes had corrosion rates which were limited by the resistivity of the concrete such that increases in the availability of oxygen at the lower depth had little impact upon the corrosion rate. The relationship between cover depth and corrosion rate can be seen in Figure 6.8.

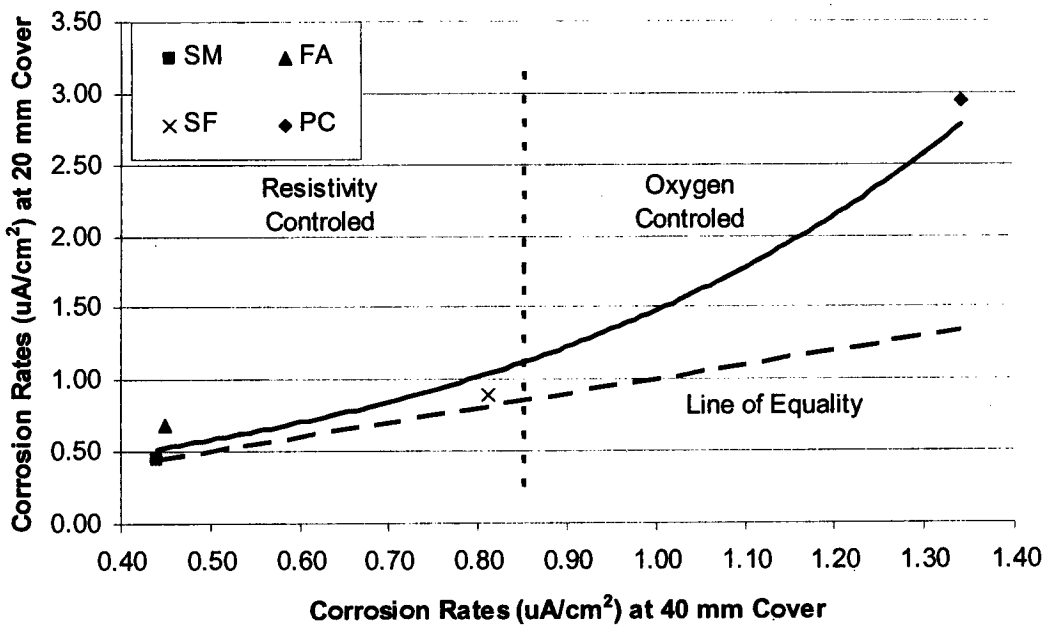

Fig 6.8: Relationship between measured corrosion rates at 40 mm cover and 20 mm cover

Figure 6.8 was based on the samples PC, SM, FA and SF as these were the only ones that had both 20 mm and 40 mm cover depth. In the initial investigation for steel in cracked concrete at cover depths of 20 mm no specimens were cast for SL, SH and TR. These mix designs, SL, SH and TR, would likely follow the same pattern but no experimental data is available. From Figure 6.6 it is evident that at low corrosion rates there was very little effect from the change in cover. As the corrosion rates increased cover was shown to have more substantial impact upon corrosion rate. The portion of the curve up to SF (0.81 $\mu A/cm^2$) at 40 mm cover represents that region which is dominated by resistivity considerations while the area beyond this represents a transition from resistivity control to oxygen control demonstrated by the PC sample. Further research would be required to reproduce the possible range of corrosion rates between SF and PC either through changes to the w/c ratio or small

additions of cement extenders, such as 5 to 15% replacement of FA or slag. This was however beyond the scope of the current investigation. The effects of cover on corrosion rate are provided as follows and are shown graphically in Figure 6.9:

$$i_{corr} = \left(1.43\frac{C_{c,90}}{f} + 0.02\right) e^{\left[\left(\frac{40-x}{20}\right)1.2\left(\frac{C_{c,90}}{f}\right)^3\right]} \quad \ldots 6.2$$

where:

x - is the cover depth (mm) between 20 and 40 mm

Equation 6.2 provides for modification of corrosion rates, given in equation 6.1, to account for variations in cover depth between 20 and 40 mm. Further investigations would be required to extend this beyond the current range to include greater cover depths.

Chloride conductivity values, as used in equations 6.1 and 6.2, provide a reasonable means of assessing the corrosion performance of reinforced concrete. The other durability index values such as water sorptivity or OPI are useful for classifying the material. However, under the situation of relatively short wetting periods compared with drying, as might be observed in the splash zone, the chloride conductivity and resistivity of the concrete are the primary influences on corrosion rate. The impact of oxygen availability, particularly for PC samples, is implicitly taken into account by means of the corrosion rate adjustment for cover depth.

The chemical effects, which appeared quite significant in the aqueous phase work and were confirmed under passive conditions, were inconsequential in the case of cracked concrete under the environmental conditions of this investigation. Sulphides would still likely lead to higher corrosion rates, than would be observed in their absence, but the effects of high resistivity (low chloride conductivity) associated with the inclusion of slag outweighed their negative influence. The corrosion rates of the various binder types under saturated conditions would represent a small range of possible values and the individual effects of pore water chemistry may be more evident. The current information does however make it possible to estimate the remaining service life of a structure once corrosion has begun, and an example will be provided in section 6.4 after a brief review of some existing damage models.

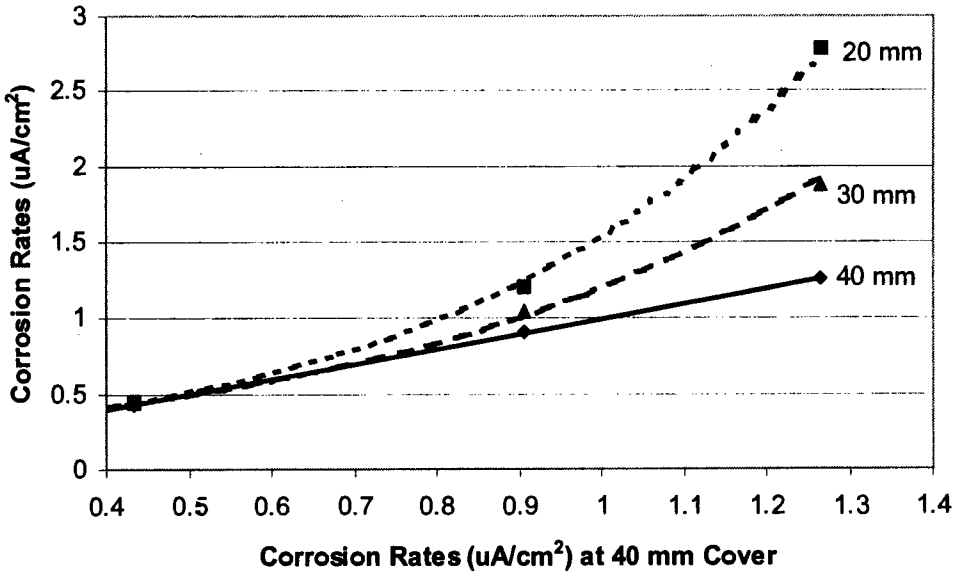

Fig 6.9: Relationship between corrosion rate and cover based on equation 6.2

The corrosion rates predicted by equation 6.2 were derived from the combined average values of 0.2 and 0.7 mm crack widths. As there is great difficulty in precisely defining cracks a combined average value was chosen particularly since other effects such as the presence of cement extenders had a far greater impact than the crack width.

6.3 Time to Cracking Models

The useful service life of a structure is difficult to accurately define as there are many possible interpretations of service life. Ferry and Flanagan (1991) for instance have identified five components of the life of an asset:

1. Functional Life - the period of time over which the need for the asset is anticipated.
2. Physical Life - the period of time over which the asset is expected to last physically, the period of time from installation until final disposal.
3. Technological life - the period until technical obsolescence dictates the replacement due to technically superior alternatives.
4. Social and Legal Life - the period until human desire or legal requirements dictate replacement; the expiry of leasehold or substantial upgrades or disposal required by law.
5. Economic Life - the period of time until economic obsolescence dictates replacement with a lower cost alternative.

Equally difficult is the definition of unacceptable deterioration of the structure and what constitutes the end of its life. Many structures can adequately perform their structural or load

carrying capacity many years after their general appearance would suggest otherwise. Andrade and Alonso (1996) list the three components of the residual life of a corroding structure as: a) loss of cross section, b) the time to cracking, c) the gradual loss of steel/concrete bond. Figure 6.10 shows the residual life of a structure based on percentage reduction of the cross section area for various corrosion rates.

The end of the service life of the structure is associated with a loss of cross sectional area between 5% and 25%. The design of a structure is obviously dependant upon the various national codes which govern design and construction from one country to another but there is generally quite a large safety factor built into the calculations to accommodate variations in material properties, construction and loading. These safety factors will effectively accommodate a certain loss in cross sectional area and bonding. A loss of cross section between 5% and 25% may therefore provide one reasonable estimate for the end of a structure's service life.

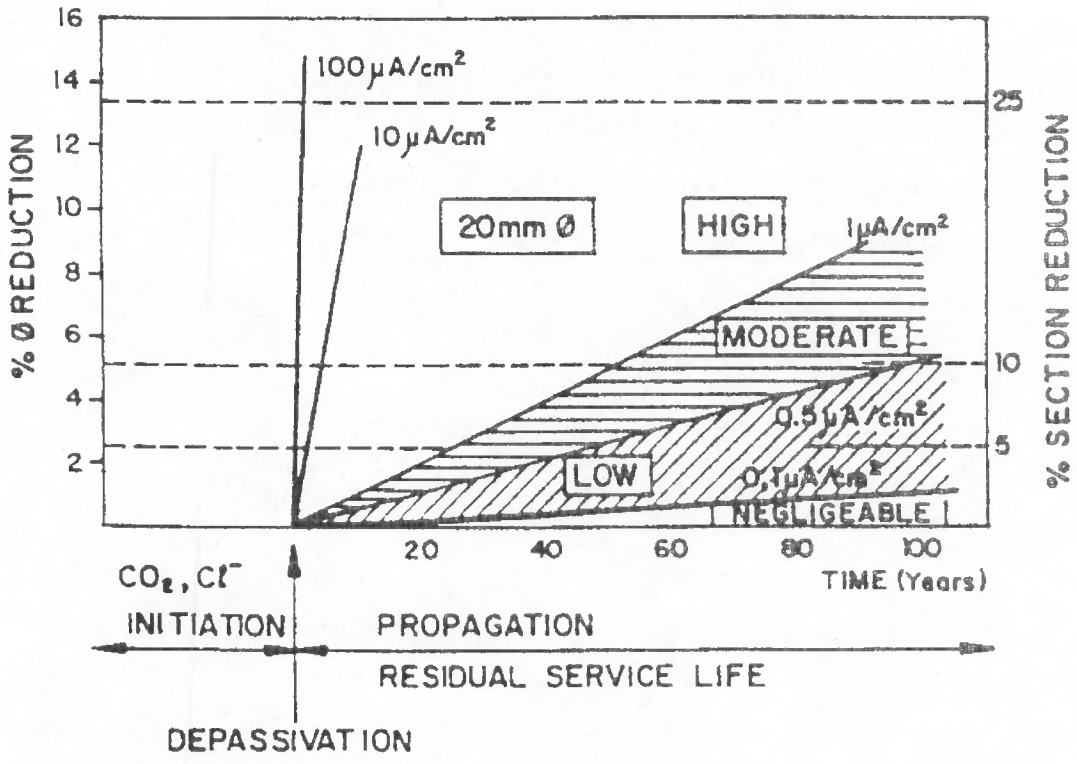

Fig 6.10: Residual service life based on loss of cross-sectional area (Andrade and Alonso, 1996)

One of the alternatives, as given by Andrade and Alonso (1996), to the loss of cross sectional area is the onset of cracking. Small cracks which result from reinforcing corrosion

are unlikely to cause significant structural problems in and of themselves. Corrosion cracks, unlike service cracks, run longitudinal with the steel and may allow for a significant acceleration of the corrosion rate as the steel is more directly exposed to the atmosphere and the ability of the cement extenders to afford protection is reduced. Thus the onset of corrosion-induced cracking may also provide a reasonable, though conservative, estimate to the end of a structure's life. Furthermore the spalling of concrete can pose a safety risk to those operating below the structure.

The relationship between corrosion rate and loss of cross section is based on Faraday's Law which states (modified from Stansbury and Buchanan, 2000):

$$m = \frac{I\,t\,M}{zF} \qquad \ldots 6.3$$

where:

m - is the mass of metal entering solution (g)

M - is the atomic mass (g/mol)

I - is the corrosion current (A)

z - is the number of equivalents (oxidation state)

F - Faraday's constant 96,500 C/mol

Faraday's law provides the relationship between mass loss and corrosion rate. The mass loss can be converted to a rate of penetration according to (modified from Stansbury and Buchanan 2000):

$$r = \frac{Mi_{corr}}{z\rho F} \qquad \ldots 6.4$$

where:

r - is the rate of penetration (assuming uniform corrosion) in cm/s

i_{corr} - is the corrosion current density (A/cm^2)

ρ - is the material density (g/cm^3)

The results from equation 6.4 indicate that a corrosion current density of 1 μA/cm^2 results in a penetration rate of approximately 11.5 μm/year. From the penetration rate it is easy to determine the loss of cross section or percentage reduction and thereby estimate the remaining service life depending on the end point which has been chosen. The principle of using loss of cross section or penetration rate allows for the estimation of the time until cracking as a result of the mass transformation of iron to its respective oxides.

6.3.1 Cracking of Concrete

Cracking of concrete is caused by the expansive pressures in the concrete associated with the formation of various iron oxides. There are numerous approaches to examining the expansive pressures associated with the corrosion of steel. Li et al. (1998) have summarized the deterioration mechanisms with respect to the tensile forces produced in the concrete at the steel/concrete interface. Consider a bar of steel embedded in concrete as shown in Figure 6.11.

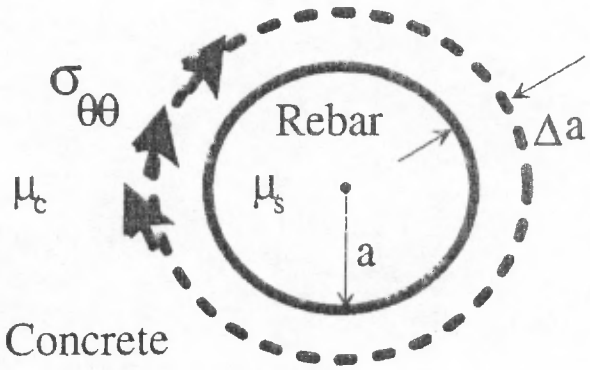

Fig 6.11: Stresses caused by reinforcing corrosion products in an unbounded medium (Li et al., 1998)

If the rebar of radius a is allowed to freely corrode it will expand by Δa which accounts for both the reduction in radius of uncorroded steel and expansion associated with the corrosion products. If the steel were placed back in the concrete, the displacement of the concrete caused by the internal pressure would be:

$$U_r^c = \frac{pa}{2\mu_c} \qquad \ldots 6.5$$

and the displacement of the steel would be:

$$U_r^s = \frac{-p(k-1)a}{4\mu_s} \qquad \ldots 6.6$$

where:

- p - is the pressure
- a - is the radius of the hole
- μ_c - the shear modulus of the concrete
- μ_s - the shear modulus of the steel
- k - is the Kolosov constant

The Kolosov constants are given as follows:

$$K = \frac{3-\nu}{1+\nu} \quad \text{for plane stress} \qquad \ldots 6.7$$

$$K = 3-4\nu \quad \text{for plane strain} \qquad \ldots 6.8$$

where:

ν - is the Poisson's ratio

Compatibility requires:

$$\left|U_r^c\right| + \left|U_r^s\right| = \Delta a \qquad \ldots 6.9$$

The stress produced in the surrounding concrete interface is therefore given as:

$$\sigma_{\theta\theta} = \frac{4\mu_s\mu_c}{2\mu_s + (k_s - 1)\mu_c}\frac{\Delta a}{a}$$

$$= C\frac{\Delta a}{a} \qquad \ldots 6.10$$

where:

$\sigma_{\theta\theta}$ - is the shear stress produced at the interface

Li et al. (1998) provide the shear modulus and Kolosov constant for steel as 81 GPa and 2 respectively with the shear modulus for concrete approximately 12 GPa, and C is therefore approximately 2.23×10^{10}. For a radial strain of 0.0001 a stress of 2.23 MPa is produced in the concrete which is sufficient to cause micro-cracking of the concrete. The previous analysis assumes an unbounded concrete such that cover effects are not included. The model is therefore useful from an initiation of damage perspective but does not provide a time to the appearance of surface cracking. Beeby (1978) has also suggested quite a simple approach to damage modeling with 0.02% reduction of the cross sectional area necessary to produce tangential strains at the bar-concrete interface of the same order as the tensile capacity of concrete.

The determination of a critical mass of corrosion product required to induce cracking that would account for the material properties of the concrete, steel and corrosion products, in addition to rebar diameter and cover was investigated by Liu and Weyers (1998). A detailed description of the model and its development can be found in Liu and Weyers (1998), Weyers (1998), and Liu (1996) and will be summarized as follows:

$$W_{crit} = \rho_{rust}\left(\pi(d_s + d_o)D + \frac{W_{st}}{\rho_{st}}\right) \qquad \ldots 6.11$$

where:

W_{crit} - critical mass of corrosion product required to induce cracking

W_{st} - amount of steel corroded = αW_{crit}

d_s - thickness of corrosion product necessary to generate tensile stresses

$$= \frac{Cf_t'}{E_{ef}}\left(\frac{a^2+b^2}{b^2-a^2}+\nu_c\right)$$

α - molecular weight of steel divided by molecular weight of corrosion product

$\alpha = 0.523$ for $Fe(OH)_3$ and 0.622 for $Fe(OH)_2$

ρ_{rust} - density of corrosion product

ρ_{st} - density of steel

d_o - thickness of pore band (interfacial transition zone) around steel concrete interface

C - cover depth of concrete

f_t' - tensile strength of concrete

D - diameter of reinforcing

a $= (D+2d_o)/2$

b $= C+(D+2d_o)/2$

E_{ft} $= E_c/(1+\varphi_{cr})$

E_c - elastic modulus of concrete

φ_{cr} - creep coefficient of concrete

ν_c - Poisson's ratio for concrete

The time to cracking is related to the critical mass of corrosion product and corrosion rate by the equation:

$$t_{cr} = \frac{W_{crit}^2}{2k_p} \qquad \ldots 6.12$$

where:

t_{cr} - time to cracking (years)

k_p $= 0.098(1/\alpha)\pi D i_{cor}$

i_{cor} - corrosion current density (mA/ft^2)

The use of equations 6.11 and 6.12 requires extensive knowledge of the material properties but, provided all the information is available, should produce an estimate of the amount of corrosion product required to induce cracking and the time to cracking. The cracking model of

Liu and Weyers was not independently verified in this investigation as the primary focus was the determination of influence of binder type on the corrosion of steel in concrete. The model does however provide an option for relating corrosion rates to degree of damage and time to cracking. Liu and Weyers (1998) have shown an increase in the mass of rust required to induce cracking for increase in cover depth from 27 mm to 70 mm. Figure 6.12 is based on average results for time to cracking presented by Liu and Weyers and converted to a critical depth of penetration for 16 mm diameter bar. The critical depth of penetration is the amount of metal loss, expressed in μm of the rebar diameter, required to initiate cracking of the concrete.

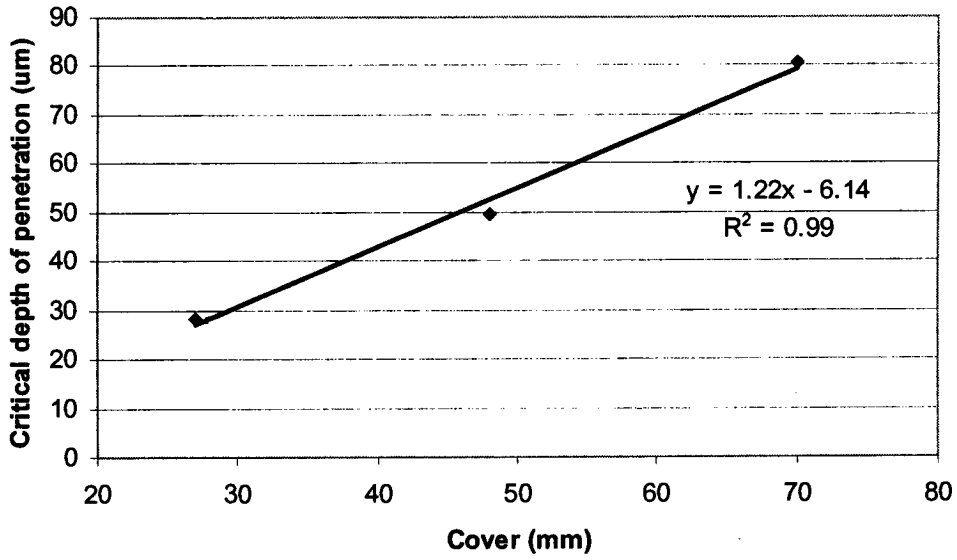

Fig 6.12: Relationship between critical depth of penetration of 16 mm diameter bar and concrete cover (based on results taken from Liu and Weyers, 1998).

An increase in the reinforcement cover depth required a greater degree of corrosion product to produce cracking at the surface of the concrete. The increase in critical depth of penetration with cover implies a greater period of time before damage becomes apparent as the cover depth increases for a given rate of corrosion. Increasing the cover depth from 30 mm to 60 mm would change the time from the first appearance of surface cracking from 2.6 years to 5.8 years assuming a uniform corrosion rate of 11.5 μm/year loss of rebar cross section. An increase in cover however, would result in lower corrosion rate thus further delaying the onset of cracking.

The determination of the time to cracking was partially based on knowledge of the composition of the corrosion products through the variable α. Suda et al. (1993) found the rust

products in concrete were only 30% crystalline magnetite, goethite and lepidocrocite compared to 45% for exposed steel in marine environments. The result is a volumetric expansion of corrosion products compared to original material between 3.0 and 3.2. According to their finite element investigation, the degree of critical corrosion to produce cracking was found to be only 2 mg/cm^2 for a 20mm bar with 40 mm cover. The amount of corrosion necessary to induce cracking will clearly be affected by the volumetric expansion of the corrosion product as shown in the work of Suda et al. (1993). The use of different cement extenders has been shown to affect the oxygen permeability of the concrete and would therefore likely affect the formation of the corrosion products. The use of cement extenders may result in corrosion products deficient in oxygen with less expansive pressures exerted on the concrete and thereby retarding the cracking mechanism. This information was not studied in the current investigation and further research would be required to provide specific knowledge for the various cement extenders under consideration. Marcotte and Hansson (1998) for instance have shown differences in the corrosion products associated with high performance concrete compared to standard industrial concrete. More work is still need to accurately quantify these variables if models similar to those proposed by Liu and Weyers are to be truly effective in predicting time to cracking.

Alonso et al. (1998) conducted an empirical examination of the influence of cover to diameter ratio, concrete quality and corrosion rate on the relationship between cracking and corrosion penetration. The approach was fairly simple but provides a basis for estimating the amount of corrosion in loss of cross section necessary to induce cracking and, by extension, the time to first cracking. The correlation coefficient of 0.92 for the relationship between corrosion penetration and cover/diameter ratio illustrates the usefulness of such an approach from an engineering perspective and is given in equation 6.13 as follows:

$$X_o = a + b\ c/\phi \qquad \ldots 6.13$$

where:

X_o - is the depth of penetration into steel rebar (μm)

a,b - regression coefficients = 7.53 and 9.32 respectively

c/Φ - cover to diameter ratio

The critical depth of penetration would produce a crack of width 0.05 mm on the surface of the concrete. According to equation 6.13, from Alonso et al. (1998), a 16 mm rebar with 40 mm cover would require a critical depth of penetration of 30.8 μm compared to 42.7 μm as taken from the results by Liu and Weyers (1998). Alonso et al. (1998) have also shown that

the size of the crack is proportional to the depth of penetration such that a crack width between 0.2 and 0.3 mm would require a penetration between 50 and 200 μm.

The density and quality of the concrete was found to have an inverse effect on the degree of corrosion required to induce cracking. Alonso et al. (1998) showed that an increase in w/c ratio and hence porosity delayed the onset of visible cracking. The higher degree of pore voids accommodated the corrosion product and retarded the development of expansive pressures. A dense concrete while slowing the actual rate of corrosion means less corrosion product is needed to produce cracking. An increase in w/c ratio from 0.52 to 0.65 for 370 kg/m^3 of cement was shown to have a fairly minor impact on the critical penetration depth while the same increase in w/c ratio for 270 kg/m^3 cement resulted in a substantial increase in the penetration depth needed to induce cracking (approximately 150 μm compared to 100 μm for 0.2 mm surface crack for w/c 0.52 and 0.65 respectively).

For the purposes of comparison in the current investigation a critical penetration depth of 30.8 μm will be chosen for the 16 mm diameter bars at 40 mm cover depth and 19.2 μm for the bars at 20 mm, based on equation 6.13, for all samples. The choice of the critical penetration depth should result in the initial appearance of surface cracking according to Alonso et al. (1998).

It is clear from the durability index values and strength data presented in chapter 5 that the material characteristics of the various concretes are different. The 28 day strengths as reproduced in Table 6.2 show similar results for most of the samples, except SH, though differences still do exist.

Table 6.2: Strength (MPa) results for 100 mm cubes (w/c = 0.58)

Mix	*Age (days)*		
Design	*28*	*56*	*90*
PC	47	53	60
SL	43	51	53
SM	43	47	48
SH	28	33	35
FA	42	51	57
SF	50	52	56
TR	47	52	57

The lower strengths of the slag bearing samples do not necessarily imply a more open pore structure as the durability indexes usually showed improved performances. SH which apparently had the most open pore structure, based on OPI and water sorptivity values, was

also found to have the lowest corrosion rate. The corrosion products that did form would likely be able to diffuse away from the rebar and thus limit the expansion pressure. SH would require a greater degree of corrosion product to produce cracking which should result in a prolonged propagation period compared to the other samples. The exact interaction however would have to be studied and validated by experimental means to determine the true effect of the cement extenders on the cracking process. In the absence of this information it is reasonable to use the chosen critical corrosion depth values of 30.8 μm and 19.2 μm (40 mm and 20 mm cover depths respectively) for comparing the influence of cement extenders on the propagation period based on the corrosion rates established in chapter 5.

6.4 Service Life Model

The corrosion rate prediction model, based on adjusted chloride conductivity values for slag concentrations above 50%, can now be used in conjunction with one of the crack propagation models to determine the time to visible cracking for concrete made with various cement extenders. In concrete which does not exhibit service cracking, the influence of chloride threshold value will significantly affect the overall life of a structure. The initiation period is considered to be that time until active corrosion begins. With chloride threshold levels from 0.08 to 0.53 percent by mass of cement, section 5.8, there is clearly a considerable variation in possible values. The lower measured chloride threshold values associated with the inclusion of cement extenders however are usually more than offset by the increased time required for the chloride ions to diffuse to the level of steel and the subsequent rate of active corrosion.

6.4.1 Initiation Period

There has been considerable work in modeling chloride transport through concrete (Glass and Buenfeld 2000, Konin et al. 1998 and Sergi et al. 1992). The transport of chlorides through uncracked concrete can generally be represented by Fick's second law of diffusion (Mackechnie 1996):

$$C_x = C_s\left[1 - erf\left(\frac{x}{2\sqrt{D_c t}}\right)\right] \qquad \ldots 6.14$$

Where:

x - depth

t - time

C_s - surface concentration of chlorides

C_x - chloride concentration at depth x

D_c - diffusion coefficient

erf - error function

The variables for determining the rate of chloride penetration used in the following example, as shown in Table 6.3, are based on values given by Mackechnie (2001) and are representative of materials commonly employed in South Africa. The values for the SF are based on 10% replacement and not 7% as used in the current study but for the purposes of discussion should provide satisfactory results. The diffusion coefficients have been modified to account for changes with time and are representative of very severe exposure conditions. Mackechnie (2001) has defined very severe exposure to be one in which the 'structure is exposed directly to sea water under sheltered conditions with little wave action'. The chloride threshold values are those determined in the current investigation.

Table 6.3: Variables for determination of time to corrosion initiation

Sample	*Chloride Threshold (% mass of cement)*	*Diffusion Coefficient ($x10^{-8}$ cm^2/s)*	*$Chloride^-$ Surface Conc. (% mass of cement)*
PC	0 53	1.40	2.0
SM	0 08	0.27	3.0
FA	0 36	0.36	2.5
SF	0 51	1.33	1.5

Mackechnie's (2001) diffusion model has been used to estimate the time to corrosion initiation based on the chloride threshold values determined in this investigation. There is considerable variation in the range of possible chloride thresholds for a given binder type. It is difficult, or rather impossible, to say with any certainty that there is a uniquely defined chloride threshold value. It is more likely that there is a certain probability range of chloride concentrations over which corrosion is likely to be initiated. Due to limitations in the number of samples in the current investigation it was not prudent to provide such statistically significant range. The individual chloride threshold concentrations provided are representative of values likely to be encountered and should be viewed as such.

It can be seen in Figure 6.13 that the inclusion of SM still delays the initiation of corrosion due to the reduced diffusion of chloride ions despite having a chloride threshold concentration of 0.08 compared to 0.53 (% by mass of cement) for PC.

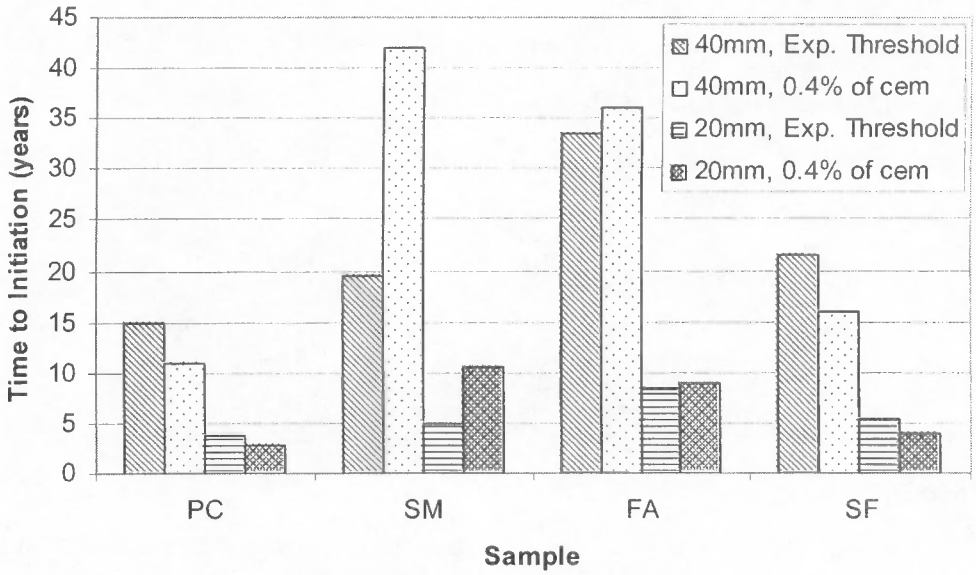

Fig 6.13: Time to corrosion initiation for 40 and 20 mm cover samples based on measured chloride thresholds and a constant 0.4% by mass of cement.

Using the measured values FA would have the longest corrosion free period of 34 years compared to 15 years for PC for a 40 mm cover depth.

If the conventional chloride threshold of 0.4% by mass of cement is assumed, the slag bearing materials show the greatest improvement. Not accounting for the possible differences in chloride threshold concentration can seriously over-estimate the onset to corrosion of a structure. Using the observed chloride threshold values compared to 0.4% results in a 52% reduction in initiation period for SM and a 36% increase in initiation period for PC. The time to corrosion initiation is still longer by including both slag and FA but not exactly what one would expect based on a uniform chloride threshold, as shown in Table 6.4.

Table 6.4: Percentage change in time (years) to corrosion initiation for 40 mm cover using measured binder specific chloride thresholds compared to constant 0.4%

Sample	*Binder specific*	*Constant*	*% change*
PC	15	11	+36
SM	20	42	-52
FA	34	36	-6
SF	22	16	+38

The chloride diffusion values provided by Mackechnie (2001) were used in the previous example but any appropriate chloride ingress model could be used in combination with

chloride threshold values. Care must also be taken in deciding which chloride threshold values are to be employed as there is a considerable range and disagreement in the literature for what are nominally the same materials. As noted in chapter 4 and 5 the chloride threshold values were variable for aqueous and solid phase studies. The process of corrosion initiation is less precisely definable than the rate at which corrosion occurs. Further study with a greater quantity of samples is necessary to confidently define the chloride threshold values. Some form of accounting for the variations in critical chloride concentration is however essential for a meaningful estimate of the initiation period.

6.4.2 Propagation Period

It was shown in chapter 5 that corrosion in cracked concrete initiated almost immediately after exposure to ponding with salt water. The chloride threshold concentration had been exceeded for all samples almost immediately and therefore the initiation period is essentially negligible. Variations in chloride threshold concentration under conditions of cracked concrete are therefore meaningless. It is from this standpoint that the comparison of the effectiveness of cement extenders in prolonging the life of a structure will now be considered. A loss of cross sectional radius due to corrosion of 30.8 μm for a 40 mm cover will be used as the end of service life, or more accurately the point at which major surface damage to the structure is likely to commence.

The choice of 30.8 μm for a 40 mm cover was based on the work of Alonso et al. (1998) and corresponds to the first appearance of surface cracking due to the expansive pressures of the corrosion products. The time to surface cracking from the onset of the propagation period for the various binder types is presented in Table 6.5. For comparative purposes the time to a loss of 5% cross sectional area of the rebar is also included. It should again be emphasized that the individual concrete types are likely to result in variations to the composition of the corrosion product which may alter the expansive pressure experienced by the concrete. More importantly the mechanics of the crack growth will vary with the specific material properties of the concrete. Furthermore the presence of an initial service crack will also affect subsequent crack development. If the end of service life is considered to be the onset of visible surface cracking due to corrosion then there is little remaining service life once the chlorides have reached the steel in sufficient concentration. The PC and SF samples provide three years or less additional protection while the use of FA adds 6 years with greatest extension of the service life accorded by SH at approximately 9 years.

Table 6.5: Predicted corrosion rates and time to cracking and loss of cross sectional area for 40 mm cover based on chloride conductivity data

Sample	*Chloride Conductivity 90 day (mS/cm)*	*Rate* ($\mu A/cm^2$)	($\mu m/yr$)	*Time (years) to* *Cracking*	*Loss of 5% Area*
PC	0.87	1.26	14.5	2.1	14
SL	0.4	0.59	6.8	4.5	30
SM	0.26	0.39	4.5	6.8	45
SH	0.61	0.30	3.4	9.1	59
FA	0.29	0.43	5.0	6.2	41
SF	0.62	0.91	10.4	3.0	19
TR	0.21	0.32	3.7	8.4	55

If the end of service life were considered to be a 5% decrease in the cross sectional area of the rebar, the extension to the service life of a structure is quite substantial with the inclusion of cement extenders, 41 years for FA compared to just 14 for PC with even greater gains associated with SM, SH and TR. Figure 6.14 shows the time to cracking (0.8% loss of cross sectional area) and time to loss of 5% cross sectional area for the different binder types.

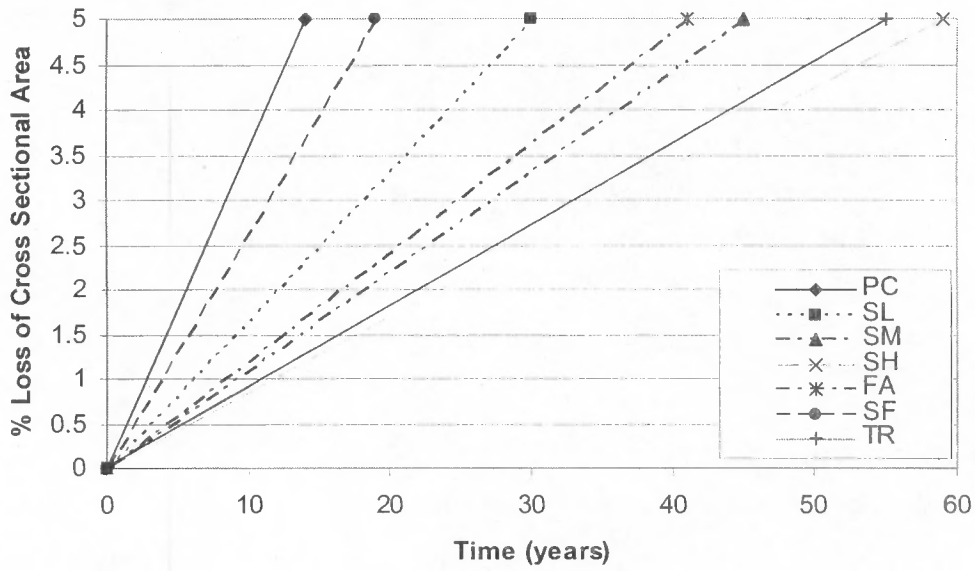

Fig 6.14: Time to loss of cross sectional area for 16 mm rebar at 40 mm cover

The time to the loss of any amount of cross sectional area for any of the mix designs studied can be determined from Figure 6.14. The corrosion rates are based on measured chloride conductivity values, calculated according to equation 6.2. The time to appearance of cracking is associated with a 0.8% (30.8 μm loss of radius) loss of cross sectional area. It should again be stressed that the corrosion rates are assumed to be constant over the period and are based

on the average stable rates as provided in section 5.10. It took approximate 26 to 48 weeks for the corrosion rates to stabilize and this gradual increase in corrosion rate is not shown in either Table 6.5 or Figure 6.14 and represents a conservative assumption with respect to service life of the structure.

A reduction in cover from 40 mm to 20 mm can have a profound effect on the time to cracking as shown in Figure 6.15. The reduction in cover results in accelerated corrosion rates thus producing corrosion products and expansive pressures at a faster rate. The lower cover to reinforcement also requires a small amount of corrosion product (loss of cross section) to produce cracking.

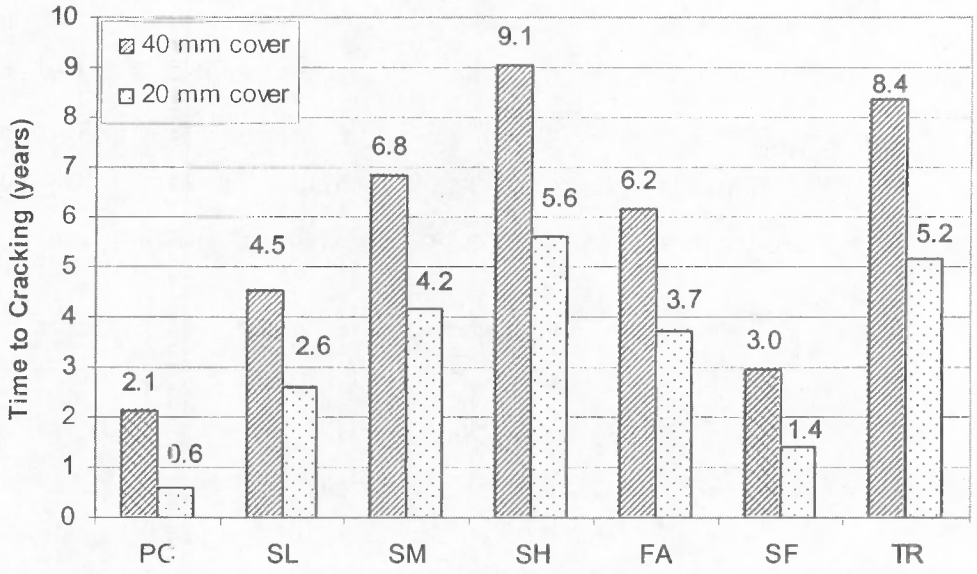

Fig 6.15: Effect of cover depth on time to cracking

The results of a reduction in cover are most significant for PC due to its dependence of corrosion rate on cover depth. Similarly PC would benefit the most from an increase in cover depths above 40 mm. No information however was obtained for cover depths greater than 40 mm in this investigation.

6.4.3 Combined Service Life Effects

Combining the initiation and propagation models provides for an estimate of the overall service life of a structure. As noted in section 6.4.2, under conditions of service cracking, there is essentially no initiation period as the chloride quickly penetrates to the depth of the steel in sufficient concentration to cause active corrosion. For the case of sound uncracked concrete both the initiation period, i.e. the time taken for chlorides to reach the steel in

sufficient concentration to induce active corrosion, and the propagation period, during which corrosion eventually lead to physical deterioration, can be combined to give an estimate of the service life of a structure. The propagation portion of the service life model uses corrosion rates determined for the case of service cracked concrete. The corrosion rates represent a maximum likely rate associated with each binder type. It is probable that with sufficient time and ingress of chloride ions the corrosion rate in sound uncracked concrete would approach the measured binder-specific rates and certainly, once cracking due to expansive pressures of the corrosion products resulted, the corrosion rates would match or exceed those measured for service cracked concrete. A further limitation of the model is the assumption that no initial corrosion occurs until the chloride threshold is reached and then suddenly the measured binder-specific corrosion rate is used to calculate the degree of damage, expressed as loss of cross section. Under real conditions in uncracked concrete it would take some time for the corrosion rates to shift from the passive values to the maximum measured rates under active conditions. The use of the maximum binder-specific corrosion rate represents a conservative assumption and in the absence of further information should provide an estimate of propagation period.

The longest time to corrosion initiation for uncracked concrete was provided by FA for the case of chloride threshold concentrations based on those determined in this investigation. A coupling of the prediction model for chloride ingress and time to cracking shows FA provided the longest service life, by a factor of 1.5 compared to the next best option (SM), based on time to first appearance of surface cracking. If some degree of surface cracking was considered acceptable and a more liberal 5% loss of cross section associated with the end of service life, then FA continues to provide the greatest long term protection due to the corrosion inhibiting effects of the materials. If a 5% loss of cross section is considered the end of service life, then the benefits of SM approach those of FA. The use of FA results in a gain of 10 years compared to SM, 34 years compared to SF and 46 years compared to PC. The combined effects of initiation and propagation periods are shown in Figure 6.16.

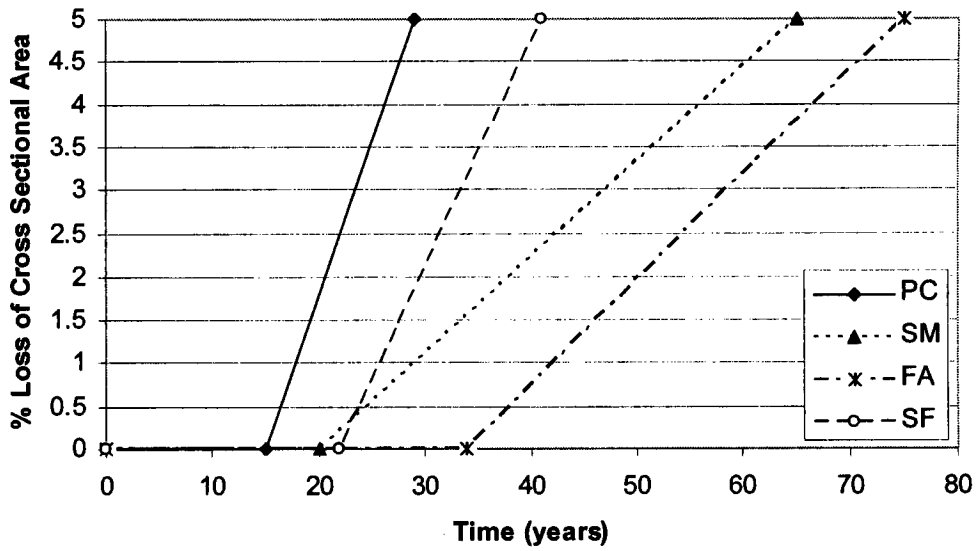

Fig 6.16: Service life modeling based on binder specific chloride thresholds and corrosion rates for 40 mm cover.

The high apparent chloride threshold value and moderate diffusion coefficient resulted in SF having the longest time to cracking despite the relatively high corrosion rate. If service cracking is likely to occur, all the gains associated with the use of cement extenders during the initiation period are removed and only their effects on controlling the corrosion rate are of importance. In this regard Figure 6.14 provides the best comparison of the protection accorded by the use of cement extenders with SH having the least damage due to reinforcing corrosion. It should be noted however that a 75% replacement of PC by slag is considerably higher than would be used in practice and TR or SM would be the most beneficial practical mix designs.

6.5 General Conclusion

A summary of the main conclusions from the individual components of this investigation were provided in section 6.1. The primary objective of this work was the investigation of the effects of cement extenders on the corrosion rates of steel in concrete. In order to more fully understand the corrosion process and factors affecting the rate of corrosion it was necessary to first examine the pore solution chemistry of concrete. Pore solution chemistry was examined through the expression of solution from samples of cement paste corresponding to the proportions for mix designs of PC, SL, SM, SH, FA, SF and TR at a w/c ratio of 0.58. The examination of the solution chemistry revealed a significant dependence of the hydroxide

concentration on binder type, such that PC had the highest concentration of hydroxides and SF the lowest. The hydroxide concentration is important from the standpoint of chloride threshold concentration and corrosion rate. All pore solutions had sufficient hydroxyl concentration to ensure adequate passivation of steel reinforcing.

Another important aspect of the chemistry of the pore solution was the determination of sulphide and thiosulphate concentration and their impact upon the dissolved oxygen content. Appreciable levels of sulphides and thiosulphate were found in the samples containing slag. The sulphide concentration was not constant with time but varied over the 90 day study period. The break-point of a 75% replacement of slag affecting sulphur chemistry, as suggested by Angus and Glasser (1985), was not observed with the materials used in this investigation. Redox potentials more than 200 mv negative to PC were observed for 25% replacement by slag. The inclusion of slag at replacement levels between 25 and 75% resulted in elevated levels of sulphides and thiosulphate causing a reducing environment in the pore solution as demonstrated by both redox potential and dissolved oxygen measurements. The dissolved oxygen content of the pore solution was found to be inversely proportionate to the concentration of sulphide and thiosulphate. Thus the slag bearing samples had the lowest levels of dissolved oxygen and most negative redox potentials.

A comparison of TR and SF shows that the slags dominated the early age process up to about 7 days while SF appeared to exert more control over the later stages. The 28 and 90 day hydroxyl concentrations were virtually identical for SF and TR. TR showed a reasonable concentration of sulphides (17 mg/l) at 7 days but these decreased quite markedly at 28 and 90 days. The low hydroxide concentration of TR would have favoured the rapid oxidation of sulphides to thiosulphate and ultimately sulphate. Both the redox potential and dissolved oxygen level slowly shifted from levels indicative of slag bearing materials to those more representative of SF. The suppressed dissolved oxygen concentrations and negative redox potentials would limit the development of the passive layer reducing its effectiveness in protecting the steel against the effects of chloride ions.

The information gathered in the investigation of the pore solution was then used to determine what quantitative effects the specific solution characteristics would have on the chloride threshold concentrations and corrosion rates. The investigation of steel samples under aqueous conditions revealed considerable variability in the threshold concentration. The chloride threshold value for initiating corrosion, based on Cl/OH ratio, ranged from 0.51 for SM to 1.39 for SF. The inclusion of sulphides was found to lower the chloride threshold for initiating corrosion in otherwise identical samples. The variability in the chloride

concentration necessary to initiate corrosion is inherent to the corrosion process as corrosion initiation by chlorides represents a transition from one form of corrosion to another. Corrosion is an ongoing process of decomposition and repair even under passive conditions and the ability and mechanism by which chlorides disrupt the passive layer are quite complex. Those sites on the steel which are defective in some way will provide the first opportunity for a breakdown in passivity. The inclusion of sulphides and thiosulphate has been shown to reduce the effectiveness of the passive layer in resisting the onset of active corrosion due to chloride ions.

The role of the total hydroxide concentration and chloride concentration was determined to be more important than simply the Cl/OH ratio. The corrosion rate increased disproportionately to the change in hydroxyl ion concentration. For example, a 4.8 times decrease in the hydroxyl concentration resulted in a 15.5 times increase in corrosion rate at a chloride concentration of 0.2 M. The effects of sulphides were not as dramatic but still evident. A comparison of SM and FA revealed corrosion rates at least two times higher for the sulphide bearing material, ceteris paribus. The primary factors affecting the corrosion of steel in aqueous solutions therefore are the hydroxide concentration and the presence of sulphides and thiosulphate during the development of the passive layer and the subsequent role of thiosulphate during active corrosion.

The negative impact of sulphides on the corrosion resistance of steel in concrete is also evident in the passivation study. The slag bearing concretes were all shown to have higher corrosion rates and more negative potentials than any of the non slag-bearing samples. The early age potentials (average over the first 16 weeks) of SL and SM were more negative than -500 mV (Ag/AgCl). Such potentials would generally indicate active corrosion associated with chloride ingress. In the present case however the negative potentials are attributed to the reducing environment caused by the presence of sulphide ions. The corrosion rates for both these samples were 0.086 $\mu A/cm^2$. The corrosion rate for SM was almost double that of PC despite having a resistivity four times higher. During the passivation of the steel the pore solution chemistry had a more significant effect on the overall corrosion process than the physical material characteristics such as resistivity. As the steel moved from a state of passivation to active corrosion this situation changed and the corrosion process became more strongly influenced by resistivity of the concrete than the chemistry of the pore solution.

Chloride threshold concentrations were determined for each of the binder types. As with the aqueous phase work there was considerable variation in the chloride threshold from one binder type to another. The chloride threshold concentrations in concrete were generally

shown to decrease with the reduction in hydroxyl concentration. The SF samples however were a notable exception. The average chloride threshold concentration for SF was almost identical to that of PC which is contrary to the aqueous phase work. It is likely that the improvements to the interfacial zone, associated with the use of SF, provided greater adhesion to the steel surface thus limiting the availability of the metal for corrosion and resulting in a comparable chloride threshold concentration despite a lower hydroxide content. As noted in chapter 5 and section 6.4 it is unlikely that there is a uniquely definable chloride threshold concentration specific to each binder type. Chloride threshold concentrations should rather be assigned a probability range over which corrosion is likely to occur. The limitations of the current investigation prevent the presentation of such a range. The binder-specific chloride thresholds however did show the relative performance of the material and provided a general guideline for what values are likely to be encountered.

The effects of cement extenders on the active corrosion rates were determined for steel at covers of 20 mm and 40 mm and crack widths of 0.2 mm and 0.7 mm. The results of the active corrosion investigation revealed a very different performance compared to both the aqueous phase and passive state. The resistivity of the concrete was found to have more of an effect than the pore solution composition or the availability of oxygen as taken from cover depths. The influence of cover and, by extension availability of oxygen, was only significant when the resistivity of the concrete was low and the corrosion rates were high. The corrosion rate of PC increased markedly when the cover was reduced from 40 mm to 20 mm. The lower cover would have allowed for a greater ingress of oxygen which was the controlling factor rather than the resistivity which was sufficiently low as to not affect the corrosion rate. For the cement extenders, a decrease in cover had little effect on the corrosion rate. The corrosion rate was limited by the resistivity of the concrete and thus an increase in the availability of oxygen did not result in a significant increase in corrosion rate. The corrosion rate was also shown to increase with crack width. The effects of crack width and cover were however small compared to the very significant effect of binder type. The inclusion of any cement extender resulted in at least a 40% reduction in the corrosion rate at a cover depth of 40 mm and a 70% reduction at a cover of 20 mm.

A marked correlation between corrosion rate and durability index values was found with the chloride conductivity which is essentially the inverse of resistivity, except that chloride conductivity is measured at an elevated pore solution chloride concentration. No meaningful correlation was found between corrosion rate and the water sorptivity or oxygen permeability indexes. The standard preconditioning of the samples for chloride conductivity determination

resulted in an index which should be applicable to any type of concrete. The relationship between the chloride conductivity, cover depth and corrosion rate is further summarized in the following section.

6.5.1 Corrosion Rate and Damage Model Summary

The corrosion rate of steel in cracked concrete was found to be strongly dependant upon the chloride conductivity values which account for resistivity and chloride binding effects of the material. Chloride conductivity values, taken at 90 days, can be used as predictive tool for estimating a representative future corrosion rate as previously provided in equation 6.2 and reproduced here:

$$i_{corr} = \left(1.43\frac{C_c}{f} - 0.02\right) e^{\left[\left(\frac{40-x}{20}\right)1.2\left(\frac{C_c}{f}\right)^3\right]}$$

where:

f - slag correction factor $= 10^{(|0.5-S|-0.5+S)}$

i_{corr} - corrosion rate μA/cm^2

C_c - chloride conductivity value (mS/cm)

S - slag concentration expressed as a decimal percentage (ie 0.25 for 25%)

x - depth of rebar (mm)

The corrosion rate predictions, based on chloride conductivity, should be valid for the range of cement replacement levels used in the current investigation. Further research will be required to extend the range and validity of the model, particularly with respect to slag replacement levels between 50 and 75%, FA concentrations above 30% and SF above 7%. The range of cover depths is also limited to 20 mm to 40 mm though fairly little change was noticed with the blended cements, and estimates based on greater depths may be reasonable but have not been validated. It should also be noted that the corrosion rates were based on mild steel round bar under slipped conditions. Both of these situations were shown in chapter 5 not to significantly affect the results such that the variations in corrosion rates between binder types was far greater than the minor influence of type of steel employed or method of crack maintenance.

One particular limitation which must be noted is the environment under which the investigation was performed. The testing of the samples and determination of corrosion rates was performed at 30°C. Variations in temperature will affect the corrosion rate of steel and if predictions are to be made for environments with different conditions some allowance must

be made. The effects of temperature on corrosion rate were discussed in chapter 5 and the corrosion rates could be modified accordingly.

The corrosion rate model presented here can be used in conjunction with one of the initiation and propagation models as given in section 6.3, and demonstrated in section 6.4, to provide an overall estimate of the service life of a structure based on knowledge of the materials to be employed. For the models accuracy to be improved, specific studies will need to be performed on the various binder types selected to extend beyond the measurement of stable corrosion rates to the time of visible damage and loss of cross sectional area.

6.6 Recommendations for Future Work

The influence of cement extenders on the corrosion characteristics of steel in concrete has been investigated in this work though many questions still remain. Cement extenders and slag in particular have been shown to have varied effects on the chloride threshold value, passive and active corrosion rates, such as the inclusion of slag resulting in lower chloride threshold concentrations, elevated passive corrosion rates and considerably reduced active corrosion rates compared to PC. A few specific areas where greater research is required have been identified during the course of the current investigation and include:

1. Further study on the cause of the high chloride threshold concentration of steel in concrete made with SF. The chloride threshold concentration of SF was found to be similar to that of PC despite having a significantly lower hydroxyl ion concentration. All other cement extenders were shown to have reduced chloride threshold concentrations compared to PC and SF.

2. Investigation of corrosion rates under different exposure conditions, particularly with RH above 95%. The specific effects of SH on the corrosion characteristics and their correlation with durability indexes may become more apparent. SH had water sorptivity and oxygen permeability indexes which suggested an open pore structure and poor corrosion resistance. The measured resistivity values however were very high and were explained by the rapid drying of the concrete. Under different exposure conditions the concrete would dry at a different rate thus affecting the resistivity and corrosion rate. While SH performed very well under the conditions of this investigation it may not do so in a more moist environment.

3. More detailed study of the effects of high replacement levels of slag between 50 and 75% on the corrosion rate and durability index values. An improvement in material performance characteristics was noticed as the percentage of slag replacement increased from 0 to 50%. The performance of the concrete at a 75% replacement was very poor and further study is needed of slag replacement levels between 50 and 75%.

4. Investigation of the cracking mechanisms in concrete made with various binder types to further the existing damage models or develop a new approach. All binder types in this investigation were assumed to behave the same under corrosion cracking. The specific mechanical properties of the concrete would result in some differences in the response to expansive pressures. The open pore structure of SH, for instance, might absorb more of the corrosion products and require a longer time before cracking becomes apparent. The subsequent corrosion induced cracking of the concrete would also result in changes to the underlying corrosion rate which must also be investigated.

5. Correlation of the corrosion rates determined in the lab with site data, specifically for the accommodation for environmental effects. The laboratory work showed a good correlation between chloride conductivity values and corrosion rate. If the chloride conductivities values are to be used as more than a qualitative comparison and employed in service life modeling they must ultimately be applied to real structures under various environmental conditions.

6.7 References

Andrade, C. and Alonso, C. 1996, *Corrosion Rate Monitoring in the Laboratory and On-Site*, **Construction and Building Materials**, Vol. 10, No. 5, pp. 315-328.

Angus, M. and Glasser, F. 1985, *The Chemical Environment in Cement Matrices*, **Materials Research Society Symposium Proceedings**, Vol. 50, pp. 547-556.

Beeby, A. 1978, **Concrete in the Oceans, Cracking and Corrosion, Technical Report No. 1**, Cement and Concrete Association, Department of Energy.

Ferry, D. and Flanagan, R. 1991, **Life Cycle Costing - A Radical Approach, Report 122**, London: Construction Industry Research and Information Association.

Glass, G. and Buenfeld, N. 2000, The *Influence of Chloride Binding on the Chloride Induced Corrosion Risk in Reinforced Concrete*, **Corrosion Science**, Vol. 42, No 2, pp. 329-344.

Glass, G. Hassanein, N., and Buenfeld, N. 1997, *Neural Network Modelling of Chloride Binding*, **Magazine of Concrete Research**, Vol. 49, No 181, pp. 323-335.

Konin, A., Francois, R. and Arliguie, G. 1998, *Penetration of Chlorides in Relation to the Micro-Cracking State into Reinforced Ordinary and High Strength Concrete*, **Materials and Structures**, Vol. 31, pp. 310-316.

Li, Z., Li, F., Zdunek, A., Landis, E and Shah, S. 1998, **Application of Acoustic Emission Technique to Detection of Reinforcing Steel Corrosion in Concrete**, *ACI Materials Journal*, Vol. 95, No. 1, pp. 68-76.

Liu, Y. and Weyers, R. 1998, *Modeling the Time-to-Corrosion Cracking in Chloride Contaminated Reinforced Concrete Structures*, **ACI Materials Journal**, Vol. 95, No. 6, pp. 675-681.

Liu, Y. 1996, **Modeling the Time-to-Corrosion Cracking of the Cover Concrete in Chloride Contaminated Reinforced Concrete Structures**, Dissertation for Doctor of Philosophy, Virginia Polytechnic Institute and State University.

Mackechnie, J. 2001, **Prediction of Reinforced Concrete Durability in the Marine Environment, Research Monograph No. 1**, Department of Civil Engineering, University of Cape Town and University of Witwatersrand.

Mackechnie, J. 1996, *Marine Exposure of Concrete under Selected South African Conditions*, **Proceedings of Third International Conference on the Performance of Concrete in Marine Environments, St. Andrews by-the Sea, Canada**, American Concrete Institute, Farmington Hills, pp. 205-216.

Marcotte, T. and Hanssor, C. 1998, *A Comparison of the Chloride-Induced Corrosion Products from Steel Reinforced Industrial Standard versus High Performance Concrete Exposed to Simulated Sea Water*, **International Symposium on High-Performance and Reactive Powder Concretes: Sherbrooke**, Vol. 4, pp. 145-162.

Sergi, G., Yu, S. and Page, C. 1992, *Diffusion of Chloride and Hydroxyl Ions in Cementitious Materials Exposed to a Saline Environment*, **Magazine of Concrete Research**, Vol. 44, No. 158, pp. 63-69.

Stansbury, E. and Buchanan, R. 2000, **Fundamentals of Electrochemical Corrosion**, ASM International, Ohio.

Suda, K., Misra, S. and Motohashi, K. 1993, *Corrosion Products of Reinforcing Bars Embedded in Concrete*, **Corrosion Science**, Vol. 35, No. 5-8, pp. 1543-1549.

Weyers, R. 1998, *Service Life Model for Concrete Structures in Chloride Laden Environments*, **ACI Materials Journal**, Vol. 95, No. 4, pp. 445-453.